University of Bath

UNIVERSITY OF
BATH

PHD

Enzyme-Triggered Catalytic Signal Amplification

Goggins, Sean

Award date:
2015

Awarding institution:
University of Bath

Link to publication

Enzyme-Triggered Catalytic Signal Amplification

Sean Goggins

A thesis submitted for the degree of Doctor of Philosophy

August 2015

Department of Chemistry | UNIVERSITY OF BATH

atlas telamon

Table of Contents

Chapter 3

Enzyme-Triggered Catalytic Signal Amplification

Chapter 4

Experimental

Chapter 5

Acknowledgements

There are a great number of people who I would like to acknowledge in making this thesis possible. First and foremost, I would like to thank Professor Christopher G. Frost for giving me the opportunity to work as part of his research group. I hope that through the work presented herein, I have been able to repay his decision to allow me to follow on from my undergraduate project and continue my postgraduate studies in his laboratory. Secondly, I would like to thank Atlas Genetics Ltd. and in particular, Dr. John Clarkson, not only for funding but also for the highly relevant and interesting project along with giving me the freedom to run with my ideas. I would also like to thank them for financial support in allowing me to present this work at the 248th ACS National Meeting & Exposition in San Francisco.

I am hugely grateful for Dr. Barrie Marsh for both his persistence and his motivation. Also, with his encyclopaedic knowledge of named reactions, I feel that there was no better post-doc from which to develop my further understanding of organic chemistry. I am also very grateful for Dr. Steve Flower for his friendly help and advice when I first arrived in the group as an undergraduate as well as for allowing me to demonstrate undergraduate laboratory experiments. I would like to thank all the other previous Frost group members for making my time here as enjoyable as it has been. Specifically, I would like to thank Dr. Hannah Edwards for her patience as my supervisor during my undergraduate project and Dr. Jonathan Sharp for showing me the actual working hours of Ph. D. student, someone whom I've since tried to emulate. Likewise, I would like to thank all the current members of the Frost group for their patience during the stressful writing-up period and I hope that I've been able to make their time here as enjoyable as mine was.

I consider myself very fortunate to have had many excellent undergraduate project students working under my supervision during my time here. In particular, French summer students Clément Bellini, Christophe Naz and Paul Legentil deserve my praise as due to their hard work, a number of publications were made possible. For similar reasons, I would also like to thank certain members of the University of Bath support staff; Dr. Anneke Lubben (MS), Dr. John Lowe (NMR) and Dr. Mary Mahon (X-Ray) for their expertise as well as Dave Elkins for keeping our laboratory functional.

To the residents of 28 South Avenue, Dr. Ben Atkinson, Dr. Liam Emmett and Dr. Dave Stanton, I thank for making the time living in Bath as entertaining as it was and to whom I wish all the very best for the future. I would also like to thank my parents and brother along with the rest of my family for their constant support and encouragement. Finally, I would like to very much thank Rebecca Jones for her love and patience over the last few years as without her, I definitely wouldn't be where I am today. I hope the trip to San Francisco was in some way compensation for her dedication and that I'm very much looking forward to taking similar excursions in the future.

Abstract

Amplification is essential in order to achieve low limits of detection (LOD) within analyte detection assays. Over recent years, chemists have developed a multitude of amplification methodologies for the detection of a variety of analytes with varying signal readouts. Typically, these methodologies are focussed upon one of four main amplification strategies; target, label, signal or receptor amplification. Herein, a thorough review of the current literature has been compiled highlighting both the advantages and disadvantages of each strategy.

Despite the increasing number of amplification methodologies being described, there is still significant demand for improving analyte assay efficiency and sensitivity. In particular, rapid and sensitive protein detection that can be performed at the point-of-care (POC) setting is highly desirable for the effective treatment and control of infectious diseases. In collaboration with medical diagnostics company Atlas Genetics Ltd., a new electrochemical substrate for the ratiometric detection of alkaline phosphatase (ALP), a commonly-used enzyme label within enzyme-linked immunosorbent assays (ELISA), was developed capable of delivering an ALP LOD of 0.3 pM within 30 minutes. When applied to the detection of C-reactive protein (CRP), a model biomarker used to diagnose inflammation, the substrate was shown to be significantly more reproducible than a commonly-used commercially-available electrochemical ALP substrate.

In order to improve the sensitivity of an ELISA, a novel signal amplification methodology was then developed. Based upon a double-catalyst signal amplification strategy, an organometallic transfer hydrogenation catalyst was utilised in combination with the enzyme label to afford a hybrid synthetic and biological amplification cascade. To achieve selective enzyme-triggered catalyst activation, an enzyme substrate termed a proligand was synthesised. In the presence of the enzyme, self-immolation of the proligand occurs to release a ligand, capable of binding to an iridium pre-catalyst to generate a ligand-accelerated active catalyst. Catalyst activity could be observed through ratiometric electrochemical analysis through the use of an electroactive aldehyde as the catalyst substrate. An ALP LOD of 7.6 pM after 33 minutes was obtained for this amplification methodology but when applied to the detection of CRP however, a significant background reaction, found to be caused by the iridium pre-catalyst, limited sensitivity. The versatility of the signal amplification methodology was nevertheless demonstrated through the enzyme-triggered catalytic reduction of a range of different aldehydes with alternative signal readouts, enabling signal transduction and amplification to be easily achieved within a single procedure.

Abbreviations

2CDCR	–	two-component dendritic chain reaction
AA	–	L-ascorbic acid
AA2P	–	L-ascorbic acid 2-phosphate
ABC	–	avidin–biotin complex
ABTS	–	2,2'-azino-bis(3-ethylbenzothiazoline-6-sulfonic acid)
ACA	–	4-acetoxycinnamaldehyde
Alloc	–	allyloxycarbonyl
ALP	–	alkaline phosphatase
AMP	–	adenosine monophosphate
AOx	–	alcohol oxidase
2AP	–	2-aminopurine
API	–	active pharmaceutical ingredient
ATP	–	adenosine triphosphate
ATPase	–	adenosine triphosphatase
BE	–	benzoylecgonine
BLIP	–	β-lactamase inhibitory protein
BPEA	–	9,10-bis(phenylethynyl)anthracene
BPP	–	bis(p-phenylene)-34-crown-10
BSA	–	bovine serum albumin
CA	–	carbonic anhydrase
CARD	–	catalysed reporter deposition
cat-ELCCA	–	catalytic assay using enzyme-linked click-chemistry assay
CDI	–	1,1'-carbonyldiimidazole
CENTA	–	7-(2-thienylacetamido)-3-((3-carboxy-4-nitrophenyl)thiomethyl)-cephalosporonic acid
CFDA	–	5-carboxyfluorescein diacetate
CoA	–	coenzyme A
COx	–	choline oxidase
CRP	–	C-reactive protein
DBU	–	1,8-diazabicyclo[5.4.0]undec-7-ene
DCF	–	2',7'-dichlorofluorescein
DCFH	–	2',7'-dichlorodihydrofluorescein
DCR	–	dendritic chain reaction
DIPEA	–	*N*,*N*-diisopropylethylamine
DMA	–	*N*,*N*-dimethylaniline
DMAP	–	4-(dimethylamino)pyridine
DMF	–	*N*,*N*-dimethylformamide

DMSO	–	dimethylsulfoxide
DNA	–	deoxyribonucleic acid
DNPH	–	dinitrophenylhydrazine
DTT	–	dithiothreitol
DPV	–	differential pulse voltammetry
EAAS	–	enzyme-amplified array sensing
EATR	–	enzyme-assisted target recycling
EB	–	elementary body
ELISA	–	enzyme-linked immunosorbent assay
EME	–	ecgonine methyl ester
ESI	–	electrospray ionisation
Fc	–	ferrocene
FLDA	–	fluorescein diacetate
FLuc	–	firefly luciferase
Fmoc	–	9-fluorenylmethoxycarbonyl
FRET	–	Förster resonance energy transfer
FSA	–	fluorescence signal amplification
FT	–	Fourier transform
β-gal	–	β-galactosidase
GOAT	–	ghrelin O-acyltransferase
GOx	–	glucose oxidase
GPES	–	general purpose electrochemical system
HCA	–	human carbonic anhydrase
HCR	–	hybridisation chain reaction
HILR	–	halide-induced ligand rearrangement
HIV	–	human immunodeficiency virus
HPLC	–	high-pressure liquid chromatography
HRP	–	horseradish peroxidase
HSD	–	hydroxysteroid dehydrogenase
IgG	–	immunoglobulin G
IL-8	–	interleukin-8
IR	–	infrared
IRMA	–	immunoradiometric assay
ITO	–	indium tin oxide
LC	–	liquid chromatography
LOD	–	limit of detection
MAO	–	monoamine oxidase
MB	–	methylene blue
MMP2	–	matrix metalloproteinase-2

4-MUG	–	4-methylumbelliferyl-β-D-galactopyranoside
MS	–	mass spectrometry
NAD	–	nicotinamide adenine dinucleotide
NCS	–	*N*-chlorosuccinimide
NMR	–	nuclear magnetic resonance
NTR	–	nitroreductase
ONP	–	*o*-nitrophenol
ONPG	–	*o*-nitrophenol-β-D-galactopyranoside
ODN	–	oligodeoxynucleotide
PAC	–	polyazacyclam
PCR	–	polymerase chain reaction
PGA	–	penicillin-G-amidase
phen	–	1,10-phenanthroline
PhK	–	phosphorylase kinase
PKA	–	protein kinase A
PLE	–	porcine liver esterase
PNP	–	*p*-nitrophenol
POC	–	point-of-care
PQ	–	paraquat (*N,N'*-dimethyl-4,4'-bipyridinium dichloride)
PSA	–	prostate specific antigen
RCA	–	rolling circle amplification
SAAC	–	signal amplification by allosteric catalysis
SCE	–	saturated calomel electrode
SOx	–	sarcosine oxidase
SPR	–	surface plasmon resonance
TACN	–	triazacyclononane
TASC	–	target-assisted self-cleavage
TBAA	–	tetrabutylammonium acetate
TBAB	–	tetrabutylammonium bromide
TBAF	–	tetrabutylammonium fluoride
TCE	–	2,2,2-trichloroethyl
TEA	–	triethylamine
TEV	–	tobacco etch virus
THF	–	tetrahydrofuran
TLC	–	thin-layer chromatography
TMB	–	3,3',5,5'-tetramethylbenzidene
TMEDA	–	*N,N,N',N'*-tetramethylethylenediamine
TMSE	–	2-(trimethylsilyl)ethyl
TOF	–	time-of-flight

Tris	–	tris(hydroxymethyl)aminomethane
TSA	–	tyramide signal amplification
UHR	–	ultrahigh resolution
UOx	–	urate oxidase
WLA	–	weak-link approach

Chapter 1

Molecular Amplification in Sensing

1.0   Introduction

Amplification is the process whereby a small input signal is converted to a large output signal by means of an amplifier. Amplifiers are most commonly associated with electronics where they are used to increase the power of an electric signal for functions such as increasing audio volume. Amplifiers are also found within certain aspects of optics, fluidics and mechanics. In nature, living organisms use amplification for purposes such as visual excitation,[1] blood clotting,[2] and biosignalling.[3] Typically, these amplified physical responses to an external stimulus are achieved through enzyme cascade mechanisms (Scheme 1.1).[4] Specific enzyme cascades are initiated when a signalling molecule (*i.e.* a hormone) is detected by a signal receptor, which in turn activates an associated enzyme. Once activated, the enzyme can catalyse the production of multiple signal relay molecules, which can go on to activate more enzymes and so on, resulting in an enzyme cascade. An example of this can be found within the fight-or-flight response exhibited by animals where, in response to a perceived threat, epinephrine is released by the body to activate an enzyme cascade for increasing blood sugar levels.[5] Through this powerful amplification mechanism, the detection a single molecule of epinephrine by a receptor can lead to the production of thousands of glucose molecules; amplifications over several orders of magnitude are observed within milliseconds.
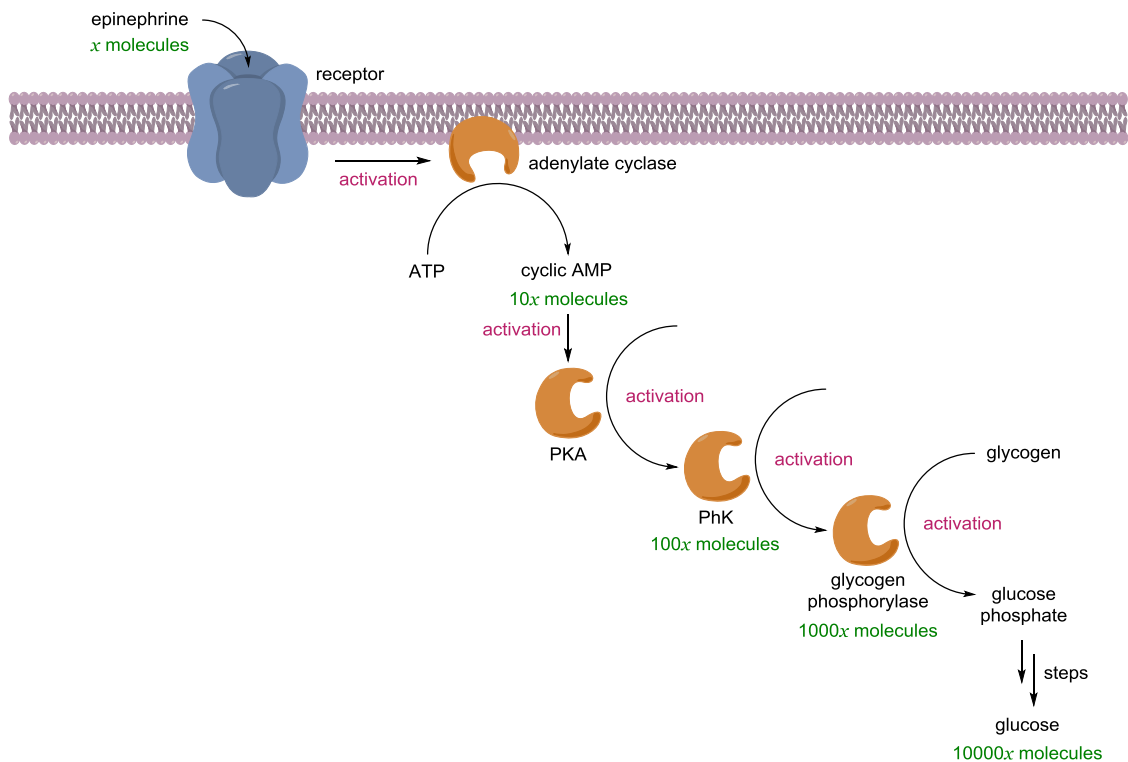
Scheme 1.1 Epinephrine-activated enzyme cascade for the amplified production of glucose.
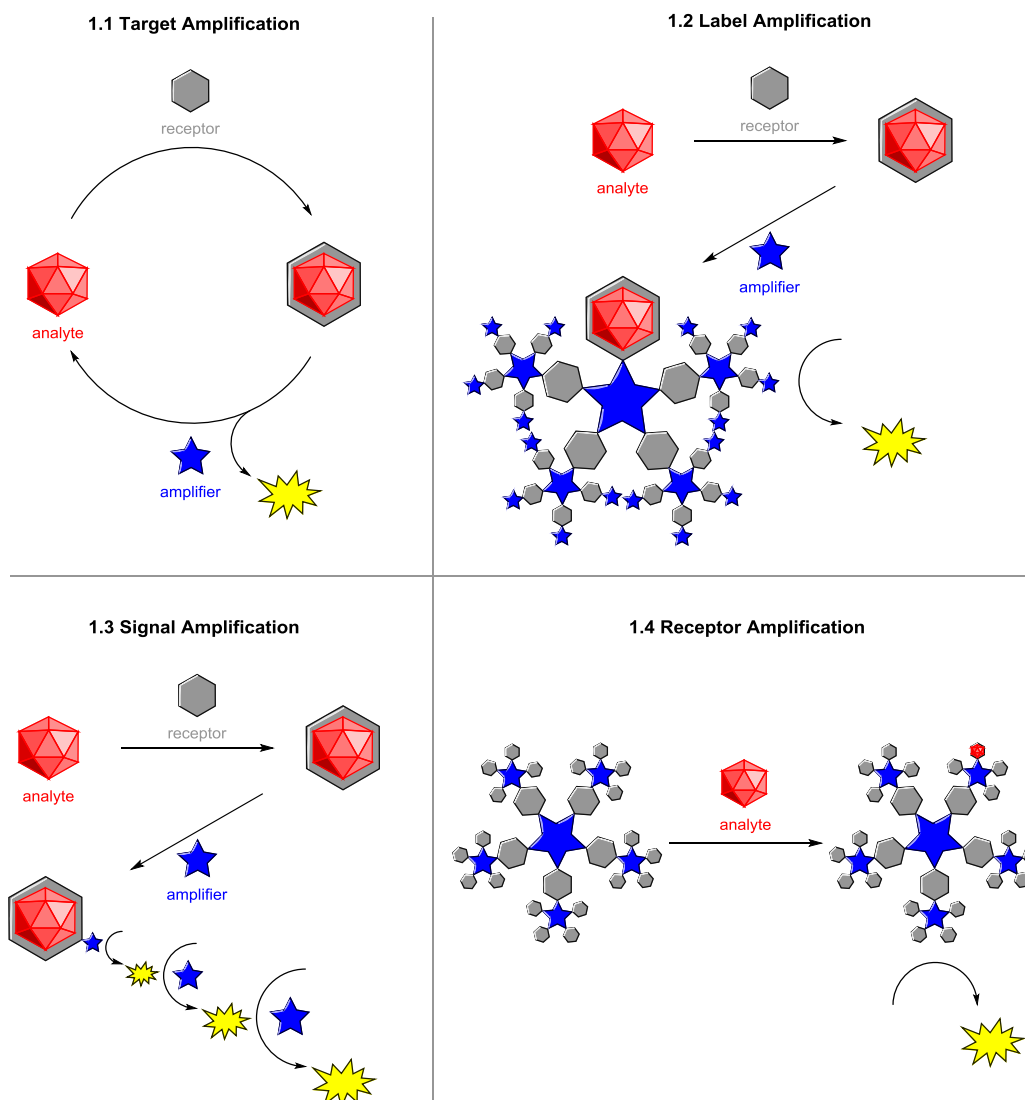
Figure 1.1 Four main approaches to achieving amplification within sensing.

The use of amplification is also found within many biological and chemical sensing techniques.[6] Since a single molecule is unable to generate a strong enough signal to be detected, some degree of amplification is paramount to achieving a detection protocol with high sensitivity. There is huge demand for the ability to detect of a large variety of different analytes in many areas of society but especially within molecular diagnostics,[7] forensic analysis,[8] and environmental monitoring.[9] There is also increasing pressure to improve the efficiency as well as the sensitivity of currently existing analyte detection assays. As such, more and more amplification methodologies for a range of different analytes are constantly being developed. The analytes requiring detection are often very structurally diverse and the readout method chosen for detection can also vary depending on the application. To accommodate for this, many different amplification methodologies have been developed to specifically detect the desired analyte with an appropriate sensitivity and using the readout method required. Despite the vast number of amplification methodologies published to date, they typically fall within one of four types of amplification

categories; target amplification, label amplification, signal amplification or receptor amplification (Figure 1.1).

Target amplification (Chapter 1.1) involves increasing the number of analyte–receptor recognition events that occur *per* analyte. This can be done by increasing the analyte concentration prior to analyte recognition through analyte replication protocols, or by recycling the analyte after a signal has been produced post-analyte recognition. Additionally, analytes that can affect multiple labels or reporter molecules due to possessing catalytic properties themselves provide inherent target amplification within their detection assays. Label amplification (Chapter 1.2) focuses on increasing the number of labels *per* analyte recognition event. Since each label is responsible for providing a signal, the ability to amplify the number of labels that represent an analyte–receptor recognition event leads to a signal increase. This can be done using polymerisation or nucleic acid replication techniques or through the use of nanostructures for either directly increasing label numbers or to provide a collective change in physical property to illicit a detectable response. Signal amplification (Chapter 1.3) is by far the most common approach to improving the sensitivity of a detection methodology and regards the use of amplifiers to enhance the signal produced from an analyte–receptor recognition event. Receptor amplification (Chapter 1.4) utilises a number of scaffolds to amplify the amount of receptors bound to the signal-generating mechanism. This increases the probability of achieving an analyte–receptor recognition event and, as a single binding event is able to affect the properties of the entire structure; an increased signal can be obtained in comparison to a single receptor system. Although the majority of amplification methodologies published to date are designed upon one of these four approaches, many are not exclusively bound to such parameters and categorised by which best describes the novel amplification method developed by the authors. This becomes apparent with regard to more recent amplification publications where the authors strive to achieve even greater detection sensitivity through a combination of strategies from different amplification categories.

1.1   Target Amplification

1.1.1   Target Replication

One strategy to improve the limit of detection (LOD) of an assay is to simply increase the number of target molecules present. If few molecules of the target are present then an efficient replication technology, that is specific only to the analyte, would dramatically increase the concentration of target molecules to a detectable level. Traditionally, target replication has been specifically developed for the amplification of nucleic acids and there have been a substantial number of different strategies developed for this purpose.[10] The polymerase chain reaction (PCR) is one such target replication methodology and it is probably the most widely known sensing amplification methodology ever produced.[11]
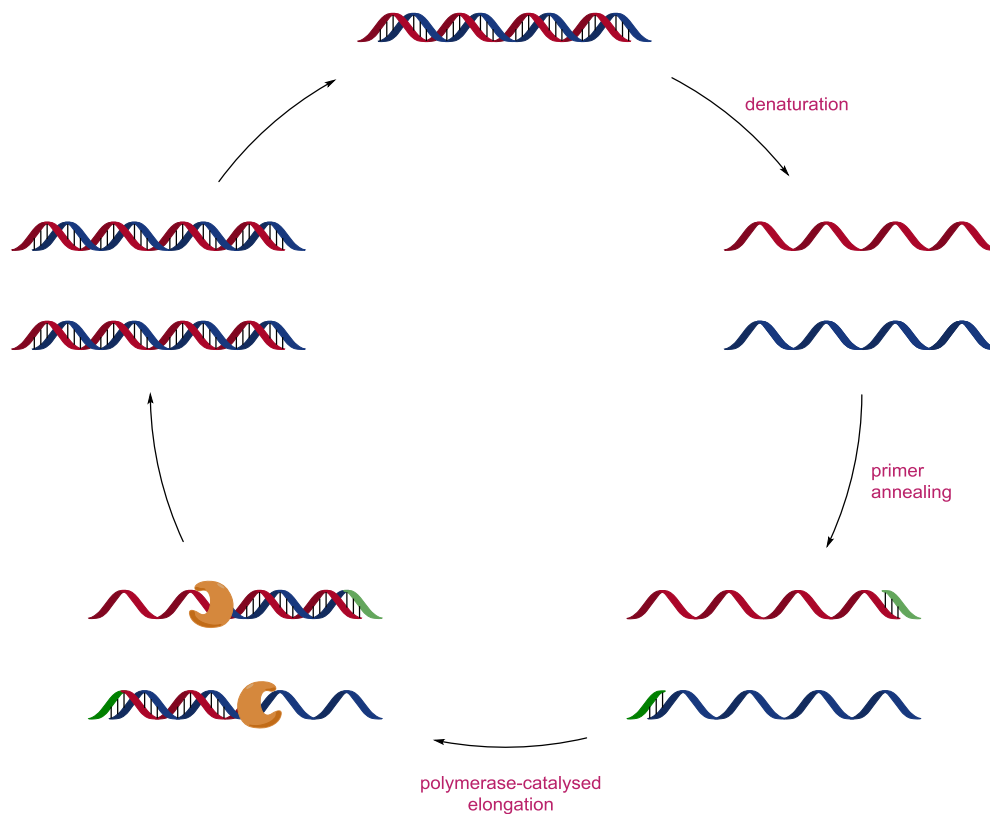
Scheme 1.2 The polymerase chain reaction (PCR) cycle.

PCR is used to amplify target strands of deoxyribonucleic acid (DNA) prior to detection and is carried out over a number of cycles (Scheme 1.2).[12] Each cycle begins with denaturation of the double-stranded DNA at elevated temperatures in order to obtain the target DNA in single-stranded form. This is followed by the annealing of DNA primers to the single-stranded DNA, which indicates the start of the specific sequence of DNA due to be replicated. Starting from the primer, an enzyme known as DNA polymerase elongates the nucleic acid sequence in a base-by-base complementary fashion to the single-stranded DNA yielding two identical copies of double-stranded DNA. These steps are repeated, often between 15 to 40 cycles, until amplification yields a detectable concentration of target DNA. As with every PCR cycle the amount of target DNA present is doubled, then DNA amplification using PCR is exponential; one of only a handful of sensing methodologies that truly exhibits exponential amplification. Because of this powerful amplification, and the fact that the process can be automated using thermal cyclers, PCR has been incorporated into many areas of science where sensitive DNA detection is paramount, such as forensics, evolutionary molecular biology and molecular diagnostics.[13] Current research into PCR has been focused towards avoiding the use of thermostable polymerases and thermal cyclers in order to reduce the time, and improve the efficiency of the protocol. A number of isothermal nucleic acid amplification technologies have since emerged,[14–15] which allows for nucleic acid sensing to be performed in the point-of-care (POC) setting.[16] One limitation of PCR is that it is

specific only to the amplification of nucleic acids. Target amplification methodologies that demonstrate the exponential amplification of other analytes as yet remain undiscovered.

1.1.2   Target Recycling

In the majority of cases, analytes to be detected are unable to be replicated as a means of providing amplification. Target amplification can still be achieved however, if the analyte can be recycled after a signal has been produced by an analyte recognition event. By doing this, one target molecule is able to act upon multiple probe molecules which are responsible for providing the positive signal. This can be described as target recycling and is another useful method of providing target amplification.
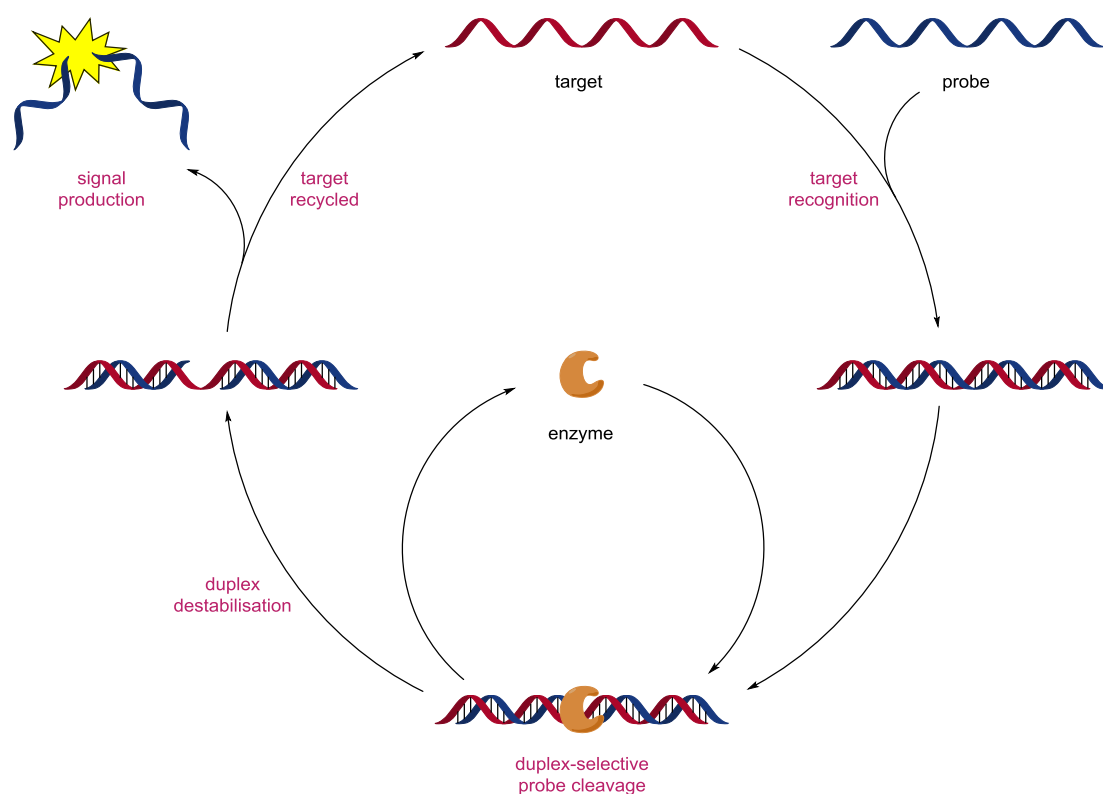
Scheme 1.3 Enzyme-assisted target recycling of nucleic acids.

An example of this is enzyme-assisted target recycling (EATR), which is also used primarily for nucleic acid detection (Scheme 1.3).[17] In this approach, single-stranded target DNA hybridises with probe oligonucleotides, which are usually in a vast excess. The resulting double-stranded DNA is acted upon by an enzyme that selectively cleaves the probe and in the process, releases a detectable signal.[18] Enzyme-cleavage also results in the destabilisation of the complex which then separates and in doing so, releases the target single-stranded DNA capable of reacting

further with more DNA probes. Although EATR produces a linear amplification compared with the exponential amplification provided by PCR, fewer false-positives occur since the procedure is less sensitive towards DNA contaminants. Additional benefits of EATR over PCR include an improved robustness and reduced cost, making it a useful amplification methodology for affordable POC diagnostics. The same concept can also be achieved with ribozymes (nucleic acid enzymes) instead of enzymes, allowing for autocatalytic variants of this method to become possible.[19]
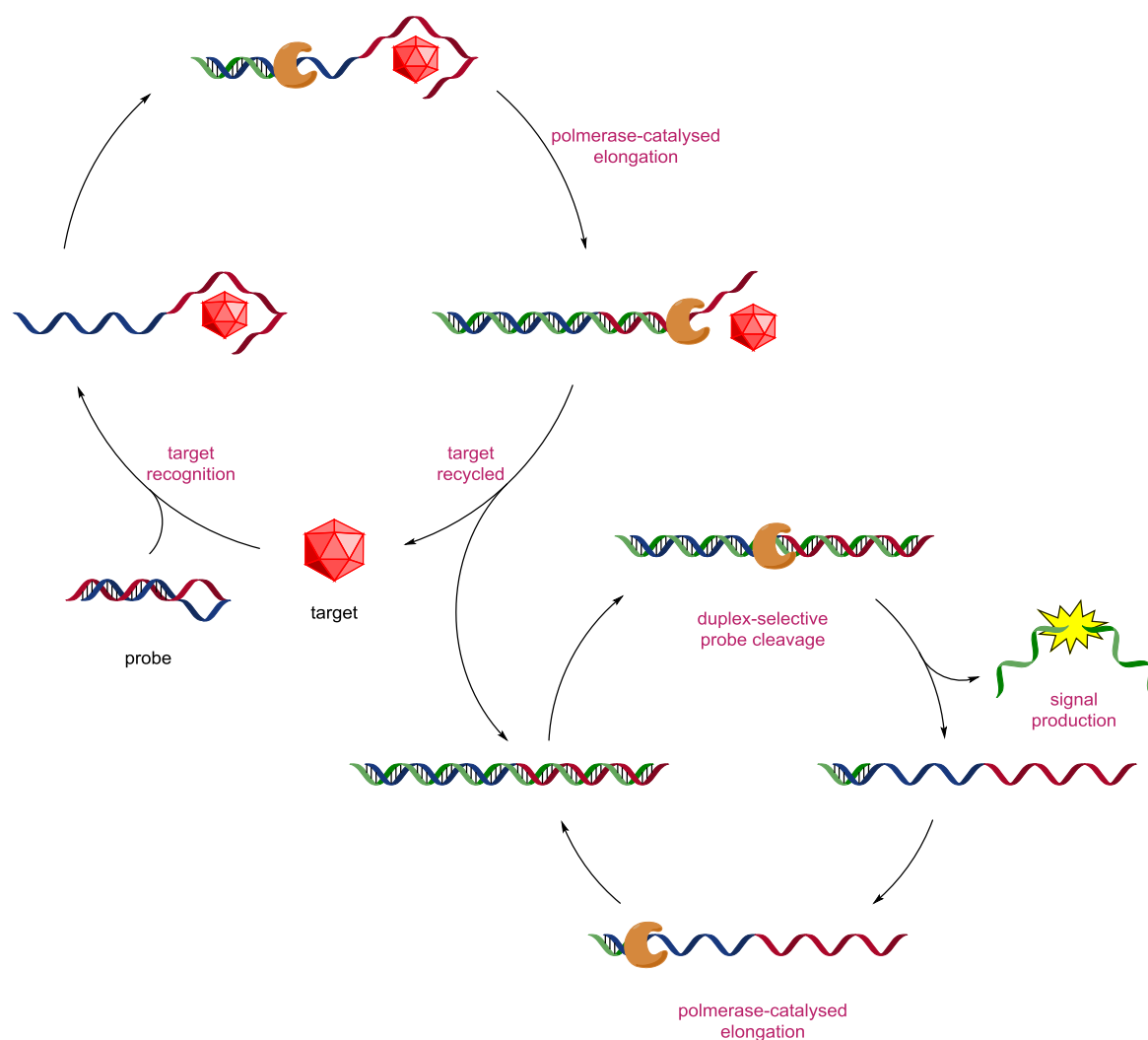
Scheme 1.4 Quadratic enzyme-assisted target recycling for small molecule detection.

Efforts have since been made towards removing the enzyme entirely through the development of self-cleaving probes.[20] In their non-hybridised form, the probes are stable towards any inter- or intramolecular reactions with itself, giving no signal in the absence of the target. In the presence of the target, target-assisted self-cleavage (TASC) occurs, destabilising the complex and leading to recycling of the target along with the production of the signal, often *via* fluorescence. This 'reagent-free' approach towards DNA sensing has inspired the development of DNA-templated reactions where target DNA can act as a catalyst for turning substrates into products.[21]

Coupling substrate turnover with signal production allows for the reaction to be monitored over time and DNA templates have been shown to provide >200-fold increase in signal in 30 seconds over a nontemplated reaction, and can achieve a turnover number of 1500 times with a LOD of 0.5 pM.[22] Recently, a quadratic target recycling amplification procedure has been described by Huang *et al.* in which two recycling pathways operate sequentially for the ultrasensitive detection of certain antibiotics (Scheme 1.4).[23] In this advancement, a hairpin DNA structure containing an aptamer probe, selectively binds to its target ampicillin. Once the hairpin has been opened by the target, a primer becomes bound and a polymerase replicates a complementary strand recycling the target in the process. The double helix produced as a result then enters its own EATR cycle producing multiple copies of short single-stranded DNA. This amplified sequence is then able to bind to electrochemically-labelled complementary sequences, preventing them from being detected at the electrode. Thus, a positive sample is observed in this case by a signal decrease. The use of a DNA aptamer for analyte recognition delivered excellent selectivity for the target, even in the presence of similar structures such as penicillin, and the LOD for this system was calculated to be 1.09 pM after a 4.5 hour amplification period which boasts a 100-fold improvement over existing methods.

Target recycling methodologies have also found use within applications other than DNA detection. For example, two EATR cycles can cross-trigger one another to achieve simultaneous self-amplification for use towards a DNA-based artificial biochemical circuit.[24] Additionally, cascaded catalytic nucleic acids have been used to control reactivity, perform logic operations and assemble complex structures.[25]

1.1.3 Target Catalysis

Another target amplification strategy is to utilise the catalytic attributes of the analyte being detected. Target catalysis, as an amplification methodology, is typically used for the detection of trace metal contaminants found in pharmaceutical ingredients and waste water streams. There has been a significant increase in the number of metal-catalysed cross-coupling reactions used in the pharmaceutical industry over recent years and as a result, metal impurities within drug compounds are becoming commonplace and are considered to pose a potential health risk.[26] Palladium is the most commonly used element within metal-catalysed reactions towards the synthesis of pharmaceuticals and consequently, restrictions have been placed upon the amount of residual palladium allowed to be found in medicinal compounds.[27] Unsurprisingly, the development of sensitive detection methodologies for palladium has been widely sought after.

Koide *et al.* were the first to exploit palladium's catalytic ability as a method of providing amplification for its detection.[28] Non-fluorescent compound **1** was designed with an allyl moiety for analyte recognition which, only in the presence of Pd^0, undergoes deallylation *via* a Tsuji–Trost-like mechanism (Scheme 1.5).[29–31] Quantitative detection of the released, highly-

fluorescent product **2** can be performed using a standard fluorometer allowing for a LOD of less than 1 ppm of palladium *per* mg sample. This efficient example of target amplification was successfully shown to detect residual Pd^0 in pharmaceutical products as well as impregnated within used glass reactor vessels. In addition, the probe has been used within a high-throughput method for the detection of palladium within ore samples towards the more efficient and economical mining of precious metals.[32] As Pd^{II} is readily reduced to Pd^0, both oxidation states of palladium are detected by this method. However, by changing the mechanism used for palladium detection to the metal-catalysed aromatic Claisen rearrangement,[33] selective detection of Pd^{II} over Pd^0 could be achieved.[34] The similar reactivity of palladium and platinum however can cause selectivity issues, but through careful selection of the solvents used in the assay and by maintaining a specific pH, this can also be overcome.[35] Improvements to this detection methodology include the introduction of reducing agents and phosphine ligands in order to increase the catalytic activity of the palladium, which in turn has led to increased sensitivity of the assay.[36–37] Furthermore, a bis-allyl ether derivative of **1** has been very recently reported that can significantly reduce background fluorescence and as such, delivers a >300-fold signal increase within a 5 minute reaction period.[38]
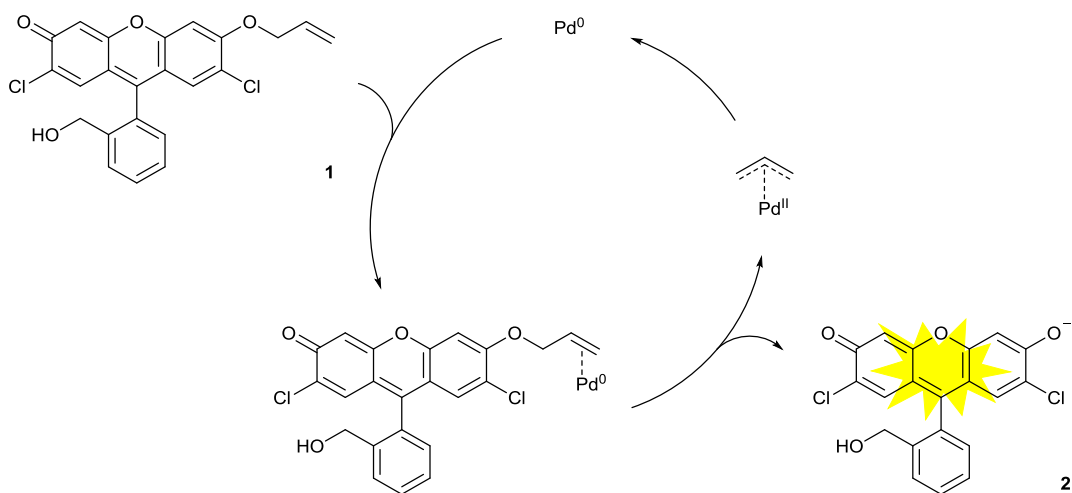
Scheme 1.5 Fluorogenic detection of palladium using a catalytic deprotection strategy.

Alternative moities have also been shown to be selective for palladium detection as a propargyl derivative of compound **1** has been shown to be able to monitor palladium accumulation in living systems *via* fluorescence.[39] Probes with different fluorescent scaffolds have also been used for palladium detection within cells.[40] Among these, naphthalimide-derived probes are considered the most accurate since fluorescence detection is ratiometric.[41] Palladium sensing is not confined to just allyl or propargyl deprotection as Jun and Ahn have utilised the catalytic cross-coupling capability of palladium to develop a 'switch-on' fluorescent detection method (Scheme 1.6).[42] In this example of target catalysis, non-fluorescent probe **3** was designed comprising of an aryl iodide for analyte recognition and a spirolactam derivative of a rhodamine dye, a common pro-fluorescent

scaffold.[43] Oxidative insertion into the carbon–halide bond induces ring-opening of the spirolactam, and subsequent reductive elimination provides highly-conjugated fluorescent product **4** whilst simultaneously regenerating the active catalyst. This highly sensitive technique allows for the specific detection of palladium at concentrations as low as 2 ppb. Following the success of these initial reports, there has been extensive research into the development of alternative probes for both the colourimetric and fluorescent detection of palladium and platinum based upon this catalytic amplification concept.[44–45]
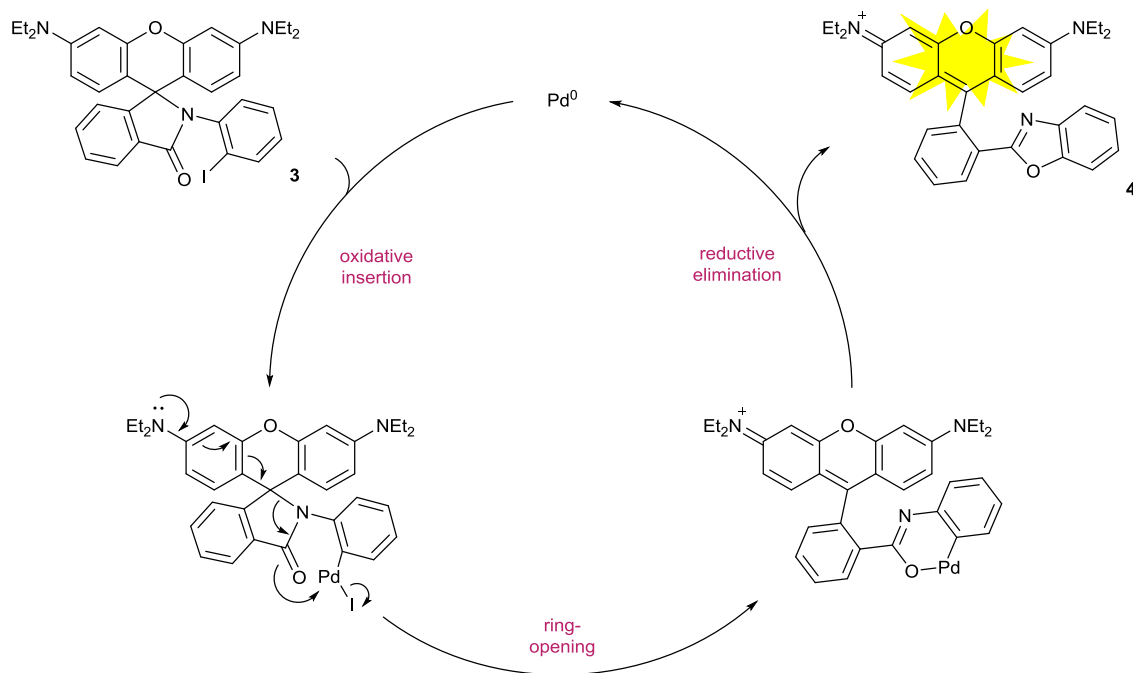
Scheme 1.6 Fluorogenic detection of palladium using a catalytic cross-coupling strategy.

In addition to the sensitive detection of metals, the detection of enzymes are also important especially within high-throughput screening for drug discovery as well as enzyme engineering.[46] Since a single enzyme is capable of generating multiple reporter molecules, amplification in the form of target catalysis is inherent within enzyme detection assays.[47] The simplest and most effective strategy is to couple enzyme-responsive functional groups with water-soluble chromogenic or fluorogenic moieties to obtain enzyme substrates that selectively exhibit a change in physical property in the presence of an enzyme.[48] For example, Sames *et al.* designed a range of fluorogenic probes for oxidoreductase enzyme detection based on this concept.[49] During their investigation, they found that one probe in particular was a highly selective substrate for 3-α-hydroxysteroid dehydrogenase (HSD), an enzyme responsible for the activation and deactivation of steroid hormones.[50] This enabled fluorescence imaging to be performed on human cells in order to

monitor the up-regulation of HSD in response to panaxytriol,[51] an active compound found in red ginseng; a common ingredient within herbal medicines.[52]
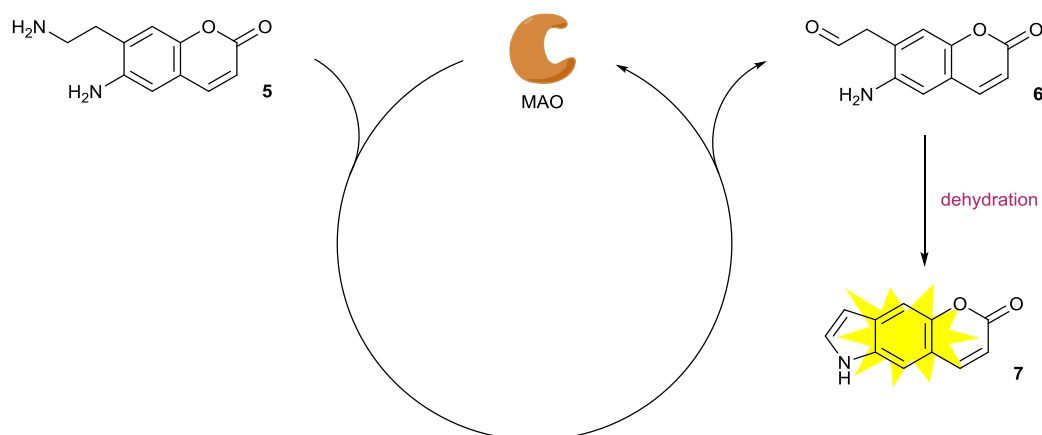
Scheme 1.7 Fluorogenic enzyme assay for the detection of MAO.

By changing the enzyme-responsive trigger unit, the group were able to simply achieve a highly selective 'switch-on' fluorescent assay for monoamine oxidase (MAO) (Scheme 1.7),[53] an enzyme associated with neurological and psychiatric diseases.[54] In this enzyme detection assay, compound **5** was exposed to MAO which catalyses the aerobic oxidation of amines to the corresponding imines.[55] This intermediate is then hydrolysed under the aqueous conditions required for enzyme activity to give aldehyde **6**, which then undergoes intramolecular cyclisation and dehydration to afford highly fluorescent indole **7**. Although not a particularly sensitive system due to the slow turnover rate of the enzyme, it did allow for the direct and continuous measurement of MAO activity in mitochondria, utilising target catalysis for amplification.

1.2   Label Amplification

1.2.1   Label Replication

Since the majority of analytes requiring detection do not possess catalytic attributes or can be easily replicated, target amplification is therefore not a realistic amplification strategy. An alternative amplification method is amplifying the label after analyte–probe recognition. This concept provides amplification by multiplying the number of labels *per* analyte recognition event. An example of this can be provided through a derivative of PCR, known as rolling circle amplification (RCA).[56] RCA is an isothermal nucleic acid amplification protocol which has found use in many applications within chemical biology, materials science and medicine.[57] Typically, circular single-stranded DNA, called a template, is linearly replicated hundreds or thousands of times to give an extremely

long strand of single-stranded DNA. Since the same DNA sequence is repeated, multiple complementary probe strands are able to hybridise to the amplified single-stranded DNA label enabling sensitive detection normally through fluorescence.[58]
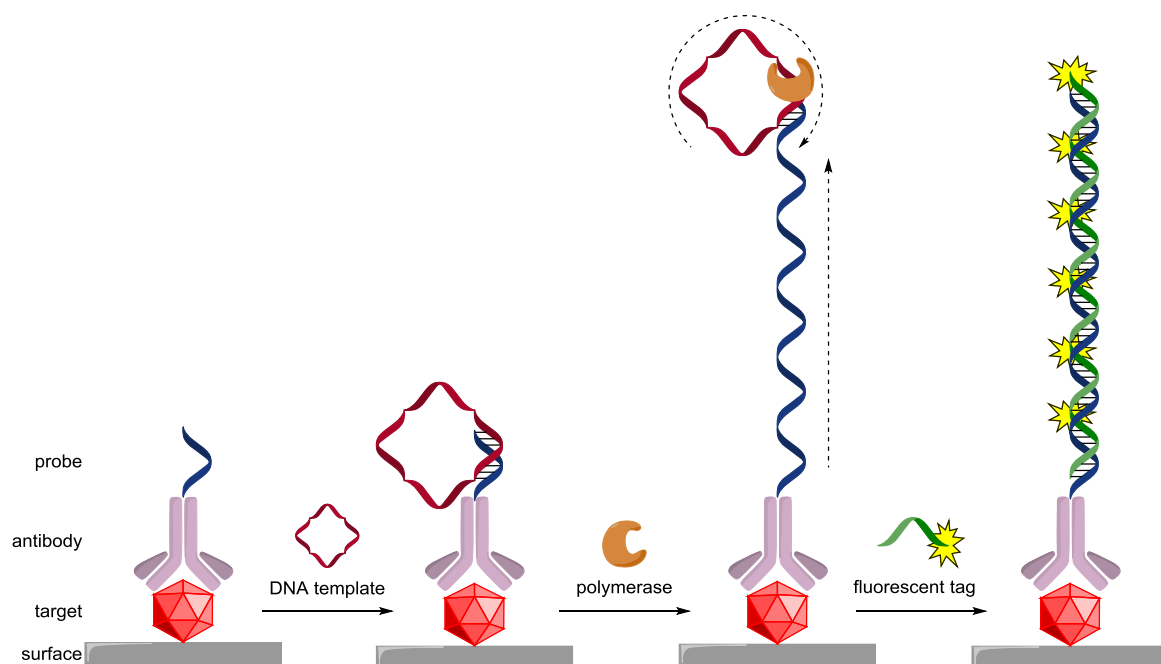
Scheme 1.8 Label amplification using RCA in a DNA-labelled immunoassay.

The application of RCA to immunoassays, known as immuno-RCA, allows for the sensitive detection of proteins through the labelling of probe antibodies with a specific DNA sequence (Scheme 1.8).[59] In the presence of the analyte, hybridisation with the circular template enables replication of the label DNA sequence using RCA, which can then be detected by fluorescence through the hybridisation of multiple complementary DNA sequences tagged with a fluorophore. This strategy allows for an enormous ratio of fluorescent molecules *per* label, and therefore *per* analyte, and as such, delivers a highly sensitive detection system. Jiang *et al.*, for example, achieved a LOD of 0.9 fM for the detection of human immunoglobulin G (IgG) using immuno-RCA.[60]

RCA has also been combined with oligonucleotide-functionalised nanoparticles for sensitive cancer cell detection by electrochemical methods with an obtained LOD of 10 cells *per* mL.[61] Increasing the sensitivity of DNA-labelled immunoassays can also be achieved by using PCR as the amplification technique.[62] Termed immuno-PCR, this technique delivers 100 to 10000-fold increase in immunoassay sensitivity and has been applied to the sensitive detection of tumour markers, viral proteins and bacterial pathogens.[63–64] However, to allow the label to be amplified by PCR, cleavage of the DNA label from the analyte–probe complex is required which can be difficult to perform efficiently without denaturising the complex and creating unwanted contaminants that can hinder the PCR amplification process.
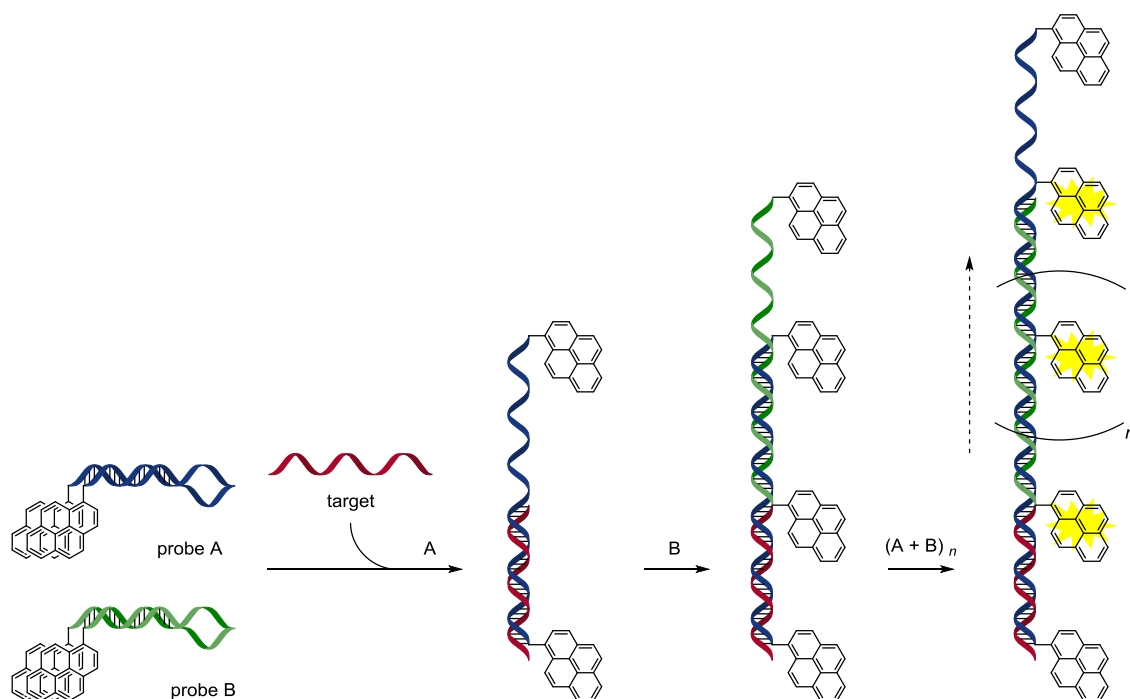
Scheme 1.9 HCR approach to label amplification.

A reagentless label replication strategy known as the hybridisation chain reaction (HCR) was developed by Dirks and Pierce, that involved two stable DNA hairpin structures that can coexist in solution until selectively triggered by the analyte.[65] Once triggered, the two strands of DNA react with one another in an alternating end-over-end fashion. By introducing 2-aminopurine (2AP), a fluorescent adenine analogue,[66] into the structure of one of the hairpin structures, HCR can be measured through fluorescent quenching. Alternatively, labelling both ends of both hairpin structures with pyrene enables a switch-on fluorescent DNA detection derivative (Scheme 1.9).[67] Of one the benefits of using pyrene is that fluorescence detection is ratiometric which minimises errors from environmental effects leading to a more accurate detection method. Not only is this amplification method isothermal and enzyme-free, it is also highly selective, as base-pair mismatches, base deletion or base insertion are all discriminated from the target, and highly sensitive as DNA detection is in the femtomolar range. These highly advantageous attributes has enabled HCR to be used for *in situ* amplification and fluorescent imaging within vertebrate embryos.[68] Silver nanoparticles can also be used within a label-free derivative of HCR for amplified electrochemical DNA detection.[69]

A synthetic approach to label replication was developed by Bowman *et al.* who achieved an amplified response through molecular recognition-selective polymerisation (Scheme 1.10).[70] In this approach, surface-bound biotin-labelled analytes are tagged with a macrophotoinitiator *via* an avidin complex. Irradiation of the surface in the presence of a monomer-containing solution induces polymerisation selectively from the photoinitiators, which therefore only occurs in the presence of the analyte. A 10 minute exposure to 365 nm wavelength light was enough to initiate polymers with a thickness greater than 100 nm, which is significant enough to see with the unaided

eye and allowed a DNA concentration of 0.5 fmol to be easily detected. It has been estimated that an amplification factor of between 10^6 to 10^7 can be achieved through this methodology.[71] This polymerisation-based amplification has also been applied to the detection of the influenza virus through macrophotoinitiator-labelled immunoassays.[72] To provide quantitative measurements, as opposed to the quantitative visual readout, fluorescent nanoparticles can also be incorporated into the polymer enabling DNA detection,[73] and antibody detection,[74] to be achieved through fluorescent polymerisation-based amplification.
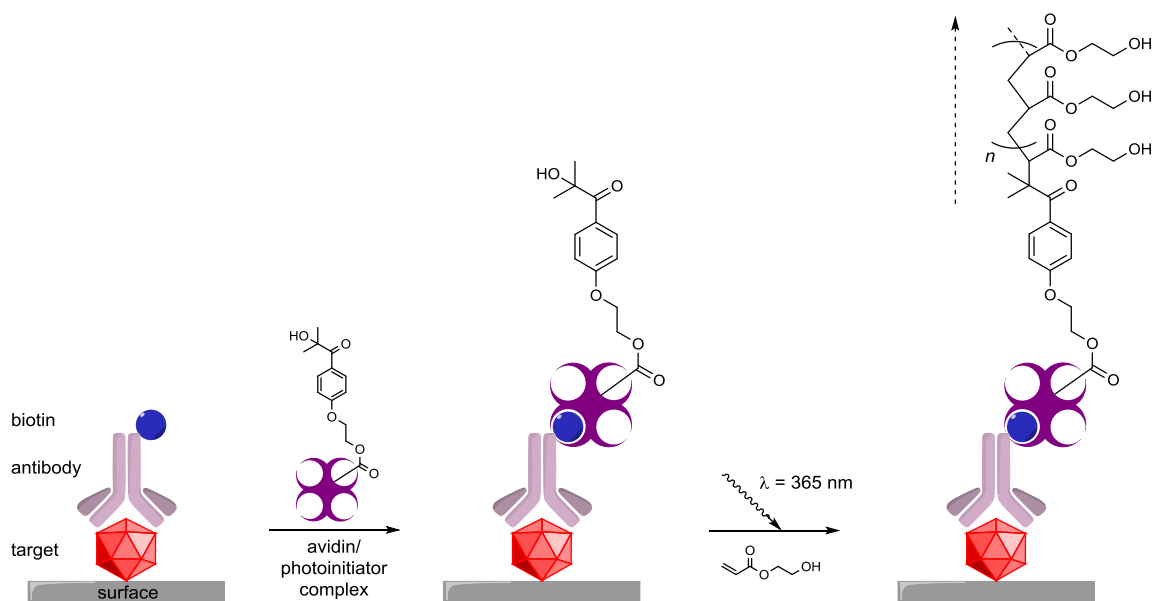
Scheme 1.10 Polymerisation-based label amplification.
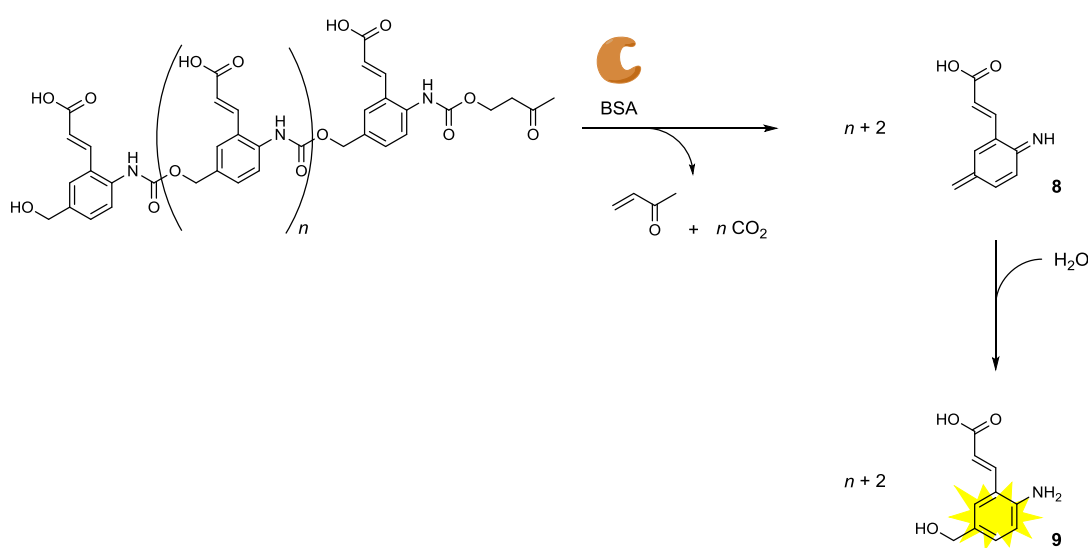
Scheme 1.11 Integer label amplification through triggered head-to-tail depolymerisation.

13

In a conceptually opposite approach, self-immolative polymers that undergo triggered depolymerisation in the presence of a specific analyte have been developed by Shabat *et al.* for catalytic protein detection (Scheme 1.11).[75] Typically, polymer chains comprised of between 15–20 pro-fluorescent monomer units and an analyte-responsive trigger unit at the head were synthesised. Cleavage of the head group occurs selectively in the presence of bovine serum albumin (BSA),[76] triggering continuous head-to-tail depolymerisation,[77] with subsequent release of the monomer units and trapping of these aza-quinone-methide intermediates **8** with water, generates aniline **9** with a consequential turn-on of fluorescence. Although full consumption and full elimination of the polymers is slow, a 1 mgmL^{-1} concentration of BSA could easily be distinguished from the background after an hour. Different monomers can easily be incorporated into the polymer allowing multiple signals to be released simultaneously upon a single trigger cleavage.[78] This has lead to self-immolative polymers being used for a number of biomedical applications as well as for amplification within diagnostic assays.[79–80]

1.2.2 Label Multiplication

In the majority of instances, label replication is typically restricted to the use of nucleic acids as labels as it relies upon nucleic acid amplification procedures such as PCR and RCA. However, these methods are dependent upon the successful conjugation of the DNA label to the antibody, which can be difficult to achieve without denaturising the antibody. Also, polymerisation methods can be irreproducible and quantification of analyte concentrations can be difficult. A more general approach to providing label amplification can be provided though multiplying the number of labels present after an analyte–receptor recognition event. In this method, the label that indicates the presence of the target is able to capture multiple identical probes in the adjacent vicinity, thus multiplying the number of labels *per* target. This is exemplified by an amplification procedure designed to increase immunosensitivity known either as tyramide signal amplification (TSA),[81] or catalysed reporter deposition (CARD).[82]

Typically, CARD is used to multiply the number of enzyme labels that represent the presence of a target protein after an initial analyte–receptor complex has been labelled with an enzyme (Scheme 1.12).[83] In this example, the target analyte is bound to a solid surface and identified with the corresponding antibody labelled with the enzyme horseradish peroxidase (HRP). In the presence of a biotin-labelled tyramine-derived substrate, the enzyme catalyses the formation of highly reactive tyramine radicals that react readily with any tyrosine units found within the adjacent protein structures.[84] This results in the macromolecular structure being covered with many biotin molecules, each of which is able to bind another enzyme *via* its streptavidin conjugate utilising the high binding affinity between biotin and streptavidin.[85] By employing this approach, one target is able to bind multiple enzyme labels which, upon addition of a pro-fluorescent substrate, leads to an amplified fluorescent output. This method is reported to deliver improved

sensitivity in comparison to other probe multiplication methods towards increasing immunoassay sensitivity such as the avidin–biotin complex (ABC) approach.[86]
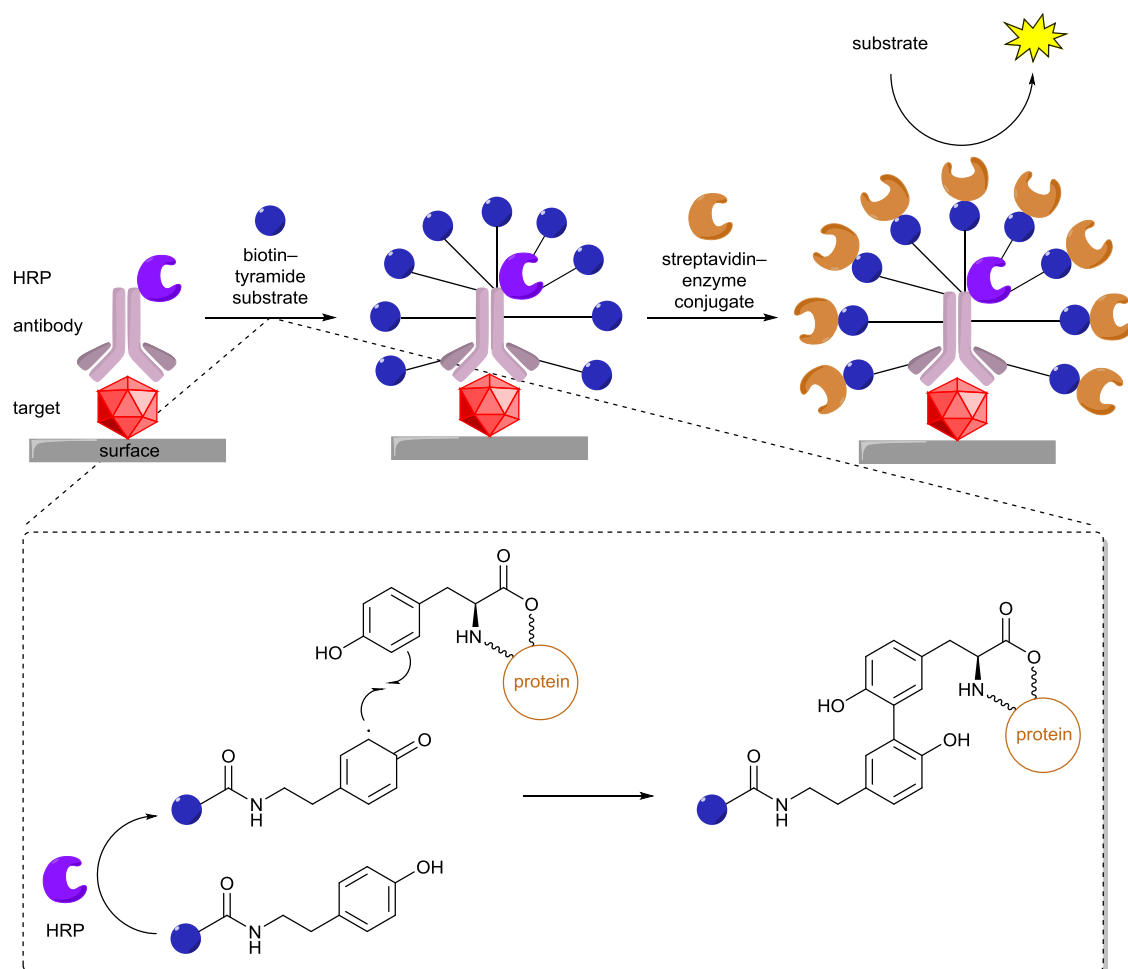
Scheme 1.12 Catalysed reporter deposition (CARD).

The ABC approach to label multiplication typically utilises the multivalent characteristics of the streptavidin tetramer avidin, in order to increase the number of labels that represent a target molecule (Scheme 1.13).[87] Similarly to CARD, target proteins are identified by appropriate antibodies after to being adsorbed onto a solid surface. Instead of being labelled with an enzyme however, the antibodies are labelled with biotin. The addition of a solution consisting of avidin and biotin-labelled HRP leads to a vast interlinked biotin–avidin network containing multiple peroxidase enzymes *per* complex. As a result, when the enzyme network is exposed to a solution containing the enzyme substrate, an amplified response is observed compared to an immunoassay that uses just one enzyme *per* target analyte. This has led to the ABC approach to label amplification to be used for a number of applications such as affinity chromatography and enzyme localisation studies, as well as for diagnostics.[88] However, like many immunoassay amplification methodologies, this system is susceptible to high background rates due to non-specific adsorption.

Not only this, but the procedure also adds multiple manipulation steps in comparison to standard immunoassays.[89]
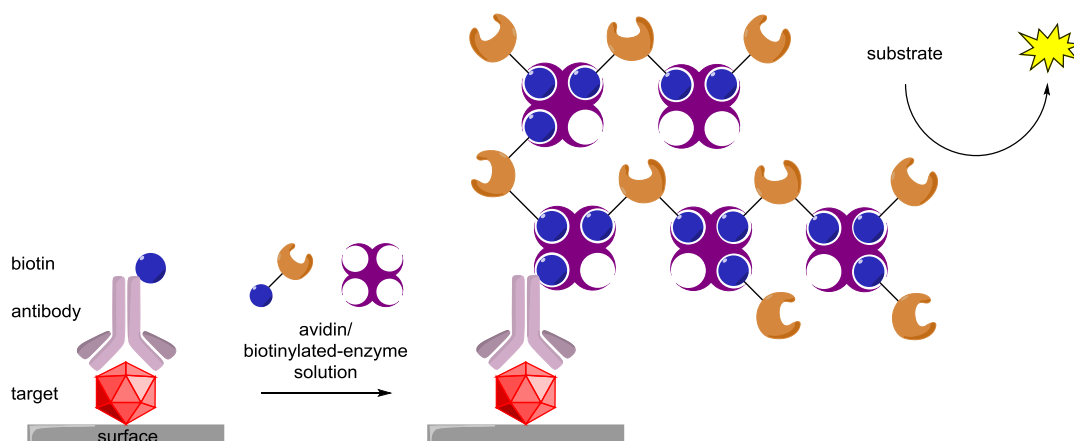
Scheme 1.13 Avidin–biotin complex (ABC) approach to label amplification.

The concept of synthesising structures possessing multivalent characteristics in order to multiply the number of labels corresponding to a single target molecule has inspired the development of many other label amplification approaches. In particular, nanostructures have found considerable success as label amplifiers, especially within biosensors, due to their small size yet large collective surface area.[90–92] For example, Rusling *et al.* described the use of carbon nanotubes as the label amplifier within an electrochemical immunosensor for sensitive cancer biomarker detection.[93] In this approach, the carbon nanotubes function as a bridge between the antibody used for target identification, and the enzyme labels. The amount of enzyme labels *per* binding event was calculated to be approximately ninety, which allowed for a LOD of 4 pgmL^{-1} for the cancer biomarker, prostate specific antigen (PSA). Similarly, this technique was also used for the attomolar detection of DNA, which equates to just 80 copies.[94] Gold nanoparticles, which are easier to functionalise than carbon nanotubes, have also been used as the label amplifier. The enzyme label to binding event ratio was found to dramatically increase through this change, since the use of 1 µm diameter gold nanoparticles allowed up to five hundred thousand enzyme labels to be attached *per* nanoparticle. Due to this massive label amplification, a LOD of 1 fgmL^{-1} was obtained for the detection of cancer biomarker interleukin-8 (IL-8).[95]

The ability to attach a large number of labels upon a single nanoparticle and that gold nanoparticles in particular are easier to functionalise through strong covalent gold–thiol bonds, has seen them incorporated into a large number of chemical and biological sensing methodologies for label amplification.[96] One extremely sensitive approach was developed by Mirkin *et al.* who functionalised gold nanoparticles with multiple copies of oligonucleotides with identical sequences to obtain what are known as "bio-barcodes".[97] These bio-barcode nanoparticles were then used as label amplifiers for the sensitive protein detection (Scheme 1.14).[98] In this approach, antibody-

functionalised magnetic capture nanoparticles are used to identify target proteins which, in the presence of the analyte, are labelled with the bio-barcodes through the formation of a highly-stable sandwich complex. The complex is then separated from the mixture magnetically and the oligonucleotide labels are released from the nanoparticle either thermally by hydrolysis or chemically, using dithiothreitol (DTT).[99] If necessary, the released oligonucleotides can also be amplified by PCR to further increase the sensitivity of the assay. Detection is often achieved scanometrically on a solid surface,[100] or by fluorescence in solution using fluorophore-labelled probes.[101] By functionalising the magnetic capture nanoparticle with DNA instead of antibodies, the bio-barcode sensing approach can be applied towards DNA detection. The sensitivity of this approach allows for target DNA detection with a LOD of 0.5 aM, which approximately equates to just 10 copies of DNA *per* 30 µL sample.[102] The bio-barcode amplification approach also exploited the versatility of nanoparticles through the simultaneous use of magnetic capture nanoparticles with different probes and different label nanoparticles which allows for the multiplex detection of either DNA,[103] or proteins.[104]
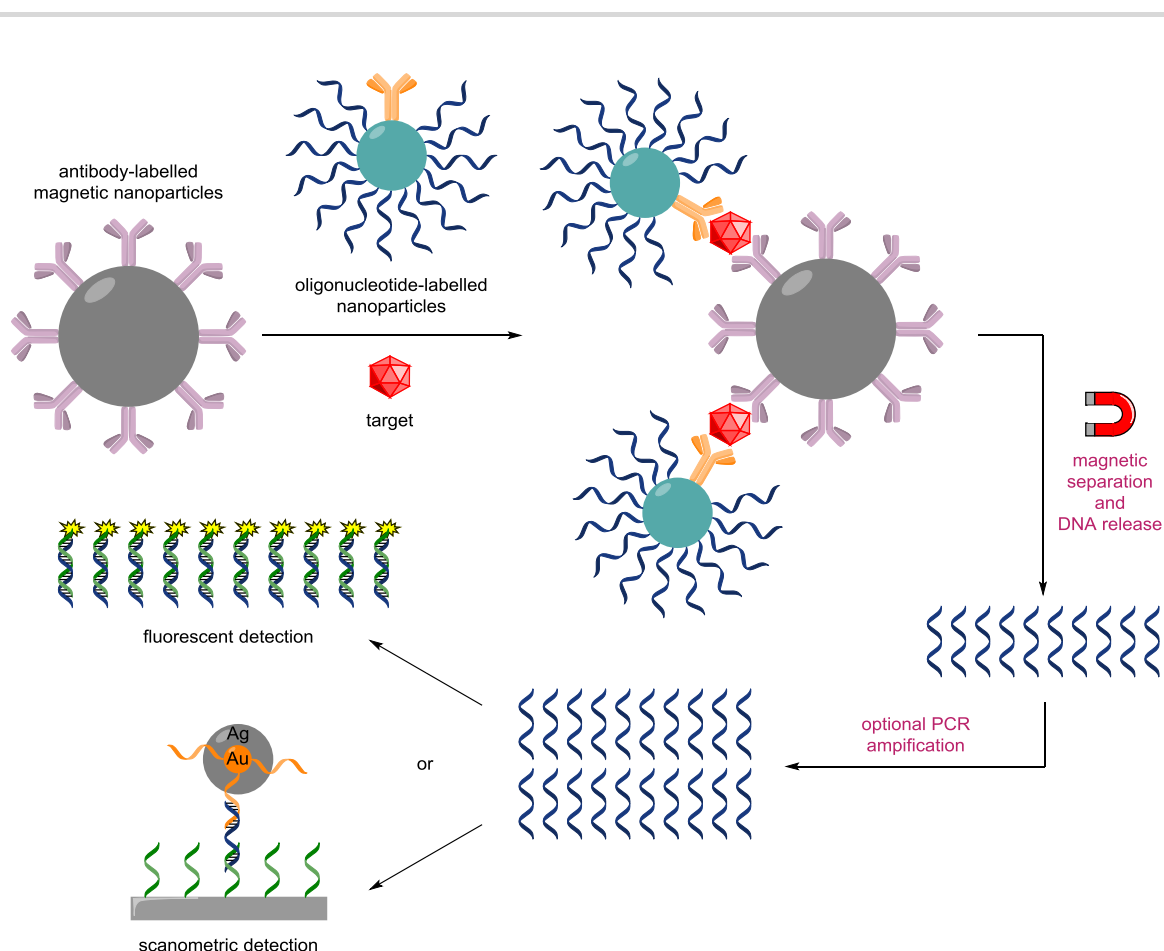
Scheme 1.14 Detection of a target protein using nanoparticle-based bio-barcode probes.

1.2.3   Label Aggregation

Another approach to label amplification can be demonstrated by an analyte's ability to affect a large number of labels in a collective fashion, as opposed to amplifying the label post an analyte–probe recognition event as seen in replication or multiplication strategies. Rather than having one reporter molecule being made responsible for the production of the signal with amplification efforts being made to increase the number of these molecules *per* analyte, it is the strategy of label aggregation to harness all the reporter molecules available to create the signal and by changing the physical properties of a collective signal in the presence of the analyte, significant amplification can be achieved. This type of collective response to minor changes in conditions is analogous to colourimetric pH indicators where a slight increase or decrease in acidity is enough to shift the equilibrium of the system, which can result in a dramatic colour change. In a similar manner, the optical properties of gold nanoparticles are known to be dependent upon the distance between each nanoparticle, which is attributed to the surface plasmon resonance (SPR) of gold.[105] Manipulation of this physical property phenomenon for label aggregation within a sensing methodology was first provided by Mirkin *et al.* for the colourimetric oligonucleotide detection (Scheme 1.15).[106]
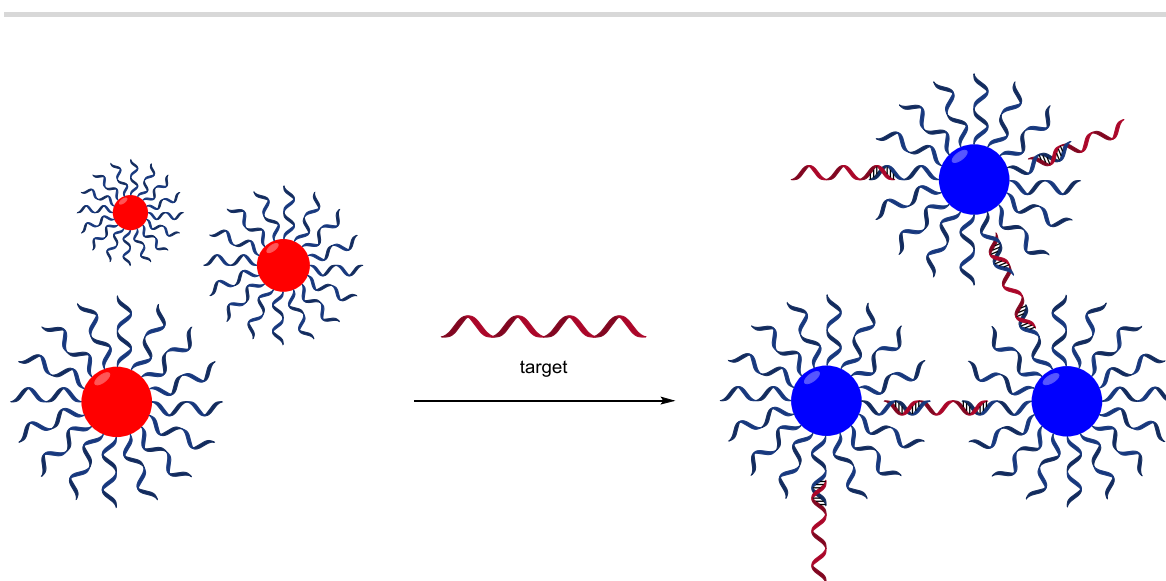
Scheme 1.15 Gold nanoparticle label aggregation for colourimetric DNA detection.

In this approach, ≈13 nm gold nanoparticles were constructed and derivatised with mercaptoalkylated probe oligonucleotides to afford a nanoparticle-containing solution with a characteristic red colour since the distance between particles is significantly greater than the particles themselves. In the presence of target oligonucleotides, hybridisation at both ends of the target causes significant aggregation of the nanoparticles and the subsequent decrease in

interparticle distance results in a colour change to blue. This simple DNA detection and label amplification method was found to be surprisingly selective as a single base-pair mismatch could be distinguished from the complementary target. Sensitivity was also high allowing for a LOD of ≈10 fM of oligonucleotide to be easily detected.
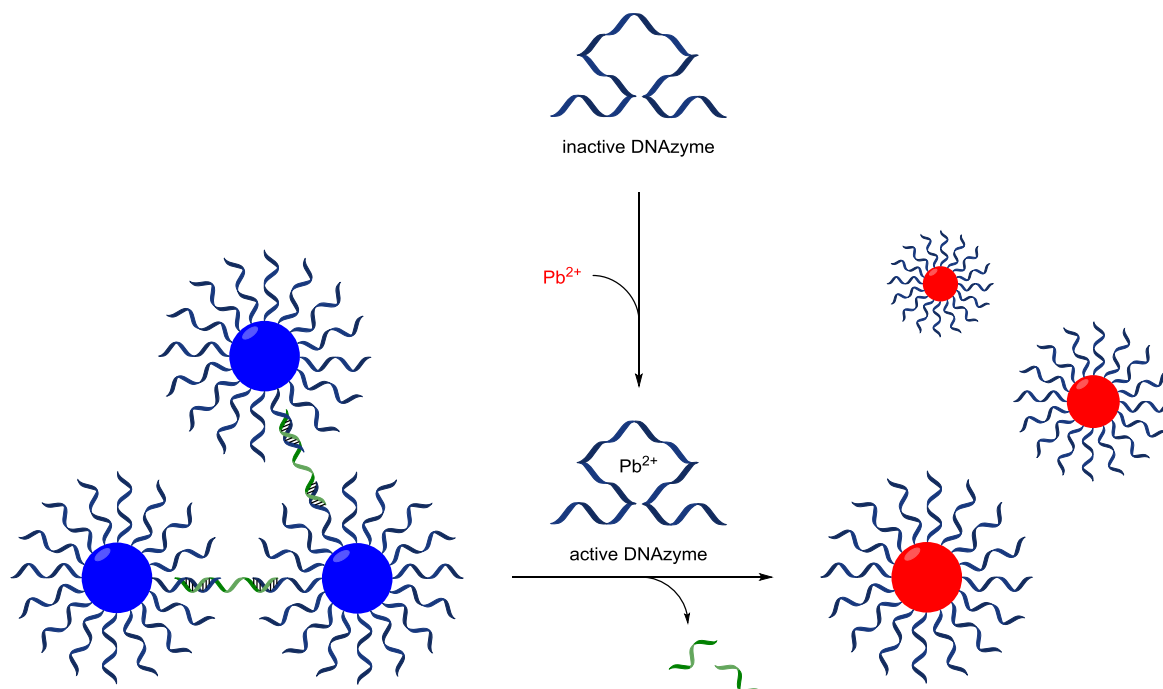
Scheme 1.16 Gold nanoparticle label deaggregation for colourimetric lead detection.

In a similar but opposite approach, Liu and Lu utilised the deaggregation of gold nanoparticles towards colourimetric lead ion detection (Scheme 1.16).[107] In this setup, an oligonucleotide probe was used to aggregate gold nanoparticles together through hybridisation at both ends. In the presence of lead, inert DNAzymes are activated which results in cleavage of the oligonucleotide substrate serving as the linkage between the nanoparticles. The dissociation of the nanoparticles results in an easily-visualised colour change from blue to red. Since DNAzymes can be synthesised to be very selective for particular cofactors,[108] this method was shown to be highly selective for lead in the presence of a host of other metal ions. The label aggregation provided by this methodology provided excellent sensitivity with a LOD of 100 nM lead concentration shown to be detectable by the unaided eye.

Label multiplication methods such as CARD and the ABC approach both suffer from a lack of versatility as there are only a limited number of labels available for amplification. Nanostructures compensate for this as their versatile nature has made them popular label amplification tools within biosensing. However, they are often cumbersome to prepare and suffer from high backgrounds due to oversensitivity from non-specific adsorption. The use of controlled

aggregation for label amplification is a simple yet effective strategy for amplification within sensing and typically has the benefit of a colour change which can be easily visualised. Despite having examples exhibiting powerful amplification, label amplification techniques are often analyte-specific and are restricted to the specific type of diagnostic assay they are designed for in order to achieve successful amplification.

1.3 Signal Amplification

Signal amplification is the process whereby the signal generated from an analyte–probe recognition event is amplified by an external amplifier. Signal amplification is the most popular amplification method employed in sensing as it is often the easiest amplification methodology to design and implement, as amplification does not involve amplifying the target or the label. Due to the high number of examples, signal amplification approaches can be divided into four distinct areas based on the mechanism of amplification: single-catalyst, double-catalyst, autoinductive and autocatalytic (Figure 1.2). As one would expect, the reaction profiles displayed by these signal amplification mechanisms are markedly different (Figure 1.3). However, it is not a case of which one provides the biggest or fastest signal, as dependent upon the application, one type of signal amplification may prove more suitable than another.
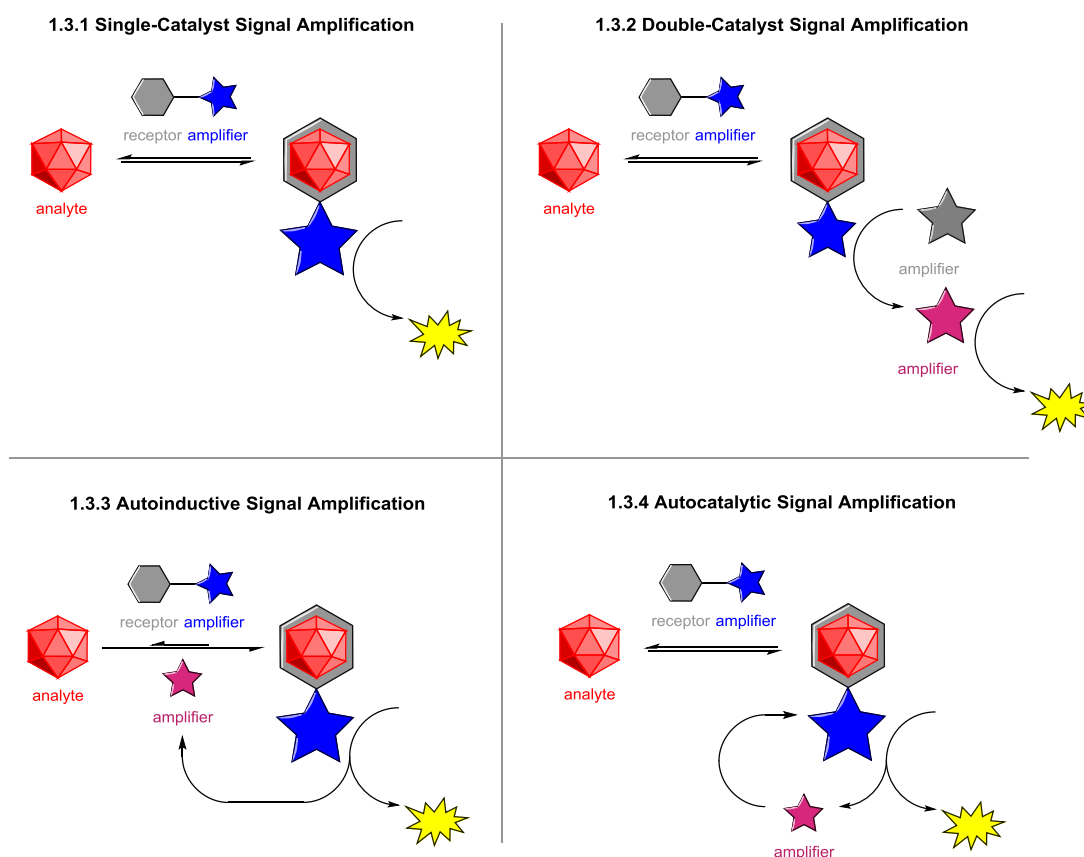
Figure 1.2 Four main signal amplification mechanisms.
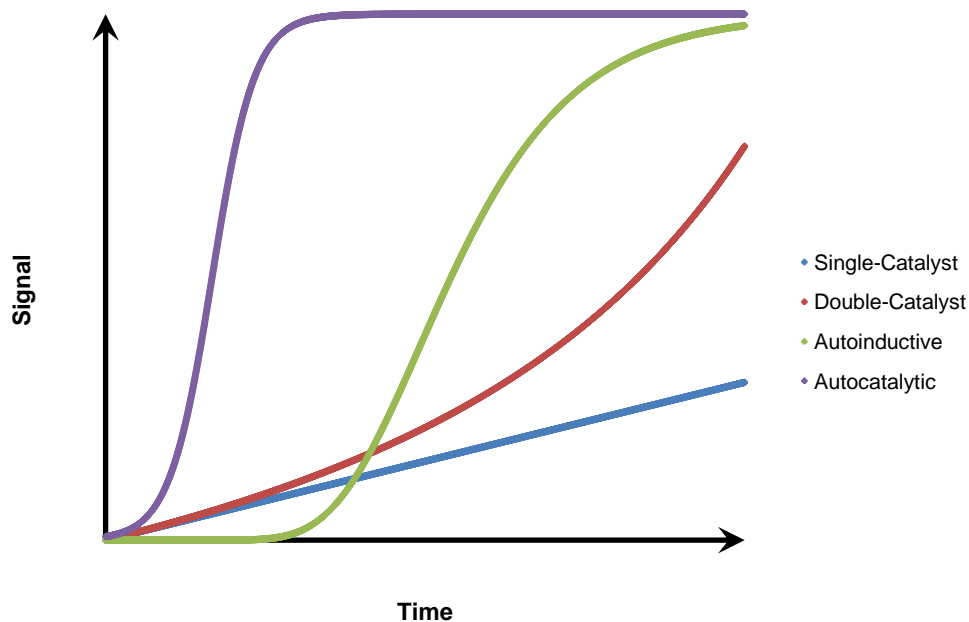
Figure 1.3 Typical signal amplification profiles observed for the different signal amplification mechanisms.

Initial developments towards implementing signal amplification within diagnostic assays were focused upon using a single amplifier such as an enzyme or a catalyst, which provides a linear increase in signal over time. A natural succession from this led to the successful combination of two consecutive signal amplifiers to achieve dual-enzyme, dual-catalyst or even hybrid enzyme–catalyst amplification cascades, which often display quadratic-type amplification profiles. The constant strive to attain even greater assay sensitivity has led to the development of complex auto-amplification strategies, such as autoinductive and autocatalytic signal amplification, where the signal-amplified products themselves can increase the rate of signal production. Autoinductive signal amplification is a system whereby the products can indirectly accelerate the rate of a kinetically meaningful step of the signal amplification mechanism whereas autocatalytic signal amplification is the process whereby the products themselves directly serve as catalysts for their own production.[109] As a result; both auto-amplification types exhibit sigmoidal amplification profiles with autocatalysis demonstrating exponential signal amplification. Again, choosing the appropriate signal amplification protocol for a diagnostic assay is dependent upon a number of factors including, but not limited to, the type of analyte being detected, the medium the amplification is being performed in, the length of time after analyte recognition that a signal is required and the readout method used. For example, an assay requiring the lowest LOD possible would look to elect an autocatalytic signal amplification method whereas an assay requiring greater accuracy would look to employ a single-catalyst signal amplification strategy.

1.3.1   Single-Catalyst Signal Amplification

Signal amplification methodologies typically use enzymes or synthetic catalysts as amplifiers due to their ability to generate multiple product molecules without themselves being chemically altered. By designing a detection system whereby the enzyme or catalyst indicate the presence of the target and product formation results in a change in physical property, then catalyst or enzyme activity, and therefore the target, can be easily detected.[110] As such, early signal amplification methodologies focused on the selective activation of the amplifier in the presence of the target analyte. Typically, this is achieved either through intrasteric or allosteric activation. Intrasteric activation involves direct competition between the analyte and an inhibitor for the catalyst or enzyme active site and allosteric activation involves structural alteration of amplifier conformation which results only from recognition of the analyte at a site on the amplifier, other than the active site.[111] Examples of both allosteric and intrasteric activation of enzymes, as well as allosteric and intrasteric activation of synthetic catalysts have all been successfully demonstrated for the detection of a wide variety of analytes.
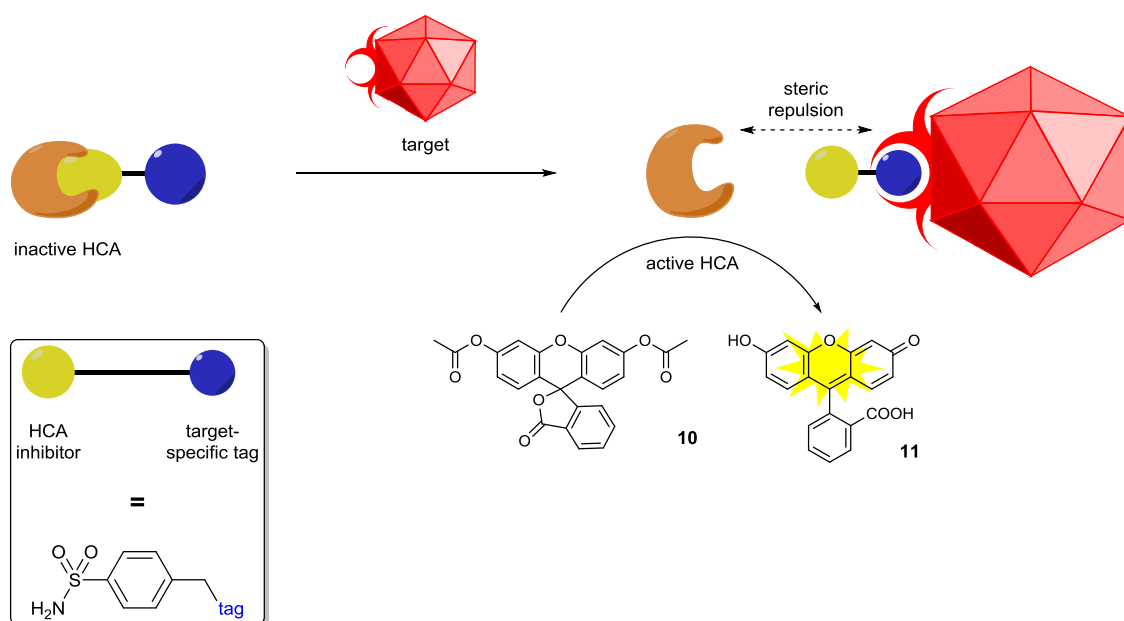
Scheme 1.17 Intrasteric enzyme activation through steric repulsion for signal-amplified protein detection.

The very high turnover rate of enzymes under physiological conditions have made them popular signal amplifiers within sensing methodologies and varying enzyme activation methods have been employed to enable selective analyte detection. Intrasteric activation of enzymes is one particular method of activation and works through initial blocking of the active site of the enzyme with an inhibitor which restricts enzyme activity. Removal of the inhibitor by an analyte-recognition event restores enzyme activity which can be detected by the addition of an appropriate

enzyme substrate. A very recent development by Tan *et al.* provides a perfect example where the activity of human carbonic anhydrase (HCA) is intrasterically regulated through a strongly bound benzenesulfonamide inhibitor which is labelled with a protein-specific tag (Scheme 1.17).[112] In the presence of the target protein, a binding event with the tag occurs which plucks the inhibitor out of the HCA active site in order to minimise steric interactions between the protein and the enzyme. Enzyme activity is thus restored and can be measured by fluorescence through hydrolysis of non-fluorescent substrate, fluorescein diacetate (FLDA) **10**. The use of an enzyme for signal amplification was found to increase fluorescence signals 70-fold. This versatile approach was demonstrated for the detection of a number of different proteins through simple alteration of the inhibitor tag.
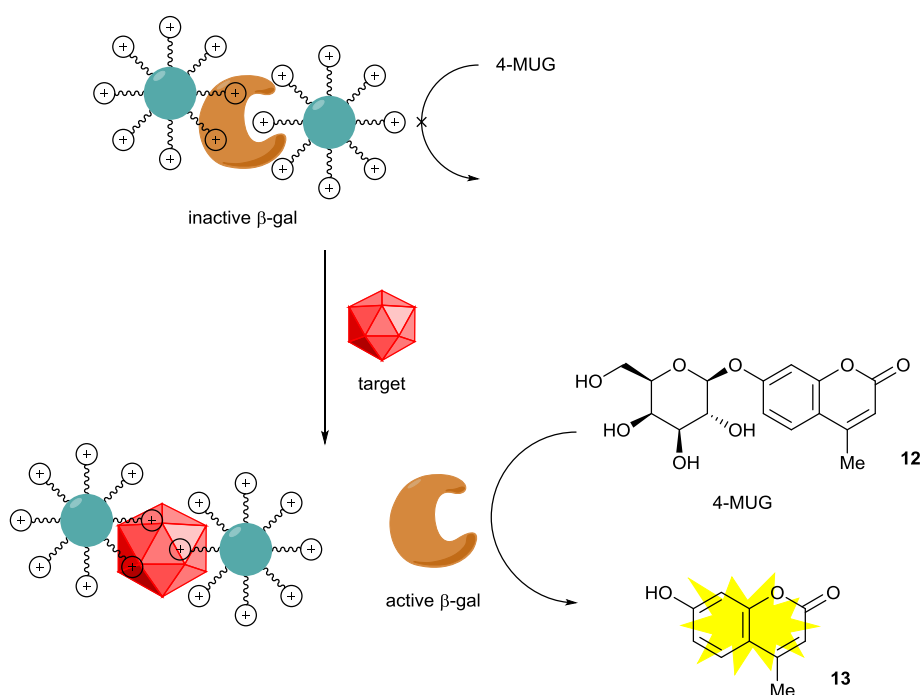
Scheme 1.18 Protein detection *via* intrasteric enzyme activation through electrostatic interactions.

Another method towards intrasteric enzyme activation for protein detection has been demonstrated by Rotello *et al*. who developed a procedure known as enzyme-amplified array sensing (EAAS) (Scheme 1.18).[113] In this method gold nanoparticles deliberately developed to possess a high cationic surface charge,[114] electrostatically bind to enzymes such as β-galactosidase (β-gal) that have a high anionic surface charge, and inhibit enzyme activity without denaturing the enzyme.[115] In the presence of specific proteins, the nanoparticles blocking the active site of the enzyme are removed, which restores enzyme activity. The addition of pro-fluorogenic substrate, 4-methylumbelliferyl-β-D-galactopyranoside (4-MUG) **12**, allows for protein detection *via* fluorescence. The amplification provided by the enzyme delivers a highly sensitive detection assay able to differentiate target proteins at 1 nM concentrations. The versatility of using enzymes as

amplifiers under physiological conditions is also demonstrated as using an alternative enzyme substrate enabled a colourimetric biosensor for bacterial infections to be developed.[116] Furthermore, this electrostatic nanoparticle approach to protein detection can be used in conjunction with fluorescent conjugated polymers, *vide infra*, to develop 'chemical nose' sensors capable of distinguishing between several different proteins simultaneously.[117]
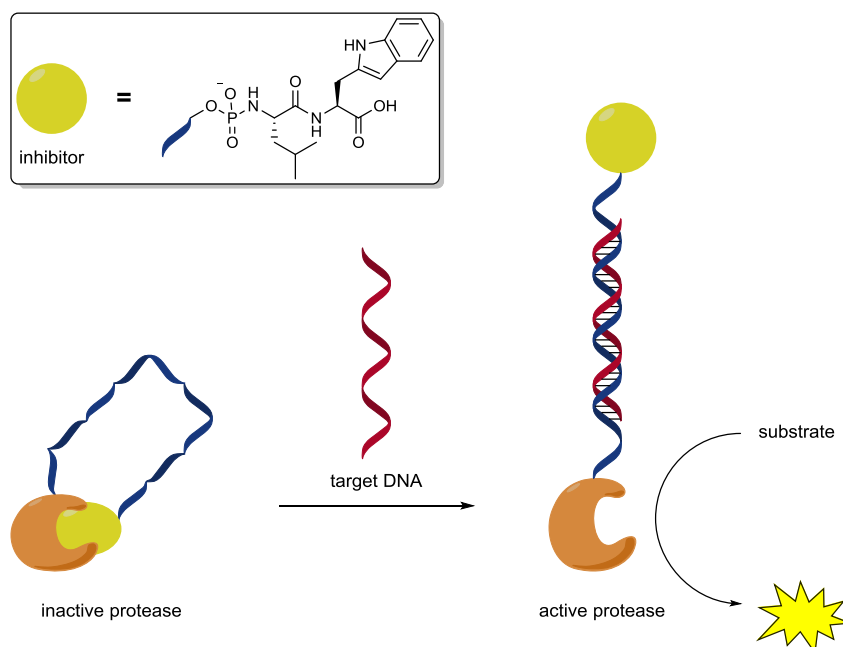
Scheme 1.19 DNA detection *via* allosteric enzyme activation through intrasteric enzyme regulation.

Enzymes have also been used in a number of amplified nucleic acid detection methodologies due their ease of conjugation to DNA as well as rapid signal production.[118] One of the first examples of such a system was described by Ghadiri *et al.* who developed a modified protease enzyme where its phosphoramidate inhibitor was covalently bound to itself through a single-stranded DNA probe (Scheme 1.19).[119] Once constructed, the modified enzyme was rendered inactive since the flexibility of the DNA probe allowed for the inhibitor to loop around and bind to the active site of the enzyme. In the presence of target DNA, hybridisation occurs forming a highly favourable rigid DNA duplex and in the process, physically removes the inhibitor from the active site of the enzyme. Enzyme activity is therefore restored and hydrolysis of a non-fluorescent substrate to a fluorescent product enables simple enzyme-amplified DNA detection *via* fluorescence. Both the sensitivity and selectivity of the concept was validated as a 10 pM concentration of DNA could be detected within 3 minutes and no discernible signal was observed in the presence of non-complementary DNA. Additionally, this approach is not limited to the use of proteases for signal amplification as the enzyme thrombin has also been conjugated to an inhibitor–DNA probe for fluorescent DNA detection.[120] The excellent control of enzyme activity

demonstrated through allosteric regulation allows for molecular logic gates to be developed, operated by different DNA sequences.[121]

Enzyme and inhibitor do not necessarily have to be covalently bound at either end of the same single-stranded DNA probe in order to achieve successful intrasteric enzyme activation as Merkx *et al.* have very recently demonstrated (Scheme 1.20).[122] In this approach, β-lactamase and a β-lactamase inhibitory protein (BLIP) were attached to separate strands of DNA that were complementary to that of the probe strand. Through a strong hybridisation interaction and the flexibility of the single-stranded probe strand, enzyme and inhibitor are brought together restricting substrate turnover. In the presence of target DNA, hybridisation with the probe strands causes significant structural rigidity and physically pulls the inhibitory protein from the enzyme active site and away from one another, thus restoring enzyme activity. Again, this can be measured by fluorescence through the introduction of a non-fluorescent enzyme substrate to afford the fluorescent product. This modular approach to intrasteric enzyme activation for sensitive DNA detection could detect down to 2 fmol of target single-stranded DNA.
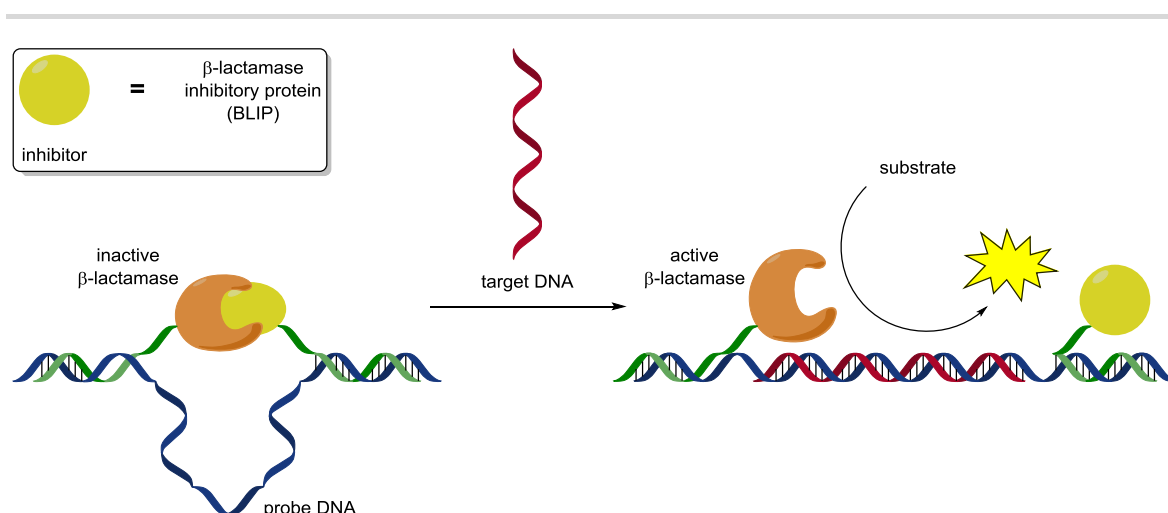
Scheme 1.20 Mechanical intrasteric enzyme activation for DNA detection.

Enzyme activity can also be regulated through selective control of specific allosteric factors. In principle, allosteric activation involves target analyte recognition at an allosteric binding site which, in turn, causes a structural conformation that activates the catalyst. The excellent versatility of being able to regulate enzyme activity through allosteric activation, rather than intrasteric activation, has seen this method used extensively for signal amplification within biosensors for molecular diagnosis.[123] Allosteric enzyme activation methods can vary tremendously, but generally either occurs through manipulation of enzyme cofactors or through modification of the enzyme structure. Enzymes are usually dependent upon cofactors, such as small organic molecules,[124] or metal ions,[125] for high catalytic activity. Therefore, a popular allosteric

enzyme activation method for sensing is to release enzyme cofactors selectively through an analyte–probe interaction at an allosteric binding site to consequently up-regulate enzyme activity.
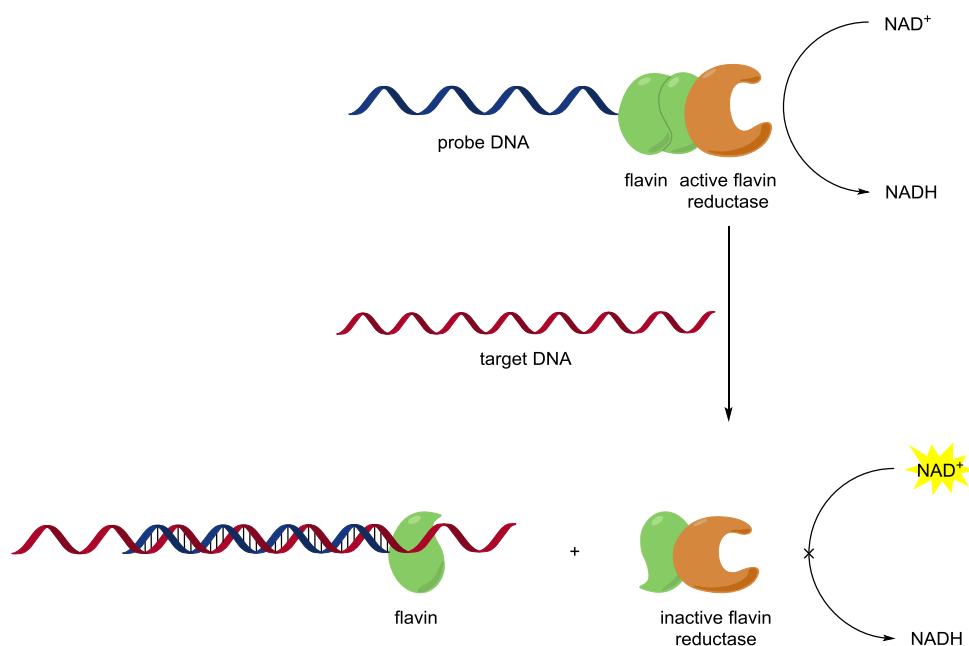
Scheme 1.21 Fluorescent DNA detection *via* allosteric organic cofactor release and consequential down-regulation of enzyme activity.

Through the manipulation of flavin, a small organic molecule cofactor, Décout *et al.* have also developed an allosteric enzyme activation method for fluorescent DNA detection (Scheme 1.21).[126] Modifying flavin with a single-stranded DNA probe was shown not to significantly interfere with its ability to act as a cofactor, thus enzyme activity remained on consuming fluorescent substrate, nicotinamide adenine dinucleotide (NAD^+). In the presence of target DNA, the rigid DNA double helix formed as a result physically removes the cofactor from the allosteric site of the enzyme, which down-regulates enzyme activity. As such, NAD^+ does not get consumed by the enzyme which means fluorescence remains on. This approach to DNA detection is reported to detect a 50 nM concentration of target DNA after a 2 hour reaction time. Although no optimisation was performed to try to increase the sensitivity of this method, inherent drawbacks to this system include a lower affinity of the modified flavin towards the enzyme and the weak fluorescence of NAD^+.

A similar approach has been demonstrated by Yan *et al.* who use molecular tweezers for enzyme-amplified DNA detection (Scheme 1.22).[127] Molecular tweezers are synthetic molecular receptors with two interaction sites bridged by a hinged spacer.[128] For the detection of DNA, the allosteric site in this example was constructed of single-stranded DNA complementary to the target, whilst enzyme and cofactor were attached to either end of the tweezer arms. In the absence of any target DNA, the tweezers are closed bringing enzyme and cofactor together and activating enzyme

activity. However, in the presence of target DNA, a rigid double helix is formed within the tweezers which prizes enzyme and cofactor apart, deactivating enzyme activity. By coupling enzyme activity with the production of blue dye resazurin **13**, which produces a greater signal than using NAD$^+$ alone, 0.75 μM target DNA could be indicated through the absence of colour production.
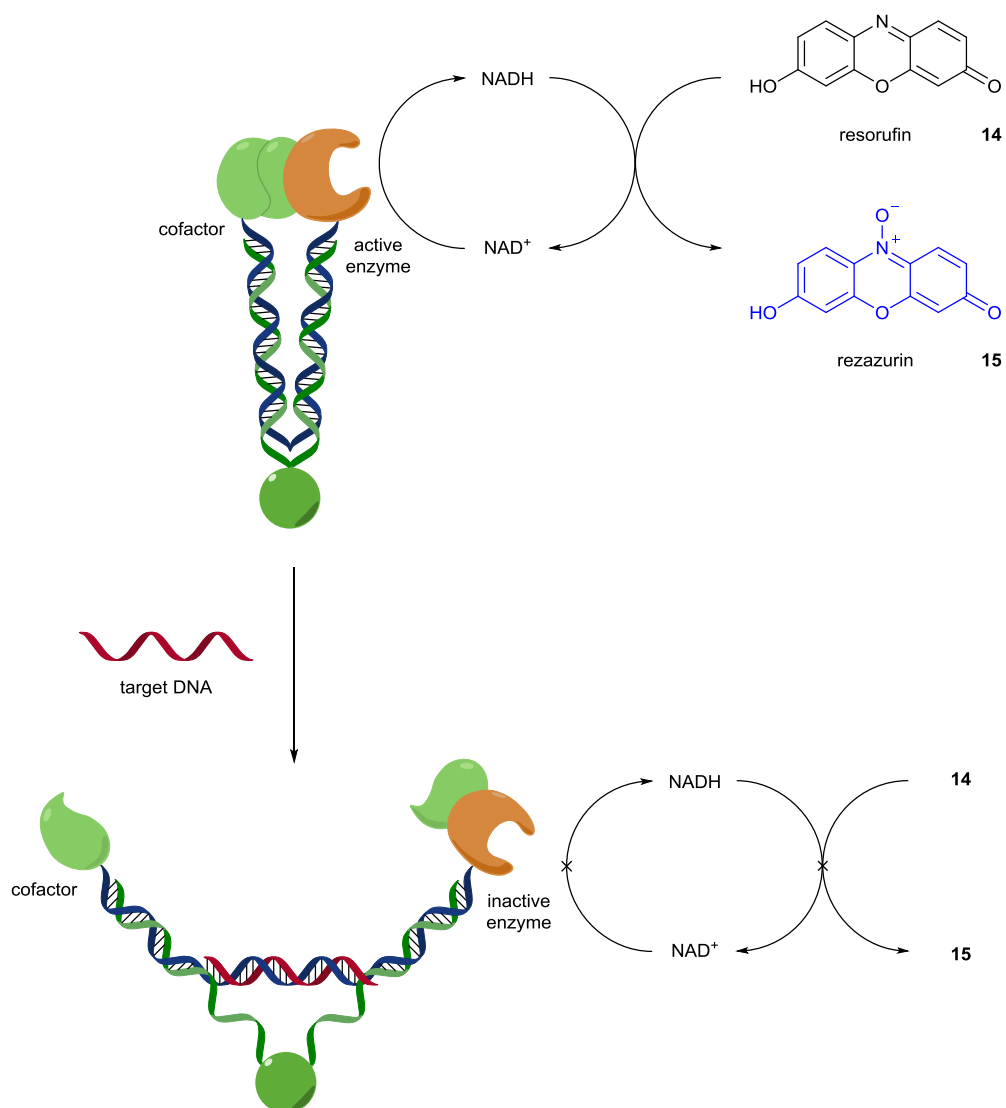
Scheme 1.22 Molecular tweezer approach to colourimetric DNA detection *via* allosteric enzyme activation.

Metal ion cofactor release has also been exploited for allosteric enzyme activation for sensing and has been demonstrated effectively by Graf and Krämer for fluorescent DNA detection (Scheme 1.23).[129] In the presence of Zn^{2+}, single-stranded DNA, complementary to that of the target, modified at each end with a terpyridine moiety forms a stable cyclic structure.[130] Upon the addition of target single-stranded DNA, a conformational change occurs to accommodate the formation of the more favourable DNA double helix and bis-chelation to the metal ion is disrupted.

The inactive apoenzyme of carbonic anhydrase (CA) then binds to the released metal to form the active holoenzyme. Enzyme activity, which indicates the presence of DNA, can be detected by the deacetylation of FLDA **10** to give the fluorescent product fluorescein **11**. Despite this elegant approach towards allosteric enzyme activation, a significant background reaction by the apoenzyme limits the sensitivity of the assay to target DNA concentrations of only 0.1 μM. This high background reaction observed with CA was considerably reduced by replacing the enzyme with a zinc-dependent aldolase which, *via* a signal transduction mechanism, results in the consumption of UV-active substrate NAD$^+$, thus developing a switch-off DNA detection method.[131]
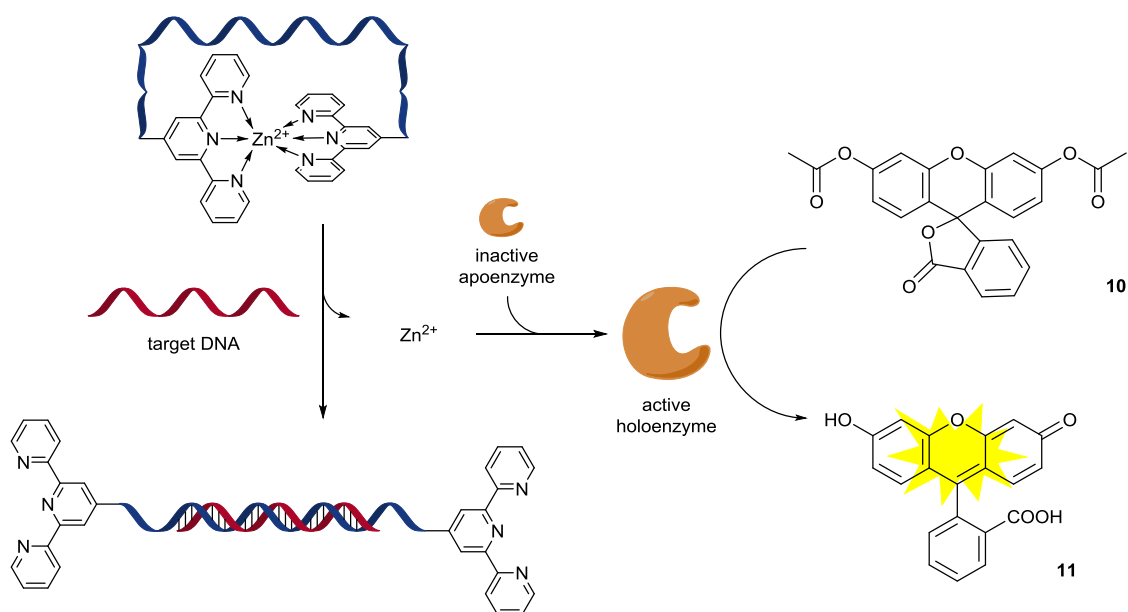

Scheme 1.23 Fluorescent DNA detection *via* allosteric metal ion cofactor release and consequential up-regulation of enzyme activity.

Although many enzymes require cofactors, releasing them in response to certain analytes still remains a substantial challenge. This approach towards allosteric enzyme activation for signal amplification relies on having a high affinity between the cofactor and enzyme as well as a low background rate of the apoenzyme in the absence of the cofactor. However, as shown previously, these criteria can be difficult to fulfill. Despite the advantages of using enzymes as amplifiers within sensing methodologies such as their high turnover number, they are expensive, can be difficult to manipulate without denaturising and they are unable to be used under non-physiological conditions. Because of this, synthetic catalysts have gained increased interest as amplifiers within sensing as they can be easier to manipulate, have a higher tolerance to changes in conditions and have application to the detection of a wider range of analytes. Similarly to enzyme activation, most catalytic signal amplification methodologies use either intrasteric or allosteric strategies for controlling catalytic activity.
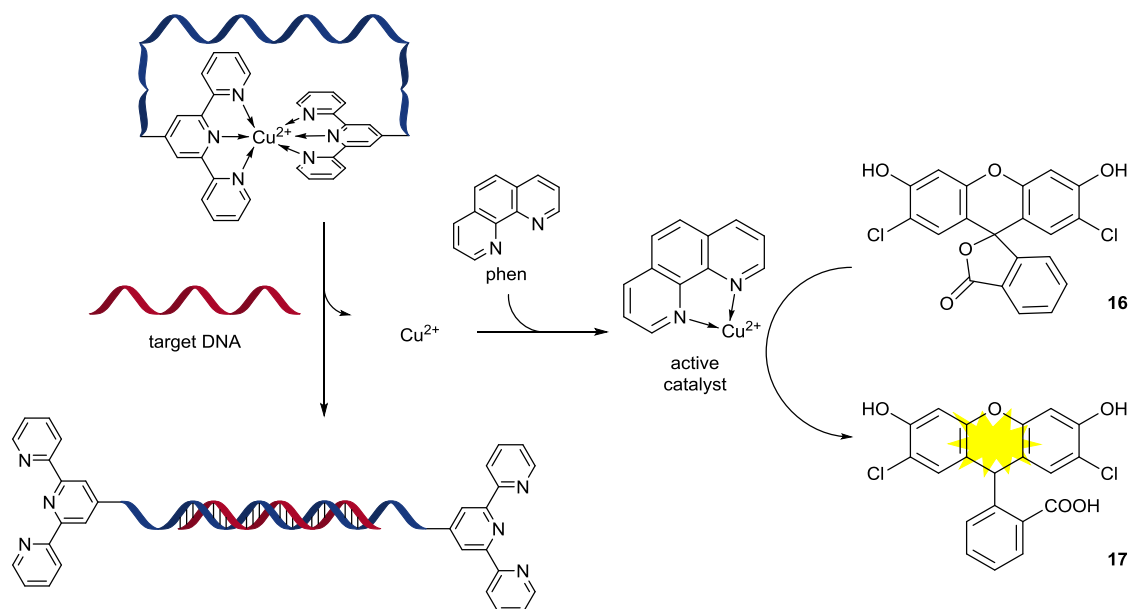
Scheme 1.24 Fluorescent DNA detection *via* allosteric metal ion release and catalyst activation

Intrasteric activation of catalysts for sensing involves target recognition at the catalyst active site. In principle, catalyst activity can be significantly reduced by physically blocking the catalyst active site with functionalised molecules. If these molecules are functionalised with analyte-responsive groups, then only in the presence of the analyte should the selective removal of the catalyst inhibitor occur, which would reveal the catalyst active site and restore catalytic activity. Simply coupling catalytic activity with signal production leads to a successful analyte detection assay with catalytic amplification. Following their initial publication on the allosteric activation of enzymes for DNA detection, Krämer *et al*. adapted the same probe, and therefore the same analyte recognition procedure, for a synthetic catalyst-amplified method for DNA detection (Scheme 1.24).[132] Building upon DNA-templated metal catalysis,[133] the authors replaced Zn^{2+} with Cu^{2+} which, in the absence of the target, still forms the same stable cyclic structure. In the presence of the target single-stranded DNA, the formation of the double helix occurs and in the same manner as shown previously, the metal is released into the system. An active catalyst is then formed between the released metal and phenanthroline (phen), a ligand capable of accelerating copper-catalysed reactions. Non-fluorescent dichlorofluorescein (DCF) **16** is then oxidised by the active Cu·phen catalyst to give the fluorescent product dichlorodihydrofluorescein (DCFH) **17**. The low turnover rate of the active catalyst however limits DNA detection to a concentration of 5 nM.

Prins *et al.* were also able to utilise intrasteric regulation of a synthetic catalyst for a colourimetric enzyme detection assay (Scheme 1.25).[134] In this example, gold nanoparticles, covered with triazacyclononane (TACN) ligands capable of binding Zn^{2+}, were prepared and the resulting cationic complexes were shown to effectively catalyse transphosphorylation reactions.[135] However, this catalytic activity could be switched off through the binding of oligoanions, such as peptides, to the catalyst through electrostatic interactions, which physically block the active site of

the catalyst. When the target protease enzyme was added, cleavage of the peptides occurred which reduces the effectiveness of the binding between blocker and nanoparticle. Destabilisation reveals the catalyst active sites and catalyses the dephosphorylation of substrate **18**, which is accompanied by the production of yellow reporter molecule *p*-nitrophenol (PNP) **19**. The benefits of this system include a close to zero background rate, a high affinity of the $[Zn^{2+} \cdot TACN]^{2+}$ complexes towards the substrate and a colourimetric detection system. Also, the catalyst-amplified enzyme detection assay was shown to be highly sensitive, capable of detecting protease subtilisin A at a concentration of 66 nM after an hour reaction time.
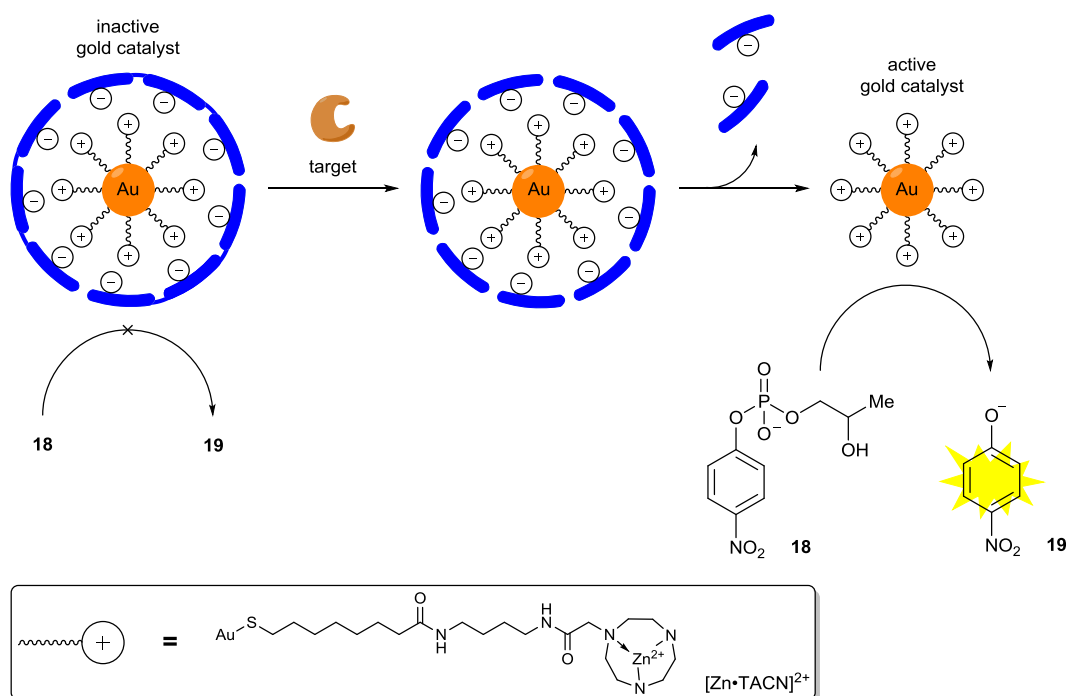
Scheme 1.25 Intrasteric activation of a synthetic catalyst for catalyst-amplified colourimetric enzyme.

Intrasteric catalyst regulation through the use of analyte-responsive probe molecules has some inherent difficulties associated with it since the catalyst inhibitor requires strong enough binding to prevent a high background reaction but not strong enough to prevent an efficient turn on of catalytic activity in response to the analyte. As such, signal amplification by allosteric catalysis (SAAC) has by far become the most popular catalytic signal amplification strategy used for sensing.[136] Primarily, this is due to the vast number of supramolecular receptors used for analyte detection and also the large number of synthetic catalysts used for amplification that can be easily coupled together for an amplified detection system.[137] Consequently, a significant number of signalling techniques based upon supramolecular systems have been developed for sensitive DNA, protein and small molecule detection.[138] Additionally, the binding affinities between different metal–ligand complexes are well-known allowing for ligand exchange to become a prominent analyte detection, and subsequent catalyst activation, mechanism for SAAC.
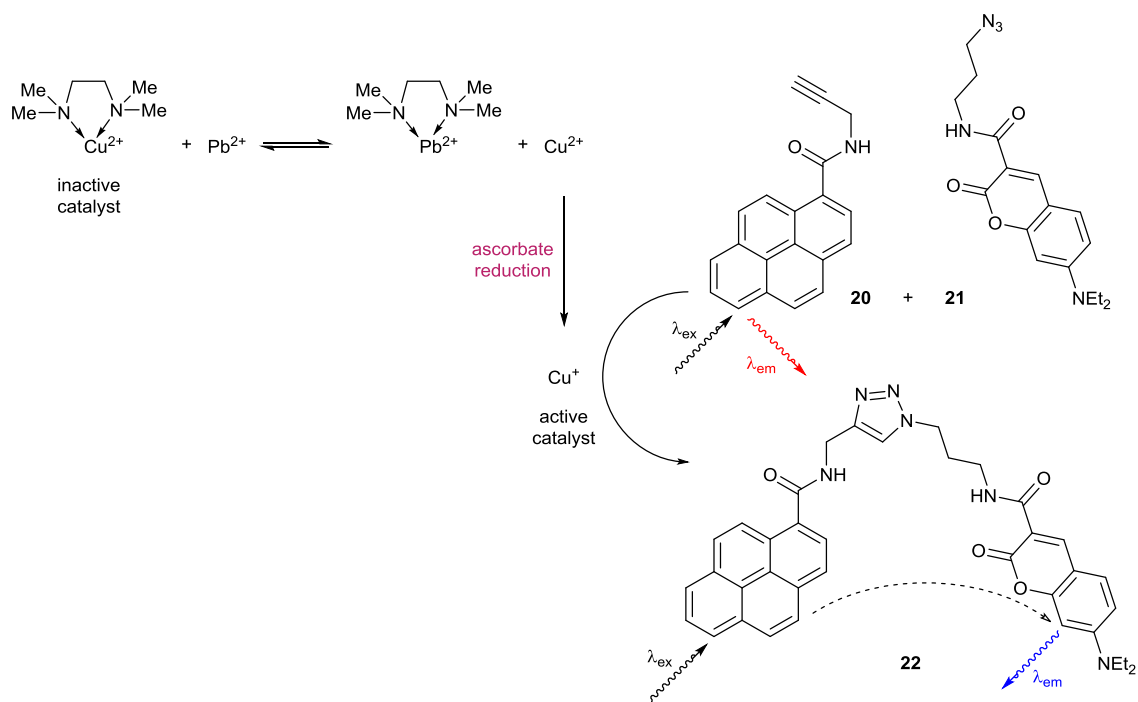
Scheme 1.26 Allosteric catalyst activation for FRET-based detection of lead ions.

Anslyn *et al.* were the first to exploit this ligand exchange for SAAC allowing for the detection of lead ions (Scheme 1.26).[139] In this approach, a Cu^{2+} complex with tetramethylethylenediamine (TMEDA) was synthesised and shown to be an inactive catalyst within a cycloaddition reaction. Metal cations, such as Pb^{2+} and Zn^{2+}, were found to competitively coordinate with TMEDA and consequently release Cu^{2+} into the system. In the presence of L-ascorbate, Cu^{2+} is reduced to Cu^{+}, the active catalyst within the Huisgen cycloaddition reaction.[140] By using FRET pair pyrene-derived alkyne **20** and coumarin-based azide **21** as the reactants, target metal ion concentration could be measured directly by fluorescence through the resulting triazole product **22**. Although being the seminal publication in the field, this approach to catalytic signal amplification is not without limitations. The analyte in question has to have orthogonal reactivity to the reaction conditions to not cause unwanted side-reactions. For example, Hg^{2+} was shown not to activate the cycloaddition reaction, but instead oxidised the reducing agent. Ligand exchange was also found to be slow, limiting the amount of active catalyst available relative to the concentration of analyte. Since the catalytic amplification is a bimolecular reaction, under the dilute assay conditions the reaction was deemed incomplete even after 18 hours, which further shows the inefficiencies in this particular catalytic system. Additionally, a high concentration of the analyte was found to interfere with the amplification reagents, potentially due to the formation of metal acetylides.

In an ensuing publication, the authors sought to overcome some of these limitations, by choosing to use a more efficient palladium catalyst as the catalytic signal amplifier (Scheme 1.27).[141] The ligand exchange strategy, which allows analyte detection through allosteric regulation, was improved by replacing the relatively unselective TMEDA ligand with a

polyazacyclam (PAC), which provided better selectivity for Cu^{2+} over other metals. Also, by designing a catalytic signal amplification methodology around a palladium catalyst, an intramolecular Pd^0-catalysed Heck reaction could be used, which provides increased ease of operation and the formation of a fluorescent product.[142] In this strategy, a Pd·PAC complex was synthesised that was shown to be inactive towards the Heck reaction. When the metal ion analyte is present, in this case Cu^{2+}, ligand exchange occurs since Cu^{2+} has a higher affinity for the PAC than Pd^{2+}, releasing Pd^{2+} into the system which is immediately reduced to the active Pd^0 by a phosphine ligand. The resulting active catalyst is able to turn non-fluorescent aryl iodide **22** into fluorescent indole **24** allowing for catalyst activity and therefore analyte concentration to be detected *via* fluorescence. Increasing catalytic activity improved the catalytic signal amplification as a detectable fluorescent signal was provided from a 30 nM concentration of Cu^{2+}. Despite this, a 90 minute reaction time was required and the ligand exchange methodology for analyte detection was shown to be unselective, since Ni^{2+}, Co^{2+} and Cd^{2+} all delivered false positive results. Better selectivity for the toxic metal ion Cd^{2+} over Ni^{2+} and Co^{2+} could be achieved by using a PAC with a bigger ring size to accommodate for the increase in ionic radius.[143] Better sensitivity was also achieved through the production of a coumarin-derived product since the presence of an electron-withdrawing ester not only increases the rate of Heck coupling but the product also has an increased quantum yield than that of indole **24**.
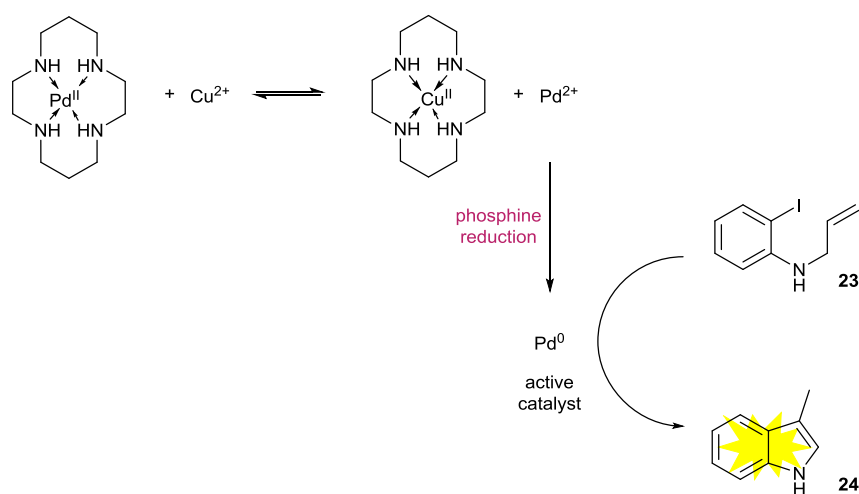
Scheme 1.27 Allosteric catalyst activation for the fluorescent detection of copper ions.

The use of PACs for analyte recognition is a major drawback for this methodology since analyte detection is limited to only metal ions. Also, ligand exchange is slow, reversible and as shown previously, unselective. To extend the application of this catalytic signal amplification methodology beyond the detection of metal ions, the group replaced the PAC with a dithiol for the fluorescent detection of carbonyl-containing small organic molecules (Scheme 1.28).[144] In this approach, target compounds containing carbonyl functionality, such as a ketone or aldehyde,

condense with the analyte-recognising dithiol to give a dithiolane, which has a considerably lower binding affinity towards metals than the free thiol. As a result, Pd^{2+} ions are released into the system and are reduced by phosphine ligands present in the assay mixture, generating the active catalyst for a Sonogashira cross-coupling reaction.[145] The coupling of phenylacetylene **25** with 9-bromo-10-(phenylethynyl)anthracene **26** produces the commonly used fluorophore 9,10-bis(phenylethynyl)anthracene (BPEA) **27**, therefore allowing analyte detection to be easily detected through fluorescence. Despite the catalytic signal amplification, significant drawbacks with using the Sonogashira cross-coupling reaction for catalytic signal amplification is its intolerance of water and some of the reaction components cause undesired quenching of anthracene fluorescence. However, the initial work published by the Anslyn group proved the concept of SAAC and has paved the way for this design to be adapted within other signal amplification methodologies that utilise allosteric control of metal ions for catalyst activation.
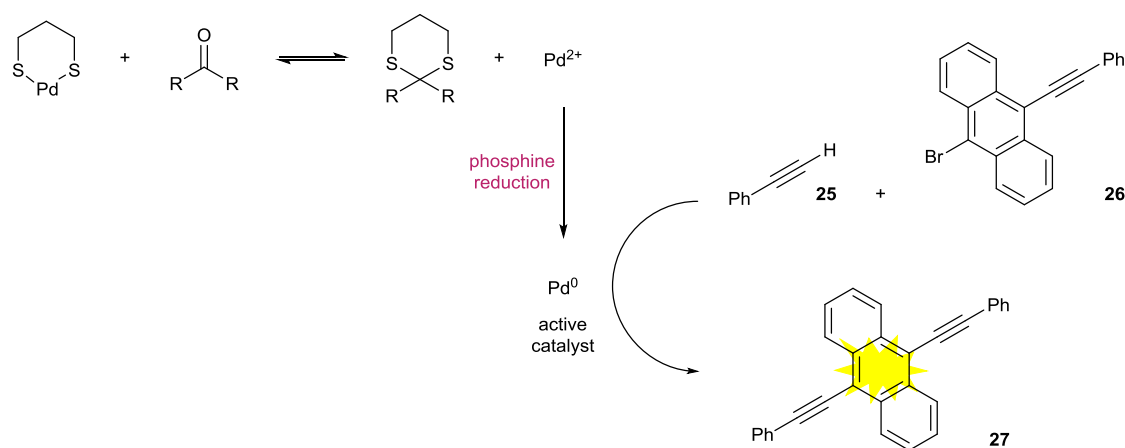
Scheme 1.28 Allosteric catalyst activation for the fluorescent detection of small, carbonyl-containing organic molecules.

One such methodology was described by Ritter and König who developed a signal transduction and signal amplification protocol using photo-activated catalysis.[146] In this procedure, a flavin derivative is used as a synthetic photoreceptor while the copper-catalysed Huisgen cycloaddition reaction is used for signal amplification (Scheme 1.29). Specifically, the stimulation of riboflavin tetraacetate **28** by a photon gives its strongly-oxidising excited state which, in the presence of an electron donor, undergoes photoreduction to afford strongly-reducing dihydroflavin tetraacetate **29**. Dihydroflavin **29** is then capable of reducing Cu^{2+} to Cu^+, thus providing the active catalyst for the cycloaddition, resulting in the formation of triazole **32** from azide **30** and alkyne **31**. Signal detection was measured through the reduction of observed fluorescence since the covalent connection between fluorophore and quencher reduces fluorescence emission.[147] In water, the reaction cascade shows light-dependent behaviour as only under irradiation is significant fluorescence quenching observed. When irradiation is stopped, disproportionation of Cu^+ to Cu^0

and Cu^{2+} occurs, which removes the active catalyst from the system and stopping the cycloaddition reaction. However, it was found that excess continuous irradiation leads to the formation of undesired by-products. Other problems associated with the assay include requiring oxygen-free conditions to prevent formation of flavin hydroperoxides and a slow background reaction in the absence of light due to spontaneous reduction of Cu^{2+} to Cu^+ by triethylamine in solution. However, the principle of transforming a non-chemical input signal, in this case light, into an amplified chemical output signal is superbly illustrated in this example, inspiring other groups to develop similar signal transduction and amplification chemical systems.
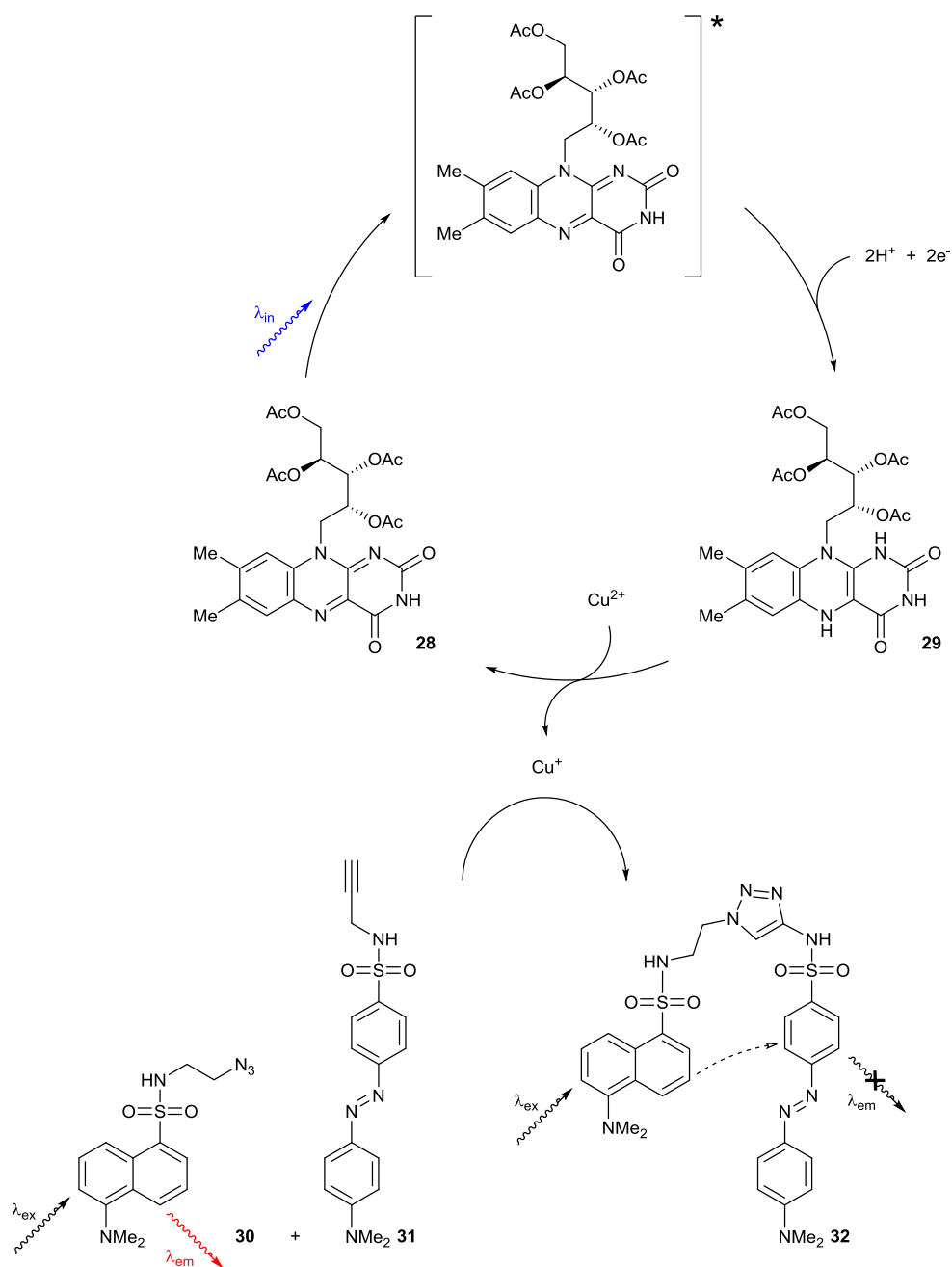
Scheme 1.29 Light-activated catalytic signal amplification.

The majority of examples of allosteric catalyst activation previously described have been based upon metal–ligand binding affinities where, analyte recognition leads to coordination disruption followed by metal ion release and consequent active catalyst formation. However, this is an imperfect approach since analyte recognition is a reversible reaction between the analyte and the active catalyst responsible for signal amplification. Also, the formation of the active catalyst is not necessarily instantaneous after analyte recognition which leads to long assay times. To overcome these problems, Mirkin *et al.* have developed synthetic enzyme mimics based upon supramolecular coordination chemistry.[148]

To achieve this, inorganic macrocycles were constructed *via* the weak-link approach (WLA) consisting of two metal centres and two hemilabile ligands.[149] The ligands are the key to this concept as they are polydentate chelates containing two sets of two differently coordinating heteroatoms; one set that strongly binds to the metal centre and one set that weakly binds to the metal centre. The dimer that initially forms has all coordinating atoms bound to a metal centre and in this 'closed' structural conformation, the ligand spacers are forced together. The introduction of small, coordinating molecules, that have a higher affinity to the metal than the weakest metal–heteroatom bond, displace the weakly binding heteroatom of the ligand. This then causes a structural conformational change to give an 'open' complex since the ligand spacers are now pulled apart. This precise control over the structural conformation of a macrocycle led to the subsequent development of a synthetic supramolecular catalyst where catalyst activity could be regulated allosterically.[150]

To obtain catalytic activity selectively as a result of a structural change in conformation, the ligand spacers were replaced with a [Cr·salen]$^{3+}$ complex proven to catalyse epoxide ring-opening reactions.[151] In the absence of the small molecule effectors, the tetrametallic supramolecular construct was shown to be in its 'closed' conformation and exhibited minimal catalytic activity towards the ring-opening of cyclohexene oxide since the catalyst active sites are pushed too close together and thus blocking one another, preventing the substrate from reaching the catalyst active site. The addition of small molecule effectors Cl$^-$ and CO result in them binding to the allosteric Rh$^+$ metal centre and causing a structural change in the macrocycle to its 'open' conformer, known as halide-induced ligand rearrangement (HILR).[152] The Cr^{3+} metal centres are then pulled apart from one another revealing the active sites for the substrate, which consequently leads to a 25-fold increase in catalytic activity. In addition, the bimetallic active site of the supramolecular catalyst was shown to have an increased rate of reaction over its monomeric counterpart, which explains the low background rate observed when the catalyst is 'closed'.[153] Since the epoxide ring-opening reaction is not attributed with a change in physical property, signal amplification *via* this approach to allosterically-regulated supramolecular catalysis could not be used for sensing purposes.

Towards this end however, the group sought to change the catalyst responsible for signal amplification to a [Zn·salen]$^{2+}$ complex capable of catalysing the acylation of 4-pyridyl carbinol **32** (Scheme 1.30).[154] As a consequence of the acylation, the pH of the reaction medium is lowered

since acetic acid is formed as a by-product and as such, signal production was achieved through a pH-responsive fluorophore **37** allowing for analyte detection to be determined using fluorescence.[155] Under an atmosphere of carbon monoxide, an 800 nM concentration of Cl⁻ ions could be distinguished from the background reaction after 6 hours. Since the supramolecular catalyst is modular by design, alternative metals can be used at the allosteric site of the supramolecular catalyst yet still maintain the same mode of activation and the same catalytic reaction for amplification. This can therefore expand the application of the signal amplification procedure towards the detection of different analytes.[156] It is thought that increased control and a reduction in background catalytic activity could be achieved through a triple-layer catalyst where the middle layer holds the active catalyst and the top and bottom layers physically block the catalyst active sites when the supramolecular structure is 'closed'.[157] Currently, the addition of the small molecule allosteric effectors can induce a structural change in the supramolecular structure to its 'open' conformer and restore catalytic activity to polymerise ε-caprolactone, [158] but has yet to be applied towards a sensing methodology.
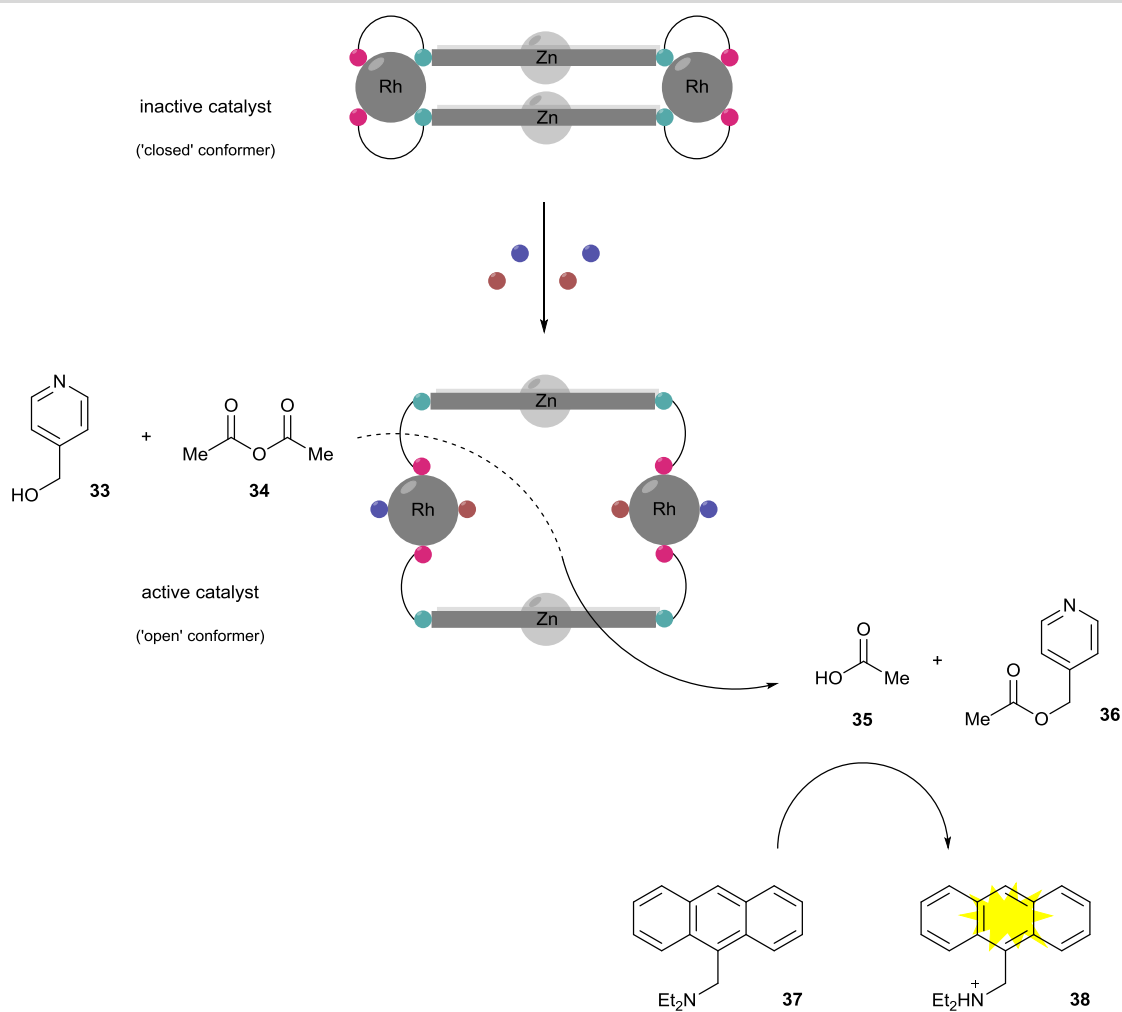
Scheme 1.30 Allosteric regulation of a supramolecular catalyst for catalytic signal amplification.

1.3.2 Double-Catalyst Signal Amplification

In principle, the addition of an extra catalytic cycle to a single-catalyst signal amplification procedure should accelerate the rate of signal production over time and in turn, would lead to a signal increase orders of magnitude higher than that of just doubling the number of catalysts of a single-catalyst system. However, in comparison to the number of single-catalyst signal amplification procedures described, the use of two sequentially-activated catalysts for signal amplification is a considerably less explored area. This could be, in part, due to the difficulty in finding catalyst combinations whereby products resulting from the first catalytic cycle are able to act as catalyst activators for the second catalytic cycle. In addition, to afford sufficient assay sensitivity, the background reaction of the second catalyst must be minimal, if not zero, to minimise false positive results. Initially, signal amplification protocols utilising a two catalyst cascade were developed as a result of applying a single catalytic amplification procedure towards the detection of a target that itself also displays catalytic activity.
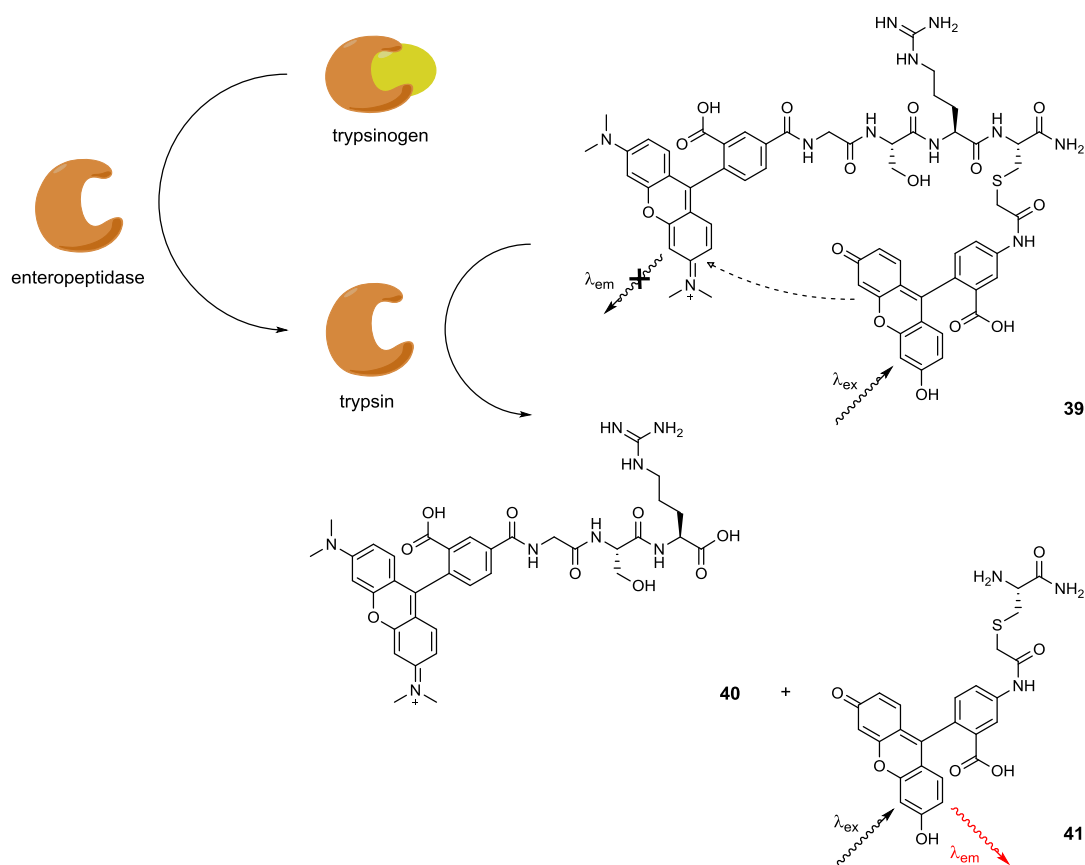
Scheme 1.31 Double-catalyst signal amplification approach to the FRET-based detection of enteropeptidase.

The first example of a double catalyst signal amplification strategy for a sensing application was demonstrated by Zuchner *et al.* for protease detection using FRET (Scheme 1.31).[159] Sensitive protease detection is of paramount importance as abnormal protease activity has

been associated with a variety of diseases, one of which includes cancer.[160] As such, there has been huge demand for the development of highly sensitive protease assays and methods to achieve high sensitivity have been through the use of enzyme cascades for signal amplification.[161]

In this particular example, an initial optimisation of a FRET-based detection assay was performed on trypsin, a digestive enzyme that selectively cleaves peptides at the carboxyl side of amino acids lysine or arginine.[162] Of the trypsin substrates synthesised and tested, peptide **39** was found to be optimal as it showed a >97% quenching efficiency in the absence of the enzyme and after trypsin was introduced, maximum fluorescence was obtained in 15 minutes, achieving a LOD of 0.1 fmol. With the second catalytic cycle of the amplification methodology optimised, the next objective was to selectively activate it.

To do this, the group chose serine protease enteropeptidase, the intestinal enzyme responsible for activating multiple digestive enzymes in response to food ingestion,[163] and whose congenital deficiency can lead to severe intestinal malabsorption.[164] Its primary mode of action is to catalyse the activation of trypsin from the inactive zymogen, trypsinogen.[165] As such, trypsin was replaced with trypsinogen and exposed to enteropeptidase to determine if the enteropeptidase could catalyse the activation of the second catalytic signal amplification. Indeed, in the presence of enteropeptidase, a fluorescent signal was obtained which was attributed to the *in situ* conversion of trypsinogen to trypsin and consequent consumption of pro-fluorescent substrate **39**. This double-catalytic signal amplification methodology achieved a LOD of 0.01 fmol for enteropeptidase after an assay time of 3 hours and demonstrated an excellent dynamic range showing a linear signal–concentration correlation over two orders of magnitude.

The high sensitivity and selectivity obtained for this dual-enzyme signal amplification approach has inspired others to do the same by developing inactive zymogens as enzyme precursors that can be activated by a clinically-relevant enzyme to produce a detectable signal. One such example can be provided by Yoo *et al.* who engineered β-lactamase zymogens for amplification and determination of protease activity (Scheme 1.32).[166] In this approach, an inactive β-lactamase zymogen was constructed using intrasteric inhibitor BLIP attached to the enzyme through a peptide linkage. In the presence of the protease, the peptide linkage is cleaved and intrasteric activation of β-lactamase occurs as BLIP is removed from the active site. β-Lactamase activity, and therefore protease activity, was measured by the change in absorbance from β-lactamase substrate, 7-(2-thienylacetamido)-3-((3-carboxy-4-nitrophenyl)thiomethyl)-cephalosporonic acid (CENTA) **42** to hydrolysed product **43**.[167] To prevent the BLIP from remaining bound to the β-lactamase after protease-catalysed amide hydrolysis, which would reduce the potential positive output signal, a number of β-lactamase mutants were synthesised and tested within the assay. Through this optimisation, a β-lactamase mutant with a lower binding affinity to BLIP was able to deliver a 68-fold signal increase from the background reaction. This mutant was then utilised as the signal-amplifying enzyme within a dual-enzyme signal amplification strategy for the detection of matrix metalloproteinase-2 (MMP2), a protease that plays a significant role within cancer progression,[168] and was shown to be detectable at concentrations down to 25 pM.
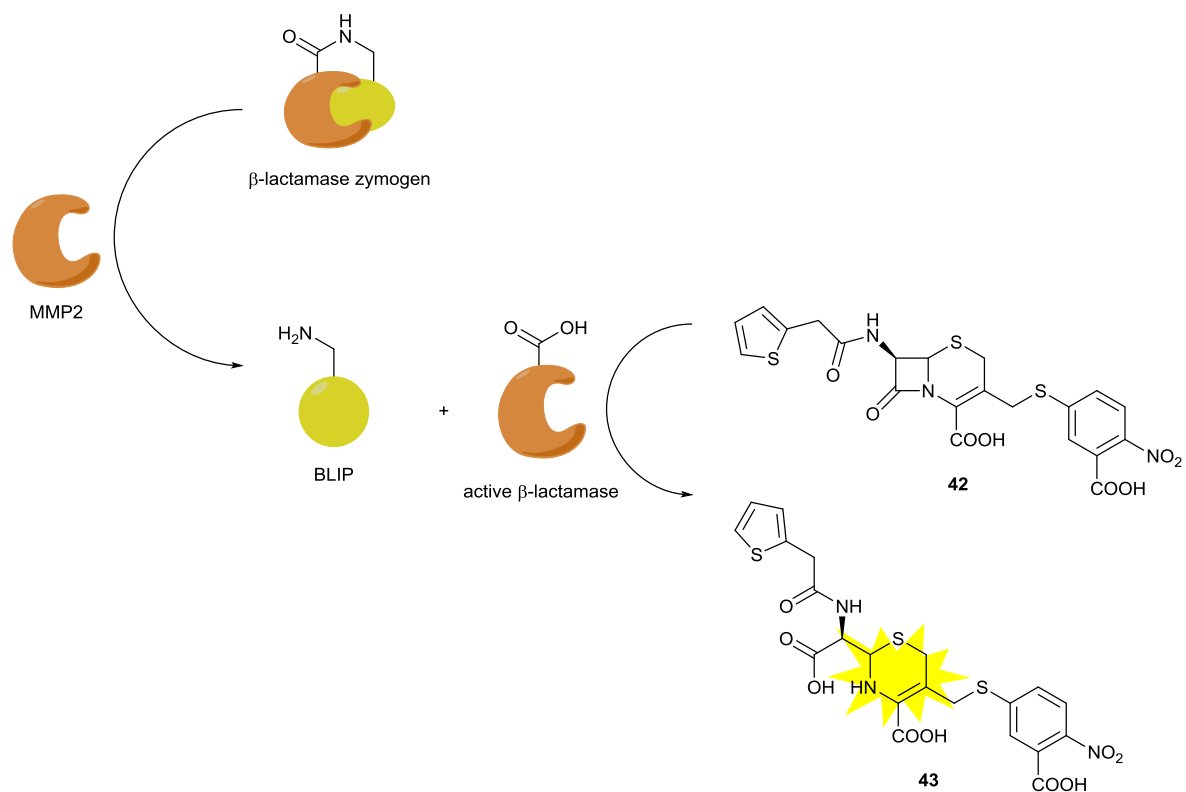
Scheme 1.32 Double-catalyst signal amplification for an absorbance-based protease detection assay.

Another approach to enzyme-triggered enzyme activation has been through the use of split-protein systems. Split proteins are two protein fragments that do not exhibit any catalytic activity separately but can come together to form an active enzyme.[169] By physically preventing the split-proteins from coming together through an enzyme-cleavable intrasteric inhibitor, an enzyme-amplified enzyme detection assay can be achieved. This tactic was exemplified by Ghosh *et al.* who utilised the split-protein system of the enzyme firefly luciferase (FLuc) for protease detection (Scheme 1.33).[170] To prevent the split-proteins from coming together, one of the split-proteins was appended with a structure comprised of two interlocking α-helices known as a coiled-coil.[171–172] In the presence of the target protease, the peptide linkage between the protein and the coiled-coil is cleaved allowing the two protein halves to reassemble to form the active FLuc. Once activated, FLuc is able to catalyse the bioluminescent oxygenation of **44**, allowing protease activity to be determined *via* luminescence. Through this dual-enzyme amplification cascade, a 1000-fold increase in the signal-to-noise ratio could be obtained for the detection of tobacco etch virus (TEV) protease. The modularity of this method has allowed other split-protein type enzymes, such as β-lactamase, to be used as the enzyme amplifier and this signal amplification method has also been applied to the detection of caspases by simply changing the enzyme-cleavable linkage between the coiled-coil and the split-protein.[173]
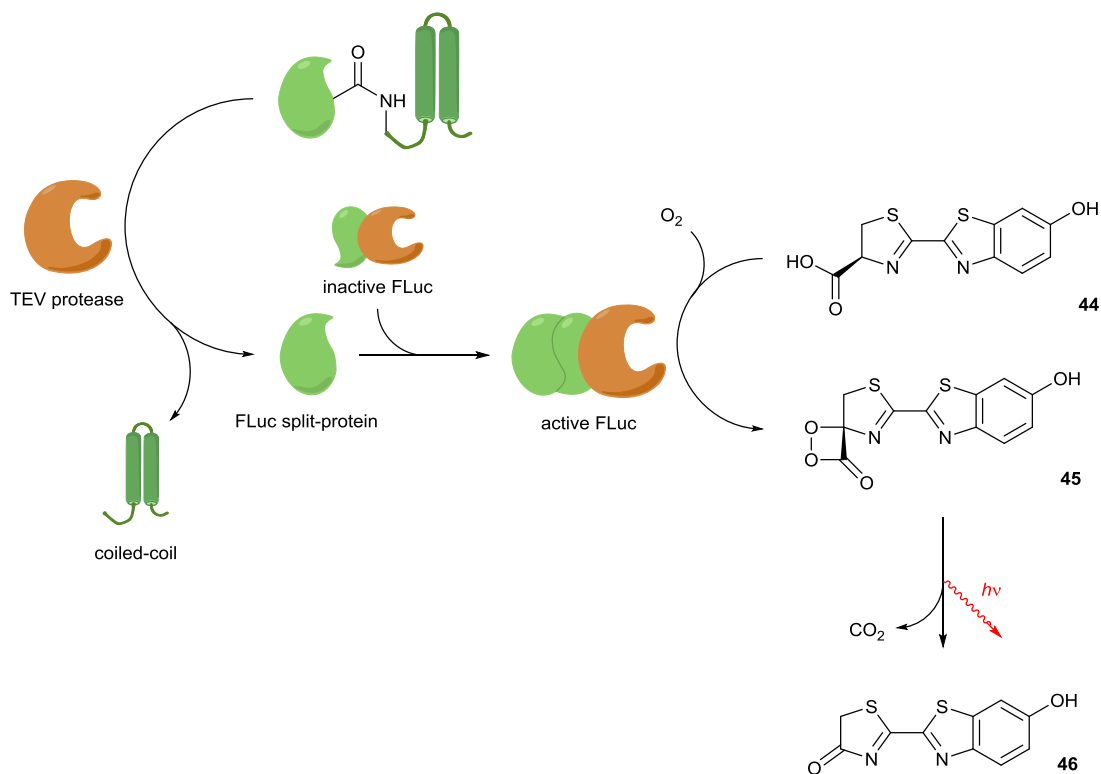
Scheme 1.33 Double-catalyst signal amplification for a bioluminescent protease detection assay.

Utilising enzyme cascades for signal amplification relies on the ability to structurally modify enzymes to restrict enzyme activity without denaturisation yet in the presence of the target, enzyme activity must be easily restored. Although a number of examples have been demonstrated, this still remains a significant challenge. A way of incorporating enzyme cascades for signal amplification without needing structural modification of enzymes is to use solid-supported enzyme substrates, as enzyme activity can be introduced and removed through physical addition and aspiration steps. Inspired by assays where catalyst activity can be measured through immunoassays,[174–175] Garner and Janda developed a catalytic assay using an enzyme-linked click-chemistry assay (cat-ELCCA) for the fluorescent detection of ghrelin *O*-acyltransferase (GOAT) (Scheme 1.34).[176] In this approach, a biotin-labelled peptide enzyme substrate is captured on a streptavidin-coated solid surface. In the presence of the target enzyme, a selective *O*-acyl transfer occurs where a serine residue is esterified with an *n*-octynoyl group. The resulting alkynylated product is then labelled with HRP *via* a click reaction, which is able to provide signal amplification through catalytic production of fluorescent compound resorufin **14** from HRP-substrate amplex red **47**. Through this unique double-enzyme signal amplification approach, a greater than 7-fold fluorescence enhancement was observed. Since GOAT is involved in the acylation of the gastric peptide hormone ghrelin,[177] this signal amplification methodology was subsequently used in the discovery of potent GOAT inhibitors as promising anti-obesity and anti-diabetes drug targets.[178]
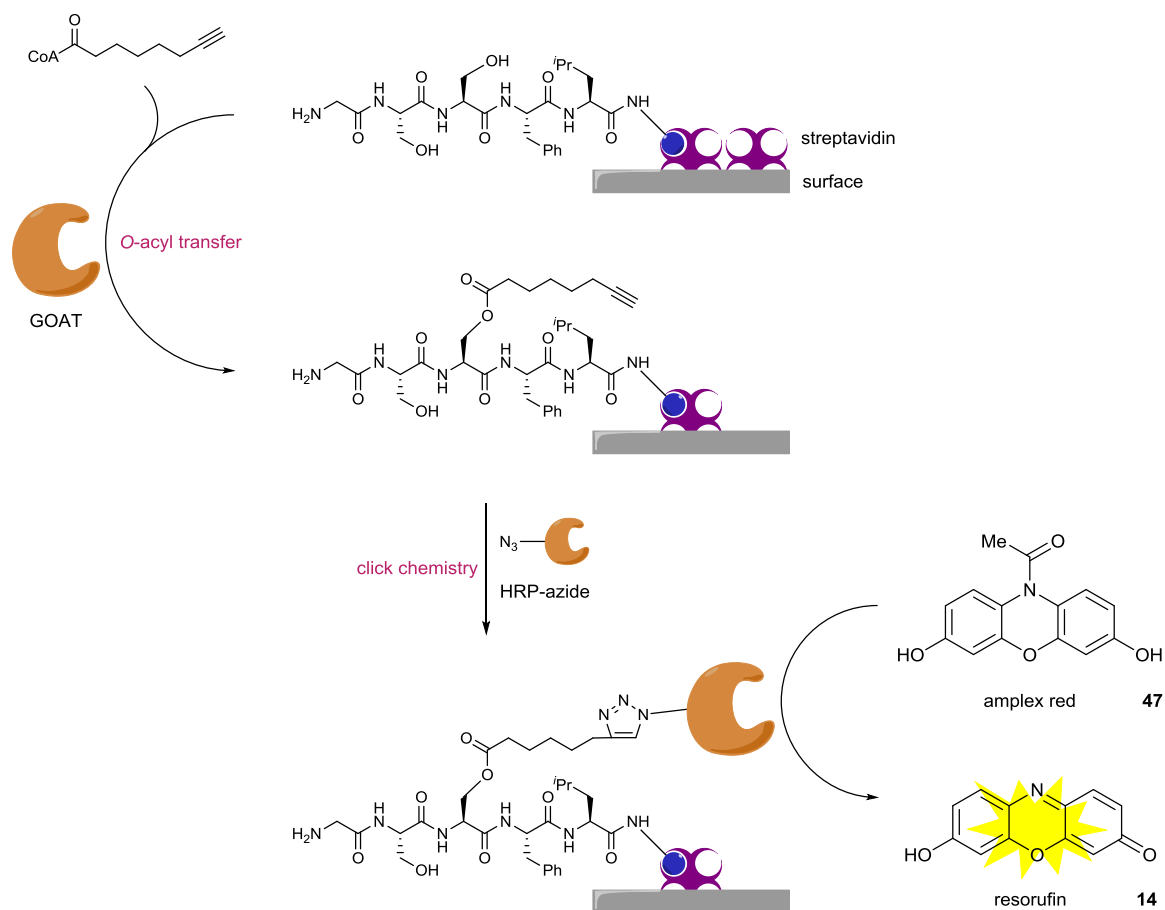
Scheme 1.34 Catalytic assay using enzyme-linked click-chemistry assay (cat-ELCCA) for the fluorescent detection of ghrelin *O*-acyltransferase (GOAT).

However, double catalyst signal amplification is not just limited to the use of enzymes for amplification. One example of the use of deoxyribozymes as a catalytic amplifier can be provided by Mao *et al.* who utilise a double catalyst signal amplification methodology for colourimetric DNA detection (Scheme 1.35).[179] Deoxyribozymes, also known as DNA enzymes or DNAzymes, are catalytic domains comprised of DNA rather than amino acids and are therefore considered to be more stable than traditional protein-based enzymes.[180] In this amplification approach, target DNA is detected using a complementary DNA probe that is also a circular template for RCA, which codes for the linear production of DNAzymes. Therefore, the target DNA acts as a primer for RCA and once hybridised, initiates the production of repeating units of DNA that form multiple DNA peroxidases after complexation to hemin. The DNA peroxidases can then catalyse the oxidation of 2,2'-azino-bis(3-ethylbenzothiazoline-6-sulfonic acid) (ABTS) **48** to afford colourimetric product **49**. This procedure showed an excellent dynamic range where DNA detection covers concentrations over four orders of magnitude and delivered a LOD of 1 pM. However, problems associated with using RCA as the initial amplification procedure include strict amplification durations as any reaction time longer than optimal, results in extensive tangling of the DNAzyme chains. Not only this, but the concentration of the circular RCA template is also important as a high enough concentration is required to ensure efficient binding to the target, yet too high a

concentration leads to unwanted binding of the template to the amplified DNA product thus preventing further amplification and folding of the DNA into the DNAzyme. A similar DNAzyme cascade has since been described by Tan *et al.* that replaces RCA with an alternative DNAzyme to deliver a double-catalyst signal amplification strategy for colourimetric protein detection.[181]
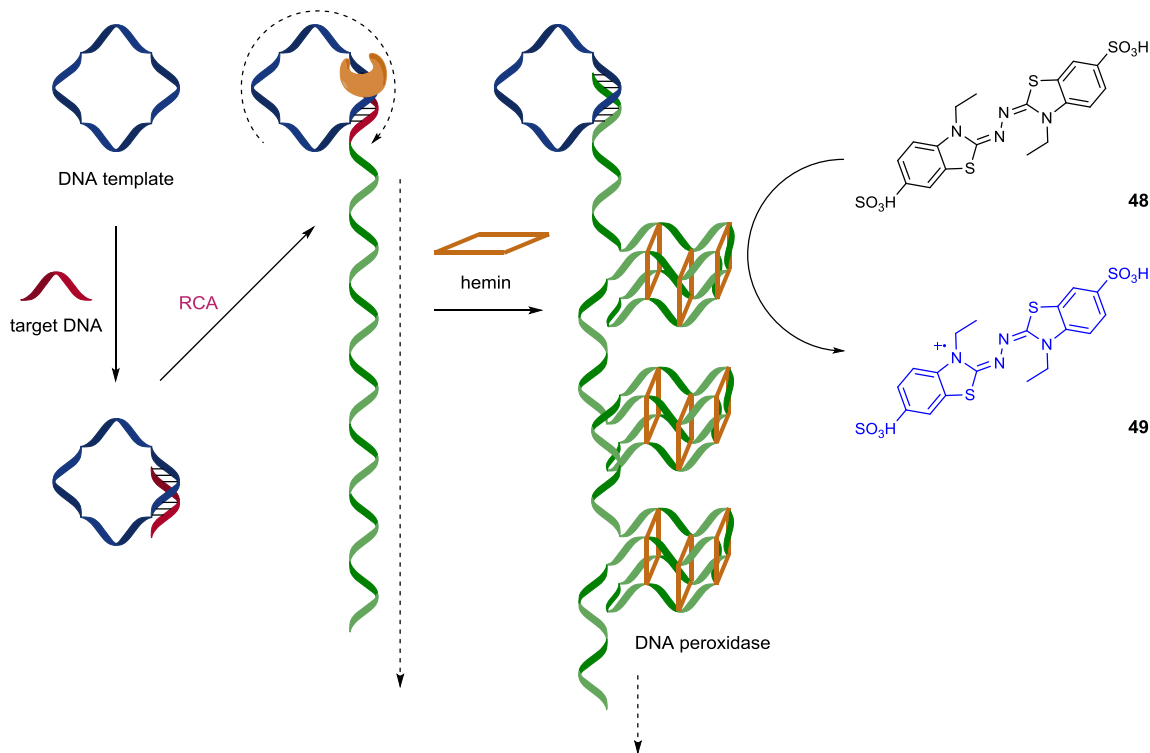
Scheme 1.35 Rolling circle amplification and DNAzyme catalytic cascade for colourimetric DNA detection.

A similar strategy has been described by Aoyama *et al.* who use ribosomal catalytic production, or translation, of protein-based enzymes for the double-catalytic chemiluminescent detection of human immunodeficiency virus (HIV) RNA.[182] For successful RNA detection, the group utilise the molecular beacon approach,[183] where in the absence of the target, the RNA probe intramolecularly binds to itself to adopt a hairpin-like conformation which cannot activate the catalytic amplification cascade. When in the presence of the target oligodeoxynucleotide (ODN), the resulting double-stranded duplex prevents the probe from adopting the hairpin-like conformation from occurring, thus revealing the riboregulator which is the specific sequence of the probe that activates translation. Once activated, the catalytic production of luciferase enzymes begins which are able to produce a chemiluminescent output signal. By using the molecular beacon probe, excellent selectivity was achieved and due to the double-catalyst signal amplification, good sensitivity was also obtained with a target ODN concentration of 50 fmol being detectable. However, because of the size of the target–probe duplex in comparison to the riboregulator sequence, inefficient allosteric activation of the transcription enzyme was observed, leading to a loss in sensitivity.
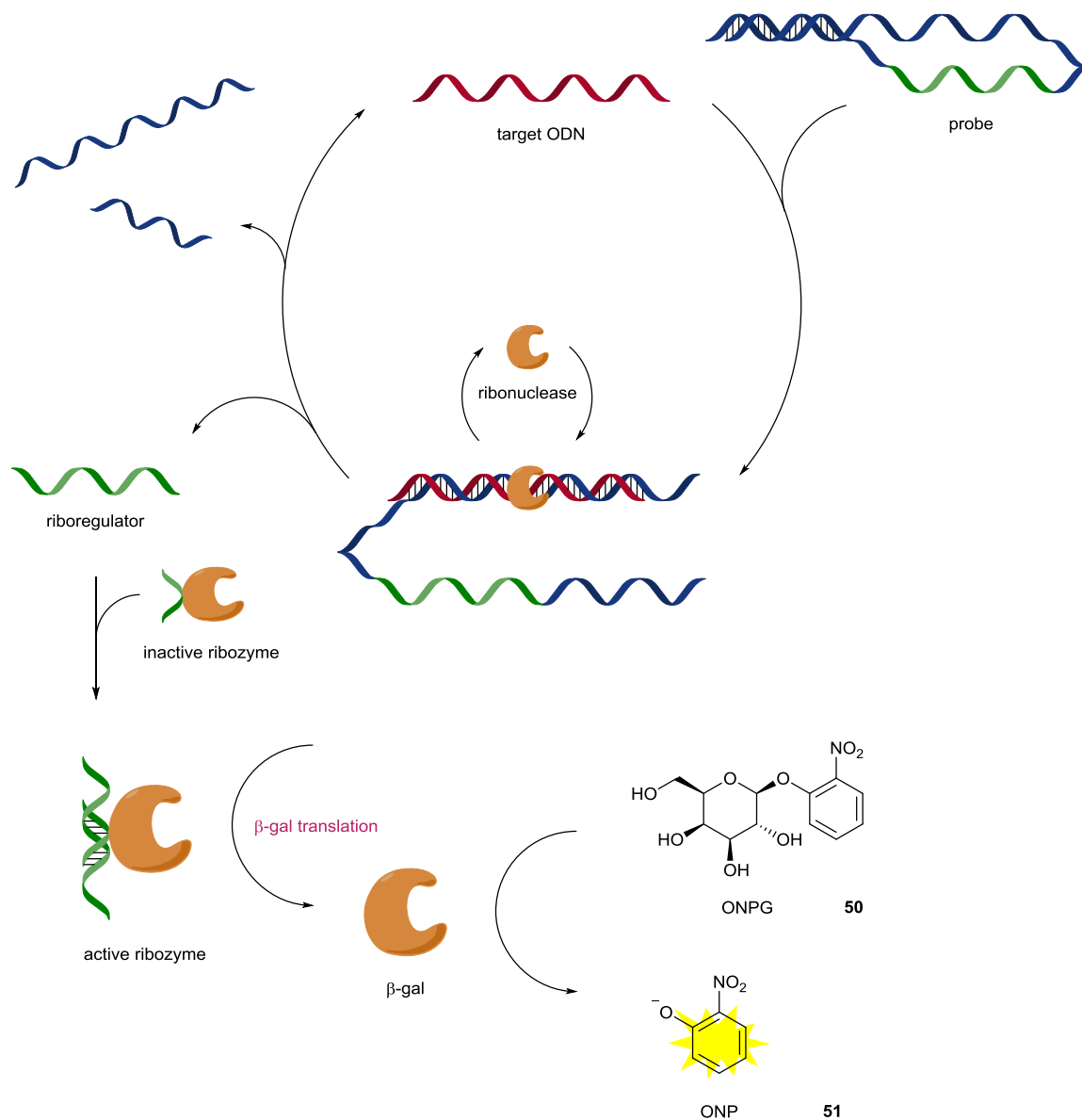
Scheme 1.36 Double-catalyst amplification cascade combined with EATR to obtain a triple-catalyst cascade for the visible detection of nucleic acids.

To address this, the group combined their double-catalyst signal amplification methodology with EATR to create a triple-catalyst cascade (Scheme 1.36).[184] In this advancement, the duplex formed as a result of target–probe hybridisation is cleaved by a ribonuclease which not only releases the riboregulator, thus making allosteric activation irreversible, but also recycles the target ODN. This both improves allosteric translation enzyme activation and allows the target ODN to react further with more probes. The extra catalytic cycle of the amplification cascade enhances both sensitivity and selectivity, obtaining a target ODN concentration LOD of 9 fmol. In addition, the riboregulator sequence can be altered to activate catalytic production of β-gal enzymes which enables the visible detection of nucleic acid sequences through conversion of *o*-nitrophenol-β-D-galactopyranoside (ONPG) **50** to *o*-nitrophenol (ONP) **51**.

The majority of double-catalyst signal amplification methodologies described to date involve the manipulation of enzyme cascades rather than the use of synthetic catalysis. This is primarily due to the well-known number and variety of enzyme cascades used in nature for a number of purposes. This leads to the easy transition from biosignalling to signal amplification within a sensing methodology by coupling the final enzyme with a colour or fluorescent production. Although selectivities and sensitivities are high, adjusting enzyme cascades towards the signal amplification of different analytes, especially when detection is required in non-aqueous solvents, can be difficult. As such, there is still demand for the easily-adaptable synthetic double-catalyst cascades for the sensitive detection of small organic molecules. Furthermore, hybrid systems that can utilise the efficiency of enzymes under physiological conditions along with the control and robustness offered by synthetic catalysts could offer excellent versatility within an amplification sensing methodology.

1.3.3   Autoinductive Signal Amplification

Autoinduction is the process whereby the reactants or products of a reaction can directly or indirectly affect the rate of the reaction, whether it is either in a positive or negative way. This process is typically associated with metabolic enzymes in the body whereby an active pharmaceutical ingredient (API) can induce or up-regulate an enzyme involved in its own metabolism.[185] By designing a system whereby the products of a reaction can induce or up-regulate the rate of its own production, then this would provide significant signal amplification if applied to a sensing methodology. Towards this end, Sella and Shabat designed the concept of the dendritic chain reaction (DCR) (Scheme 1.37).[186]

Dendrimers themselves are uniform molecular trees made up of highly-branched, repeating units, often with reactive functionality on the end groups, which are attached to a central core.[187] Because of their unique supra- and macromolecular properties, dendrimers have found application within multiple fields such as medicine, catalysis and in particular, sensing.[188] The concept of constructing dendrimers comprised of repeating units capable of undergoing elimination mechanisms initially allowed dendrimers to be shown to selectively release their cargo in response to a specific stimulus such as, drug compounds under reductive conditions,[189] coloured compounds when exposed to palladium,[190] and fluorescent compounds in response to light.[191] The spontaneous disassembly, or self-immolation, of dendrimers in response to a specific stimulus has provided a distinctive molecular amplification approach to sensing since one analyte can trigger the disassembly of a dendrimer with multiple reporter end groups.[192] However, dendritic amplification only multiplies the initial input molecule by the number of end-groups attached to the dendrimer core. For example, in a sensing methodology for the detection of the explosive triacetone triperoxide, a dendrimer with three reporter molecules was shown to provide three times the signal compared with a non-dendritic reporter.[193] In order to provide amplification more akin to a catalyst

or an enzyme in which signal amplification increases over time, DCR was designed to take advantage of the multivalent capabilities of dendrimers by attaching signal transducers as well as reporter molecules to the central core. Once released, the signal transducers could be manipulated into inducing further dendrimer disassembly, therefore leading to an autoinductive signal amplification mechanism being in effect.
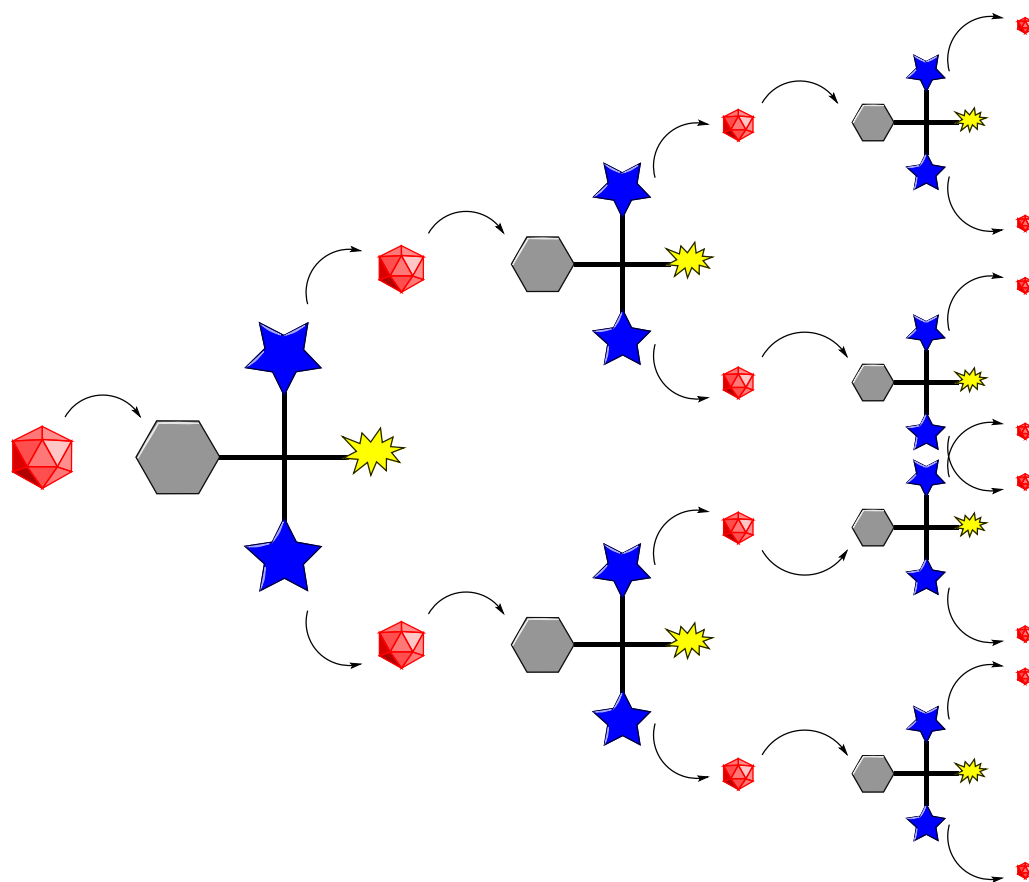
Scheme 1.37 Amplification concept of the dendritic chain reaction (DCR).

The successful achievement of an autoinductive signal amplification methodology through the use of dendrimers was through the clever design of dendron **52**, which consists of a *p*-nitroaniline reporter molecule, two molecules of choline to relay the signal and a phenylboronic acid used for analyte recognition (Figure 1.4). In the presence of hydrogen peroxide, aryl boronic acids are known to undergo oxidation to their corresponding phenolates,[194] *via* a Baeyer–Villiger-type mechanism,[195] analogous to the Dakin oxidation.[196] This functional group transformation had previously been exploited for the fluorescent stoichiometric detection of hydrogen peroxide.[197]
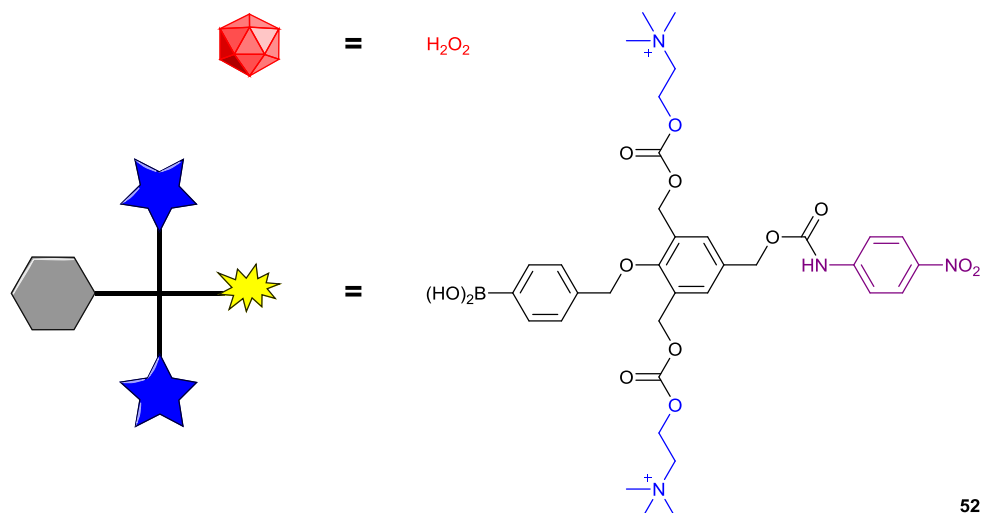
Figure 1.4 Structure of dendron **52**; responsive to the signal propagating molecule, hydrogen peroxide.
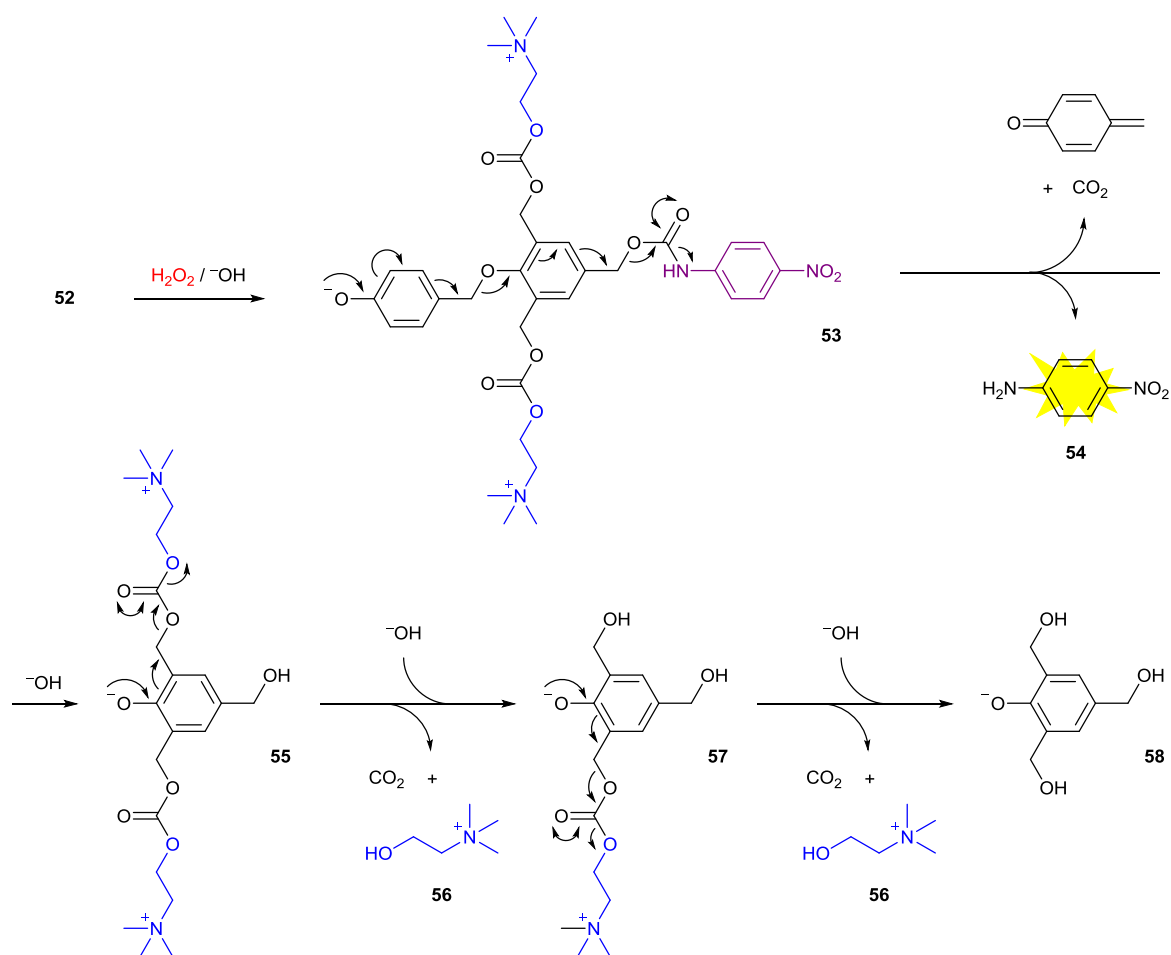
Scheme 1.38 Breakdown mechanism of dendron **51** initiated by hydrogen peroxide.

In DCR, phenolate **52** produced as a result of the oxidation is unstable under the mild alkaline assay conditions and undergoes multiple quinone methide eliminations,[198] followed by entropically-favourable decarboxylation to release colourimetric reporter **54** and two equivalents of

choline **56** to propagate the signal (Scheme 1.38). This is performed by the enzyme choline oxidase (COx), which twice oxidises choline to afford trimethylglycine **59** and in the process, generates two equivalents of hydrogen peroxide capable of initialising the breakdown of more molecules of dendrons **52** (Scheme 1.39). The requirement of COx for signal propagation is especially apparent at low concentrations of hydrogen peroxide, as a >50-fold signal enhancement is observed in comparison to a system without COx. The exponential production of hydrogen peroxide and subsequent exponential decay of all dendrons **52** leads to rapid signal production with full conversion observed after 50 minutes. The DCR was then applied to the colourimetric detection of penicillin-G-amidase (PGA), through the use of a choline-releasing probe, and showed a significant signal increase in comparison to a classic probe-based approach, allowing for PGA concentrations of 0.1 μgmL^{-1} to be detected.
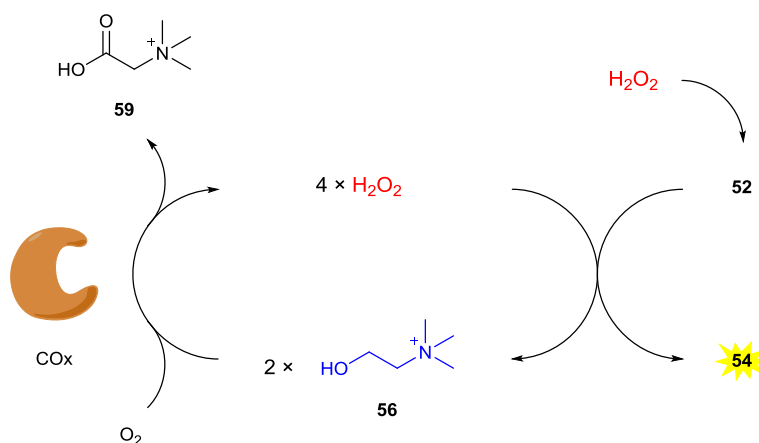
Scheme 1.39 Signal propagation in DCR: enzyme-catalysed hydrogen peroxide formation.

One of the major benefits of using DCR as a signal amplification technique is its modularity. For example, by changing the boronic acid trigger with a silyl-protected phenol enables an autoinductive exponential signal amplification procedure for the sensitive detection of fluoride ions.[199] Additionally, the enzyme amplifier could be replaced with other enzymes capable of producing hydrogen peroxide, such as alcohol oxidase (AOx).[200] Despite its wide application, a major weakness of DCR, like many exponential signal amplification methodologies, is the high background rate observed in the absence of the trigger, which arises from undesired hydrolytic cleavage of the carbonate linkages.[201] Another difficulty lies in the synthesis of the dendrimers as a large number of challenging synthetic steps are often required to successfully obtain them.
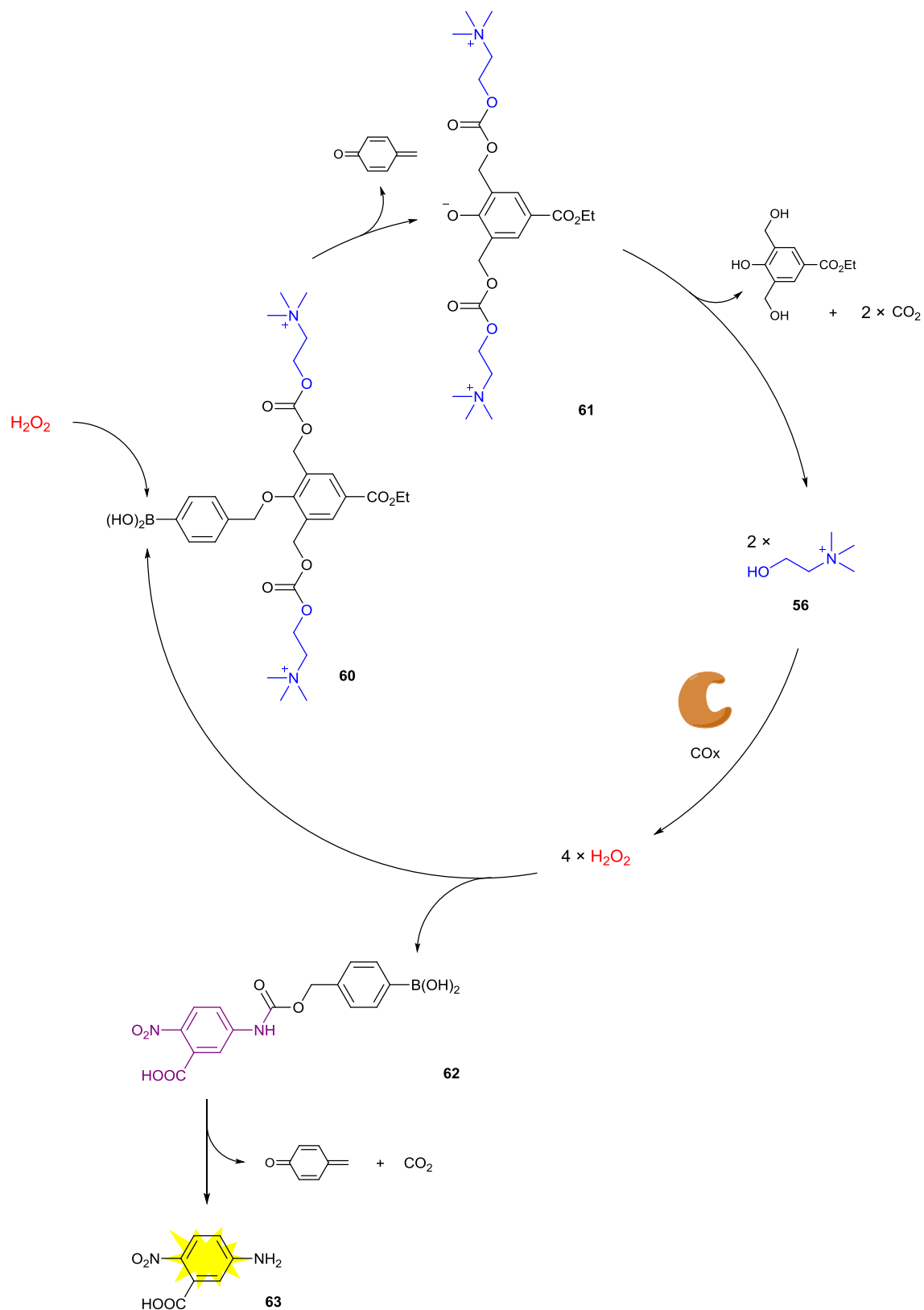
Scheme 1.40 Two-component dendritic chain reaction (2CDCR).

To address these issues, the group developed a two-component dendritic chain reaction (2CDCR) where one reagent **60** contains the trigger unit responsible for analyte detection and signal transduction while the second reagent **62** was solely responsible for signal production

(Scheme 1.40).[202] Through this two-component methodology, the unwanted background signal was suppressed as hydrolysis of **60** does not directly lead to signal production. Also, by separating analyte detection and signal production into different compounds, a mix-and-match approach to sensing can be applied to allow DCR signal amplification to be applied to a fluorescence detection assay. Alternative enzyme amplifiers have also been incorporated into 2CDCR as a number of glucose-containing dendritic amplifier components were tested using glucose oxidase (GOx) as the enzyme amplifier.[203] Additionally, the use of a quinone-based detection component allowed for the 2CDCR to be applied to the detection of thiols.[204] Autoinductive signal amplification can also be achieved in the absence of the enzyme amplifier by utilising the hydroquinone–quinone oxidation by molecular oxygen as a method for generating hydrogen peroxide *in situ* without the need for additional biological components.[205–206]
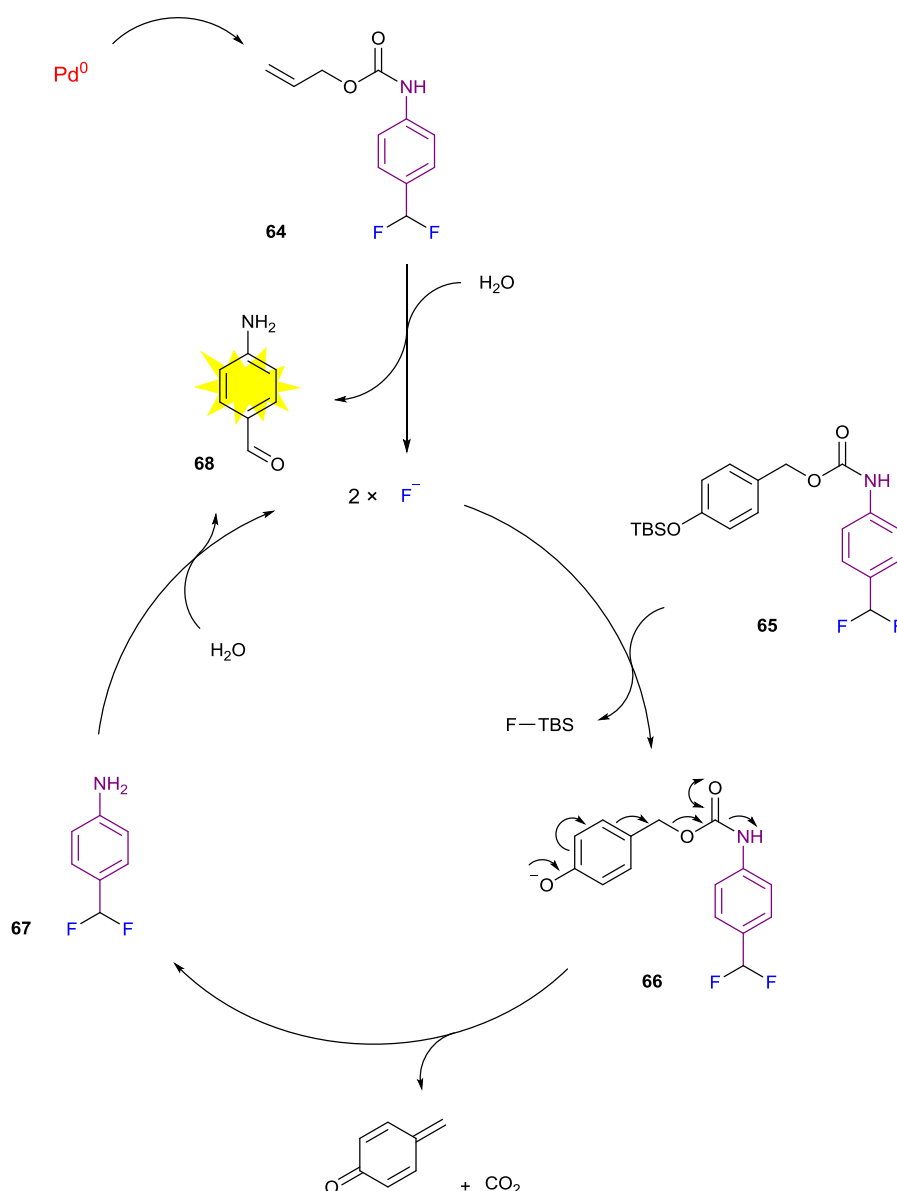
Scheme 1.41 Two-component small molecule autoinductive signal amplification for colourimetric palladium detection.

An example of a two-component autoinductive signal amplification protocol used in combination with target amplification for increased sensitivity was described by Baker and Phillips for the colourimetric detection of palladium (Scheme 1.41).[207] To achieve this autoinductive signal amplification methodology, the first component **64** of the two was equipped with an allyl carbamate trigger, for selective palladium detection, and two fluoride leaving groups as the amplified signal relay. In the presence of palladium therefore, catalytic deallylation and decarboxylation occurs to give 4-(difluoromethyl)aniline which undergoes a double 1,6-elimination to produce two fluoride ions. The second component **65**, a colourimetric probe for fluoride detection itself,[208] was equipped with a silyl protecting group, sensitive to the fluoride relay signal, along with another two equivalents of fluoride to further amplify the signal. After initial breakdown of **64** in response to the analyte, silyl deprotection of **65** occurs due to the generated fluoride and intermediate phenolate **66** also undergoes a 1,6-elimination and decarboxylation to afford another equivalent of aniline **67**, capable of eliminating further to afford another two equivalents of fluoride. Colourimetric detection occurs following elimination of **67** as the compound 4-aminobenzaldehyde **68** produced as the elimination by-product is yellow. This two-component autoinductive signal amplification strategy in combination with an analyte that exhibits target catalysis allows for a LOD of 0.36 ppm palladium, a concentration of palladium typically found in roadside dust.[209]

The reagents used to within this assay are thermally-stable and inexpensive and the colour produced can be seen with the naked eye enabling this methodology to be used in resource-limited environments. However, reaction times are slow with >24 hour assay times required to detect palladium concentrations close to the LOD. Also, due to the slow hydrolysis of **65**, an amplified background reaction limits assay sensitivity, although the introduction of allylic ethers as elimination linkers have shown promise in minimising background reactions yet maintaining signal propogation.[210] The modularity of the small molecule autoinductive signal amplification approach has enabled an extension of compound **65** to be developed for fluorescent fluoride detection.[211]

The ability of a signal amplification protocol to generate products that not only provides a detectable signal but can also increase the rate at which the signal is produced, has allowed previously inaccessible detection limits to be achieved. Inspired by DCR, the majority of autoinductive signal amplification approaches currently described revolve around small molecule-based systems which allow for thermally-stable, inexpensive reagents to be used for analyte detection, signal amplification and signal production in a simple manner. Current challenges involve improving reaction times to allow for these signal amplification methodologies to be applied within the POC setting. In addition, suppression of the high background rates associated with spontaneous hydrolysis of the reagents should allow for better detection limits to be obtained.
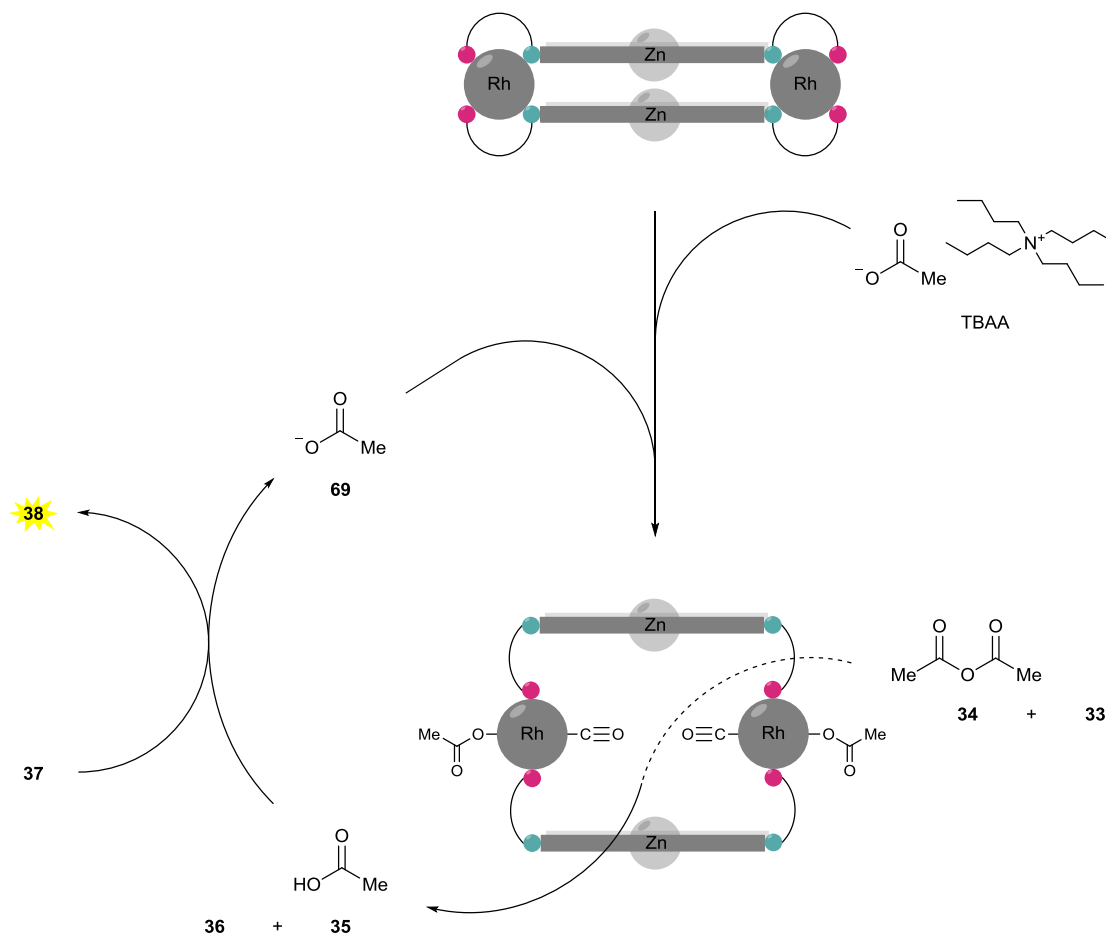
1.3.4 *Autocatalytic Signal Amplification*

Autocatalysis is the process whereby the product of a reaction is able to catalyse the production of itself.[212] This fascinating phenomenon has been intensively studied for the past forty years since autocatalysis may have played a significant role in the origins of life.[213–214] Early synthetic examples of autocatalysis involved the self-replication of small oligonucleotides where the product can act as a template, assisting the formation of more oligonucleotides.[215–217] Synthetic template-assisted autocatalysis,[218–219] has also been applied to the self-replication of peptides,[220] as well as small molecules.[221] Metal-catalysed autocatalysis was first described by Soai *et al.* where the alcohol formed as the product was able to act as a ligand within a zinc-catalysed alkyl addition to aldehydes, promoting the formation of more of itself.[222] Since the reaction can be performed asymmetrically, this reaction can be applied to selectively amplify one enantiomer over another and therefore increase the enantiometric excess of a near racemic mixture.[223–226] This powerful asymmetric amplification method has even been used to discriminate between carbon-12/carbon-13 chirality,[227] which has huge implications for determining the origins of homochirality.[228–229]

Although considerable effort has been made towards enantioselective amplification using autocatalysis,[230] the application of autocatalysis towards a signal amplification methodology has been comparatively less explored. To date, only two autocatalytic signal amplification methodologies for sensing have been published and both are advancements upon signal amplification concepts already described herein. The first of the two was developed by Yoon and Mirkin who manipulated their supramolecular catalysts to be activated by the product allowing for autocatalytic signal amplification to be applied towards the fluorescent detection of acetate anions (Scheme 1.42).[231]

In a previous example, supramolecular constructs based upon the WLA were shown to rearrange selectively in the presence of the chloride analyte to reveal a bimetallic active site for a Lewis acid-catalysed acylation reaction. Since the by-product of this acylation is acetic acid, the authors hypothesised that an autocatalytic variant of SAAC could be achievable if the produced acetate anion could bind to the allosteric site of the pre-catalyst and also induce ligand rearrangement. Thus, in the presence of tetrabutylammonium acetate (TBAA), used as the model analyte, and under a carbon monoxide atmosphere, catalytic activity was shown to be switched on through the production of fluorescence. Initially, a minor amount of the catalysts are activated leading to slow product formation. However, as more acetate is produced, an increase in catalyst activation is observed leading to an acceleration of catalytic activity until the reaction reaches its saturation point when full consumption of the substrate occurs. This is confirmed by a study of the reaction kinetics; the conversion–time graphs display sigmoidal curves characteristic of autocatalytic product generation which starts with a slow induction period followed by an exponential increase before reaching a plateau.[232] Similarly to PCR, analyte concentration correlates with the time taken to reach exponential signal amplification. Importantly for autocatalytic signal amplification protocols, almost no conversion was observed in the absence of

acetate. Although variations at the allosteric site of the catalyst amplifier and the use of alternative pH-responsive reporters for different readouts would allow this autocatalytic signal amplification protocol to be used within multiple applications, the current procedure described appears to be limited towards only acetate detection.

Scheme 1.42 Supramolecular autocatalytic signal amplification for fluorescent acetate detection.

A more flexible approach to autocatalytic signal amplification was provided by Phillips *et al.*, who described an autocatalytic variant of their two-component autoinductive signal amplification procedure for colourimetric palladium detection (Scheme 1.43).[233] To achieve autocatalysis, signal amplification reagent **72** was designed, inspired by amine proliferation compounds used within photolithography,[234] with a 9-fluorenylmethoxycarbonyl (Fmoc) reporter moiety and a piperidine unit which were connected *via* an aniline linker. Analyte-responsive reagent **70** was equipped with an allyl carbamate trigger for selective palladium detection adjoined with a signal propagating piperidine group *via* an electron-rich aniline, which facilitates elimination upon analyte recognition.[235] In the presence of palladium, deallylation and elimination of **70** occurs releasing the piperidine catalyst. Since palladium also exhibits target catalysis, multiple equivalents of piperidine can be released *per* molecule of palladium thereby increasing assay sensitivity. After

release, piperidine acts as a catalytic base, deprotonating **72** to release another equivalent of piperidine and the dibenzofulvene chromophore **73**. Proton transfer then occurs regenerating the original catalytic base and creating another catalyst. This cycle repeats until full consumption of signal amplification reagent **72** occurs and full conversion is obtained.
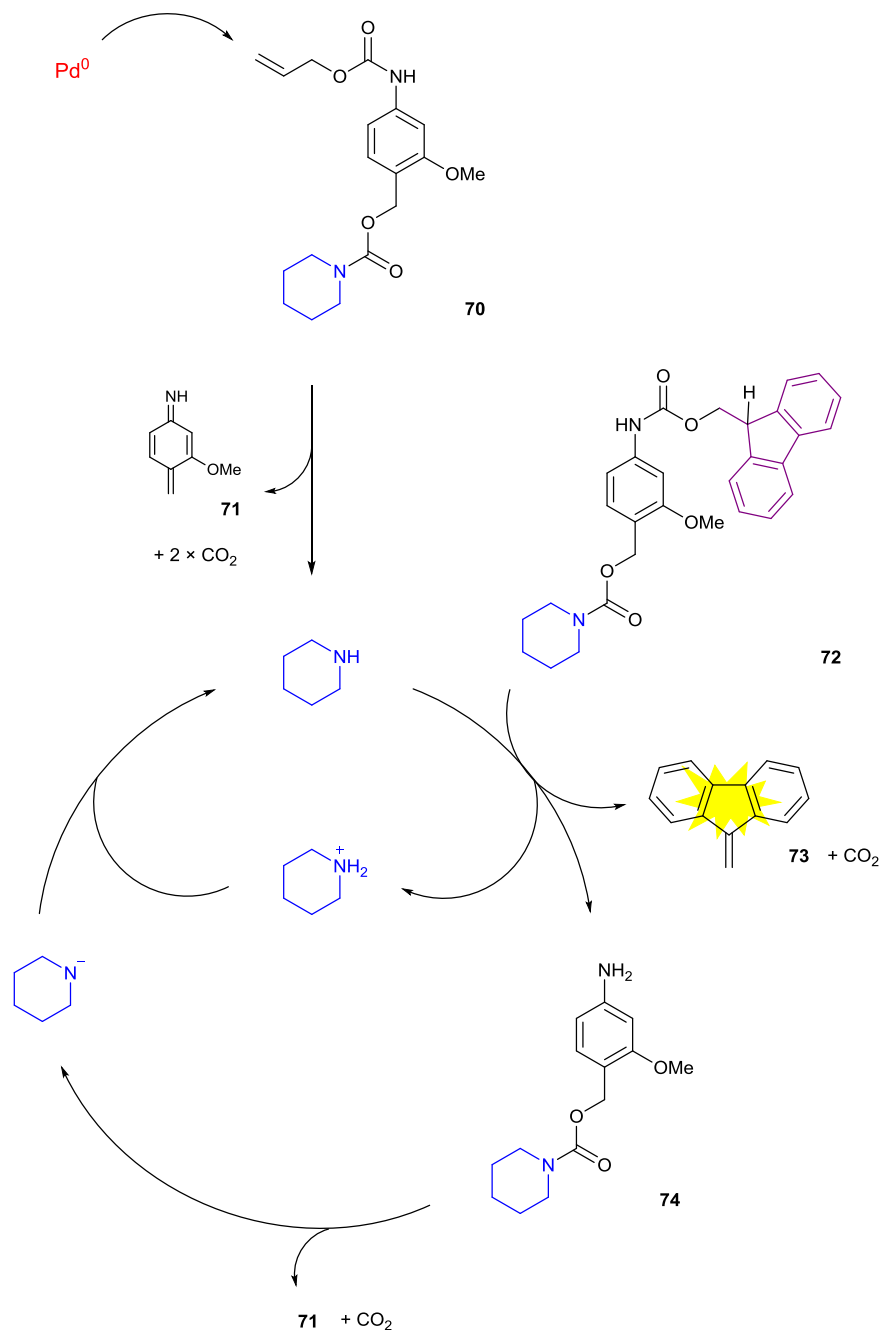
Scheme 1.43 Small molecule autocatalytic signal amplification for colourimetric palladium detection.

A piperidine catalytic loading of 0.1 mol% was shown to initiate full breakdown of **72** over 18 hours and exhibited a sigmoidal reaction profile over this time period which indicates that an autocatalytic mechanism was in effect. This two-component small molecule approach to

autocatalytic signal amplification was capable of reaching a LOD of 12 ppm for palladium and variations of 2 ppm in palladium concentration could be easily distinguished. Despite >1000-fold signal amplification, the long induction time required for low analyte concentrations prevents this methodology from being employed for POC diagnostics. However, this methodology could see use within areas such as stimuli-responsive materials where high amplification is required but a specific timeframe in which this occurs is less important.[236]

Autocatalytic signal amplification has the potential to fulfil the needs of diagnostic assays which suffer from a lack of sensitivity and is capable of detecting analyte concentrations unreachable by other signal amplification methods. The development of such protocols is still in its infancy with only two examples successfully demonstrated to date. They have however, shown that autocatalytic signal amplification is achievable through completely different methods and should inspire the next influx of amplification approaches to match, if not better, current detection limits. Future efforts should also be aimed at providing autocatalytic signal amplification towards detection of biological samples allowing them to be incorporated within medical diagnostic applications. Furthermore, the time taken to induce exponential amplification should be dramatically shortened to enable autocatalytic signal amplification to be applied to the POC setting.

1.4   Receptor Amplification

Within a detection assay, signal production typically occurs after the result of an analyte–probe recognition event. Increasing the number of analyte receptors upon the probe would therefore lead to an increase in the probability of an analyte–probe recognition event occurring and therefore faster signal production. This concept is perfectly exemplified by Amir and Shabat who were able to increase the number of analyte-responsive triggers on a dendrimer in order to achieve an amplified signal response (Figure 1.5).[237] In this example, three dendrimer derivatives were synthesised containing one, two or four enzyme responsive triggers connected to a single reporter molecule. Since the removal of just a single trigger is capable of releasing the reporter molecule, the dendrimer with the most receptors should deliver the fastest response. Indeed, in the presence of the enzyme target, dendrimer **76** with two enzyme triggers was shown to eliminate twice as fast as dendrimer **75** containing only one enzyme trigger. However, due to slow elimination kinetics associated with the increased number of eliminations required, dendrimer **77** with four enzyme triggers attached to the reporter molecule was actually shown to produce a considerably slower signal. Still, this dendritic approach to receptor amplification was successfully coupled to a dendritic signal amplifier to significantly reduce the time-to-result yet still provide an amplified signal for the detection of PGA.[238] It is on this basic principle that the majority of receptor amplification methodologies are based upon.

Similarly, but conceptually opposite, to label amplification, receptor amplification methodologies utilise the multivalent characteristics of a range of molecular structures to

sufficiently amplify the number of receptors adjoined to the signal producer. This has allowed structures such as polymers, micelles and hydrogels to all being successfully employed as receptor amplifiers within sensing methodologies.
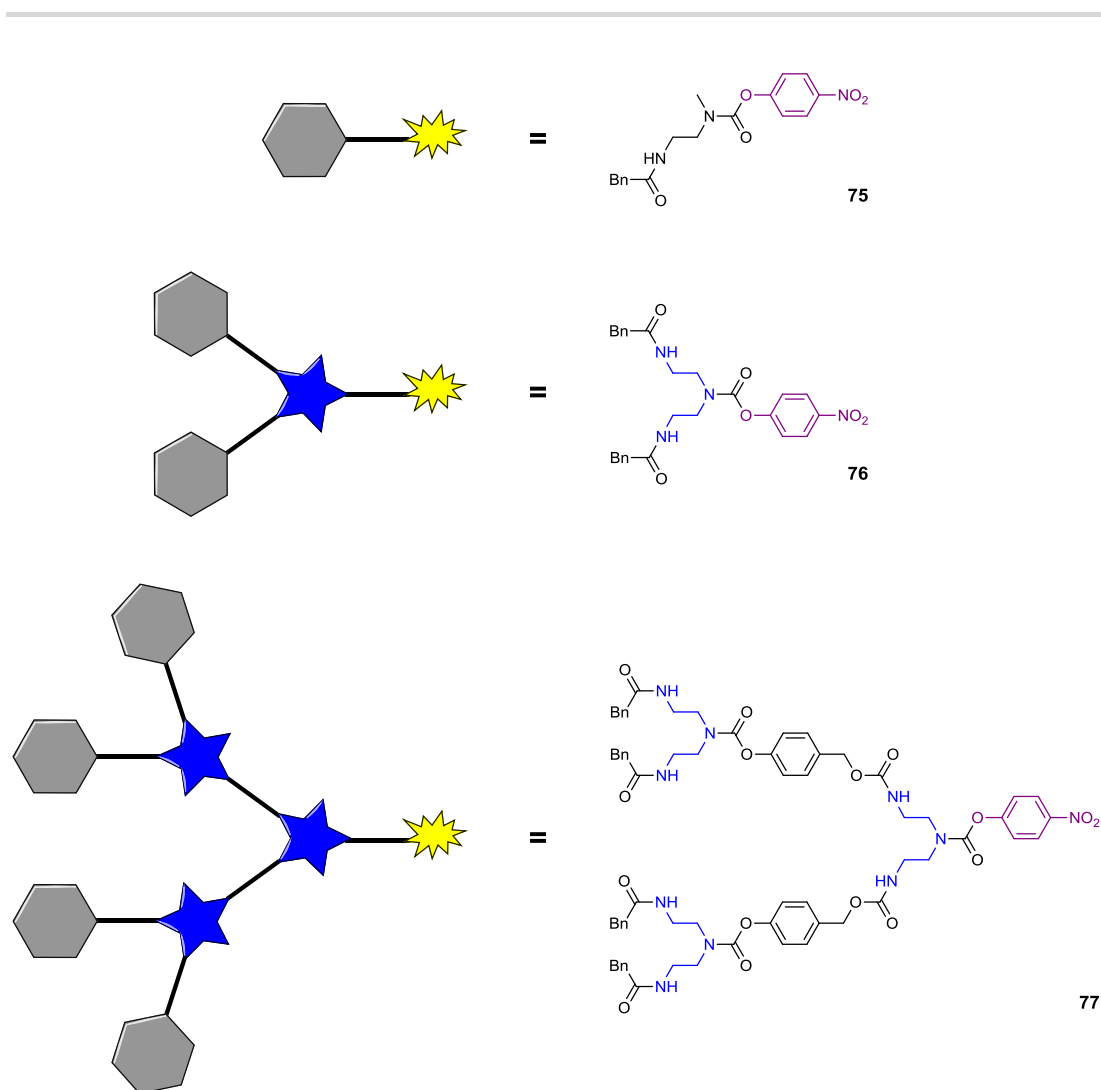

Figure 1.5 Concept of receiver amplification and the structures of dendrimers **75**, **76** and **77**.

1.4.1   Polymers

Prior to the introduction of self-immolative dendrimers, the development of conjugated polymers was fundamental to enabling receiver amplification as this allows communication between repeating units of the polymer.[239] Functionalising the conjugated polymers, known as "molecular wires", with analyte-responsive receptors generates a single compound with multiple linked receptors. However, it was the use of fluorescent conjugated polymers developed by Swager *et al.* that adapted the molecular wire approach to be used for receptor amplification within a sensing application (Scheme 1.44).[240]
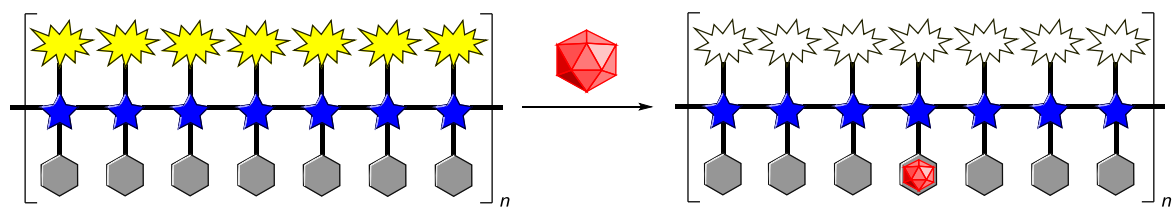
Scheme 1.44 The molecular wire approach to receptor amplification.

78
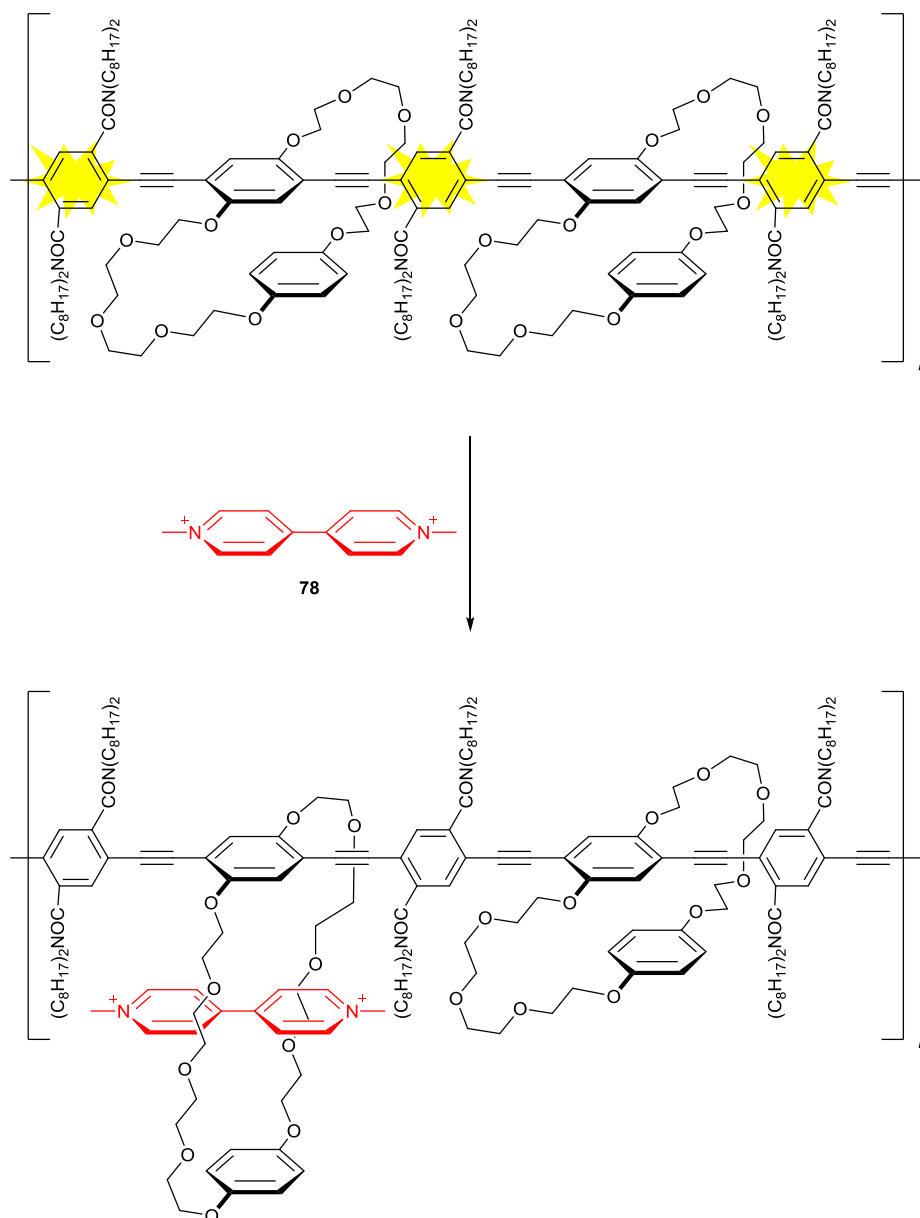
Scheme 1.45 The molecular wire approach for the fluorescence detection of PQ.

In a seminal publication, Zhou and Swager described the use of cyclophane receptors attached to a polyphenylacetylene backbone for the fluorescent detection of paraquat (PQ) (Scheme 1.45).[241] A strongly fluorescent molecular wire was synthesised through palladium-catalysed cross coupling of 4-iodophenylacetylene monomers equipped with   bis(*p*-phenylene)-34-crown-10

(BPP), an excellent binder of PQ.[242] In the presence of the analyte **78**, PQ was shown to dramatically quench the fluorescence of the conjugated polymer in comparison to the monomer. In fact, a 65-fold increase in quenching was observed through the molecular wire approach, which was attributed to energy migration transmitted throughout the polymer. In other words, a single analyte binding to a single receptor is able to exhort fluorescence quenching over the entire polymer. At high molecular weight polymers though, a marked decrease in sensitivity is observed due to the length of the polymer being longer than the diffusion length of excitation. Attempts to increase the diffusion length of excitation by enhancing the delocalisation throughout the polymer backbone in order to improve sensitivity were unsuccessful.[243] Increased sensitivity can be achieved however through deposition of the molecular wires into thin films as energy migration can then occur between individual polymers.[244]

The concept of receiver amplification employed by this method has allowed amplification to be applied to the large array of simple analyte receptor systems previously developed, enabling lower LODs to be obtained through these conjugated polymer-based chemical sensors.[245] The considerable number of polymerisation techniques, as well as the number of analyte receptors available, has meant that the amplified detection of small ions, explosives and biomolecules can be achieved using fluorescent conjugated polymers.[246] Not only this, but modification of the polymer backbone has allowed for colorimetric derivatives of receiver-amplified polymer-based detection methods to become possible allowing analyte detection to be achieved with the unaided eye.[247]
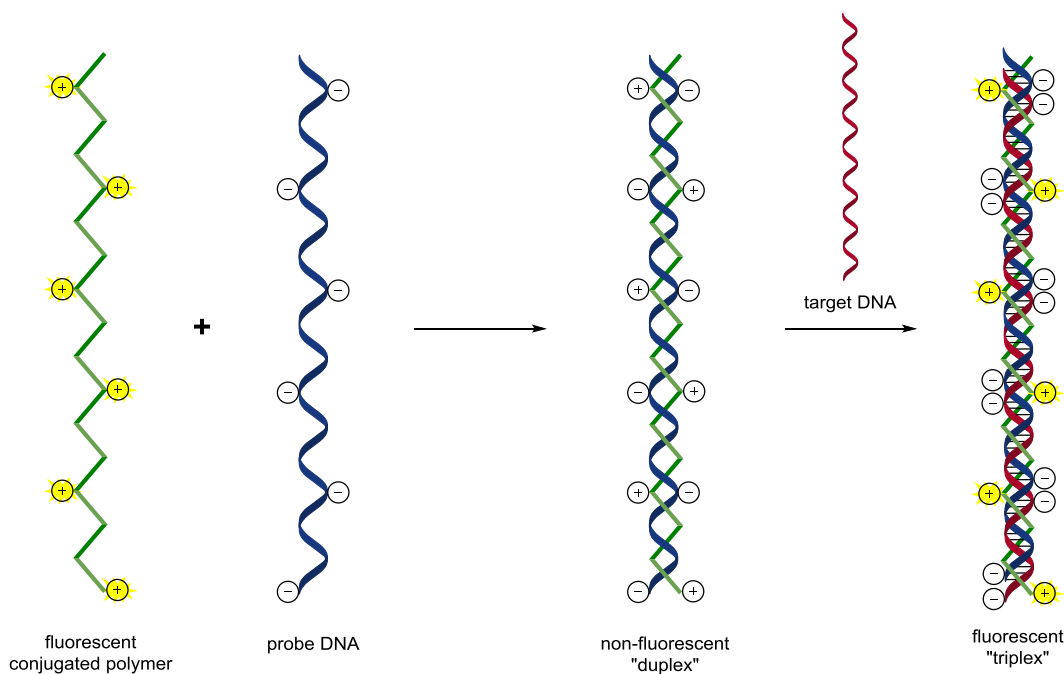
Scheme 1.46 Conjugated polymers for fluorescence detection of nucleic acids.

Typically, conjugated polymers display fluorescence and it is in the presence of the analyte that fluorescence is quenched. In contrast, Leclerc *et al.* demonstrated the use of conjugated-polymers for signal-amplified switch-on fluorescent nucleic acid detection (Scheme 1.46).[248] In this invention, a cationic, water soluble, thiophene-derived conjugated polymer,[249] and an anionic, complementary strand of probe DNA initially come together through electrostatic interactions. The complexes then aggregate together because of their poor solubility in aqueous media and due to the close proximity of the polymers, as well as polymer stiffening, fluorescence quenching is observed.[250] In the presence of target DNA, hybridisation preferentially occurs with the probe DNA and a stable triplex is formed where the conjugated polymer is wrapped around the DNA double helix, bound to the anionic phosphate backbone. The resulting uniform, helical structure of the conjugated polymer, along with the triplex being more soluble in water, leads to dequenching and a switch on of fluorescence. This technique was shown to be surprisingly selective as well as sensitive since a two base pair mismatch can be easily discriminated and a LOD of 2.4 aM after an assay time of 1 hour can be achieved. Labelling the probe DNA with a fluorophore whose optimal absorption wavelength is identical to the emission wavelength of the conjugated polymer can provide FRET enhancement within the detection methodology.[251] This not only improves selectively since a single base pair mismatch could be distinguished, but also improves sensitivity as a LOD corresponding to 3 zM could be achieved after just a 5 minute assay time. This increase in sensitivity is attributed to additional fluorescence signal amplification (FSA),[252] as one conjugated polymer is capable of exciting a large number of fluorophores.[253]

1.4.2   Encapsulated Reagents

The concept of encapsulation to segregate reaction reagents and slowly release them in response to product formation for reaction rate acceleration is a well-known method of providing chemical amplification.[254–255] Manipulating this premise towards a sensing methodology requires modification of the capsule to release its contents selectively in the presence of the analyte and a change in physical property must accompany content release in order for effective analyte detection.

The discovery of fluorophores that undergo self-quenching at high concentrations,[256] such as fluorescein,[257] has enabled the development of 'switch-on' fluorescent sensing methodologies utilising polymeric assemblies and supramolecular structures that display stimuli-responsive fluorescence emission characteristics.[258] In a prime example of this, Matile *et al.* described the use of synthetic supramolecular pores within vesicles for the fluorescent detection of enzyme activity (Scheme 1.47).[259] Artificial rigid-rod molecules capable of self-assembling into β-barrels,[260] were constructed and then filled with anionic enzyme substrate adenosine triphosphate (ATP) **80**, which can bind to the cationic inner wall of the barrel through electrostatic interactions. The blocked barrels were then slipped into the lipid bilayer of a vesicle containing a high concentration of 5-

carboxyfluorescein **79** and as such, were non-fluorescent. Since a large number of synthetic pores, or analyte receptors, are present *per* vesicle and only one is needed to be unblocked to release its cargo then significant receptor amplification is demonstrated by this approach. In the presence of the analyte, a nonspecific adenosine triphosphatase (ATPase) enzyme,[261] dephosphorylation of ATP to adenosine monophatase (AMP) **81** occurs. Due to the decrease in size and the reduced number of anionic binding sites, AMP is unable to sufficiently block the barrel and is expelled. Once the barrel is unblocked, this allows the release of the trapped molecules within the vesicle through the synthetic pores and into the reaction medium. Consequently, dilution of 5-carboxyfluorescein **79** prevents self-quenching leading to the observed turn-on of fluorescence.
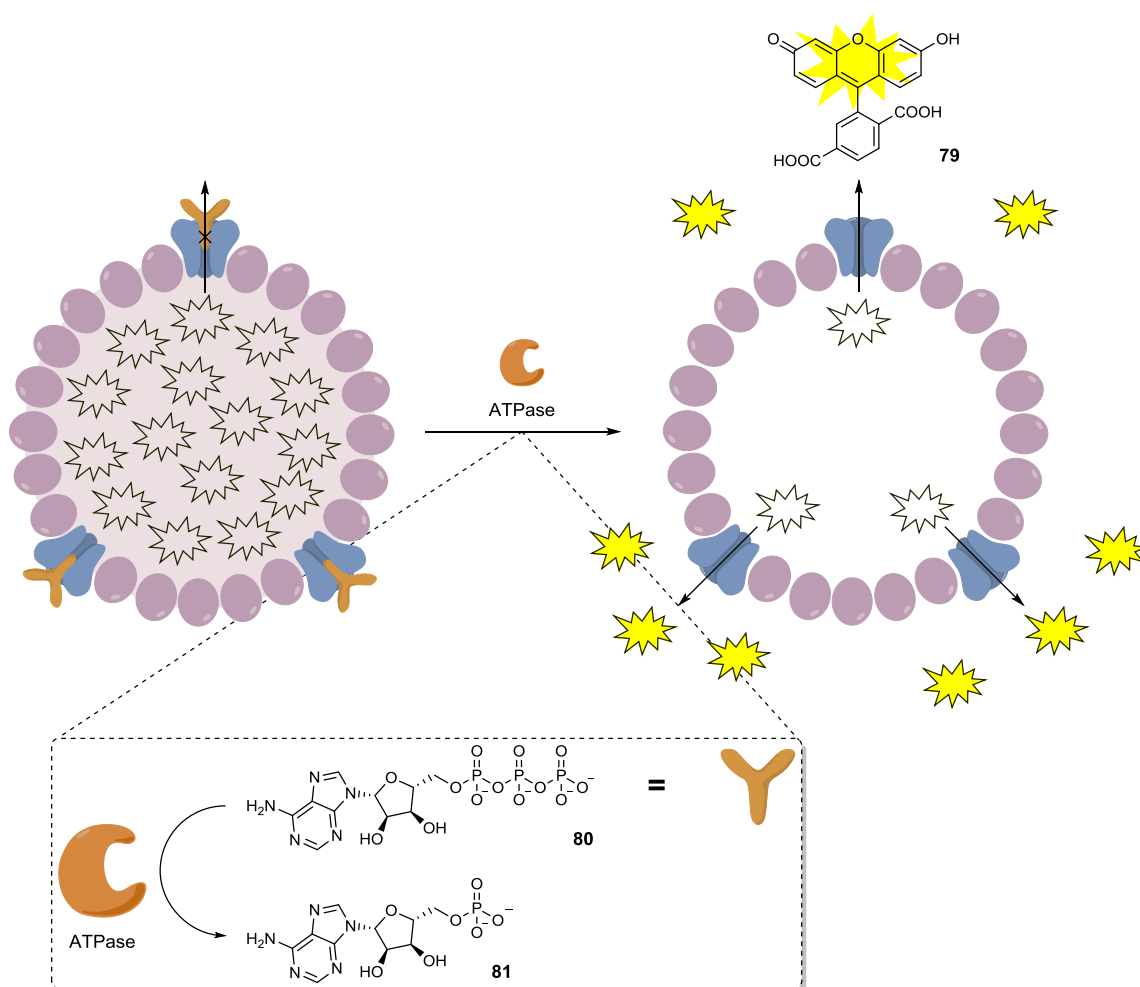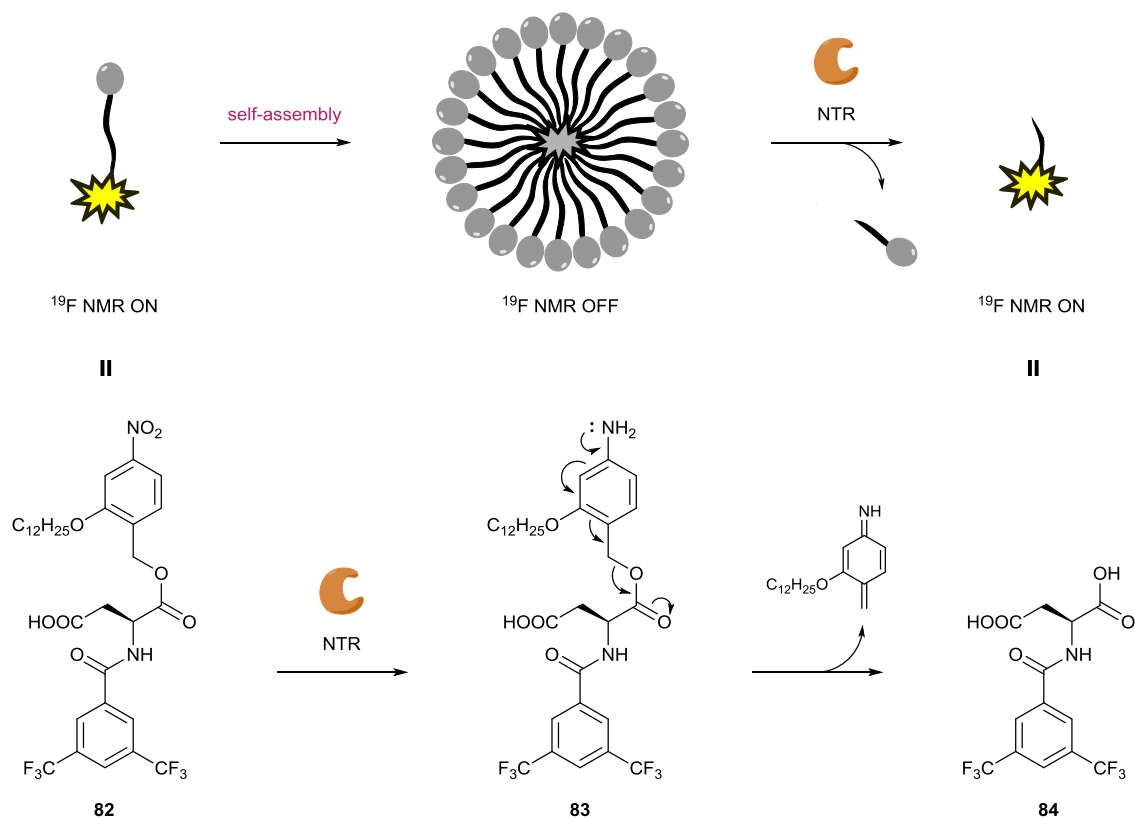

Scheme 1.47 Fluorometric detection of enzyme activity with synthetic supramolecular pores.

The versatility of this amplification methodology was also shown as it was easily adapted to the detection of other enzymes, such as aldolases and phosphatases, through the use of the appropriate unmodified enzyme substrates as pore blockers. However, the advantage of not requiring labelled enzyme substrates is highly dependent on the enzyme substrate showing high affinity for the pores and the enzyme product having a significantly lower affinity. In particular, to

enable vesicle receptor amplification for the fluorescent detection of ATP, an analyte detection method without synthetic pores had to be used.[262] Despite this, the rigid-rod approach for the development of synthetic, multifunctional pores capable of responding to changes in pH, concentration and voltage,[263] has enabled a variety of different analytes to be detected using synthetic and bioengineered membranes.[264]

Scheme 1.48 Receptor amplification through self-assembling probes for the ^{19}F NMR detection of enzyme activity.

Similarly to self-quenching fluorophores, the phenomenon of molecular signal changes at high label concentrations also occurs with self-assembling fluorine-containing compounds when using ^{19}F nuclear magnetic resonance (NMR) as the detection method. Developed by Hamachi *et al.*, a detailed study was conducted into the different combinations of monomers that could be obtained through modification of the fluorine-containing tail group, the linker and the analyte-responsive head group and the effect this would have upon self-assembly.[265] The successful formation of spherical, self-assembled nanoprobes, with the fluorine-containing tail-groups on the inside, was determined by a switch-off of the ^{19}F NMR signal. Since the outside of the nanoprobe is covered with the analyte-responsive head groups and modification or removal of just one could disrupt aggregate formation, then considerable receptor amplification can be achieved.

To adapt this observation towards a sensing methodology, the group used nitrobenzene head groups for the ^{19}F NMR detection of the enzyme nitroreductase (NTR) (Scheme 1.48).[266] In this approach, enzyme-catalysed reduction of the nitro group upon probe **82** to the corresponding aniline **83** generates an unstable intermediate that undergoes 1,6-elimination to afford reporter molecule **84**. Subsequently, disaggregation of the nanoprobes occurs and a switch-on of the ^{19}F NMR signal is observed. Importantly, due to the designed elimination procedure, a shift in the ^{19}F NMR signal is also observed which confirms the detection of enzyme activity *via* the proposed mechanism as opposed to nanoprobe disaggregation occurring through other means. The adaptability of this technique was also demonstrated as by changing the head group to a specific peptide chain, the amplified ^{19}F NMR detection of cancer biomarker MMP2 could be achieved. The nanoprobes also exhibit excellent biocompatibility and this method has been demonstrated for both cell surface,[267] and intracellular protein imaging.[268]
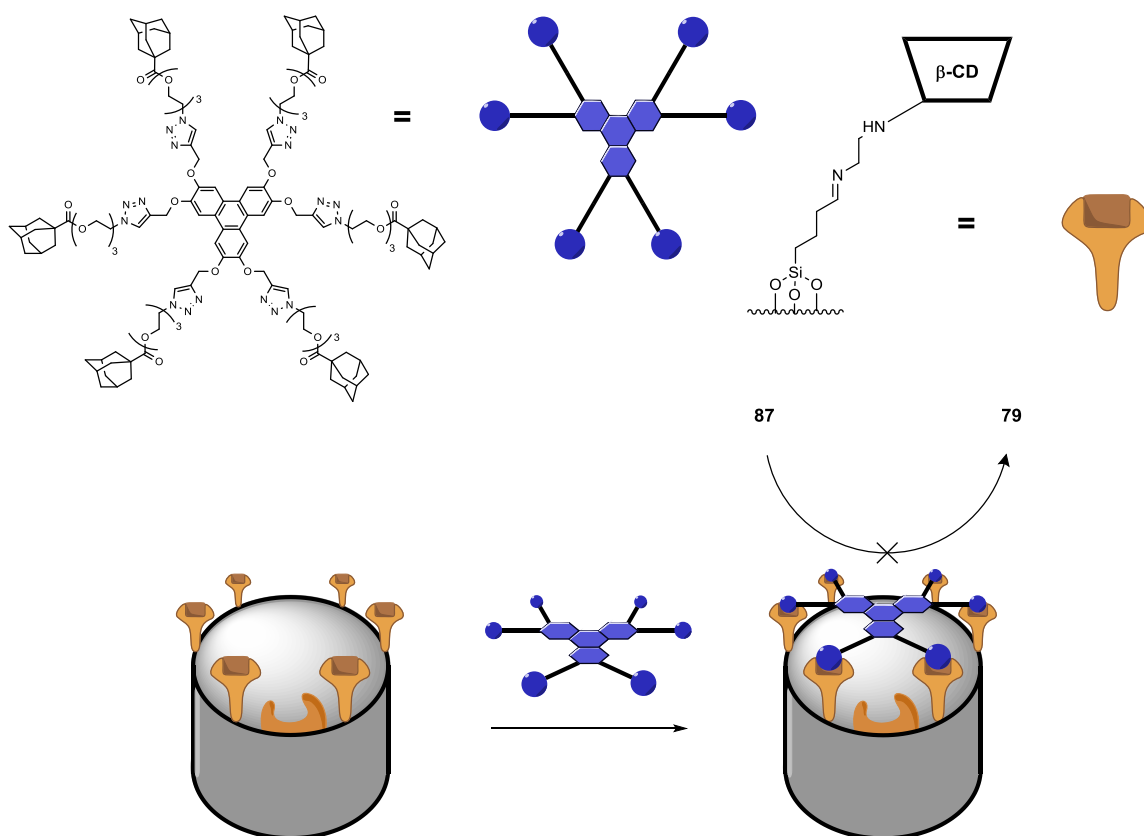
Scheme 1.49 Structure of both the size-selective gate and the hinge, and their use in the construction of pH-controlled, enzyme-encapsulated, mesoporous silica nanoparticles.

Stimuli-responsive release of encapsulated reagents,[269] has enormous application to a number of biomedical applications such as drug delivery and self-healing materials.[270] As such, a considerable number of analyte-triggered reagent release methodologies are not necessarily designed for sensing purposes.[271–272] Recently, advances have been made from encapsulated

reagents to encapsulated enzymes in an effort to provide further amplification as well as to achieve programmed enzymatic reactions.[273] From a sensing perspective, one particular contribution of note was provided by Xue and Zink who demonstrated an enzyme chemical amplifier using mechanised nanoparticles.[274]
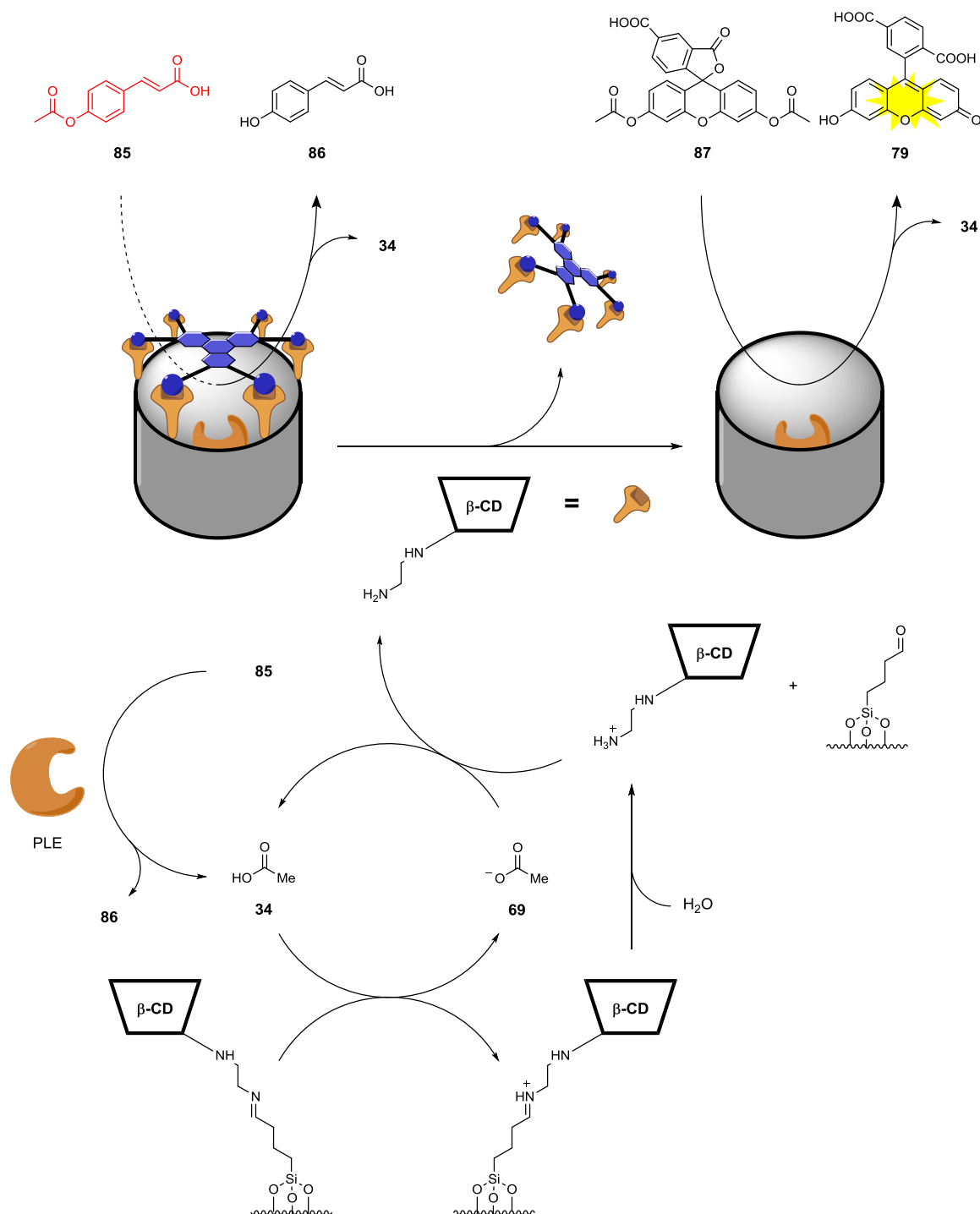

Scheme 1.50 Size-selective, pH-controlled, enzyme-encapsulated mesoporous silica nanoparticles for the fluorescence detection of small, acylated compounds.

In this method, size-selective pH-controlled silica nanoparticles were constructed containing porcine liver esterase (PLE) and capped with a star-like gate through imine hinges (Scheme 1.49).[275] The gate allows the coexistence of the enzyme and enzyme substrate in the same media yet prevents their interaction through size-exclusion. System activation occurs in the presence of the analyte, 4-acetoxycinnamaldehyde (ACA) **85**, which is small enough to fit through the gate and is subsequently hydrolysed by the enzyme (Scheme 1.50).[276] The acid produced as a result of enzyme hydrolysis is then capable of catalysing the hydrolysis of the imine hinges holding the gate in place. Once all the linkages are broken, the gate is removed from the nanoparticle which therefore allows interaction between the enzyme and pro-fluorescent enzyme substrate, 5-carboxyfluorescein diacetate (CFDA) **87**. Enzyme-catalysed hydrolysis of enzyme substrate CFDA not only allows enzyme activity to be measured by fluorescence but also produces further equivalents of acid, which leads to further gate removal and therefore an increased rate of fluorescence production. Although the system demonstrated autoinductive amplification, reaction times were long owing to the slow turnover rate of the enzyme. Also, this methodology is limited to the detection of acylated compounds that are small enough to fit through the gaps in the gate. Despite this, background rates are negligible showing that enzyme activity can be effectively controlled using size-selectivity and this methodology could have wider application within biosensing due to both the high biofunctionality and biocompatibility of mesoporous silica nanoparticles.[277]
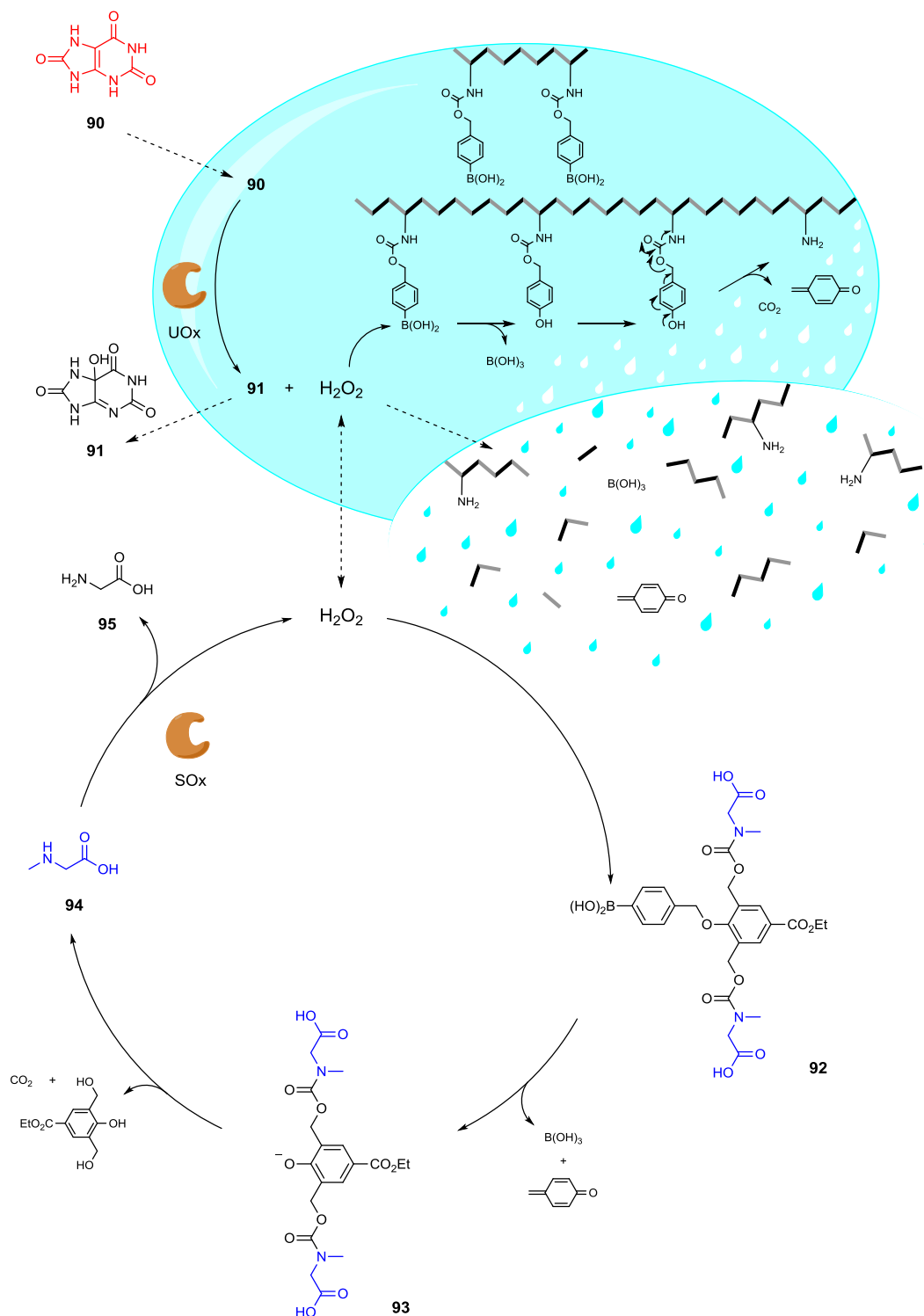
1.4.3   Hydrogels

Hydrogels are hydrophilic polymer networks that can absorb up to 99% of their own weight in water without dissolution.[278] They possess the ability to contain a large number of analyte receptors either physically encased within the polymer matrix or covalently bound to the polymer and can induce a considerable physical response in the presence of specific stimuli.[279] This, along with their high biocompatibility,[280] has seen the inclusion of hydrogels within a number of sensing applications such as temperature and pH monitoring,[281] as well as for the detection of biologically-related material.[282] Typically, the physical response elicited is either through swelling or shrinkage of the hydrogel and this response can be measured through changes in optical transmission,[283] or refractive index.[284] However, these methods require sophisticated instrumentation to afford an accurate readout and as a result, there has been efforts made to induce complete disintegration of the hydrogel in response to an analyte allowing for naked eye detection. Furthermore, by accompanying full dissolution of the hydrogel with a colour change, then an unambiguous positive result can be easily determined by eye. One such methodology was developed by Tan *et al.*, who developed an aptamer-based colourimetric hydrogel platform for the visual detection of cocaine **88** (Scheme 1.51).[285]
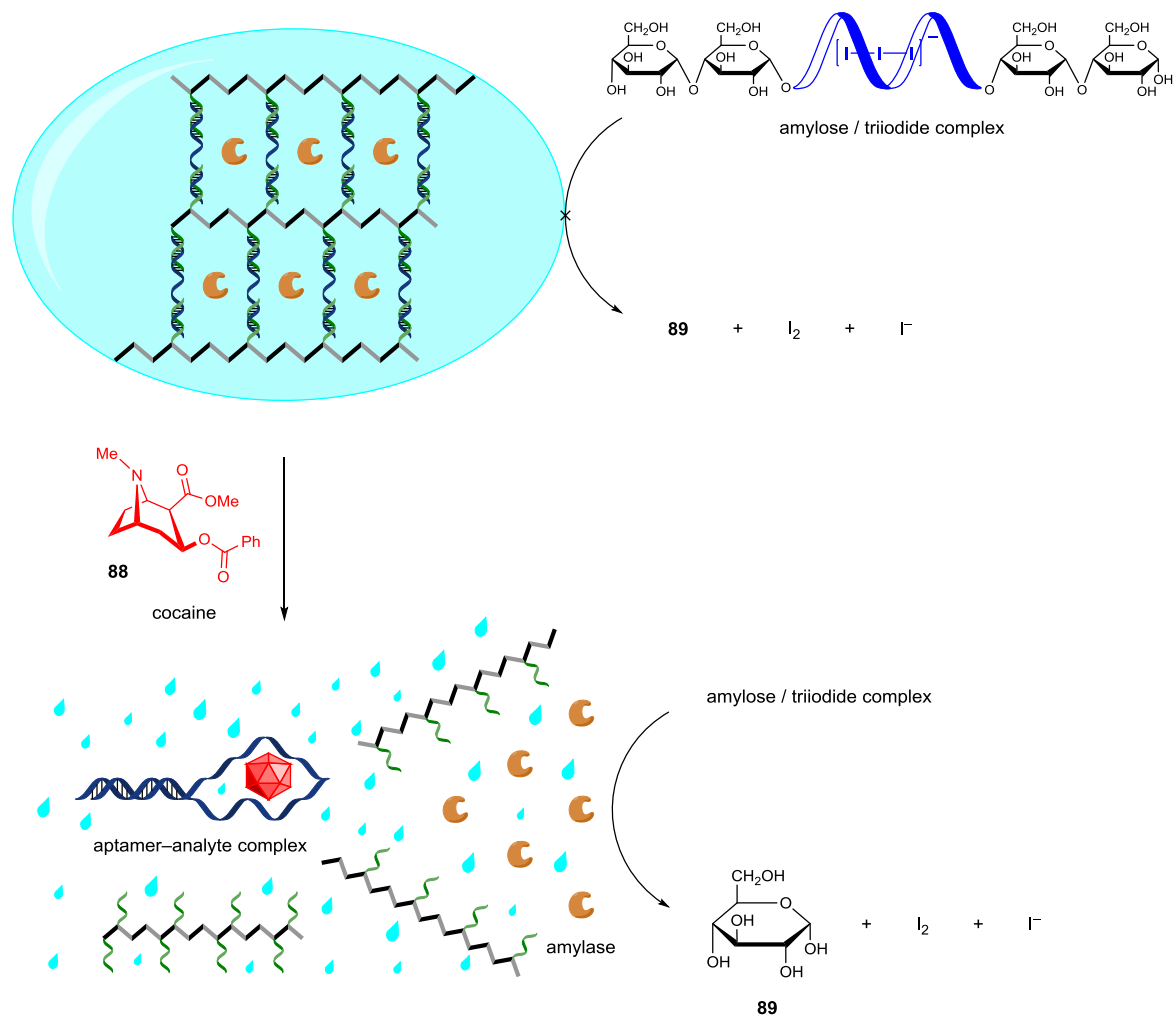
Scheme 1.51 An aptamer-bound, enzyme-encapsulated hydrogel for colourimetric cocaine detection.

In this procedure, amylase enzyme amplifiers were trapped within a cross-linked polymer hydrogel that was dependent on DNA aptamers, that are selective for cocaine, for structural support.[286] In the presence of the analyte, competitive binding for the aptamers occur leading to hydrogel destabilisation and then inevitable dissolution of the hydrogel with concomitant release of amylase enzymes. Thus, the enzyme-catalysed breakdown of amylose is initiated and when the assay medium is stained with iodine, the characteristic blue colour associated by the presence of amylose does not appear.[287] The combined receiver amplification of the hydrogel and the signal amplification delivered by the enzyme enabled cocaine detection to less than 20 ng with the naked eye within 10 minutes. Due to the use of DNA aptamers for analyte detection high selectivity for cocaine over structurally similar compounds such as benzoylecgonine (BE) and ecgonine methyl ester (EME) was also observed. Enzyme trapping, compared with some enzyme conjugation methods, is extremely mild yet effective as no loss of enzyme activity was seen between trapping and activation. Also, no undesired substrate breakdown was seen in the absence of the analyte since the hydrogel and the enzyme substrate are both polymers. As glucose **89** is produced as a result of

the enzyme-catalysed breakdown of amylose, cocaine detection can also be measured quantitatively with a commercially available personal glucose meter.[288]

Scheme 1.52 DCR-enhanced, chemically-reactive supramolecular hydrogel for the visual detection of uric acid.

Supramolecular hydrogels, hydrogels constructed solely on the self-assembly of small molecule hydrogelators rather than through chemical cross-linking or polymerisation, are becoming

increasingly popular because in addition to being able to support biomaterial within the hydrophilic gel, hydrophobic molecules such as fluorophores can also be supported within the supramolecular framework itself.[289] As such, a considerable number of supramolecular hydrogels have been used for a number of fluorescent chemosensors that respond to molecular recognition and enzyme activity.[290] Of particular note is the supramolecular hydrogel-based sensing techniques developed by Hamachi *et al.* that have been shown to be easily adaptable towards the fluorescent detection of polyanions,[291] polycations,[292] and PSA.[293] However, continuing the endeavour for analyte detection without instrumentation, the group very recently successfully coupled their chemically reactive supramolecular hydrogel with a DCR-type amplification procedure for the naked-eye detection of uric acid in human plasma (Scheme 1.52).[294]

In this protocol, supramolecular hydrogels designed to be selective towards hydrogen peroxide, were constructed containing three components; analyte selective enzyme urate oxidase (UOx), signal transducing self-immolative compound **92**, and signal amplifying enzyme sarcosine oxidase (SOx). Despite the high number of encapsulated reagents, the hydrogels were shown to be physically stable. In the presence of uric acid **90**, a biomarker for gout,[295] UOx catalyses its oxidation to 5-hydroxyisourate **91** producing hydrogen peroxide as a byproduct, which can go on to oxidise signal transducing reagent **92** to its corresponding phenol **93**. This intermediate is unstable under the assay conditions and eliminates to produce two equivalents of sarcosine **94**. Signal amplifying enzyme SOx then catalyses the oxidative demethylation of sarcosine **94** to glycine **95** producing more molecules of hydrogen peroxide in the process. This can go on to react with more equivalents of **92** or react with phenylboronic acid residues upon the hydrogel framework. Oxidation and subsequent elimination of these residues is enough to destabilise the matrix and cause collapse of the hydrogel, a physical effect visible by eye. This system was capable of detecting 80 μgmL^{-1}, the threshold level of hyperuricemia, with the naked eye following a 3 hour incubation. The sensitivity was attributed to the amplification provided by DCR, allowing for a 5-fold decrease in analyte concentration that could be detected *via* this method. In addition, by swapping SOx with GOx, the detection method was easily adapted towards the detection of glucose. This mix-and-match approach using different enzymes allows the system to provide logic-gate output responses from different biological substance input signals.[296]

1.5   Conclusion

Molecular amplification in sensing can now be achieved through a considerable variety of different approaches; whether focussed on target, label, signal or receptor amplification. The selection of which amplification strategy to choose is not necessarily a case of which one provides the greatest amplification but more a matter of which one is most suitable as part of a particular detection assay. This is dependent on the analyte being detected, the medium the analyte is being detected from, the medium the amplification is taking place in and the desired readout signal. Factors such as the

required selectivity and sensitivity, as well as time and cost, also play an important role in selecting the most suitable amplification method.

Analyte detection methods are constantly evolving. Reversible affinity-based analyte recognition has made way to irreversible reaction-based analyte recognition in order to improve sensitivity.[297] In addition; simple indicator-based approaches to sensing are now being made obsolete by easy-to-perform, amplified detection assays. Recently, single-amplifier techniques have been elaborated with multiple amplifiers in a bid to achieve even greater sensitivity. Current efforts are being made not only towards the inclusion of multiple amplifiers but also the incorporation of different amplification approaches, such as target and signal amplification within the same detection assay. However, the strive to obtain lower and lower detection limits by more and more powerful amplification methods can lead to over-complication and problems with false-positive results from accidental activation. This is particularly true with regards to the attractive exponential amplification displayed by autocatalytic methods. Therefore, analyte selectivity is becoming increasingly important not just sensitivity.

Future amplification methodologies will always aim for a detection limit of a single molecule within a complex mixture with the naked eye. This is not the only goal within sensing though as complex diseases, such as cancer, require the successful detection of a panel of biomarkers prior to diagnosis, not just one. Therefore, the ability for amplification methodologies to demonstrate multiplexed detection without interference is highly desirable. General reagent-based amplification strategies are also in high demand as the ability to choose an appropriate reagent for a specific analyte with a particular readout where amplification is guaranteed will prove to be very adventitious within clinical diagnosis. Previously, it has been highlighted that the best results are obtained in systems that rely on cascades of amplification events and that most amplification protocols rely on hybrid systems. Current objectives within sensing should therefore be to develop amplification cascades that utilise both biological and synthetic components for selective and sensitive analyte detection assays.

Chapter 2

Ratiometric Electrochemical Detection of Alkaline Phosphatase[298]

2.0   Introduction

2.0.1   Atlas Genetics Ltd.

The work described within this thesis was conducted under the sponsorship of University of Bath spin-out company, Atlas Genetics Ltd. ("Atlas"). Atlas is a medical diagnostics company focused on decentralised, near-patient and point-of-care (POC) testing.[299] In order to achieve rapid disease diagnosis for POC testing, Atlas have been in the process of developing and commercialising the ultra-rapid io™ diagnostic platform. The io™ platform comprises of a small, inexpensive desktop instrument capable of reading test-specific disposable cartridges that combine to provide an accurate test result in around 30 minutes (Figure 2.1). This aims to give clinicians and other healthcare professionals a fully-automated device that enables disease diagnosis without the need for central laboratory testing and the associated long test-to-diagnosis time. Actionable test results that are provided whilst patients are still present are essential for the effective treatment and control of diseases where infection rates are escalating. As a result, Atlas have been initially targeting sexually transmitted infections (STIs), as an estimated one million people acquire a curable bacterial STI every day,[300] and hospital acquired infections (HAIs), which are the cause of almost 99,000 deaths in the United States every year.[301]

Figure 2.1 The ultra-rapid Atlas io™ diagnostic platform that comprises of desktop instrument and disposable cartridge.

2.0.2 Previous Work

Atlas' current proprietary technology involves the biomolecular recognition of target bacterial deoxyribonucleic acid (DNA) in combination with electrochemical endpoint detection.[302] The main advantages of developing an electrochemical biosensor include the specificity, speed, portability and low cost in comparison with optical detection techniques such as colourimetry and fluorescence.[303] In addition, samples do not need to be purified or transparent prior to detection and the instrument does not require complex calibration to maintain accuracy. Miniaturisation has also allowed electrochemical biosensors to be easily adapted for POC detection.[304]
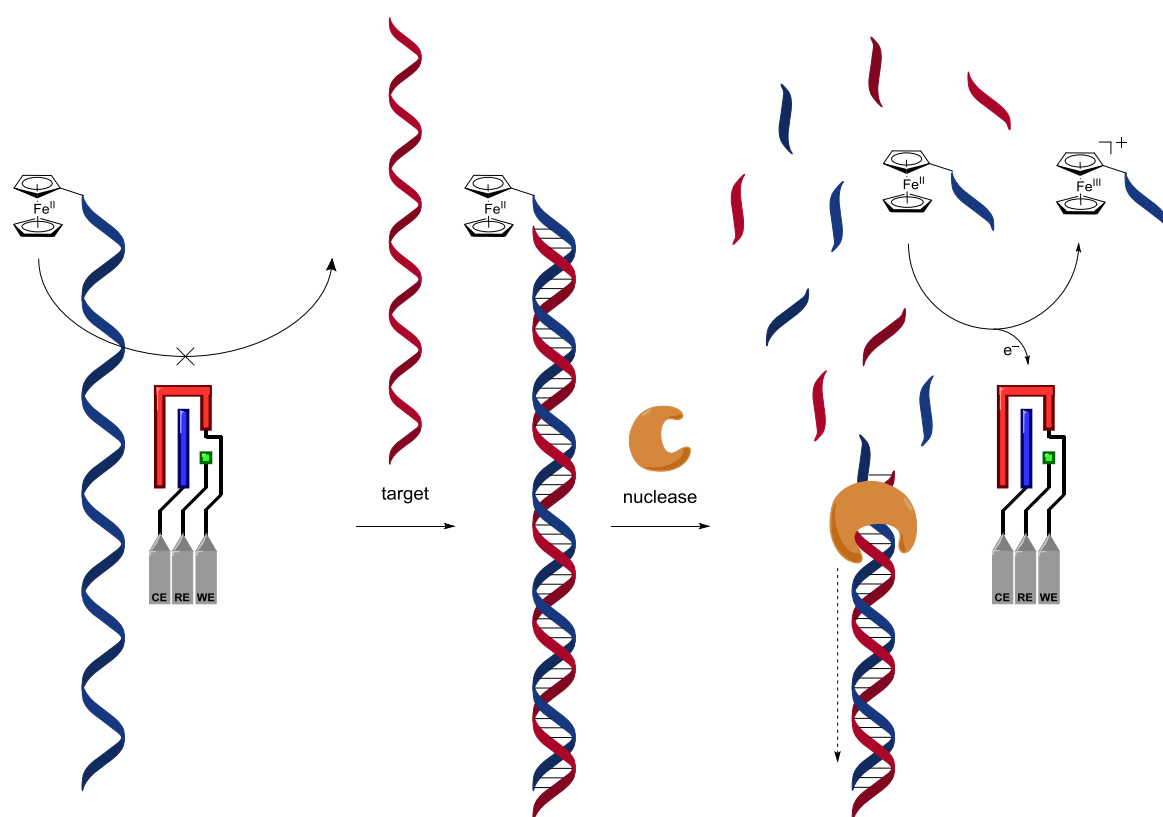
Scheme 2.1 Exonuclease-assisted double-stranded DNA cleavage for electrochemical signal amplification.

In collaboration with Atlas, previous work undertaken in the Frost group involved the development of an amplified electrochemical biosensor for DNA detection. This was demonstrated through the enzymatic digestion of ferrocene-labelled oligonucleotides (Scheme 2.1). Principally, the redox-labelled complementary probe is too large to diffuse to the electrode and as such, a low background current in the absence of the target strand is observed. Upon hybridisation to the target, the resulting DNA duplex is digested by a nuclease enzyme which splits the oligonucleotide into smaller fragments, allowing release of the redox label. The selective digestion of the probe–target complex is accompanied by a large increase in current, demonstrating excellent sensitivity for DNA detection by this method. This has been successfully achieved with both ferrocene-labelled

single-stranded DNA using an endonuclease enzyme,[305] as well as with ferrocene-labelled double-stranded DNA using an exonuclease enzyme.[306] Additional work has focussed on providing further amplification through label dimerisation to double the number of redox labels *per* probe, as well as the development of redox labels with discrete oxidation potentials for multiplex electrochemical DNA detection.[307] So far, through functionalisation of the cyclopentadienyl rings upon the ferrocene as well as a study into the hydrophobicity effect of the linker between the ferrocene and the oligonucleotide,[308] a successful pentaplex has been demonstrated allowing for four nucleic acid-based STIs along with an internal control to be detected in just one voltage sweep (Figure 2.2). Not only this, but the combined autonomous amplification procedures allow the system to obtain a LOD of 25 elementary bodies (EBs), or 3 copies of DNA, *per* sample in just 25 minutes.[309] The research accomplished during this collaboration is now undergoing integration into the Atlas io™ platform which will enable fully-automatable, sensitive, multiplex electrochemical DNA detection for a plethora of bacterial infections from a single sample.
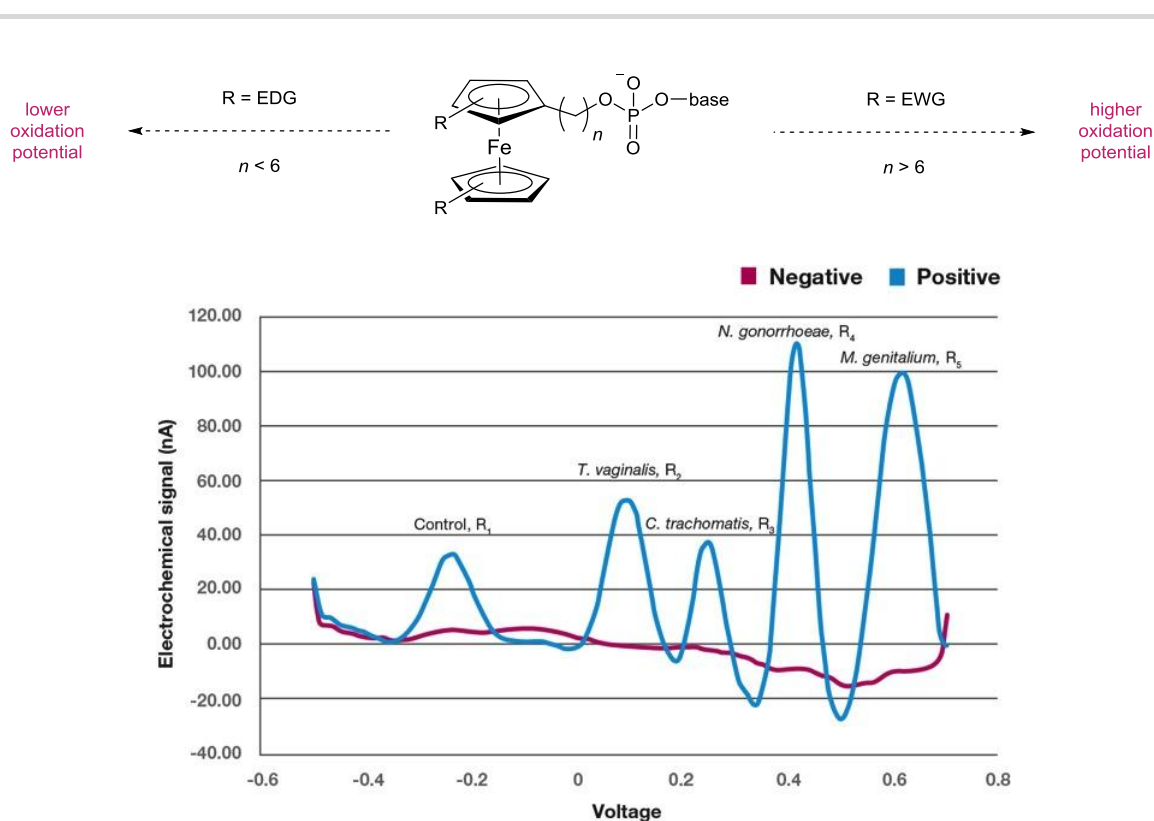
Figure 2.2 Representative pentaplex for the simultaneous electrochemical DNA of four bacterial infections plus an internal control through ferrocene derivatisation.

To complement the existing DNA detection methodology, a sensitive and selective method for electrochemical protein detection that could be utilised within a POC device was required. This would allow for diseases such as syphilis and the human immunodeficiency virus (HIV), both of which have seen sharp increases in recent observed infection rates, to be accurately and rapidly detected.[310] Also, this would allow for the rapid detection of troponin, a protein biomarker for cardiac injury that can be used to diagnose cardiovascular disease or predict an imminent cardiac arrest.[311]

A successful detection assay is dependent upon two key aspects; high selectivity and high sensitivity. High selectivity is required so the assay only delivers a positive signal in the presence of the desired biomarker and due to the complexity of a biological mixture, poor selectivity can easily occur thus leading to false positives. High sensitivity is required to deliver a detectable signal when only a low concentration of the biomarker is present, thus eliminating the possibility of false negatives, and therefore a missed diagnosis, from occurring. For the successful detection of proteins, a number of methods exist such as immunostaining,[312] immunoprecipitation,[313] and immunoelectrophoresis.[314] However, for simplicity, as well as for both high selectivity and sensitivity, the method of choice for this project was the immunoassay.[315] Therefore, the primary objective for this project was to develop an immunoassay with electrochemical endpoint detection tailored for use within a POC device.

2.1   Electrochemical Immunoassays

2.1.1   Background to Immunoassays

The term immunoassay broadly covers any diagnostic assay that uses antibodies as analytical reagents to bind to antigens in a sample solution and produces a detectable signal as a result of this interaction that is proportional to the concentration of the antigen.[316] Historically, the first labelled immunoassays were immunoradiometric assays (IRMA) where antibodies were tagged with radioactive labels which enabled antigen concentration to be determined by radiation.[317] However, due to the obvious safety concern of laboratory personnel being exposed to radiation, along with the need for special facilities, expensive counting equipment and the disposal of radioactive waste, a safer, inexpensive alternative to radiolabels was sought. The successful coupling of antibodies to enzymes without denaturising either component enabled enzymes to be that alternative.[318] Inevitably, the development of enzyme immunoassays (EIA),[319] and the solid-phase derivative enzyme linked immunosorbent assays (ELISA),[320] were reported shortly after this discovery and quickly replaced IRMAs. Since then, EIAs and ELISAs have both been integrated within automated systems and are routinely used within central medical laboratories around the world for the detection of a whole range of analytes.[321]

For non-purified or unprocessed samples, ELISAs are typically more suitable than EIAs as washing steps within the protocol will lead to a lower chance of false positives occurring. However, many types of ELISA formats exist and different enzymes can be used as the enzyme label for signal production.[322] Direct ELISA involves antigen adsorption onto the solid phase prior to antibody–enzyme labelling but as this is an ill-defined process which depends heavily on the antigen, it is often not the most sensitive type.[323] Competitive EIAs are rapid and simple to perform but since they utilise restricted antigen and enzyme concentrations, these benefits are lost when executed on solid-phase as any desorption or denaturisation has a significant impact on these concentrations which leads to signal variability and irreproducibility.[324] Indirect or 'sandwich' ELISAs are often the most selective format as they utilise two antibodies; one absorbed onto the solid-phase for antigen capture and another conjugated to an enzyme for antigen labelling (Scheme 2.2).[325] Although they require extra steps during the protocol, sandwich ELISAs are the standard choice of ELISA format for medical diagnostics purposes due to the unrivalled selectivity it offers.
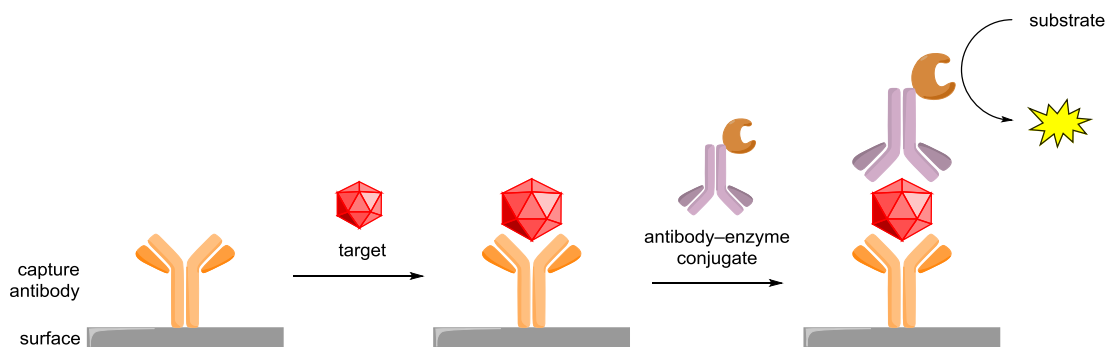
Scheme 2.2 Typical construction of a sandwich ELISA.

Although many enzymes can be successfully conjugated to antibodies, typically only three are used with ELISAs; horseradish peroxidase (HRP), β-D-galactosidase (β-gal) and alkaline phosphatase (ALP).[326] This is due the purity, specificity and sensitivity of the enzyme, as well as the ease of conjugation and the efficacy and stability of the corresponding enzyme–antibody conjugate. HRP is inexpensive, is readily available and importantly, has a high turnover rate.[327] Also, there are a considerable number of chromogenic substrates that have been developed for HRP activity detection which makes it a popular choice within ELISAs that are monitored through spectroscopic means. Comparatively fewer electrochemical substrates for HRP exist as they tend to undergo electro-oxidation or autooxidation in the absence of the enzyme, which leads to high backgrounds and potential false positive results.[328] In addition to the substrate, HRP requires hydrogen peroxide to facilitate oxidation which would add another layer of complexity for integration within an automated system. β-gal is also readily available, inexpensive and easily conjugated to antibodies but has a significantly slower turnover rate in comparison to HRP.[329] Although sensitive chromogenic and fluorogenic substrates have been developed for β-gal

detection, far fewer electrochemical substrates exist.[330] Of the ones that do, they are often derived from highly conjugated organic compounds which, despite having accessible oxidation potentials, are poorly soluble in aqueous media and contribute extensively to electrode fouling, limiting assay sensitivity. ALP has similar attributes to HRP in that it has a very high turnover rate, is readily available and easily conjugated but it is comparatively expensive however.[331] There are also a range of colourimetric, fluorometric and electrochemical substrates that have been developed for ALP making it an ideal choice as the enzyme label within an electrochemical ELISA.

2.1.2 *Electrochemical Substrates for Alkaline Phosphatase*

Once it had been decided that electrochemical biomarker detection was going to be achieved through an ALP-labelled sandwich ELISA, an investigation into previously developed electrochemical substrates for ALP was launched (Figure 2.3). One of the first, and one of the simplest compounds developed as a substrate for electrochemical ALP detection was phenyl phosphate **96** (Scheme 2.3).[332] In the presence of ALP, dephosphorylation of **96** occurs to give phenolate **97** which is oxidised at 670 mV *vs.* Ag/AgCl. The LOD for this detection system was 5 nmolL^{-1}. Despite none of the other assay components being electroactive individually, as a mixture, a large background current was observed at the high potential required for phenol oxidation and as such, **97** had to be separated from the assay mixture by reverse phase liquid chromatography (LC) prior to electrochemical detection.
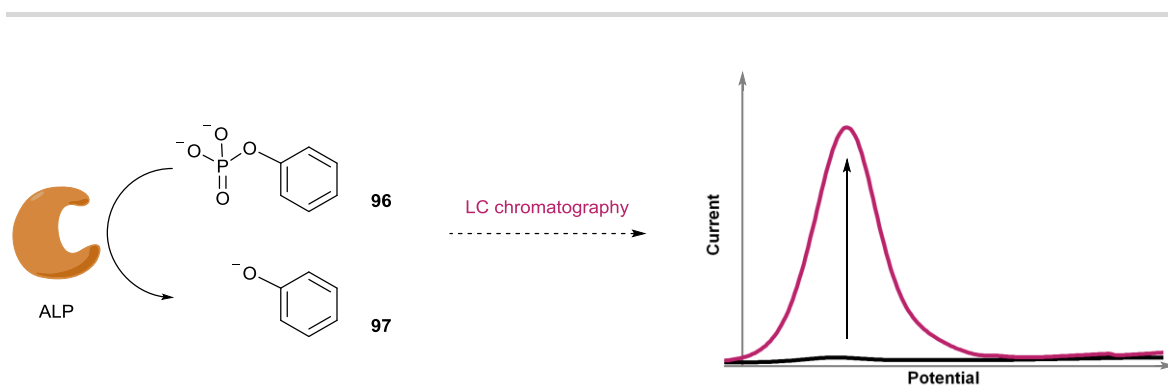
Scheme 2.3 Electrochemical detection of ALP using phenyl phosphate **96** as substrate.

In order to lower the oxidation potential of the hydrolysed product and therefore reduce the high background and remove the need for product separation, electron rich aryl derivatives of phenyl phosphate **96** such as 4-aminophenyl phosphate **98**,[333] 4-hydroxyphenol phosphate **99**,[334] and α-naphthol phosphate **100**,[335] have all been used as electrochemical ALP substrates with the latter often proving to be the most stable and the most sensitive. Reactivity is compromised

however, since electron-rich phenyl phosphates are less reactive towards hydrolysis. In order to increase reactivity, phenyl phosphates with electron-withdrawing groups such as *p*-nitrophenyl phosphate **101**,[336] and *p*-cyanophenyl phosphate **102**,[337] have also been employed as electrochemical substrates for ALP. However, the electrochemical oxidation of phenols generates phenoxy radicals, which are known to undergo radical polymerisation,[338] the main contributor to electrode fouling and leads to subsequent loss of electrochemical sensitivity. To help alleviate this, 3-indoxyl phosphate **103** has also used as an ALP substrate since the product is substantially more stable after oxidation.[339] Despite this, aerobic dimerisation of the enzyme product is required to generate the electroactive species and once formed, the dimer is insoluble in water which again leads to electrode fouling. Hydroquinone diphosphate **104** has been developed as an alternative that has been shown not to produce electrode fouling in electrochemical immunoassays.[340] In addition, the hydroquinone product has a two-electron oxidation at the electrode that produces a significantly larger amperometric response than phenol or α-naphthol. The use of hydroquinone diphosphate **104** has been limited however since it requires two enzyme-catalysed dephosphorylations before the electroactive species is generated and the substrate is also not commercially available.

98, R = NH$_2$
99, R = OH

101, R = NO$_2$
102, R = CN

104, R = OPO$_3{}^{2-}$

100

103

105
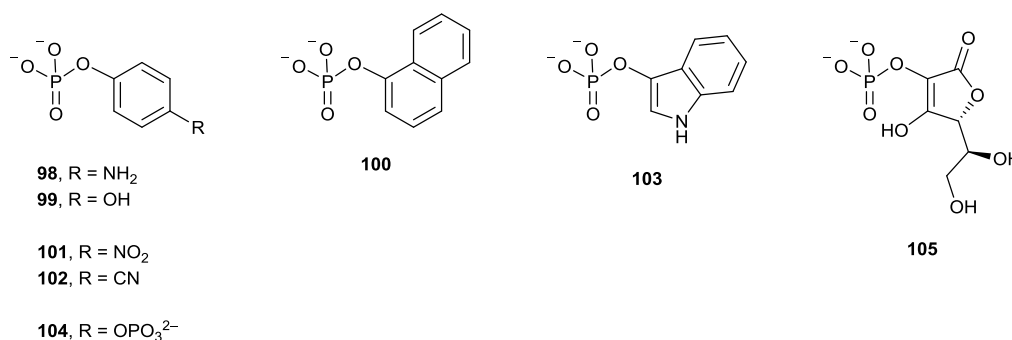
Figure 2.3 Structures of commonly-used organic substrates for electrochemical ALP detection.

One substrate that is commercially available, is L-ascorbic acid 2-phosphate (AA2P) **105** which is a mono-phosphate whose product, ascorbic acid (AA), also has a favourable two-electron oxidation at the electrode and a low oxidation potential of 400 mV *vs.* Ag/AgCl.[341] It has also been shown to be a far superior substrate in comparison to the previous substrates and subsequently, AA2P **105** has been adopted as the industry standard ALP substrate for electrochemical detection.[342] Despite this, AA has a broad oxidation potential range as the electrons given at the electrode are inequivalent. Also, AA requires acidic media to deliver optimal current which conflicts with the optimum pH for ALP activity.[343] To increase AA sensitivity, and electrochemical immunoassays in general, substantial effort has gone into immunosensor fabrication and electrode modification.[344] However, many of these approaches are inapplicable towards integration within a POC test since they are expensive and cannot be easily mass-produced. Therefore, in order to

improve electrochemical immunoassays for application with POC testing, further research needs to be performed regarding electrochemical enzyme substrates.
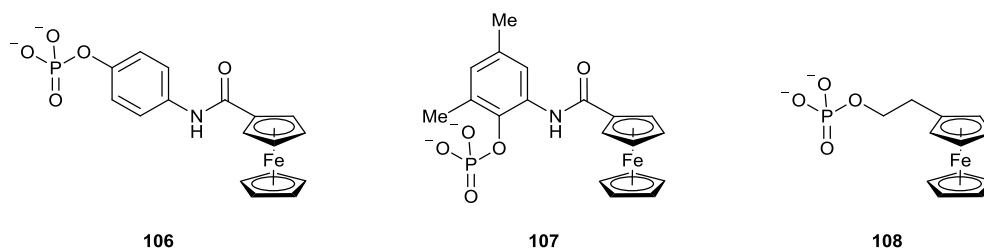
**Figure 2.4** Structures of ferrocene-derived substrates for electrochemical ALP detection.

When designing any electrochemical labels or substrates for biological detection methods, ferrocene is one of the first electroactive species that is considered due to its facile oxidation potential, good stability in aqueous media and compatibility with biological components, as well as being easily derivatised.[345] Despite these excellent attributes, the number of ferrocene-derived substrates for ALP described in the literature to date are limited to just three (Figure 2.4).[346] The first, 4-ferrocenamidophenyl phosphate **106** developed by Bannister *et al.*, had an oxidation potential identical to that of the phenol product at 180 mV *vs.* a saturated calomel electrode (SCE) and successful ALP detection was reliant on the phenol product exhibiting a higher peak current than the starting material.[347] Nevertheless, an ALP concentration of 1.2 pmolL^{-1} could still be detected *via* this method. It was noted therein that in order to obtain further enzymatic amplification, future electrochemical enzyme substrates should be designed so that the product should have a significantly lower oxidation potential than the substrate and that this difference should be approximately 100 to 200 mV so that the oxidation potentials of both substrate and product are electrochemically distinguishable.

The second structurally similar compound, 4-ferrocenamido-4,6-dimethylphenyl phosphate **107**, was developed by Degrand *et al.* as its corresponding phenol product could be separated from **107** by the use of polymer-coated glassy carbon electrode even though they possess the same oxidation potential of 350 mV *vs.* SCE.[348] The increase in hydrophobicity is required as this provided an acceptable separation in comparison with **106** which couldn't be easily separated from the product using the polymer and therefore led to a high background current.[349] An ALP LOD of 2.8 pmolL^{-1} could be achieved by the use of these modified electrodes but due to accumulation of the product within the polymer, the electrodes could only be used once. The third and simplest derivative, 2-(ferrocenyl)ethyl phosphate **108**, was also developed by Limoges and Degrand as a substrate that would allow the polymer-modified electrodes to be re-used.[350] **108** and its corresponding alcohol product 2-(ferrocenyl)ethanol again have the same oxidation potential, 300 mV *vs.* Ag/AgCl, but could still be efficiently separated by the polymer and was capable of being

reused several times *via* cathodic stripping voltammetry without a noticeable drop in sensitivity being observed, with an LOD of this substrate being approximately 2 pmolL^{-1}. Despite the good sensitivity, having to use modified electrodes can be expensive and small changes in polymer thickness can result in fluctuations in sensitivity; factors typically avoided for mass-produced POC tests. To avoid the use of modified electrodes, an electrochemical system whereby substrate and product have distinguishable oxidation potentials, known as ratiometric sensing, would be highly advantageous.

2.1.3   Ratiometric Detection for Point-of-Care Sensing
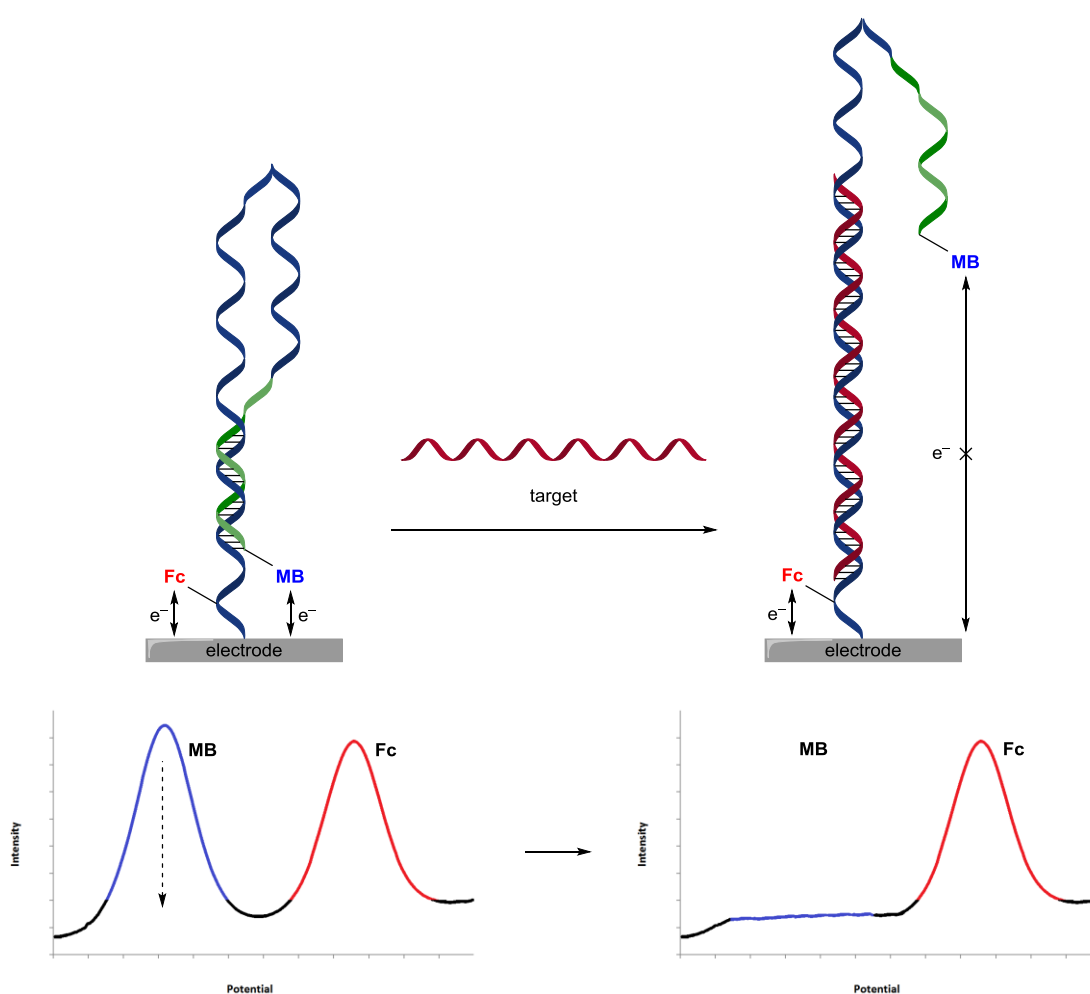
Scheme 2.4 Ratiometric electrochemical DNA detection using gold electrodes modified with a molecular beacon probe labelled at both ends with electroactive tags with unique oxidation potentials.

Despite the vast array of electrochemical biosensors published to date,[351] very few have been integrated within POC devices for a number of reasons, such as reproducibility, robustness and reliability. This is primarily due to problems associated with miniaturisation where variations in

electrode surface area and reagent concentrations are unavoidable yet small changes in either, can lead to a significant change in current. Typically, each new electrode is required to undergo a number of background scans after being installed into a device and the signal produced resulting from an assay would be referenced against this calibration. However, this is a time-consuming method and obviously inapplicable to the POC setting. Since signal intensities can vary dramatically to small differences within the sensing environment such as temperature, pH and polarity, as well as instrument and probe variation, then accurate, quantitative sensing can be difficult to achieve, especially when these differences are amplified within a POC device. To reduce the effect of these variables, a ratiometric detection system is desired.[352]
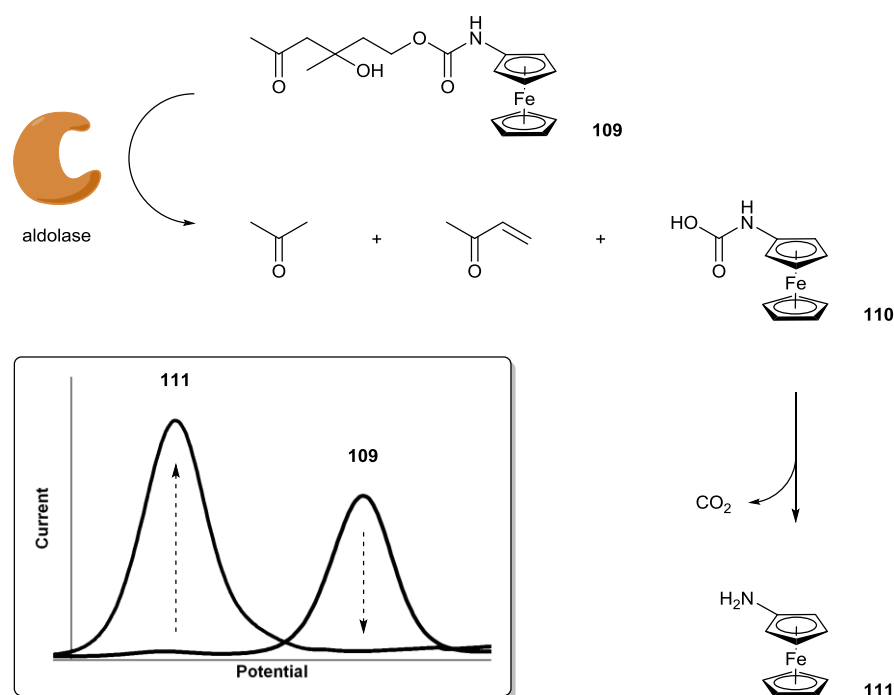
Scheme 2.5 Ratiometric electrochemical detection of aldolase activity where ferrocene-derived enzyme substrate **109** and product **111** have unique oxidation potentials.

With the plethora of organic fluorophores currently available, it is no surprise that the majority of ratiometric sensing platforms are based upon fluorescence detection.[353] Until only very recently, there were no examples whatsoever of ratiometric sensing being performed electrochemically. The first ratiometric electrochemical DNA sensing method was initially developed by Ellington *et al.* (Scheme 2.4),[354] where surface-bound oligonucleotide-derived molecular beacons,[355] were labelled at both ends with electroactive moieties, typically ferrocene (Fc) and methylene blue (MB), that have unique oxidation potentials. In the presence of target DNA, a decrease in current for one label is observed while the other label exhibits a constant current. This in-built internal control allows the electrochemical detection to be a lot more robust,

reproducible and reliable. It is no wonder that these benefits have quickly been exploited towards other ratiometric electrochemical DNA detection systems,[356] and has been extended towards protein,[357–358] heavy metal,[359–360] and small molecule,[361] sensing strategies.

The only example of enzyme activity being measured through ratiometric electrochemical sensing was described by Shabat *et al.* (Scheme 2.5).[362] In this development, ferrocene carbamate **109** was synthesised and exposed to an aldolase antibody. In the presence of the aldoase, substrate **109** undergoes a retro-aldol and a retro-Michael elimination followed by decarboxylation of intermediate **110** to achieve aminoferrocene **111**. Substrate **109** and product **111** were found to have a difference in oxidation potentials of approximately 150 mV and as such, were distinguishable *via* differential pulse voltammetry (DPV). This example was used as the primary inspiration for designing a ferrocene-derivative that could be applied to the ratiometric electrochemical detection of alkaline phosphate.

2.3   Ratiometric Electrochemical Enzyme-Linked Immunosorbent Assay

2.3.1   *Enzyme Substrate Design and Synthesis*
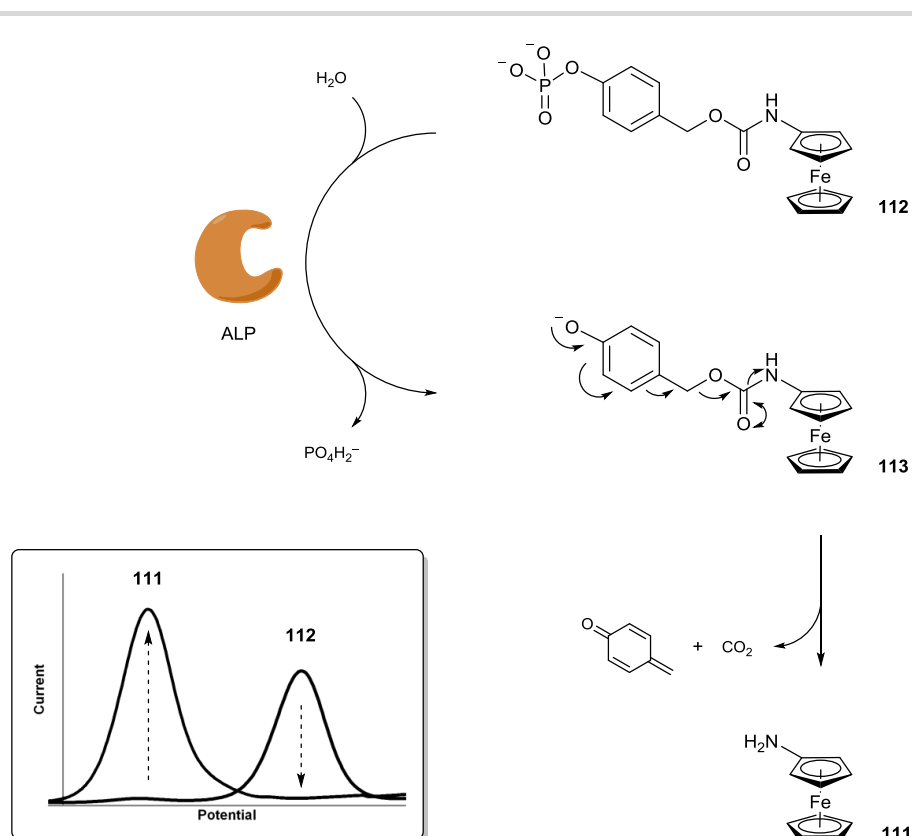
Scheme 2.6 Designed structure of ALP substrate **112** and the proposed elimination mechanism to yield product aminoferrocene **111** where substrate and product should have unique oxidation potentials

In order to achieve the ratiometric electrochemical detection of alkaline phosphatase activity, ferrocene phosphate **112** was designed (Scheme 2.6). It was proposed that in the presence of ALP, enzyme-catalysed dephosphorylation of **112** would first occur. The intermediate phenolate **113** would then be unstable under the basic conditions preferred by the enzyme and would undergo 1,6-elimination followed by decarboxylation to release aminoferrocene **111**. Retrosynthetic analysis of **112** (Scheme 2.7) revealed two key intermediates; ferrocenylisocyanate **115** and benzyl alcohol **116**. Ferrocenylisocyanate **115** could be installed *via* a Curtius rearrangement of ferrocenoyl azide **117**, which in turn could be obtained through a simple functional group interconversion from commercially available ferrocenecarboxylic acid **118**. Since the synthesis of ferrocenylisocyanate **115** is known, the starting point for the investigation was to be the synthesis of the benzyl alcohol.
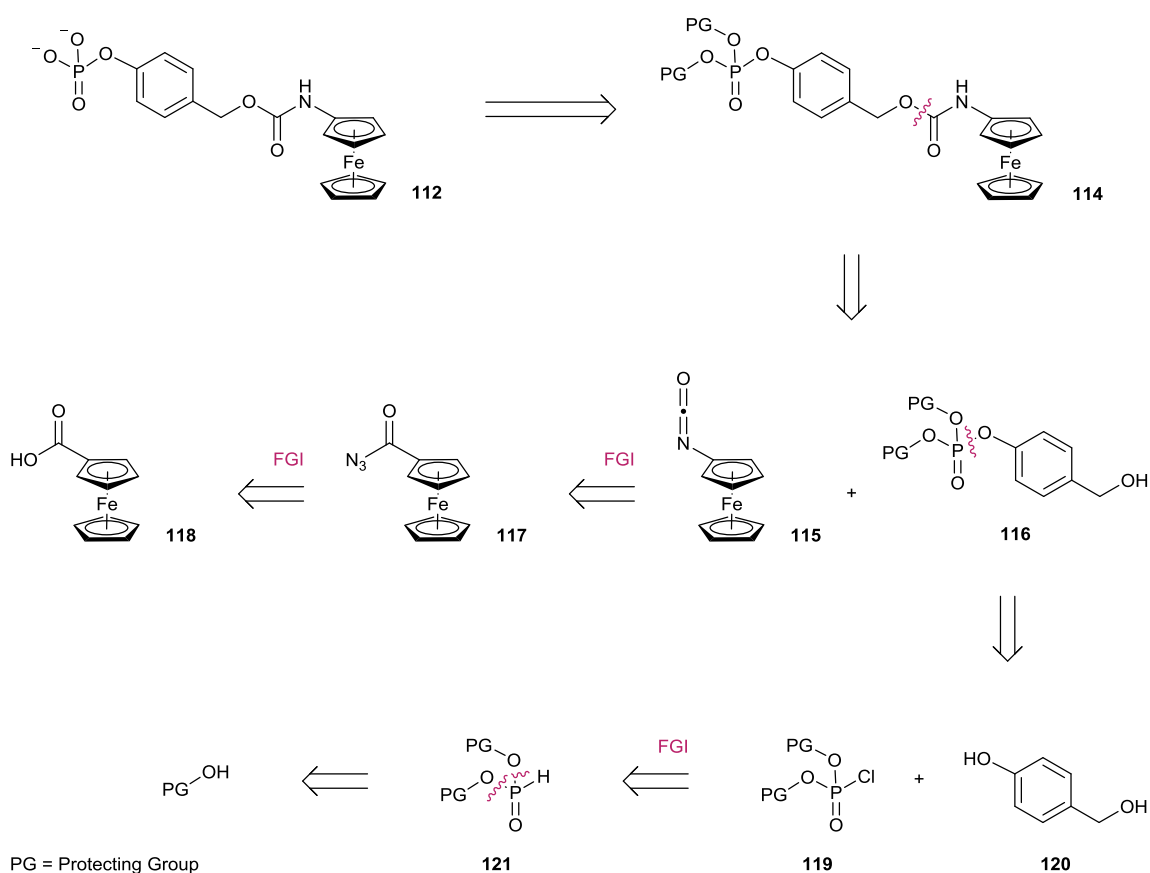
Scheme 2.7 Retrosynthetic analysis of ALP substrate **112**.

Prior to the investigation, there was only one previous example of a benzyl alcohol with a bis-protected phosphate in the *para* position **116**, where the protecting groups could be removed under mild conditions.[363] Therefore, the investigation began with the synthesis of that specific benzyl alcohol **124** where the phosphate is protected with two 2-(trimethylsilyl)ethyl (TMSE) groups (Scheme 2.8). Attempts to reproduce the synthesis of **124** from commercially available 2-(trimethylsilyl)ethanol **122** and 4-hydroxybenzyl alcohol **120** using literature conditions,[364] were

unsuccessful. This is thought to be due to selectivity issues between the phenol and the benzyl alcohol, as well as instability of the protecting groups under purification by silica gel chromatography, known to induce a Peterson elimination of TMSE groups.[365] In the absence of alternatives, further retrosynthetic analysis of the benzyl alcohol was performed (Scheme 2.9).
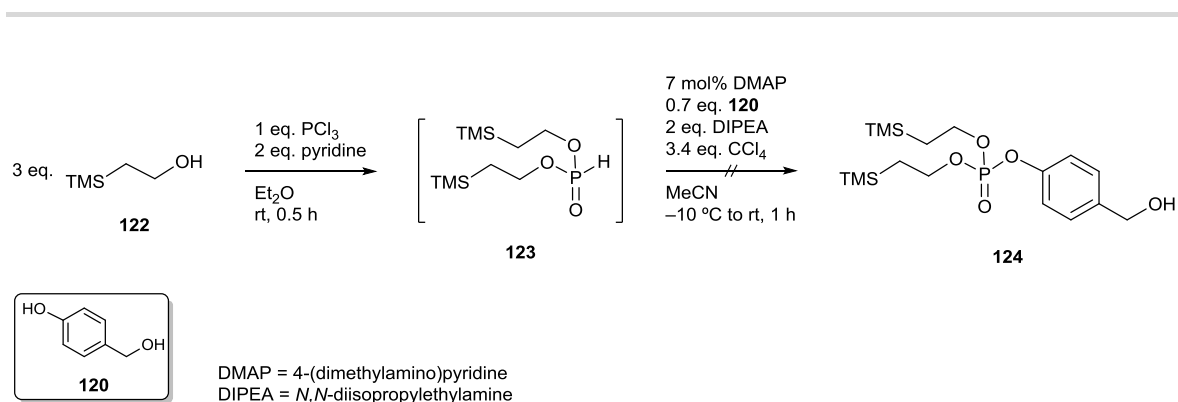

Scheme 2.8 Attempted synthetic route towards bis(TMSE)-protected phosphate **124**.

Selectivity issues could be prevented through masking the alcohol as an aldehyde **125** and the phosphorylated phenol could be simply achieved by combining commercially available 4-hydroxybenzaldehyde **126** with a protected phosphorochloridate. Again, options were limited as the only commercially available phosphorochloridate with protecting groups that could be removed under mild conditions was bis(2,2,2-trichloroethyl (TCE)) phosphorochloridate **127**. Lacking in other choices, phenol **126** and chlorophosphate **127** were reacted together in the presence of base and progress was monitored by thin layer chromatography (TLC) analysis (Scheme 2.10). Despite full consumption of the starting material and the appearance of a new product being observed within 2 hours, only starting material was recovered after silica gel column chromatography. This is attributed to the electron-withdrawing nature of the aldehyde, in combination with the mildly acidic conditions of the silica, activating the phosphate towards undesired hydrolysis upon purification. As an alternative method of purification, recrystallisation of crude **128** was attempted and successfully achieved from hot ether, albeit achieving only 7% yield. Methods to improve on this yield through the use of different solvents and solvent mixtures were unsuccessful. Nevertheless, with benzaldehyde **128** in hand it was taken forward to the next step.

PG = Protecting Group
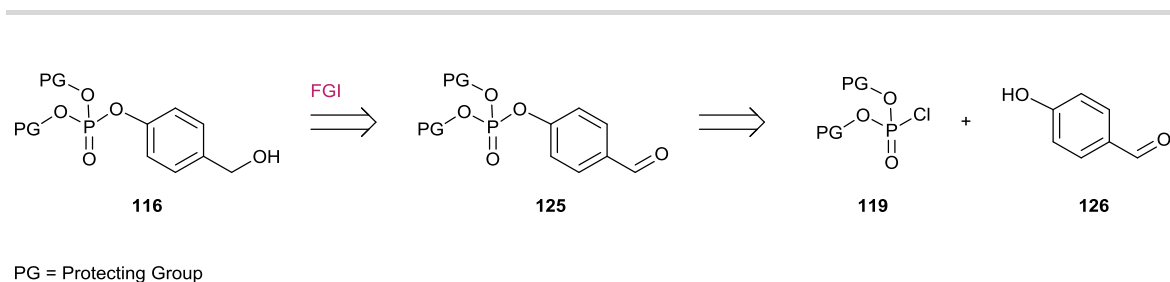
Scheme 2.9 Alternative retrosynthetic analysis of benzyl alcohol **116**.
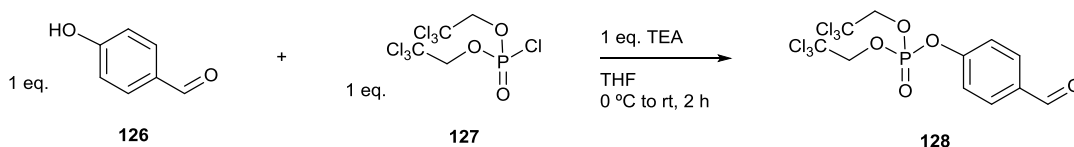
Scheme 2.10 Synthesis of 4-formylphenyl bis(TCE) phosphate **128**.
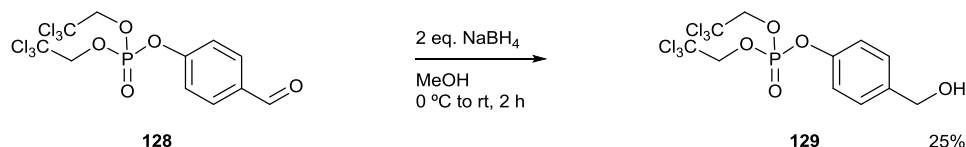
Scheme 2.11 Synthesis of 4-(hydroxymethyl)phenyl bis(TCE) phosphate **129**.

Typically, reduction of benzaldehydes to benzyl alcohols is achieved using sodium borohydride in methanol.[366] However, under these standard conditions; the desired product was only obtained in poor yield (Scheme 2.11). This was thought to be due to the solvent, as methanol could be a strong enough nucleophile to inflict an S_N2 reaction upon the phosphate, especially considering the good leaving group ability of an electron-deficient phenol. Disappointed with 2% overall yield for the two steps, it was decided to take the reaction mixture forward from the phosphorylation step crude, since TLC analysis previously revealed full conversion from starting material to product, and perform the reduction using a different solvent (Scheme 2.12). Thus, telescoping the two reaction procedures and using tetrahydrofuran (THF) as reaction solvent for the reduction delivered benzyl alcohol **129** in a much improved isolated yield over the two steps. In addition, the procedure could be performed on a 4 mmol scale allowing for >1 g of benzyl alcohol **129** to be achieved in a single operation.
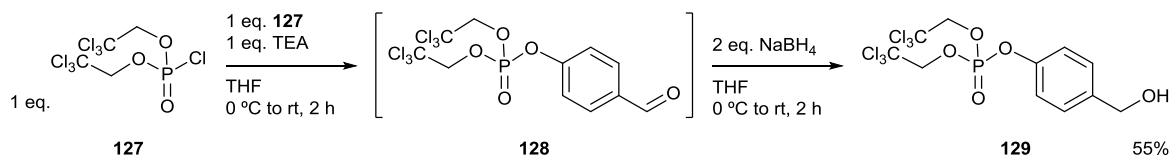
Scheme 2.12 Telescoped synthesis of 4-(hydroxymethyl)phenyl bis(TCE) phosphate **130**.

With the desired benzyl alcohol in hand, the next objective was to couple it with ferrocenoyl azide **117**. Ferrocenoyl azide was synthesised in a straightforward manner from

commercially available ferrocenecarboxylic acid **118** employing a literature procedure (Scheme 2.13).[367] A suspension of **118** was transformed into ferrocenoyl chloride **130** using oxalyl chloride, followed by exposure of crude **130** to sodium azide under Schotten–Baumann conditions,[368–369] to afford ferrocenoyl azide **117** in good yield. With carbonyl azide **117** in hand, it was then necessary to couple it with benzyl alcohol **129** *via* ferrocenyl isocyanate **115** (Scheme 2.14). Thus, **117** was heated to reflux in a sealed vessel to induce a thermal Curtius rearrangement,[370] to obtain isocyanate **115**, which was reacted with benzyl alcohol **129** *in situ* to afford the desired ferrocene carbamate **131** in moderate yield over the reaction sequence.

DMF = *N,N*-dimethylformamide
TBAB = tetrabutylammonium bromide
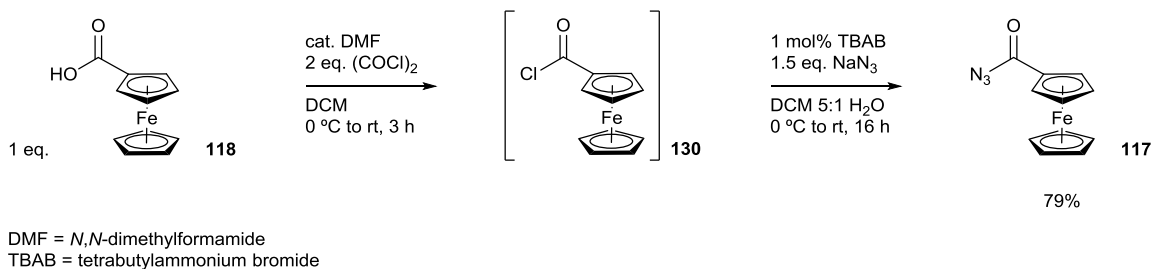
Scheme 2.13 Synthesis of ferrocenoyl azide **117**.
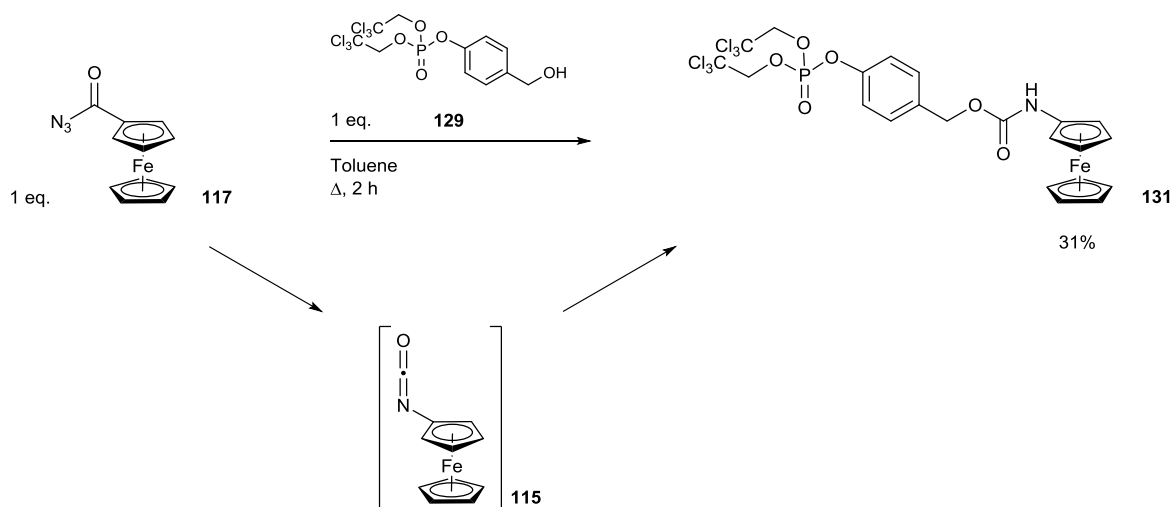
Scheme 2.14 Synthesis of 4-((bis((TCE)oxy)phosphoryl)oxy)benzyl ferrocenylcarbamate **131**.

Deprotection of the TCE protecting groups is typically achieved using zinc or a zinc–copper couple where metal insertion between the carbon–chlorine bond facilitates β-elimination. Therefore, bis(TCE)-protected phosphate **131** was exposed to standard deprotection conditions of zinc powder in pyridine (Scheme 2.15).[371] However, although the desired phosphoric acid **132** was observed by crude ^{31}P NMR, isolation of the product from the excess reactants proved impossible. As such, an alternative protecting group strategy that afforded cleaner deprotection conditions was required.
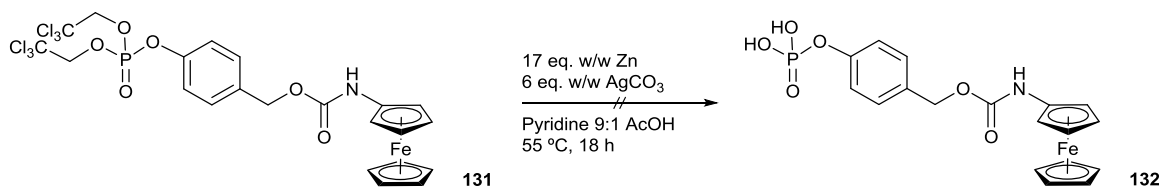
Scheme 2.15 Attempted deprotection of bis(TCE) phosphate **131**.

Having exhausted all of the commercial sources of phosphorochloridates, retrosynthetic analysis revealed that they can be obtained from the corresponding protected phosphites (Scheme 2.7). Although many are commercially available, only dibenzyl phosphite **133** possessed easily removable protecting groups and was subsequently used as the starting material for the synthesis of dibenzyl phosphorochloridate **134**. Phosphites are known to be easily transformed to their corresponding phosphorochloridates through simple treatment with *N*-chlorosuccinimide (NCS) in high yield.[372] Due to the high reactivity and instability during purification of phosphorochloridates, it was decided to react **134** immediately once synthesised with phenol **126** in order to prevent loss of yield. Also, since it has already been discovered that 4-formylphenyl phosphates are unstable to silica gel column chromatography, it was also decided to reduce the crude aldehyde **135** product once formed. Thus, in a highly telescoped procedure, dibenzyl phosphorochloridate **134** was synthesised through electrophilic chlorination of commercially available dibenzyl phosphite **133** with NCS and was subsequently used to phosphorylate 4-hydroxybenzaldehyde **126** (Scheme 2.16). The dibenzyl (4-formylphenyl) phosphate **135** formed was then reduced with sodium borohydride to furnish the desired dibenzyl (4-(hydroxymethyl)phenyl) phosphate **136** in good overall yield over the three steps. With **136** in hand, it was reacted with ferrocenoyl azide **117** *via* the Curtius rearrangement to form the desired dibenzyl-protected ferrocene phosphate **137** in moderate yield (Scheme 2.17).

NCS = *N*-chlorosuccinimide
TEA = triethylamine
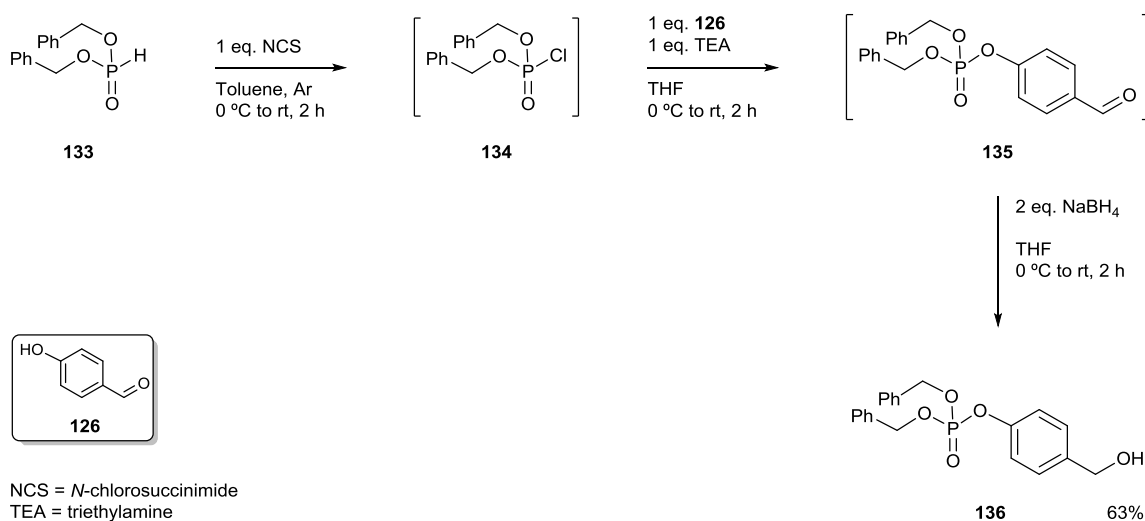
Scheme 2.16 Telescoped synthesis of dibenzyl (4-(hydroxymethyl)phenyl) phosphate **135**.
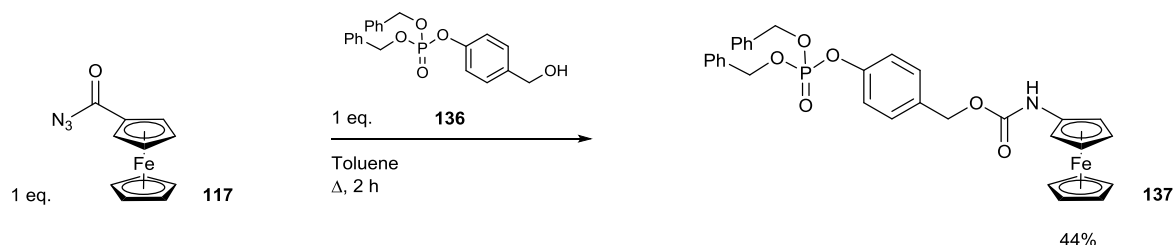
**Scheme 2.17** Synthesis of dibenzyl (4-(hydroxymethyl)phenyl) phosphate **136**.

Benzyl ether deprotection is typically achieved through hydrogenolysis catalysed by a heterogeneous metal source such as palladium on carbon.[373] As such, dibenzyl-protected phosphate **136** was subjected to standard hydrogenolysis conditions of catalytic palladium on carbon in a protic solvent under an atmosphere of hydrogen (Scheme 2.18). Although full consumption of starting material was seen, the desired deprotected phosphoric acid **132** was not observed. Instead, aminoferrocene **111** was isolated as the major product due to the concurrent hydrogenation of the benzyl linker. Since the linker is unstable towards the deprotection conditions, an orthogonal protecting group was required.
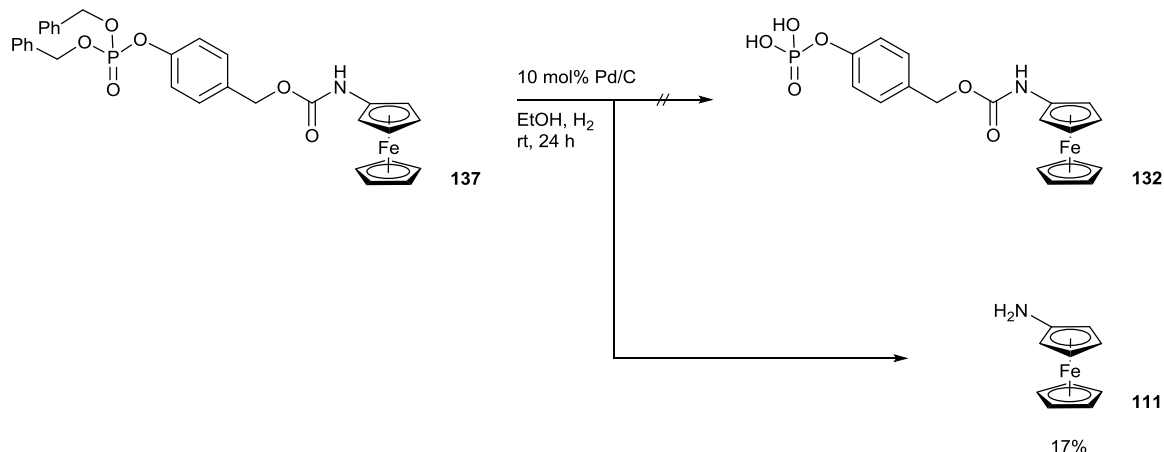
Scheme 2.18 Attempted deprotection dibenzyl phosphate **136**.

With no other phosphites bearing two protecting groups remaining that were commercially available, it was necessary to synthesise them. Retrosynthetic analysis showed that they can be easily obtained through the reaction of phosphorous trichloride with two equivalents of an alcohol (Scheme 2.7).[374] Thus, the synthesis of hydrogen phosphites bearing two functional groups that could be removed under mild conditions were attempted. The intermediate phosphites are known to be synthesised in high yield and in good chemical purity and are often taken forward crude to the next step.[375] As such, the procedure for constructing the phosphites was attached to the beginning

of the already highly telescoped procedure for the synthesis of the 4-(hydroxymethyl)phenyl phosphates (Scheme 2.19).
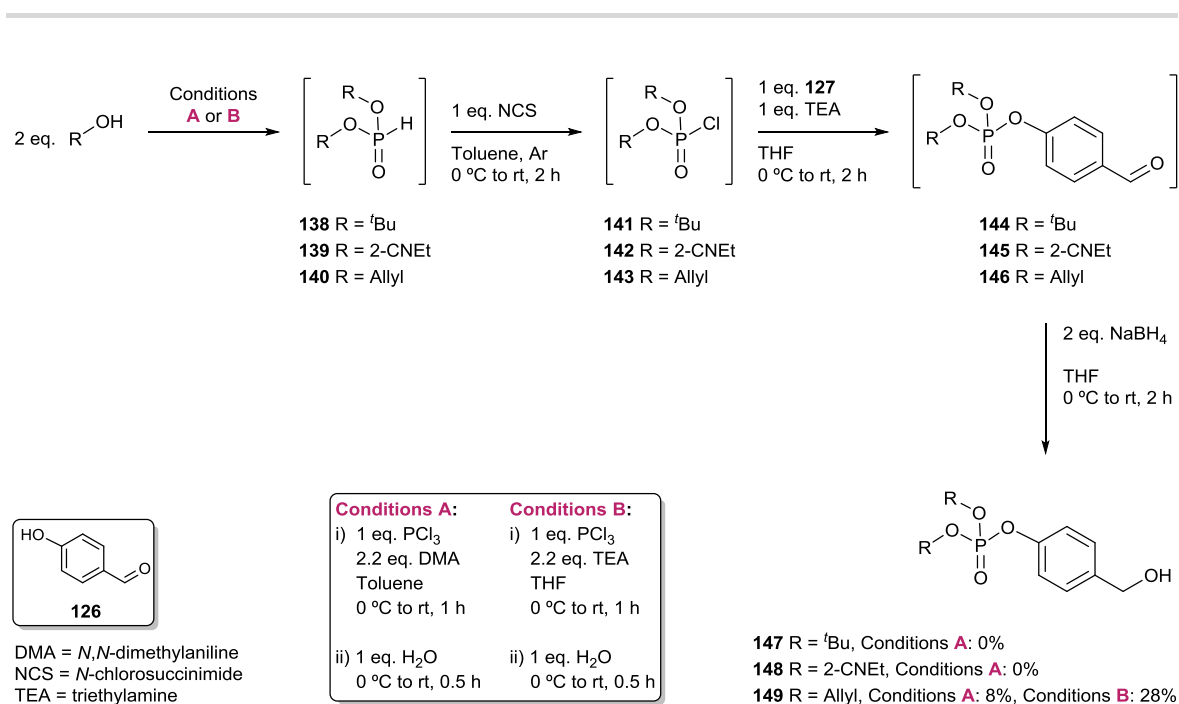

Scheme 2.19 Synthetic route to obtain protected (4-(hydroxymethyl)phenyl) phosphates bearing orthogonal protecting groups.

Firstly, *tert*-butyl alcohol was employed as the alcohol since phosphates bearing *tert*-butyl groups can be removed in strong, dry acid.[376] However, the desired dibutyl-protected phosphate was not observed *via* this method as the bulky *tert*-butyl groups sterically prevent an S_N2 reaction at the phosphorous centre of **141** from occurring during the phenol phosphorylation step. Secondly, 3-hydroxypropionitrile was used as the alcohol as cyanoethyl groups can be removed from phosphates through simple treatment with 1,8-diazabicyclo[5.4.0]undec-7-ene (DBU).[377] However, once again the desired bis-cyanoethyl-protected phosphate was not observed due to the high water solubility of the intermediate phosphite **139** and as such, was unable to be extracted. Thirdly, allyl alcohol was tried as the protecting group-containing alcohol as palladium-catalysed phosphate deallylation can be easily performed under acidic conditions.[378] Pleasingly, the desired diallyl-protected phosphate **149** was obtained from this highly telescoped procedure, albeit in poor yield. By changing the solvent and the base used in the phosphite synthesis to facilitate an easier extraction, the isolated yield was trebled over the four steps. In addition, the introduction of a hydroxide workup after the aldehyde reduction removes any unreacted 4-hydroxybenzylalcohol **120**, which greatly simplifies purification since co-elution of **120** with product **149** was unavoidable. The procedure could also be scaled up to 50 mmol scale to allow 4 grams of diallyl phosphate **149** to be obtained in a single operation.
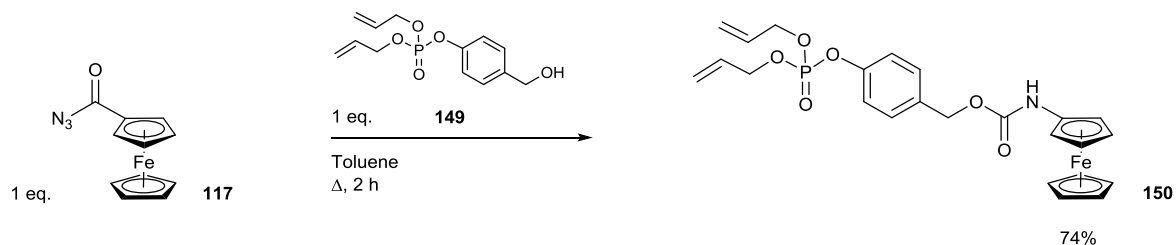
Scheme 2.19 Synthesis of 4-((bis(allyloxy)phosphoryl)oxy)benzyl ferrocenylcarbamate.

With another bis-protected 4-(hydroxymethyl)phenyl phosphate in hand, **149** was reacted with ferrocenoyl azide **117** in an identical manner as previous and the desired ferrocenylcarbamate **150** was obtained cleanly in good yield (Scheme 2.19). Next, **150** was exposed to a number of palladium-catalysed deallylation procedures which were analysed by ^{31}P NMR (Table 2.1).
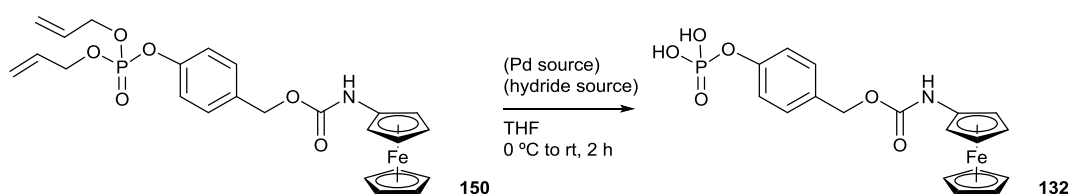

Pd Source	Hydride Source	^{31}P NMR Conversion (%) [a]
10 mol% Pd(PPh$_3$)$_4$	2 eq. Et$_3$SiH, 2 eq. AcOH	>99%
10 mol% Pd(PPh$_3$)$_4$	10 eq. TEA, 15 eq. HCOOH	>99%
10 mol% Pd nanoparticles	10 eq. TEA, 15 eq. HCOOH	0%
10 mol% Pd EnCat®	10 eq. TEA, 15 eq. HCOOH	decomp.
10 mol% Pd/C	10 eq. TEA, 15 eq. HCOOH	decomp.
10 mol% Pd/silica	10 eq. TEA, 15 eq. HCOOH	~30% [b]
polymer-bound Pd(PPh$_3$)$_4$	10 eq. TEA, 15 eq. HCOOH	>99%
polymer-bound Pd(PPh$_3$)$_4$	2 eq. ^{n}Bu$_3$SnH	decomp.
polymer-bound Pd(PPh$_3$)$_4$	10 eq. NH$_4$OOCH	0%

[a] estimated using relative peak heights. [b] mono-deprotected phosphate.

Table 2.1 Palladium-catalysed deprotection of bis(allyl)-protected ferrocenylcarbamate **150**.

Initially, literature conditions using catalytic tetrakis(triphenylphosphine) palladium with triethylsilane as the reducing agent afforded complete conversion of starting material **150** to product **132**.[379] However, problems with isolation of phosphoric acid **132** from the catalyst as well as silyl by-products prompted a cleaner alternative. Fortunately, replacing the silane with transfer

hydrogenation conditions of triethylamine (TEA) and formic acid also delivered complete conversion.[380] Removing the catalyst from the product though still proved problematic so therefore, a range of heterogeneous palladium catalysts were screened which would enable catalyst removal to be achieved simply by filtration. The use of palladium nanoparticles just returned starting material, while encapsulated palladium and palladium on carbon both led to decomposition of **150**, possibly due to hydrogenolysis of the benzyl linker. Palladium on silica showed improved reactivity as small conversion to the mono-deallylated product was observed. Gratifyingly, polymer-supported tetrakis(triphenylphosphine) palladium delivered quantitative conversion and was easily removed by simple gravity filtration. Efforts to enable a simpler purification through the use of different hydride sources such as tributyltin hydride,[381] and ammonium formate,[382] only decomposed or returned starting material respectively.
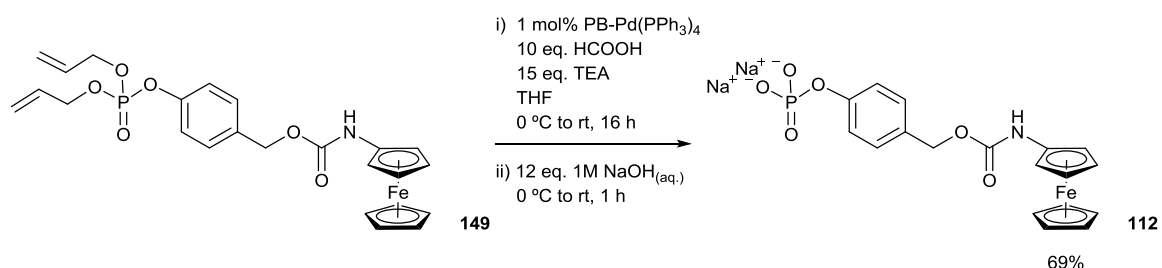
Scheme 2.20 Optimised synthesis of 4-(((ferrocenylcarbamoyl)oxy)methyl)phenyl phosphate **112**.

Unable to purify phosphoric acid **132** through silica gel column chromatography without decomposition, the phosphate salt **112** was prepared to allow purification through alternative means. Thus, treatment of crude **132** with twelve equivalents of 1M sodium hydroxide provided **112**, along with ten equivalents of sodium formate (Scheme 2.20). Although methods for the attempted recrystallisation of **112** proved unsuccessful, purification of **112** could be achieved *via* preparative reverse phase C_{18}-silica gel column chromatography. Furthermore, the catalytic loading of the polymer-bound palladium could be reduced to 1 mol% yet still achieve quantitative ^{31}P NMR conversion for the deprotection despite the reaction time needing to be extended to 16 hours. With the designed ratiometric substrate now successfully synthesised and isolated, it was necessary to establish whether **112** would act as an appropriate substrate for ALP.

2.3.2   *Mechanistic, Electrochemical and Stability Studies*

In order to determine if designed substrate **112** could be hydrolysed by ALP, it was decided that enzyme and substrate should simply be combined in a buffered solution and any interaction between the two components could be monitored by ^{31}P NMR. Due to the seemingly different

magnetic environments of the substrate compared with the released phosphate, it was thought that the peak shifts of the two would be distinguishable on a ^{31}P NMR spectrum. When a 20 mM solution of **112** was exposed to 10 UmL[−1] of ALP, a single peak at 2.7 ppm was observed after 12 minutes which differed from the peak position of 0.1 ppm for **112**. However, to confirm that the appearance of the new peak coincides with the disappearance of the substrate peak, ALP concentration was reduced to 2 UmL[−1] which would allow the reaction to be monitored in greater detail (Figure 2.5). Over time, the peak corresponding with the **112** slowly disappears and the peak corresponding with the released phosphate appears at the same rate. In a background experiment where a solution of **112** is monitored by ^{31}P NMR over time in the absence of the enzyme, no released phosphate peak is observed confirming that dephosphorylation of **112** occurs selectively in the presence of the enzyme. Due to the requirement for a protic buffer, other reaction products such as quinone methide, its water-trapped derivative 4-hydroxybenzyl alcohol **120**, or aminoferrocene **111** could not be detected by ^{1}H NMR. An attempt to scale up the reaction and extract **111** from the buffer in order to confirm its release from the linker in the presence of ALP was unsuccessful.
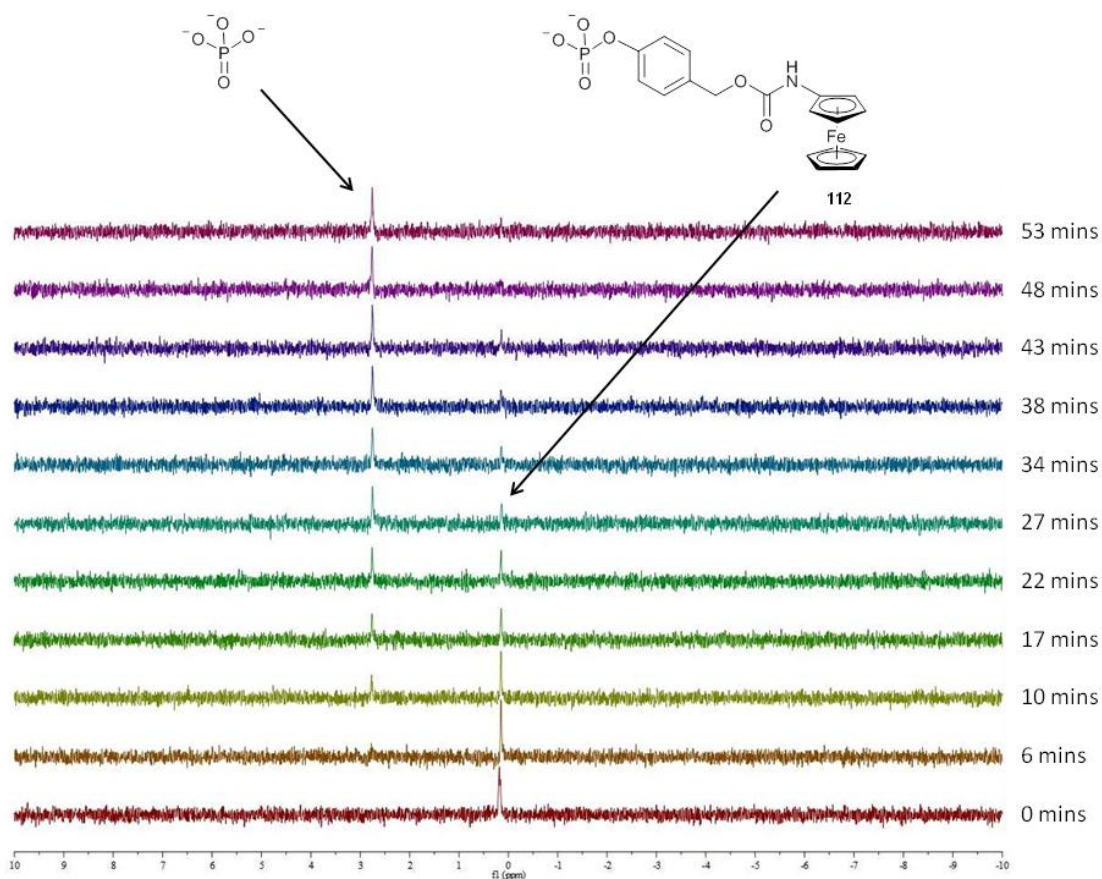
Figure 2.5 Stacked ^{31}P NMR spectra of enzyme substrate **112** over time after the addition of ALP.
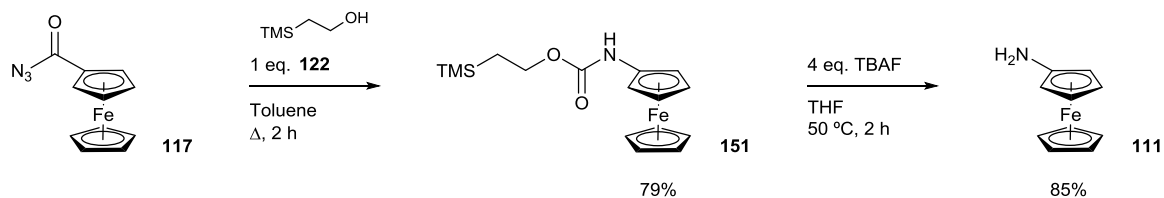
Scheme 2.21 Synthesis of aminoferrocene **111** from ferrocenoyl azide **117** *via* ferrocenylcarbamate **151**.
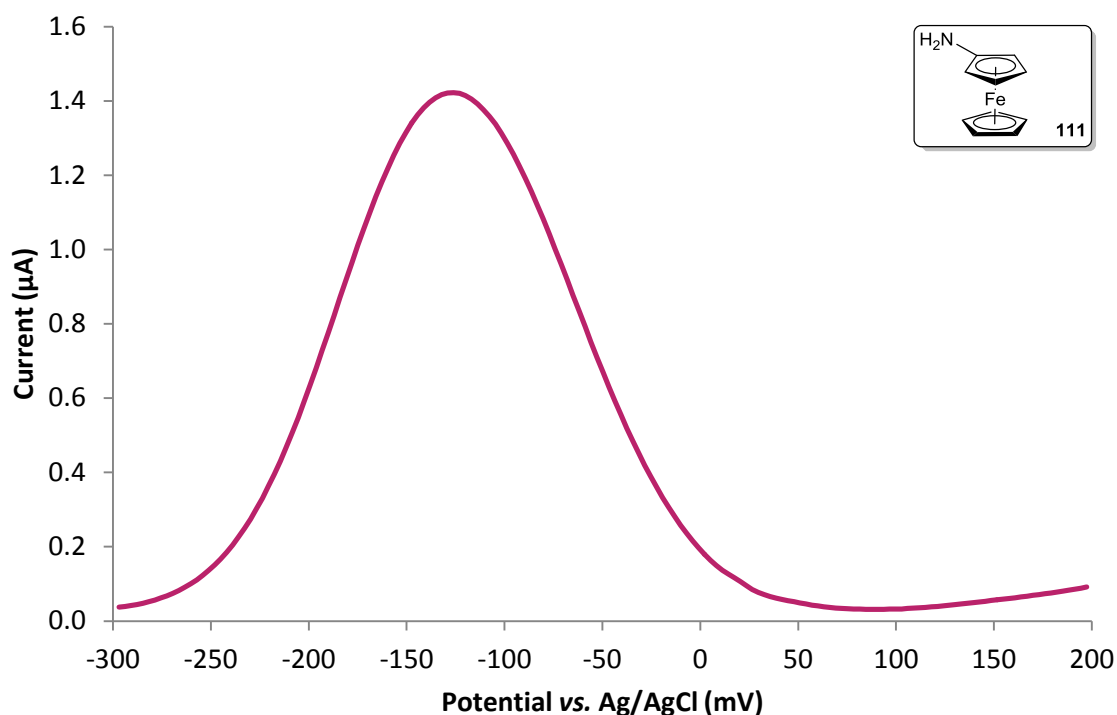
Figure 2.6 Differential pulse voltammogram of a 1 mM solution of aminoferrocene **111** in pH 9 Tris buffer.

To identify whether aminoferrocene **111** was being released from the linker subsequent to enzyme-catalysed dephosphorylation, an authentic sample of **111** was to be synthesised and its oxidation potential compared with that of the reaction between **112** and ALP. Thus, aminoferrocene **111** was synthesised in good yield according to a literature procedure and its spectroscopic data was shown to be identical with that of literature precedent (Scheme 2.21).[383] With aminoferrocene successfully synthesised, separate solutions of ALP substrate **112** and ALP product **111** in pH 9 Tris buffer, an optimal buffer for ALP activity,[384] were made up and subjected to electrochemical analysis. Using differential pulse voltammetry (DPV), a 1 mM solution of aminoferrocene **111** was found to have an oxidation potential of −130 mV *vs.* Ag/AgCl (Figure 2.6), whereas ALP substrate **112** was found to have an oxidation potential of 85 mV *vs.* Ag/AgCl (Figure 2.7). A difference in oxidation potential of 215 mV between substrate and product suggests

that both should be electrochemically distinguishable and in order to determine this, an equimolar solution of **111** and **112** was exposed to electrochemical analysis (Figure 2.8).
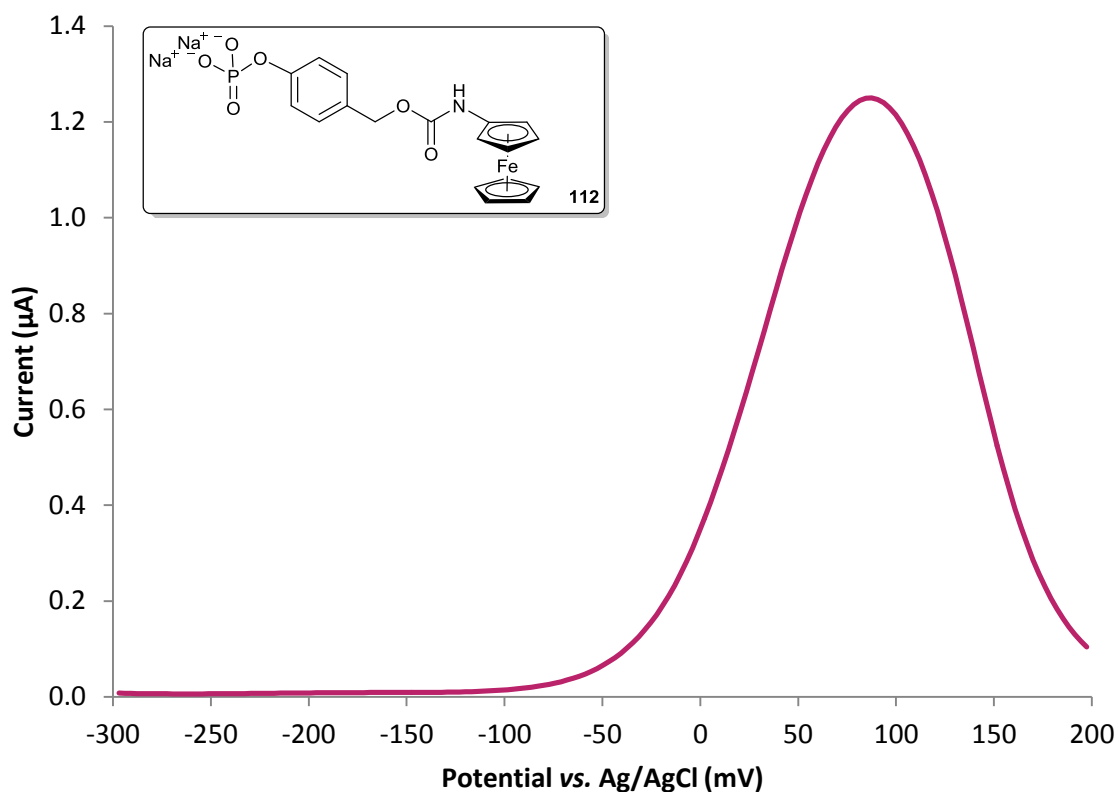
Figure 2.7 Differential pulse voltammogram of a 1 mM solution of ALP substrate **112** in pH 9 Tris buffer.

As desired, both substrate and product were distinguishable electrochemically and as such, allows for reaction conversions to be obtained through peak integration in a similar manner that organic reaction conversions can be calculated through peak integration of ^{1}H NMR spectra. Thus, at any given time point, the enzyme-catalysed conversion of **112** to **111** can be calculated by the following equation:

$$\text{Conversion (\%)} = \left(\frac{\int \mathbf{111}}{(\int \mathbf{111} + \int \mathbf{112})} \right) \times 100$$

To test this and to confirm whether aminoferrocene **111** is released as a result of ALP acting upon the substrate, a 1 mM solution of **112** was treated with 1000 UL^{-1} of ALP and stirred for 30 minutes, which is the acceptable waiting period for a POC diagnostic test result (Scheme 2.22).[385] After this time, a sample was taken and analysed electrochemically. Pleasingly, quantitative conversion of substrate to product was observed as only one peak at −130 mV corresponding to aminoferrocene **111** was apparent on the voltammogram. Importantly, a repeat reaction in the

absence of the enzyme showed no conversion after 30 minutes as only one peak at 85 mV corresponding to substrate **112** was seen on the voltammogram.
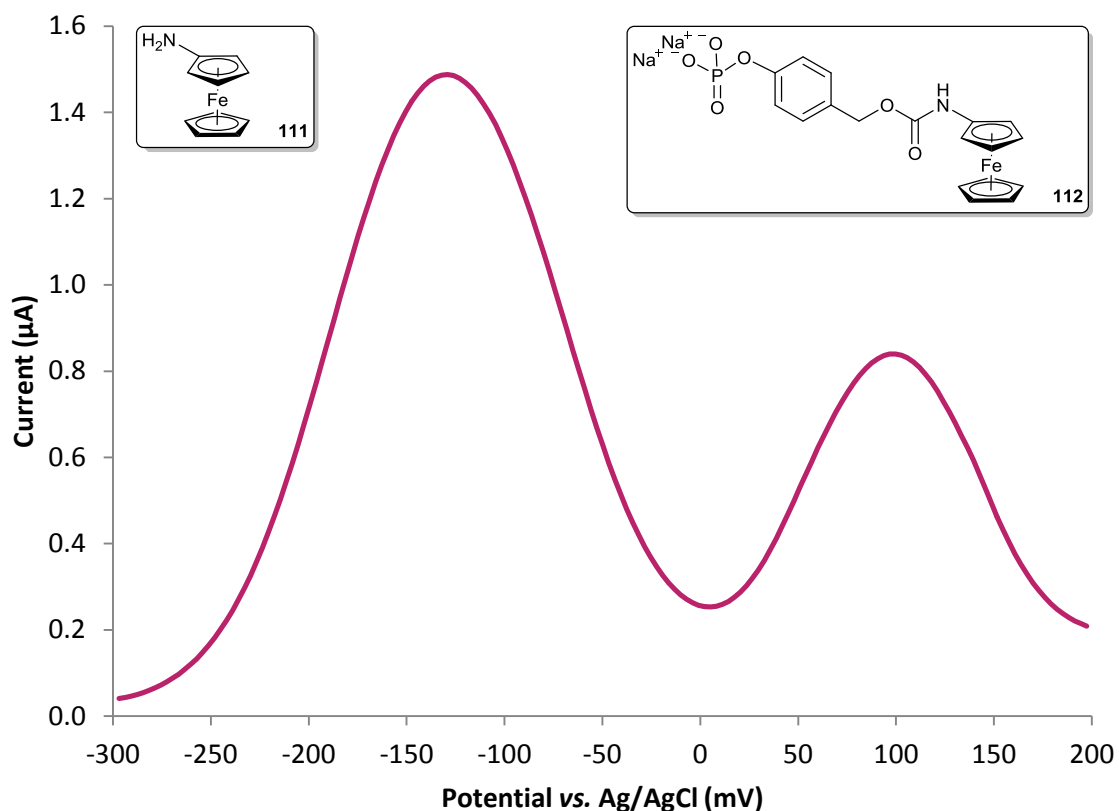
Figure 2.8 Differential pulse voltammogram of a solution containing 0.5 mM of **111** and 0.5 mM of **112** in pH 9 Tris buffer.
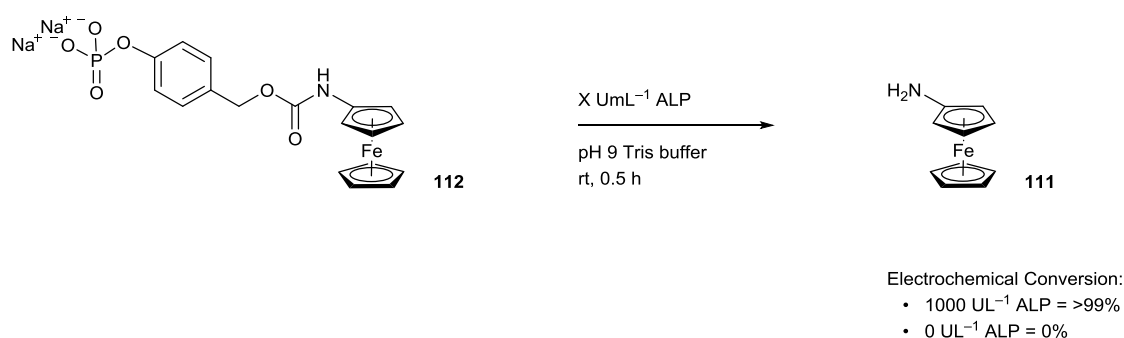
Scheme 2.22 Electrochemically-determined conversion of a 1 mM solution of enzyme substrate **112** to enzyme product **111** in the presence, and absence, of ALP.

Although no conversion was seen without the enzyme, it was necessary to perform stability studies upon substrate **112** as unwanted hydrolytic degradation could occur and lead towards false positive results. Two stability studies were performed; one solid in a screw-top vial and one in buffered solution at various concentrations (Table 2.2). After twelve months at room temperature,

the solid enzyme substrate had exhibited a colour change from orange to brown but only showed 30% degradation to aminoferrocene as determined electrochemically. This is assumed to be due to adventitious hydrolysis of the substrate by atmospheric moisture and as such, subsequent storage of **112** has been in a desiccator to maintain compound purity. In solution, substrate **112** showed excellent stability at high concentrations in buffer with minimal degradation observed after 5 weeks. However, at more dilute concentrations, degradation is more apparent as full degradation of the substrate is seen within 3 weeks. As a result, subsequent ALP detection assays were performed using a solution of **112** made from a stock 10 mM concentration that was freshly prepared every week.

Storage Time	Concentration of **112**		
	1 mM	0.1 mM	0.01 mM
21 days	0.5%	17%	100%
35 days	1%	48%	100%

Table 2.2 Degradation of **112** at various concentrations in pH 9 Tris buffer at room temperature.

Having achieved the selective ratiometric electrochemical detection of ALP and established that enzyme detection occurs through the proposed mechanism also in addition to substrate stability, the next objective was to optimise the detection assay in order to attain the lowest LOD possible.

2.3.3   Optimisation of the Enzyme Detection Assay

Pleased with obtaining quantitative conversion in the presence of ALP after 30 minutes, the reaction was repeated and monitored over time to determine the efficiency of the assay (Figure 2.9). In addition, the concentration of enzyme was gradually lowered to identify the detection limit of the current conditions. It was discovered that at the high concentration of ALP of 1000 UL^{-1}, quantitative conversion was actually achieved within 6 minutes. Enzyme concentrations of 250 UL^{-1} or higher, also delivered quantitative conversion within the 30 minute timeframe. Under these assay conditions, no conversion was seen in the absence of the enzyme and as such, a LOD of 5 UL^{-1} could be obtained.

An investigation into how the rate of reaction changes with enzyme substrate concentration, known as Michaelis–Menten analysis,[386–387] was next to be performed. To do this, a standard enzyme concentration of 100 UL^{-1} was chosen to identify any increase or decrease in rate

was observed with increases or decreases in substrate concentration. Substrate concentrations either side of 1 mM were made and tested against the standard ALP concentration and the reaction was again monitored over time (Figure 2.10). Increasing the substrate concentration from 1 mM does not significantly improve the rate of reaction as at this concentration of enzyme, all molecules of enzyme are in the form of the enzyme–substrate complex and is therefore approaching the maximum rate, V_{max}. However, decreasing the substrate concentration led to an increase in conversion and concentrations lower than 0.25 mM delivered quantitative conversion within 30 minutes. Lowering the concentration further to 0.05 mM allowed for 100 UL^{-1} of ALP to give full conversion within just 9 minutes. Unfortunately, due to the rapid conversion observed and infrequent sampling, initial rates cannot be calculated and as such, the maximum rate V_{max} and the Michaelis constant K_M, for ALP could not be obtained *via* this method. Substrate concentrations lower than 0.05 mM were unable to give a strong enough signal to enable conversion to be calculated. Although there was minimal difference in rate between 0.05 mM and 0.5 mM substrate concentration, a concentration of 0.5 mM was the concentration taken forward and used in subsequent assays due to the significant increase in the observed current as well as improved reliability when calculating conversions.
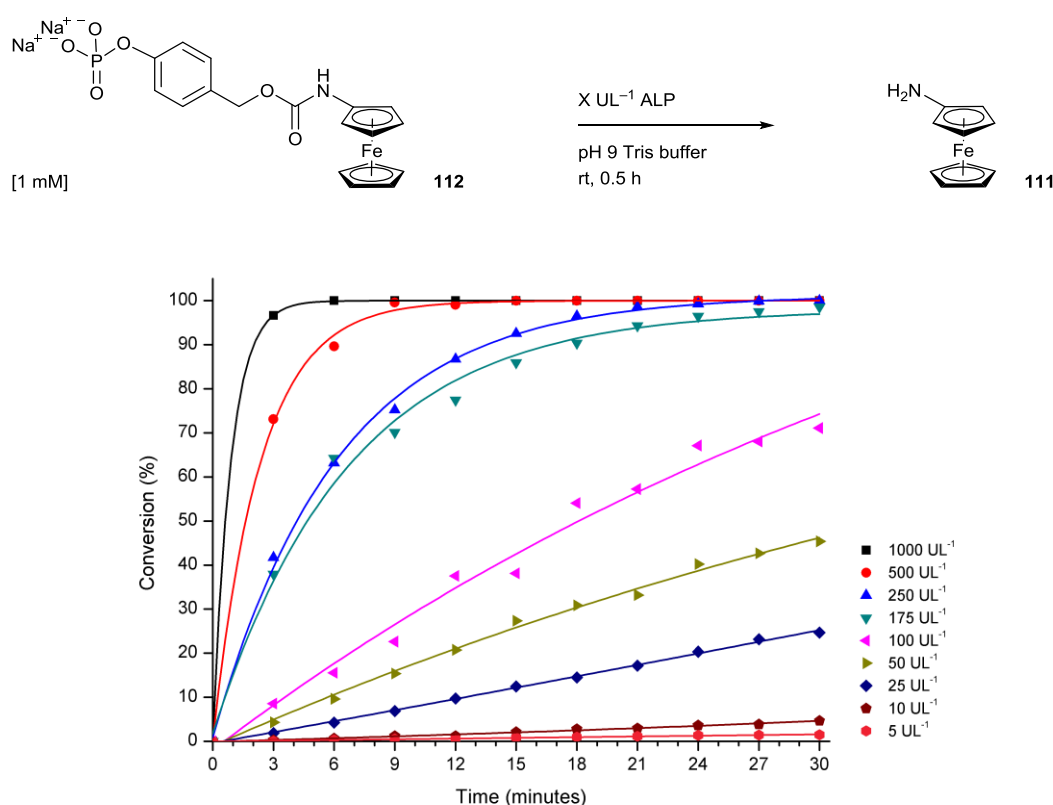

Figure 2.9 ALP-catalysed conversion of enzyme substrate **112** to enzyme product **111** in the presence of different concentrations of ALP at room temperature.
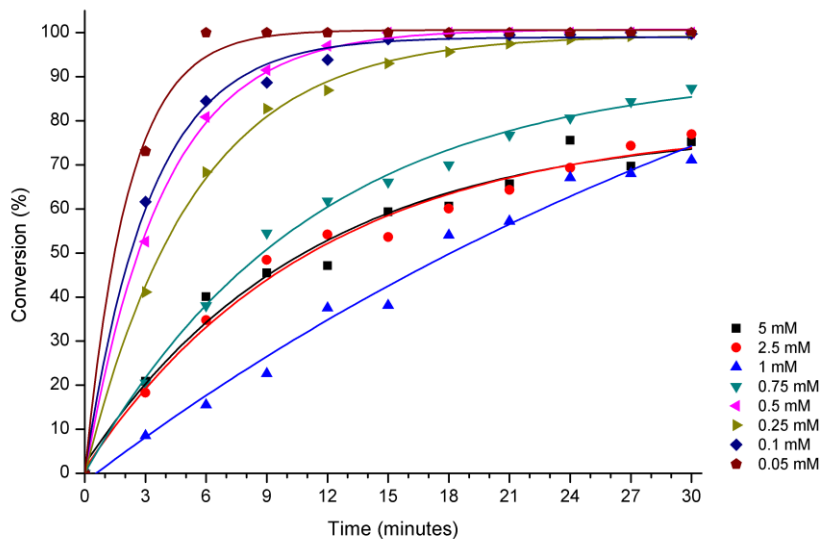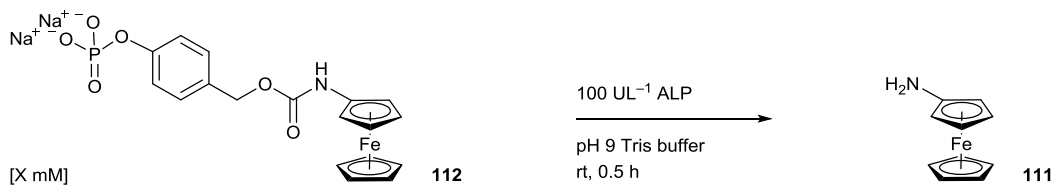
Figure 2.10 ALP-catalysed conversion of enzyme substrate **112** to enzyme product **111** at different substrate concentrations at room temperature.
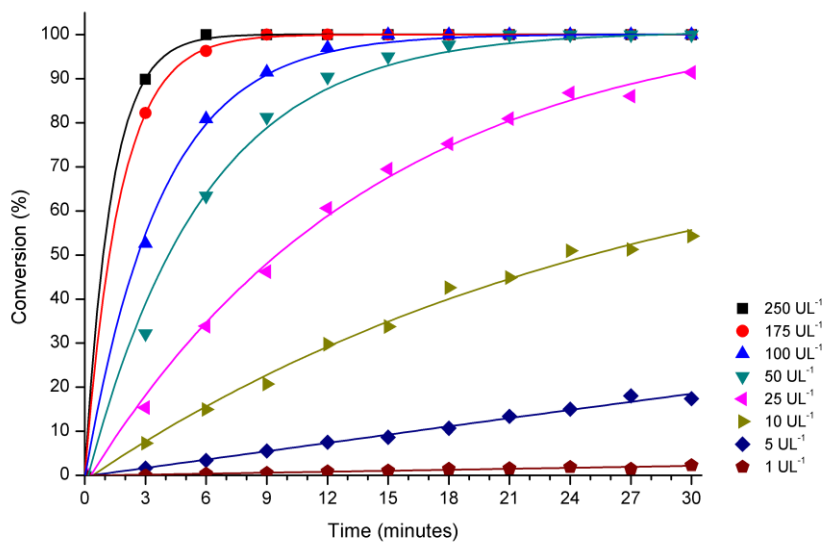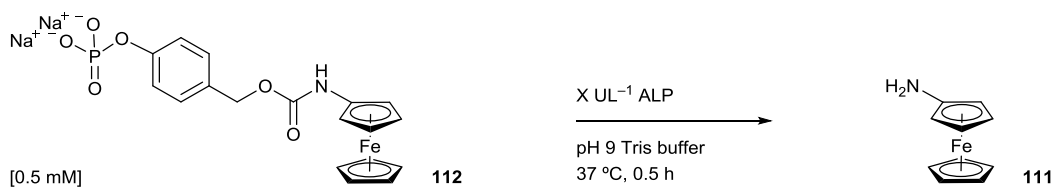
Figure 2.11 ALP-catalysed conversion of enzyme substrate **112** to enzyme product **111** in the presence of different concentrations of ALP at 37 °C.
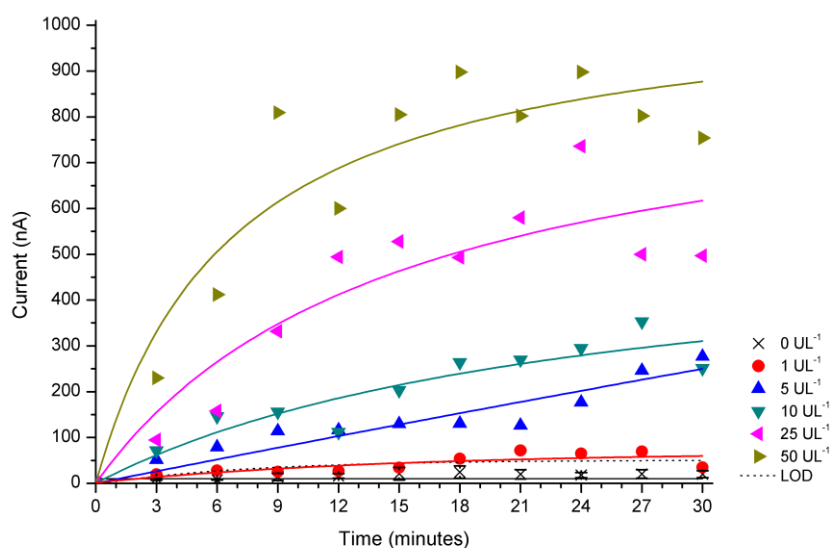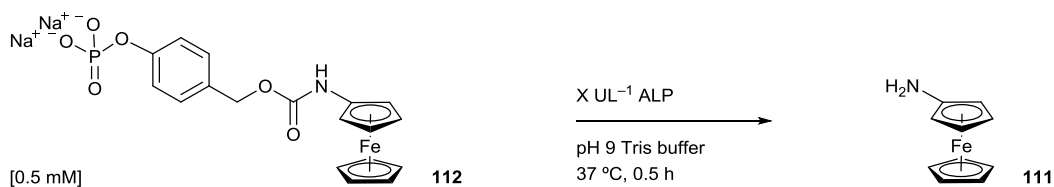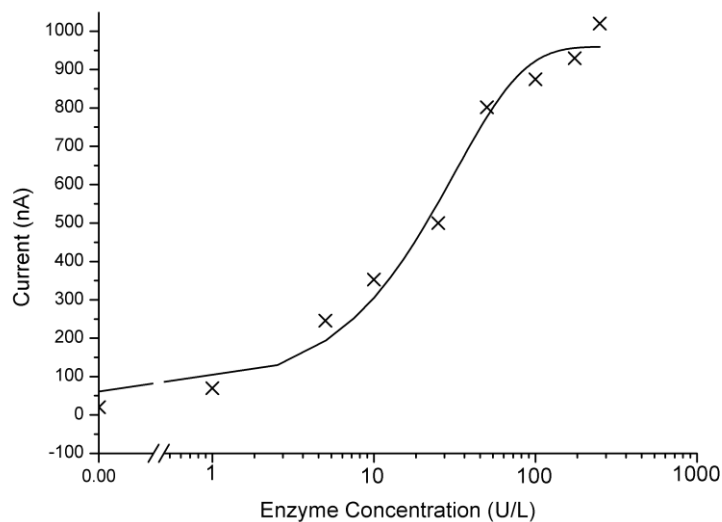
Figure 2.12 Amperometric response from aminoferrocene **111** at −130 mV over time in the presence of different concentrations of ALP at 37 °C. Error bars indicate standard deviation (*n* = 3). The LOD is calculated as 3 × the standard deviation from the mean background.

Typically, the optimal working temperature for mammalian enzymes such as ALP is 37 °C and as a result, the next improvement to the assay was to increase the temperature.[388] Accordingly, the ALP detection assays were repeated with the optimised substrate concentration at 37 °C (Figure 2.11). The desired increase in sensitivity was indeed observed as ALP concentrations of 50 UL^{-1} and higher were able to deliver quantitative conversions within the 30 minute assay duration. The increase in temperature also allowed an ALP concentration of 1 UL^{-1} to be distinguished from the background rate. However, in order to calculate an accurate LOD, the average background current needs to be determined and compared to the current obtained for the enzyme product under different concentrations of ALP. Therefore, the raw current of aminoferrocene **111** at −130 mV obtained for the assays ran with enzyme concentrations of 50 UL^{-1} and lower was plotted against time (Figure 2.12).

The fluctuations in current due to a culmination of problems associated with POC sensing such as sampling and electrode errors are immediately apparent when using solely current as the output signal. This reinforces the increase in accuracy that can be attained by using ratiometric sensing as the detection method. Fortunately, the observed background current is sufficiently low and consistently low as demonstrated by the tight error bars. This enables an ALP concentration of 5 UL^{-1} to be easily distinguished from the background when using substrate **112** and product **111** as an amperometric detection system. A plot of the current response of **111** against the log of the

enzyme concentration allows for a LOD for ALP to be calculated at 0.3 pM after a 27 minute incubation period at 37 °C (Figure 2.13).


Figure 2.13 A plot of the amperometric response obtained from aminoferrocene **111** at −130 mV after 27 minutes at 37 °C *vs.* the $\log_{10}$ of the ALP concentration. $R^2 = 0.98$.

2.3.4   *Application of the Enzyme Substrate towards Immunosorbent Assays*

With the concentration of the substrate and the temperature of the assay optimised, the next goal was to apply the substrate to a solid-supported immunoassay. Prior to this however, the substrate was tested with an ALP–conjugate in order to determine whether structural modification of the enzyme would significantly disrupt enzyme activity. In addition, the considerable size of the protein could hinder the approach of the substrate, which may also contribute to a decrease in turnover number. To test this potential problem, the streptavidin–ALP conjugate was chosen as streptavidin can be utilised to tag ALP to biotin-labelled antibodies *via* the highly favourable streptavidin–biotin binding. This could be useful information with regard to a successful immunoassay design that could be incorporated onto a cartridge in the future. As such, a 0.5 mM solution of ferrocene-derived ALP substrate **112** was exposed to varying concentrations of streptavidin–ALP at 37 °C (Figure 2.14).

Pleasingly, protein–enzyme conjugation did not lead to a significant decrease in enzyme activity towards substrate **112** as positive conversions were observed. Protein–enzyme concentrations higher than 25 mgL^{-1} delivered quantitative electrochemical conversions in 30 minutes. Again, in the absence of the protein–enzyme conjugate, no electrochemical conversion

was observed. This allowed for a protein–enzyme detection limit to be in the micromolar range as 0.5 mgL^{-1} could be distinguished from the background rate.
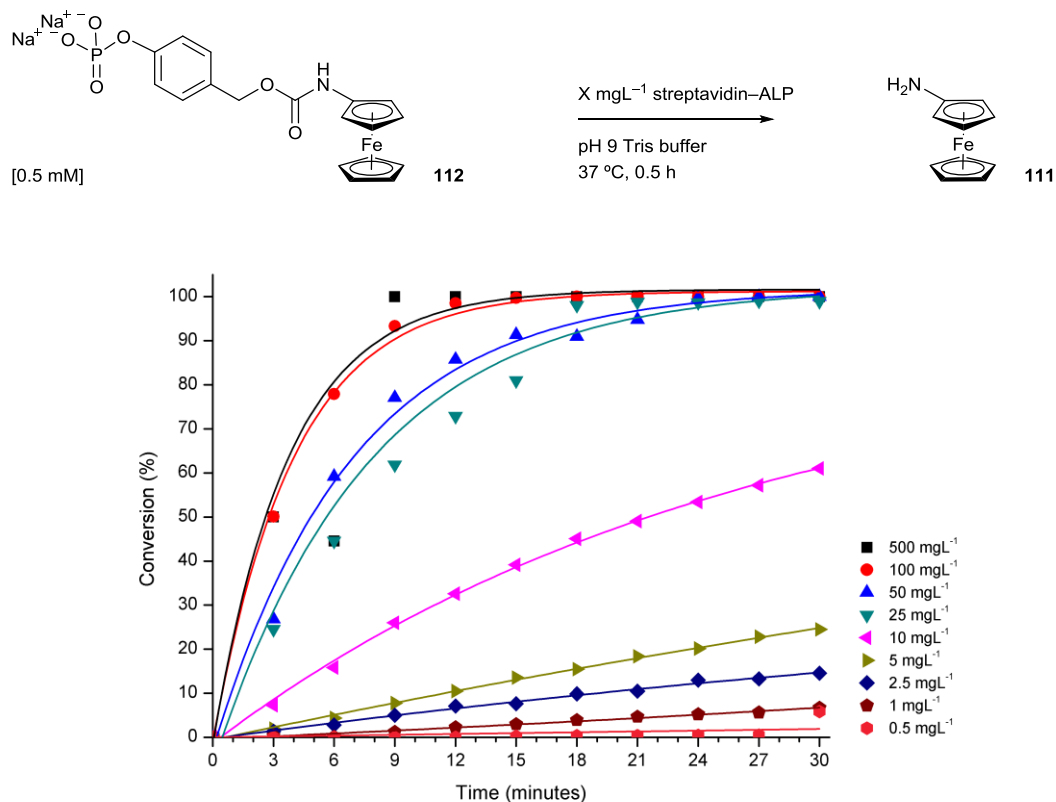

Figure 2.14 ALP-catalysed conversion of enzyme substrate **112** to enzyme product **111** in the presence of different concentrations of streptavidin–ALP conjugate at 37 °C.
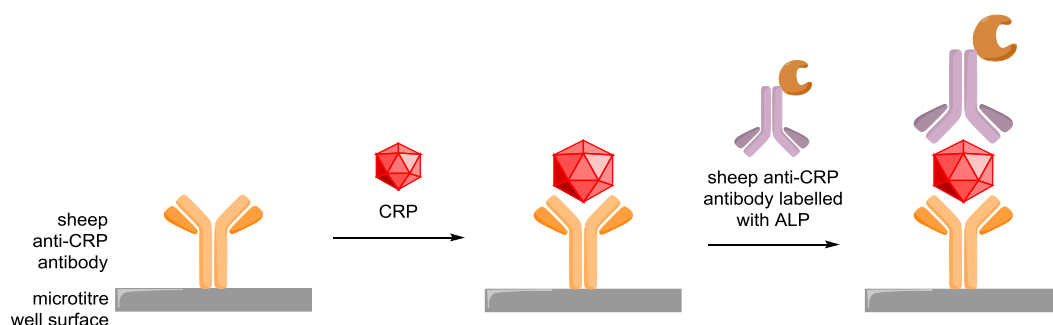

Scheme 2.23 Construction of the ALP-labelled sandwich ELISA for electrochemical CRP detection.

Since determining that enzyme conjugation does not prevent substrate turnover, the next test was to apply substrate **112** towards an immunosorbent assay for ratiometric electrochemical protein detection. A commercial ELISA kit for the detection of C-reactive protein (CRP) that uses ALP as the enzyme label was chosen as a model immunoassay. CRP is a plasma protein that is

produced by the body as a response to inflammation and because of this, it has been used extensively as a diagnostic biomarker primarily for the detection of inflammation but it can also be used to indicate impending major cardiovascular events such as coronary heart disease.[389] The sandwich ELISA was constructed according to the manufacturer's procedure (Scheme 2.23) using an array of standard CRP concentrations and exposed to a 0.5 mM solution of ALP substrate **112** (Figure 2.15).
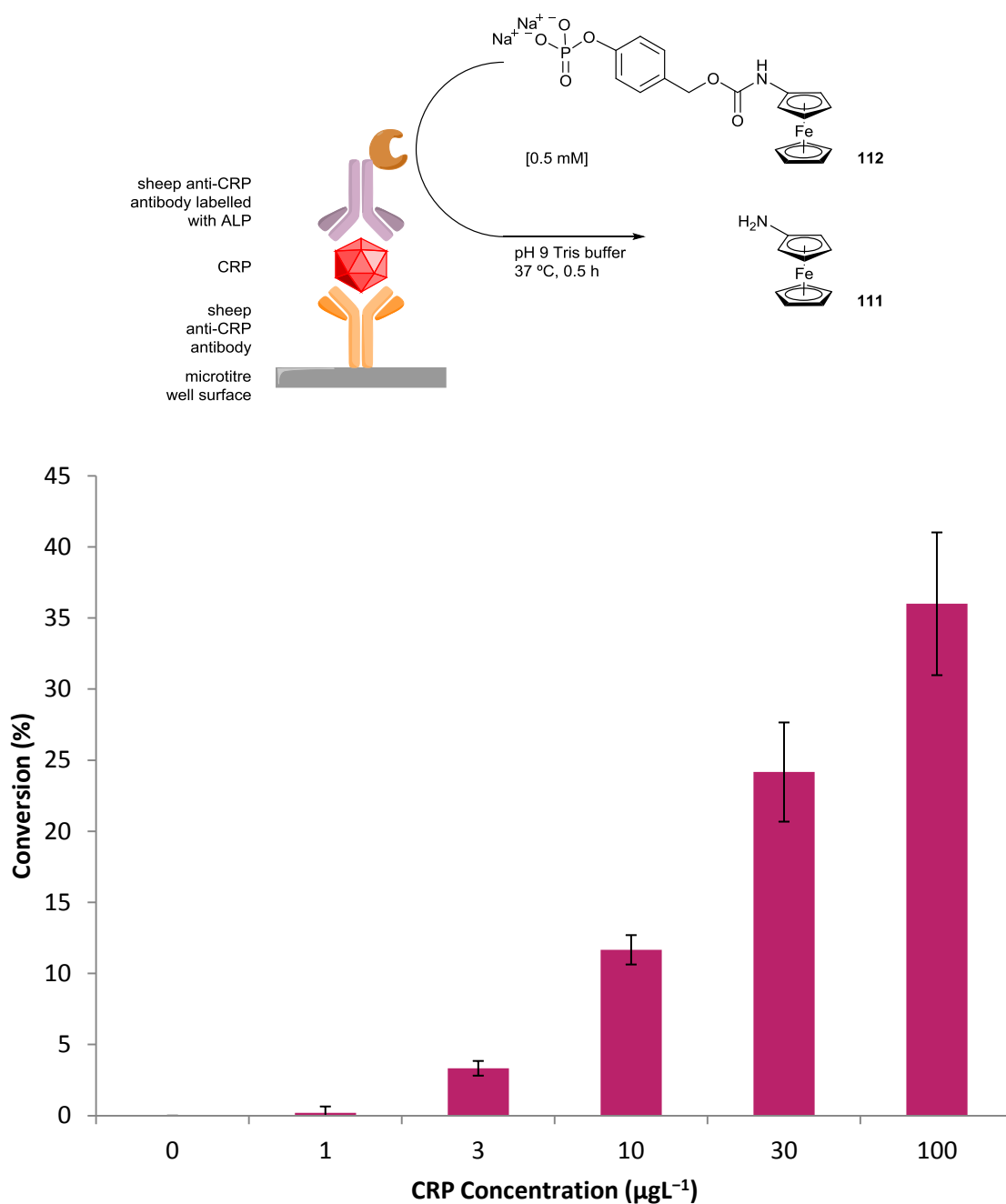

Figure 2.15 Electrochemical conversion obtained for different concentrations of CRP with ALP substrate **112** at room temperature. Error bars indicate standard deviation ($n = 6$).
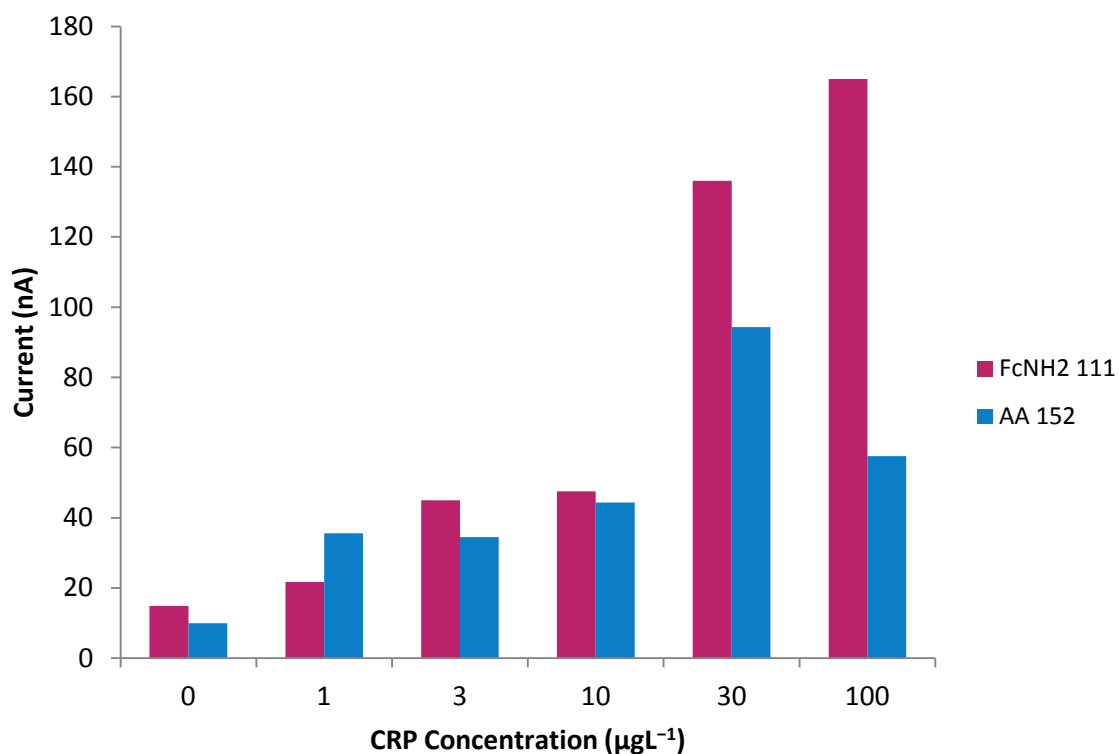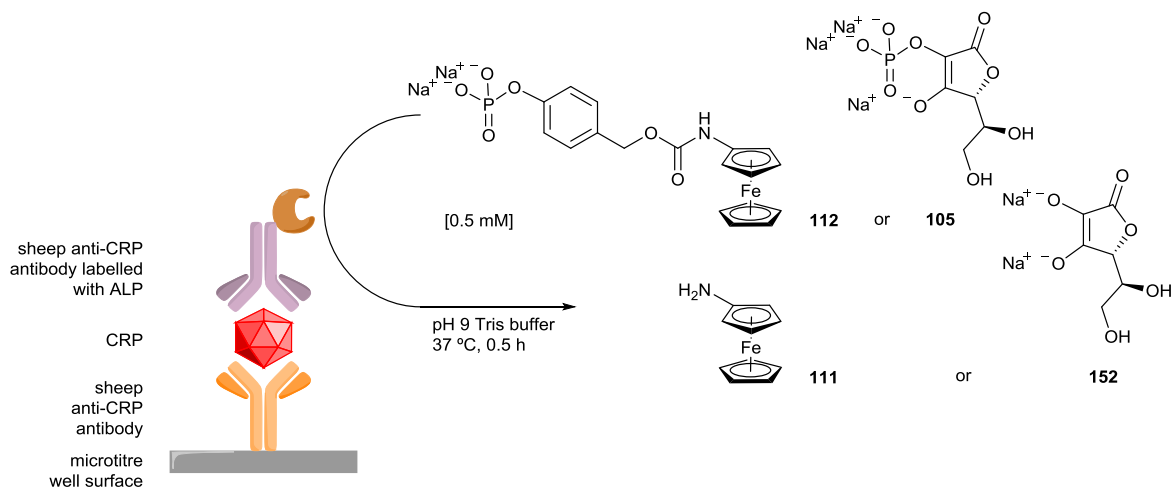
Figure 2.16 Current obtained for different concentrations of CRP with either ALP substrate **112** or AA2P **105** at 37 °C.

Gratifyingly, positive conversions were observed for most CRP concentrations tested and no conversion was seen in the absence of CRP which demonstrates the low susceptibility of ratiometric sensing towards false positive results. Quantitative conversions were unable to be attained using an ALP-labelled ELISA in comparison to the tests composed with the free enzyme as this is thought to be due to the lack of mechanical stirring and the enzyme label being surface-bound. However, the use of the ratiometric electrochemical detection method was shown to have excellent reproducibility as shown by the tight error bars which indicate the standard deviation observed over six replicate experiments.
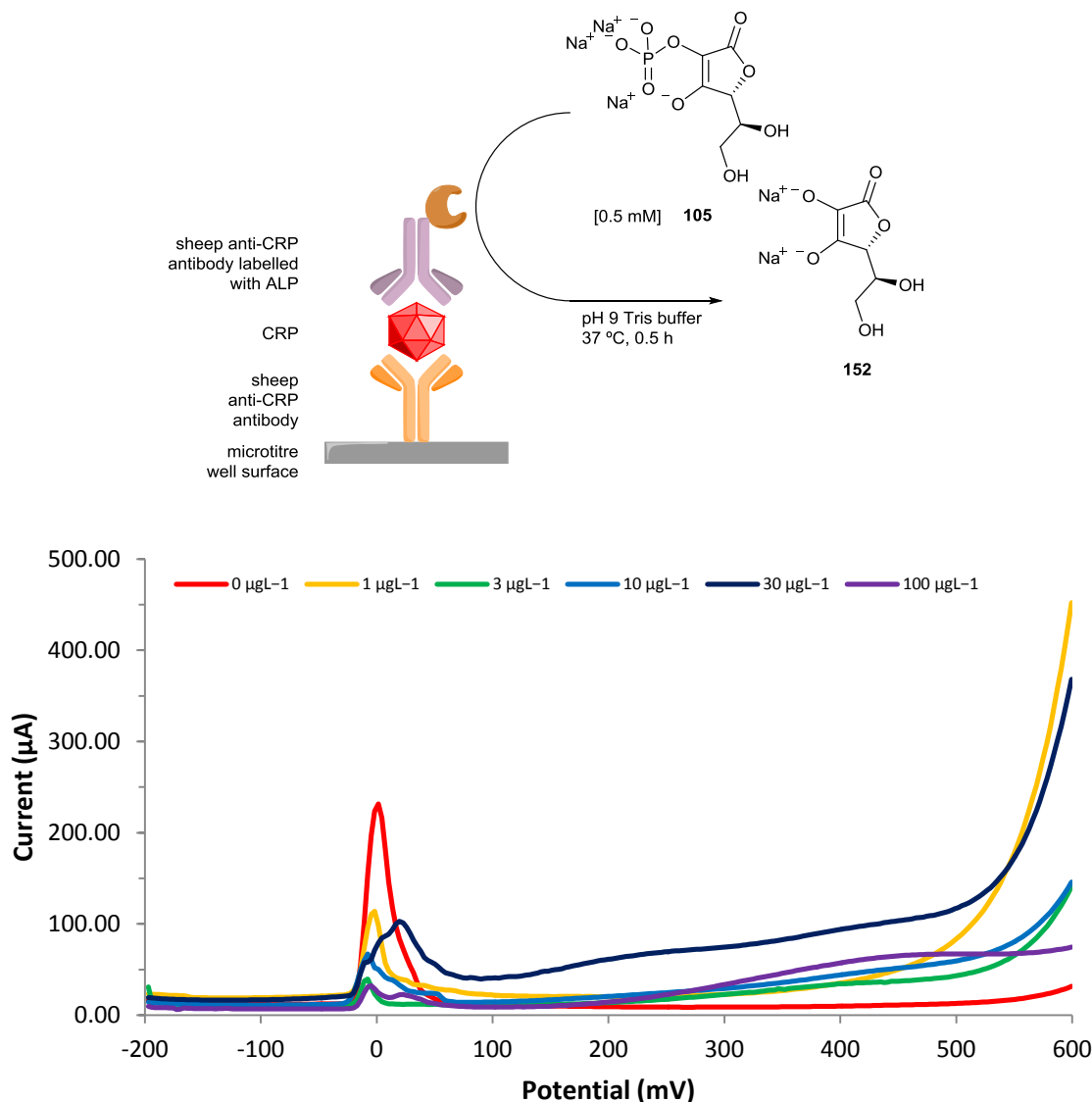
Figure 2.17 Voltammogram overlays of electrochemical CRP ELISAs using substrate AA2P **105**. Oxidation potential for product AA **152** is typically between 350 and 500 mV. Spikes observed at 0 mV is due to the oxidation of the silver reference electrode.

To compare ALP substrate **112** with a commonly-used substrate, the ELISAs were repeated but this time electrochemical detection was achieved using either **112** or commercially available substrate AA2P **105** as the enzyme substrate (Figure 2.16). In addition, the temperature of the incubation with the enzyme substrate was increased to 37 °C to increase enzyme activity and therefore improve the current response for the products of both substrates. Similar current responses were observed for both substrates at low concentrations of CRP but at higher concentrations, substrate **112** was capable of delivering a significantly higher current than AA2P **105**. Despite the similar current responses, the Gaussian peak observed for the product of substrate **112** imparts a greater confidence in the output signal in comparison to the broad hump observed for AA **152**, the product of AA2P **105**, whose absolute oxidation potential can vary considerably (Figure 2.17). Not only this, but ratiometric electrochemical detection offers a much greater

reliability and improved accuracy for inclusion within an electrochemical POC device over a 'switch on' detection method.

2.4 Conclusion

2.4.1 Project Summary

Towards implementation within a commercial point-of-care biosensor for rapid and sensitive protein detection, a novel electrochemical substrate for the ratiometric detection of the enzyme alkaline phosphatase was designed. Through a highly telescoped procedure, the substrate was successfully synthesised in just 3 steps in 14% overall yield. Once synthesised, the substrate was shown to be stable indefinitely as a pure solid stored in a desiccator and also demonstrated satisfactory stability as a concentrated solution in alkaline buffer. The substrate was shown to have a significantly different oxidation potential from that of the product which enables ALP detection to be ratiometric. Through ^{31}P NMR experiments, ALP was shown to act upon the substrate and using electrochemical analysis, the desired product was detected at the electrode demonstrating its release from the desired elimination of the dephosphorylated intermediate.

An optimisation of the ratiometric ALP detection assay revealed an optimal substrate concentration of 0.5 mM that delivered both quantitative conversion and a large current response within 30 minutes. Increasing the temperature of the detection assay also improved the rate of conversion allowing for a LOD of 0.3 pM ALP concentration to be detected within this timeframe. Protein-conjugated enzymes were shown not to affect reaction conversion as a streptavidin–ALP conjugate also demonstrated high activity allowing for less than 1 mgL^{-1} of the enzyme conjugate to be detected.

Since ALP is often used as the enzyme label within enzyme-linked immunosorbent assays, the substrate was also applied to the ratiometric electrochemical detection of proteins *via* an ELISA. Moderate conversions were obtained for the detection of model analyte C-reactive protein, but more importantly, conversions were highly reproducible owing to the ratiometric detection method. In comparison to L-ascorbic acid 2-phosphate (AA2P), a commonly-used switch-on substrate for ALP, the developed substrate delivered similar current responses when applied to the electrochemical detection of CRP. However, because of its ratiometric detection method, the developed substrate offers significant improvements over AA2P such as greater confidence in absolute oxidation potential as well as reproducibility. As such, the substrate described herein is considerably better suited for application as an electrochemical ELISA substrate within a rapid POC device for sensitive protein detection.

2.4.1 Future Work

Including the substrate developed herein, only two substrates for ratiometric electrochemical enzyme detection have been described to date; one for catalytic antibodies that demonstrates aldolase activity and the one herein for alkaline phosphatase. To increase the number of hydrolytic enzymes that can be detected through ratiometric electrochemical detection, and therefore expand the repertoire of potential point-of-care biosensors, other ferrocene-derived substrates that contain alternative enzyme-cleavable functional groups could be developed. For example, substrates containing sulfate **153**, amide **154**, acetate **155** or sugar moieties **156**, would enable the ratiometric electrochemical detection of sulfatase, protease, esterase or glycosylase enzymes respectively, *via* the same elimination mechanism (Figure 2.18).
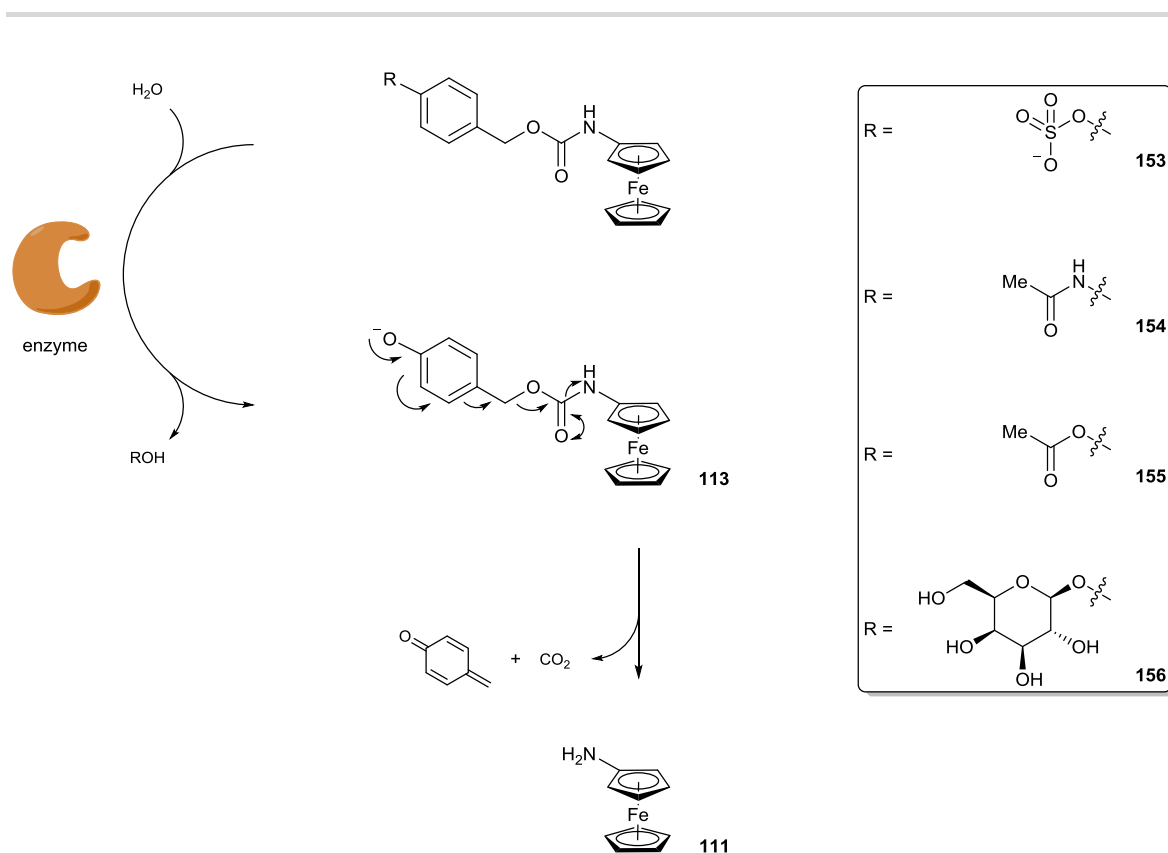
Figure 2.18 The design of different ferrocene-derived substrates for the potential ratiometric electrochemical detection of alternative enzymes.

Additionally, the use of traditional alcohol protecting groups such as allyl **157** or silyl **158** groups as the analyte-responsive trigger could extend this methodology towards the ratiometric electrochemical detection of palladium or fluoride respectively, both of which being of diagnostic interest (Figure 2.19). Furthermore, masked phenols such as phenylboronic acid **159** could also be used as the trigger moiety for the ratiometric electrochemical detection of hydrogen peroxide. By extension, this could allow for the indirect detection of hydrogen peroxide-producing enzymes such as glucose oxidase, and therefore the possibility for the diagnosis of diabetes, through this method.

Inversely, hydrogen peroxide consuming enzymes such as horseradish peroxidase could also be detected with this probe enabling a reverse protein detection strategy to be achieved using more popular HRP-labelled ELISAs (Figure 2.20).
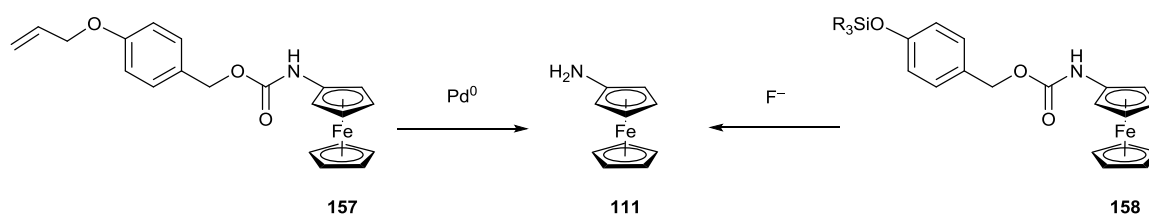
Figure 2.19 The design of different ferrocene-derived probes for the potential ratiometric electrochemical detection of palladium or fluoride.
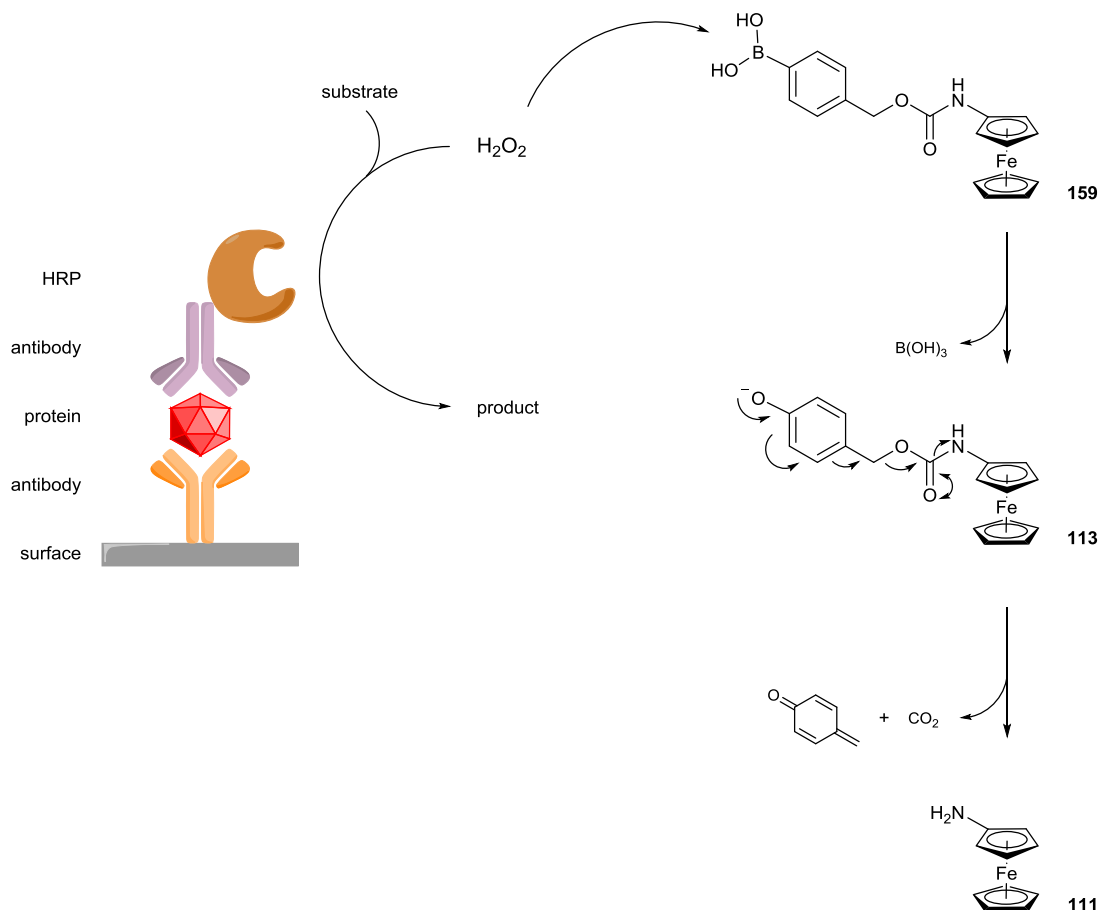
Figure 2.20 The design of a boronic acid-containing ferrocene-derived probe for the direct ratiometric electrochemical detection of hydrogen peroxide, or proteins *via* an inverse HRP-labelled ELISA.

Chapter 3

Enzyme-Triggered Catalytic Signal Amplification[390–391]

3.0   Introduction

3.0.1   Signal-Amplified Enzyme-Linked Immunosorbent Assays

In order to improve the sensitivity of a diagnostic assay, some degree of amplification is absolutely essential. Although enzyme-linked immunosorbent assays (ELISAs) contain inherent amplification from the enzyme, efforts have been directed at replacing the enzyme with alternatives that either have a higher turnover rate or can provide increased amplification through other means. Considerable success has been achieved by replacing the enzyme label with nucleic acid labels, which has allowed nucleic acid amplification techniques such as the polymerase chain reaction (PCR) and rolling circle amplification (RCA) to be used for signal amplification purposes. Typically, detection limits are improved up to 10000-fold by this method. Despite achieving these excellent sensitivities, the amplification procedure is complex in comparison to a standard ELISA and as such, are not be easily integrated into a rapid point-of-care (POC) device.[392]
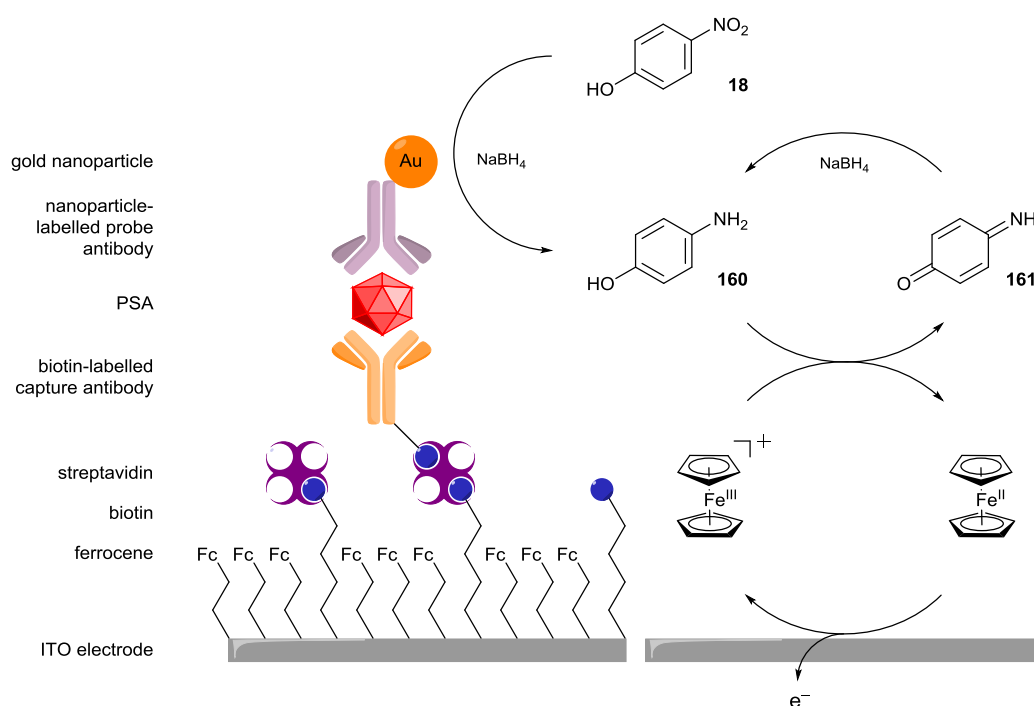
Scheme 3.1 Gold nanoparticle-labelled sandwich immunoassay for the electrochemical detection of PSA.

Alternatively, nanoparticles possessing useful characteristics such as catalytic activity and multivalency have also become popular enzyme replacements within amplified

immunoassays.[393–394] For example, Yang *et al.* described the use of gold nanoparticles as the immunoassay label within an electrochemical immunoassay for sensitive protein detection (Scheme 3.1).[395] First, capture antibodies were immobilised onto a ferrocene-coated indium tin oxide (ITO) electrode *via* a streptavidin–biotin linkage. In the presence of the target, prostate specific antigen (PSA), a standard sandwich immunoassay is formed with the antibody-coated gold nanoparticles. The gold nanoparticles were then demonstrated to catalyse the reduction of *p*-nitrophenol (PNP) **18** to *p*-aminophenol **160**, which can be detected at a facile oxidation potential due to the ferrocene-modified electrodes. Further amplification is provided through redox cycling as the oxidised quinone product **161** can be reduced by the reducing agent present.[396] Together; a competitive detection limit of 1 fgmL^{-1} for PSA was obtained. Similar electrochemical immunoassays that use platinum nanoparticles as the enzyme label replacement have also been described.[397]
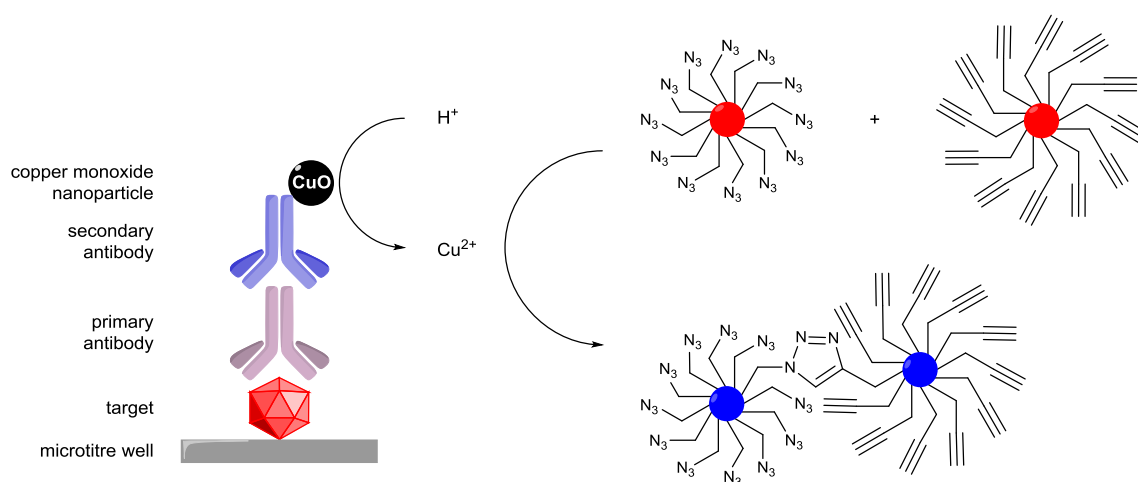
Scheme 3.2 Copper oxide nanoparticle-labelled sandwich immunoassay for colourimetric HIV antigen detection.

Nanoparticles have also been used as antibody labels to provide a colourimetric detection method within immunoassays. One example specifically was described by Jiang *et al.*, who used copper oxide nanoparticle labels to catalyse the aggregation of gold nanoparticles for the detection of human immunodeficiency virus (HIV) antigens (Scheme 3.2).[398] Here, a direct immunoassay was constructed where the antigen was adsorbed onto the surface of the microtitre well and identified with a primary antibody. This complex was then labelled with a secondary antibody tagged with copper oxide nanoparticles. In the presence of the nanoparticles, and therefore the analyte, the introduction of a strong, acidic solution to the assay dissolves the copper nanoparticles, releasing Cu^{2+} ions into the system. Once released, the Cu^{2+} ions can catalyse the Huisgen cycloaddition reaction between two sets of gold nanoparticles; one set covered with terminal alkynes and the other covered with alkyl azides. After a significant number of gold nanoparticles have been knitted together, the aggregation causes the colour of the solution to change from red to

blue. In the absence of the antigen, the copper catalyst is not produced and the gold nanoparticles remain separate keeping the detection solution red. Although not explicitly stated, the LOD obtained for this detection method was said to rival that of a traditional fluorescence ELISA.
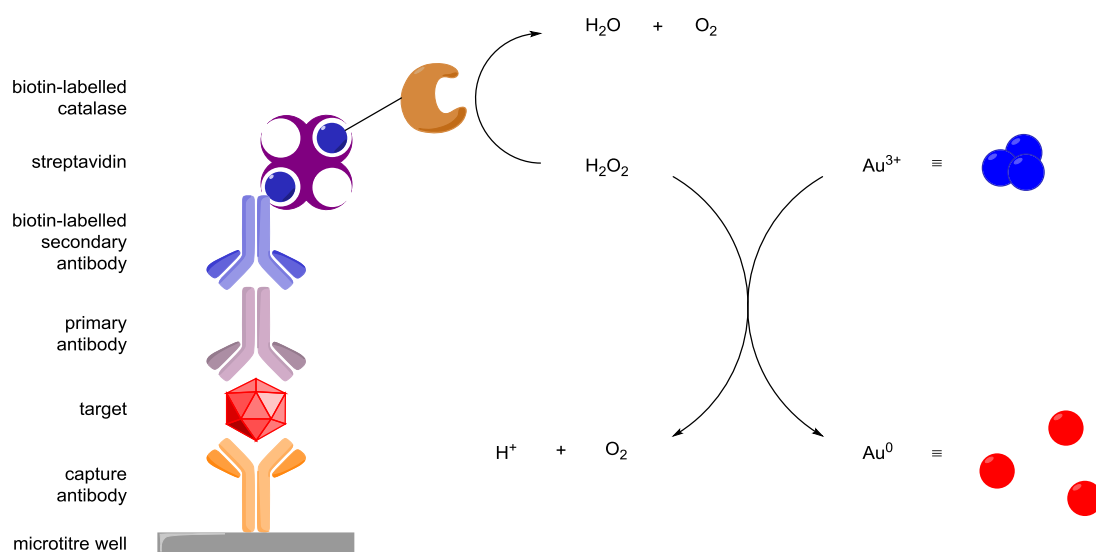
Scheme 3.3 Plasmonic ELISA for the colourimetric detection of disease biomarkers with the naked eye.

Rather than replacing the enzyme, recent efforts to increase the sensitivity ELISAs have been aimed towards the application of additional amplifiers. Of particular note, de la Rica and Stevens developed a plasmonic ELISA for the visual detection of disease biomarkers (Scheme 3.2).[399] In this example, a traditional sandwich ELISA labelled with catalase, an enzyme that catalyses the breakdown of hydrogen peroxide, was constructed. In the presence of the target, and therefore the enzyme, hydrogen peroxide is broken down to water and molecular oxygen which allows the solution containing Au^{3+} ions to form ill-defined nanoparticles that aggregate together leading to a blue colour to be developed. In the absence of the target, hydrogen peroxide remains in solution and reduces the Au^{3+} ions in the solution to Au^0. This leads to the formation of regular, spherical nanoparticles that do not aggregate together and causes a red colour to be developed. This example of gold nanoparticle label amplification in conjunction with enzyme signal amplification allowed for a limit of detection (LOD) of 1 agmL^{-1} for the detection of PSA and enabled the visual detection of HIV antigens at concentrations that were undetectable by a traditional nucleic acid-based test. This has since given rise to the development of a number of biodiagnostic tests that utilise plasmonic nanomaterials for both amplification and signal production.[400] However, it has been identified that successful and accurate signal production is highly dependent on a freshly prepared and precise concentration of hydrogen peroxide.[401] Because of this and the poor stability of hydrogen peroxide in storage, this method would not be suitable for integration within a POC device.

3.0.2   Project Aims

Although there have been several disclosures regarding amplification techniques aimed towards improving the sensitivity of ELISAs, few utilise electrochemical endpoint detection and those that do,[93,395] are too impractical to be integrated into a POC device. Continuing on from the substrate development for the ratiometric electrochemical detection of alkaline phosphatase (ALP)-labelled ELISAs, the next objective was to design a signal amplification protocol for ALP that utilised the same endpoint detection method. This should improve the sensitivity of the ELISA and therefore lower the LOD of the system, yet still allow detection to be achieved using ratiometric electrochemical analysis.

3.1   Signal-Amplified Ratiometric Electrochemical Enzyme-Linked Immunosorbent Assay

3.1.1   Signal Amplification Concept

As previously discussed, a large number of ELISA amplification methodologies are aimed at replacing the enzyme label with alternative amplifiers such as nanoparticles that offer either an improved turnover rate or an orthogonal detection method that doesn't require substrate development. However, amplifier–antibody conjugation can be inefficient and signal production can be slow and labour intensive. As such, their application within POC sensing is limited. Fundamentally, a strategy that replaces the enzyme of an ELISA with another amplifier appears counterintuitive and efforts should be made towards building upon the inherent amplification of an ELISA. Towards this end, a double-catalyst signal amplification concept for an ELISA was designed (Figure 3.1).
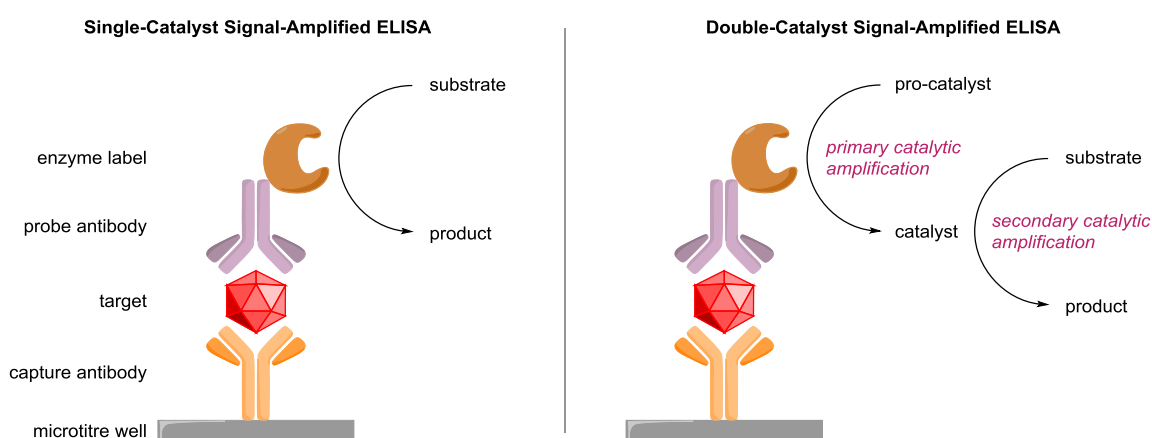
Figure 3.1 Concept of a double-catalyst signal amplification protocol for increasing ELISA sensitivity in comparison with a traditional single-catalyst signal amplification protocol.

Prior to beginning of this project, the idea of a double-catalyst signal amplification procedure for an ELISA had only been illustrated in principle.[402] A number of amplification methodologies that utilise either enzyme cycling,[403] or redox cycling,[404] as post-enzyme amplification procedures have been described and can offer improved LODs. However, accidental triggering of these cycling methods can lead to high background signals and the possibility of false positive results. The successful demonstration of an enzyme-triggered catalyst activation procedure for ELISA signal amplification had remained elusive until, when during the development of this project, Tang *et al.* described an elegant first example (Scheme 3.4).[405]
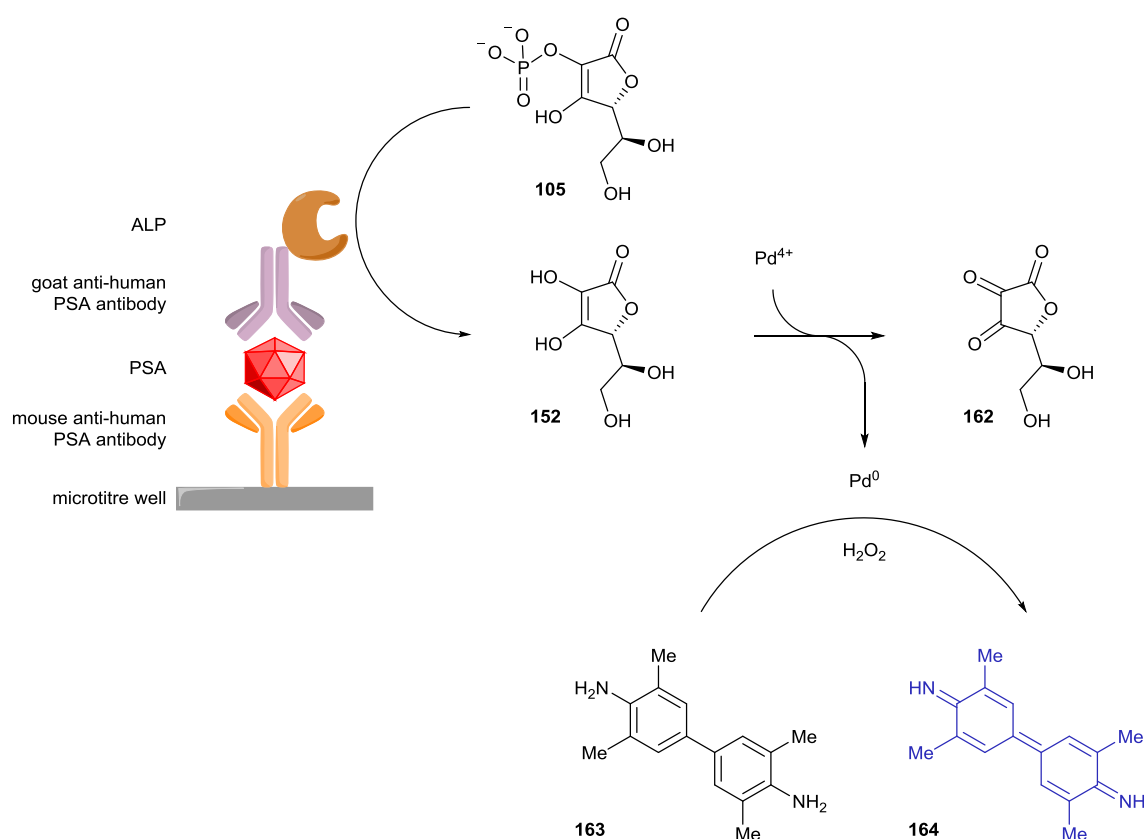
Scheme 3.4 Double-catalyst ELISA signal amplification protocol for the colourimetric detection of PSA.

In this example, a typical sandwich ELISA was constructed aimed towards the detection of PSA and using ALP as the enzyme label. In the presence of the enzyme, and therefore the target, commercially available ALP substrate L-ascorbic acid 2-phosphate (AA2P) **105** becomes hydrolysed to ascorbic acid (AA) **152**. AA was then able to reduce a palladate species to the active catalytic palladium nanostructures that aggregate upon the surface of non-participating gold nanoparticles.[406] As a peroxidase mimic, the palladium nanostructures can catalyse the hydrogen peroxide-mediated oxidation of 3,3',5,5'-tetramethylbenzidene (TMB) **163** to its corresponding blue diimine **164**.[407] Through an extensive screening process, a positive colourimetric signal was shown to only be produced by the palladium nano-catalysts which themselves were only created in

the presence of ALP, consequently leading to a low background signal. Importantly, the double-catalyst signal amplification procedure was shown to be significantly more sensitive than a traditional single-catalyst ELISA and could deliver an LOD of 0.05 ngmL^{-1} for the detection of PSA. However, due to the number of reagents required to acquire a positive signal, the procedure is considerably labour-intensive and requires the time-consuming preparation of gold nanoparticles. Nevertheless, the powerful concept of enzyme-triggered catalyst activation as a signal amplification protocol for improving immunoassay sensitivity had been proven.

3.1.2 Secondary Catalytic Signal Amplification

At the outset of this investigation, development of the second catalytic amplification step was the primary focus as this would be the step responsible for the production of the ratiometric electrochemical signal. For the active catalytic species, an organometallic catalyst was initially considered since catalytic activity could be regulated through careful control of ligands. However, for successful deployment into an electrochemical POC biosensor, the catalyst must fulfil a number of criteria, such as; high efficiency, excellent water-tolerance, low toxicity and good reliability. Specifically, a rapid catalytic transformation that is tolerant of enzyme-friendly conditions was paramount.
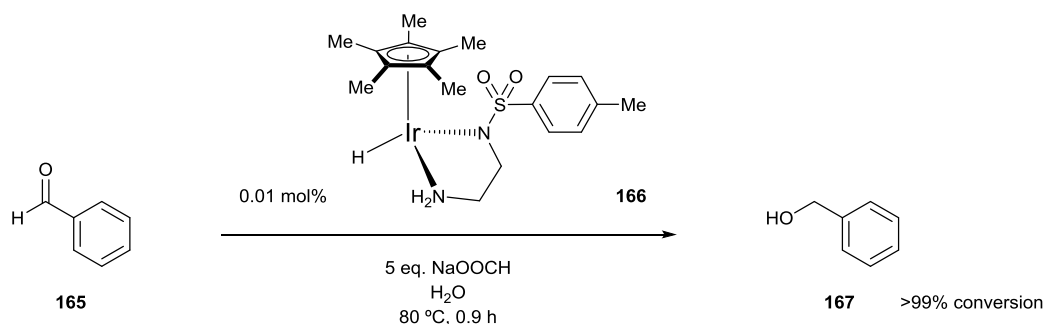
Scheme 3.5 Iridium-catalysed transfer hydrogenation of benzaldehyde **165** to benzyl alcohol **167**.

Among the comprehensive number of catalytic organic transformations that occur in aqueous media, many involve the use of high pressures, high temperatures or long reaction times and were therefore unsuitable.[408] In contrast, a range of water-soluble iridium-based catalysts have recently shown high efficiency within applications such as hydrogen storage,[409] and water oxidation,[410] as well as in a number of organic transformations such as reductive amination,[411] *N*-alkylation,[412] and the oxidation of alcohols.[413] One transformation in particular that possessed the desired characteristics to be employed within this signal amplification concept was the iridium-catalysed transfer hydrogenation reaction.[414–417] When applied to the reduction of benzaldehyde

165, a transfer hydrogenation iridium–diamine complex **166** has been shown to deliver quantitative conversion to benzyl alcohol **167** at a catalytic loading of 0.01 mol% in water within an hour (Scheme 3.5).[418] Also, by increasing the catalytic loading, reaction times could be shortened to just 5 minutes whilst maintaining quantitative conversions.
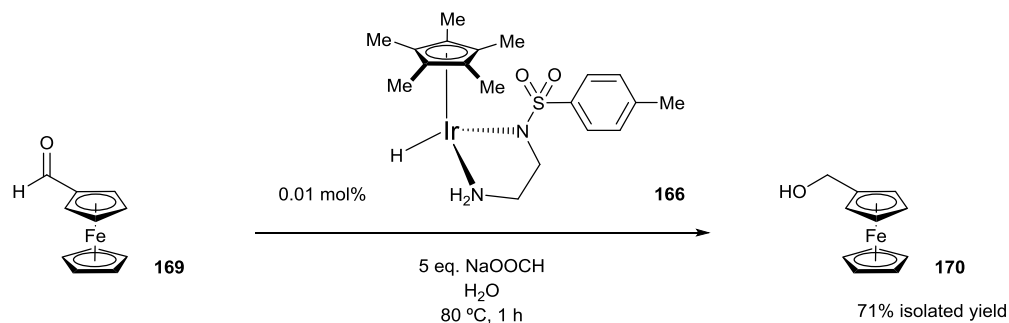

Scheme 3.6 Literature conditions applied to the iridium-catalysed transfer hydrogenation of ferrocenecarboxaldehyde **169** to ferrocenemethanol **170**.
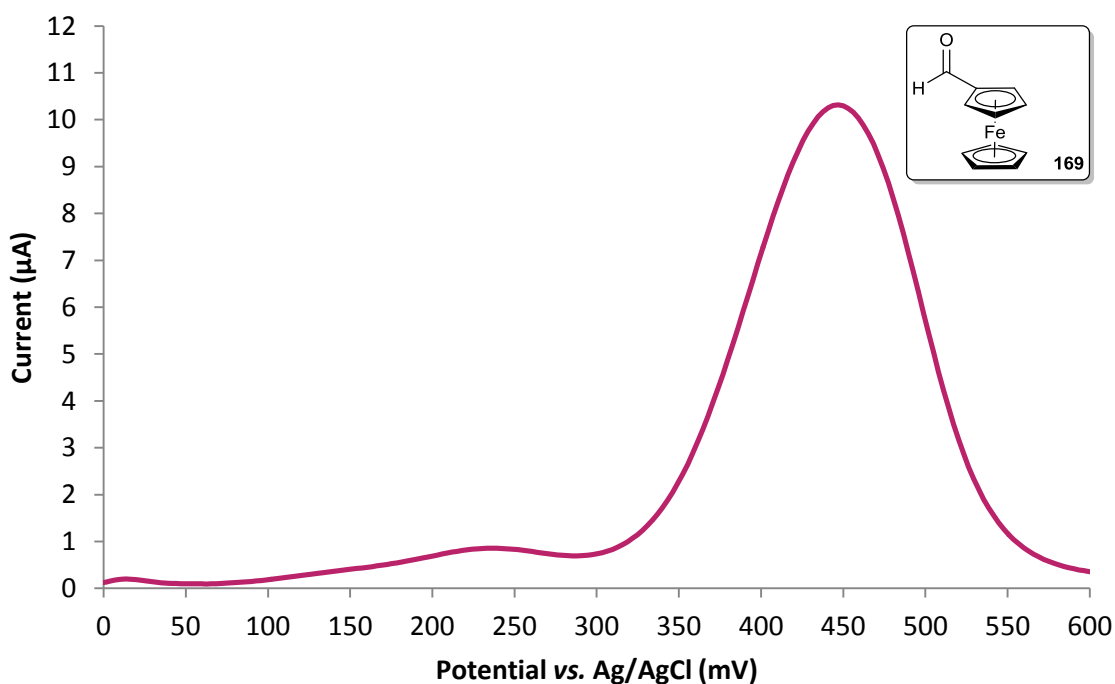
Figure 3.2 Differential pulse voltammogram of a 1 mM solution of ferrocenecarboxaldehyde **169** in pH 9 Tris buffer.

Impressed with the efficiency and low catalytic loading of this process, the investigation therefore began with the application of these literature conditions to an electrochemically-active aldehyde (Scheme 3.6). Naturally, due to its facile oxidation potential, excellent stability in aqueous media and good compatibility with biological material, commercially available

ferrocenecarboxaldehyde **168** was chosen as the initial electroactive aldehyde. Pleasingly, conversion to the desired product, ferrocenemethanol **170**, was observed and could be isolated in a 71% yield.
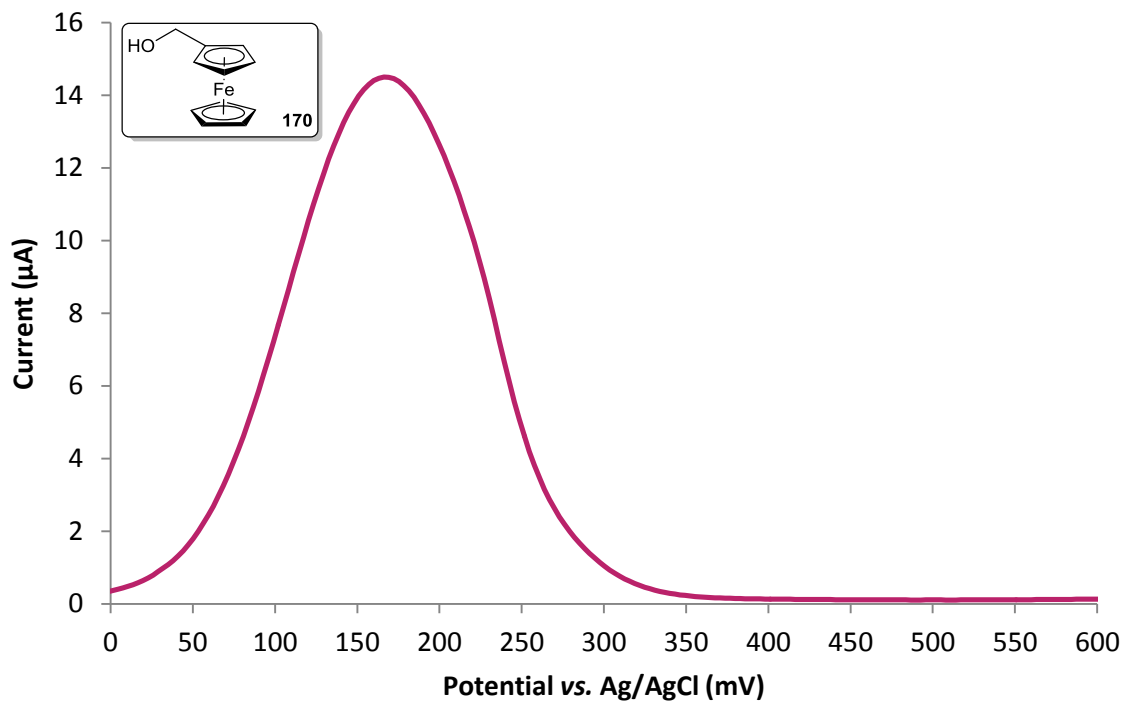
Figure 3.3 Differential pulse voltammogram of a 1 mM solution of ferrocenemethanol **170** in pH 9 Tris buffer.
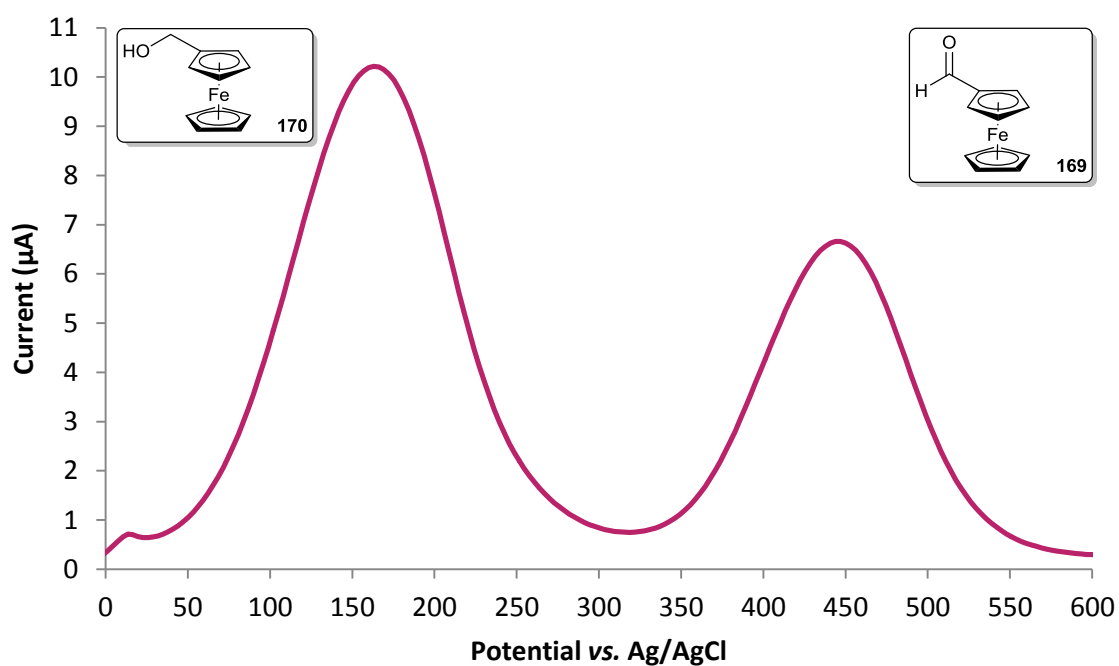

Figure 3.4 Differential pulse voltammogram of a solution containing 0.5 mM of ferrocenecarboxaldehyde **169** and 0.5 mM of ferrocenemethanol **170** in pH 9 Tris buffer.

With ferrocenemethanol **170** in hand, it was necessary to perform electrochemical analysis on both the starting material **169** and product **170** in order to determine if they were electrochemically distinguishable. Using differential pulse voltammetry (DPV), a 1 mM solution of ferrocenecarboxaldehyde **169** was found to have an oxidation potential of 450 mV *vs.* Ag/AgCl (Figure 3.2), whereas a 1 mM solution of ferrocenemethanol **170** was found to have an oxidation potential of 170 mV *vs.* Ag/AgCl (Figure 3.3). A difference in oxidation potential of 280 mV between starting material and product suggests that both should be electrochemically distinguishable and as such, an equimolar solution of **169** and **170** was made up and exposed to electrochemical analysis (Figure 3.4).

As desired, both starting material and product had sufficiently different oxidation potentials that enabled them to be separable on a voltammogram. This therefore allowed for the iridium-catalysed conversion of aldehyde **169** to alcohol **170** to be obtained through electrochemical analysis of the crude reaction mixture. Peak integration of the resulting voltammogram would allow accurate reaction conversions to be calculated by the following equation:

$$\text{Conversion (\%)} = \left(\frac{\int \mathbf{170}}{(\int \mathbf{170} + \int \mathbf{169})} \right) \times 100$$

Satisfied that the iridium-catalysed transfer hydrogenation reaction could be employed as the secondary catalytic signal amplification cycle, an optimisation of the reaction conditions was performed in order to reduce the unfavourably high temperature and long reaction time that would be unsuitable for application within a POC device (Scheme 3.7). To achieve this, the catalytic loading was initially increased and since the reaction was heterogeneous, a biocompatible organic co-solvent was introduced to improve the solubility of the substrate as well as reduce errors associated with reaction sampling. Together, this allowed for quantitative isolated yield to be obtained at room temperature in just 30 minutes. Additionally, this result was obtained without the need to pre-form the catalyst as pre-catalyst and ligand **171** could simply be added separately to generate the active catalyst *in situ*. This could lend extra applicability of this catalytic transformation towards signal amplification within a POC setting.
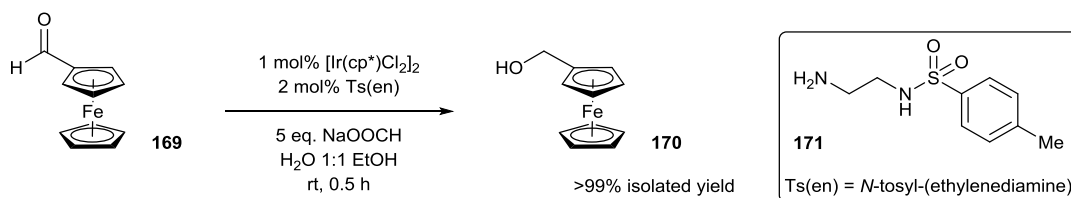
Scheme 3.7 Optimised conditions for the iridium-catalysed transfer hydrogenation of ferrocenecarboxaldehyde **169** to ferrocenemethanol **170**.

It has been shown that varying the substituents upon the aryl ring of the ligand can affect the rate of the transfer hydrogenation reaction.[419] Therefore, a range of ligands with varying substituents upon the aromatic ring were synthesised and tested within the transfer hydrogenation reaction to determine if any provided an increase in rate over the standard *N*-tosyl-(ethylenediamine) **171** ligand. The mono-sulfonamide(ethylenediamine) ligands were synthesised from the reaction between ethylenediamine **172** and the corresponding sulfonyl chlorides under standard conditions in moderate to good yields (Table 3.1).
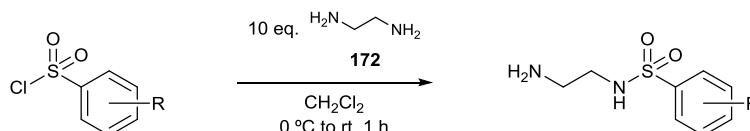
Product	R	Yield (%) [a]
171	4-Me	49%
173	H	25%
174	4-^{t}Bu	77%
175	2,4,6-Me$_3$	77%
176	2,4,6-^{i}Pr$_3$	77%
177	4-F	21%
178	4-Br	66%
179	4-OMe	37%
180	4-NO$_2$	29%
181	4-CF$_3$	59%

[a] isolated yields.

Table 3.1 Preparation of ligands **171, 173–181**.

With a range of ligands in hand containing substituents with varying steric and electronic demand, it was necessary to test them within the iridium-catalysed transfer hydrogenation reaction (Table 3.2). To determine either positive or negative effects of the ligand, the reaction was performed at half the optimised catalytic loading and was sampled after just 9 minutes. After sample dilution, the reaction was analysed by ratiometric electrochemical detection in order to calculate the reaction conversion.

Typically, electron-poor benzenesulfonamides deliver an accelerated rate when utilised within the iridium-catalysed transfer hydrogenation reaction. However, when applied to the

reduction of ferrocenecarboxaldehyde **169**, both electron-poor benzenesulfonamides, *p*-nitro **180** and *p*-trifluoromethyl **181**, did not perform as well as standard *p*-methyl ligand **171**. At the opposite end of the Hammett scale, electron-rich benzenesulfonamide *p*-methoxy ligand **179**, also delivered poor conversion. However, the mildly electron-rich alkyl-substituted ligands offered best conversions with 2,4,6-trimethylbenzenesulfonamide **175** delivering a slightly better conversion than the tosyl derivative. As a result, mesityl derivative **175** was taken as the optimal ligand for this reaction and was used in all further reactions. Increasing the steric bulk of the ligand was shown to severely restrict reaction conversion as 2,4,6-triisopropylbenzenesulfonamide **176** performed little better than the background rate. This is thought to be due to either prevention of active catalyst formation or blocking the approach of the catalyst substrate. Significantly, in the absence of any ligand, minimal conversion was observed thus reinforcing the importance of the ligand with regards to obtaining high catalyst turnover frequencies. Therefore, as a method for selective catalyst activation, careful control of the ligand could be crucial in achieving a positive conversion in the presence of the enzyme yet a negative conversion in its absence.
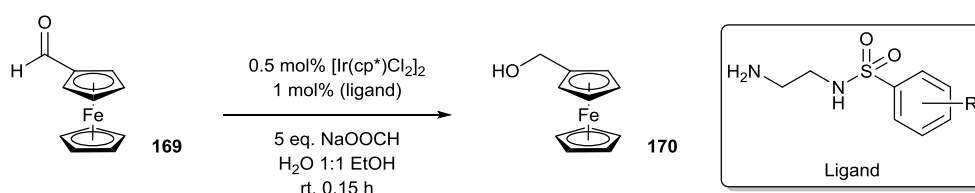
Ligand	R	Conversion (%) [a]
none	-	1%
171	4-Me	40%
173	H	22%
174	4-^{t}Bu	39%
175	2,4,6-Me$_3$	43%
176	2,4,6-^{i}Pr$_3$	3%
177	4-F	39%
178	4-Br	18%
179	4-OMe	18%
180	4-NO$_2$	25%
181	4-CF$_3$	32%

[a] determined by ratiometric electrochemical analysis.

Table 3.2 Screen of ligands **171, 173–181** within the iridium-catalysed transfer hydrogenation reaction.
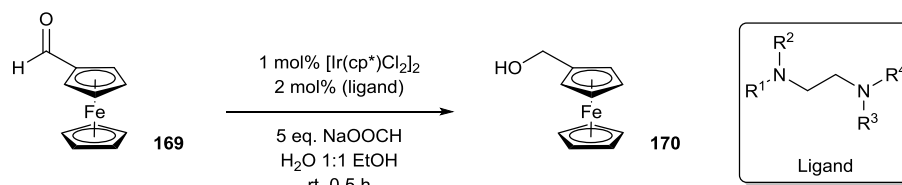
3.1.3 Primary Catalytic Signal Amplification

To switch on catalytic activity selectively in the presence of an enzyme, a programmed release of the ligand was required. In principle, if an enzyme could release the ligand into the system, then the iridium-catalysed transfer hydrogenation reaction would undergo ligand acceleration and conversion of ferrocenecarboxaldehyde **169** to ferrocenemethanol **170** would be observed by electrochemical analysis. On the other hand, if an enzyme was not present, then the ligand would not be released into the system and the transfer hydrogenation reaction would not undergo ligand acceleration leaving only ferrocenecarboxaldehyde **169** to be observed on the voltammogram. Chemical modification of the ligand structure was initially considered as an option to prevent the ligand from binding to the metal and increasing its rate within transfer hydrogenation reaction. It was presumed that modification of the ligand with an enzyme-cleavable trigger and a linker that could undergo a designed elimination, would allow ligand release in the presence of the enzyme. Prior to that however, a range of *N*-methylated ethylenediamines were tested as ligands (Table 3.3), along with their *N*-mesitylsulfonamide derivatives (Scheme 3.8), within the iridium-catalysed transfer hydrogenation reaction (Table 3.4). This would determine both how much, and where substitution was required in order to prevent a successful metal–ligand binding event and subsequent rate acceleration from occurring.
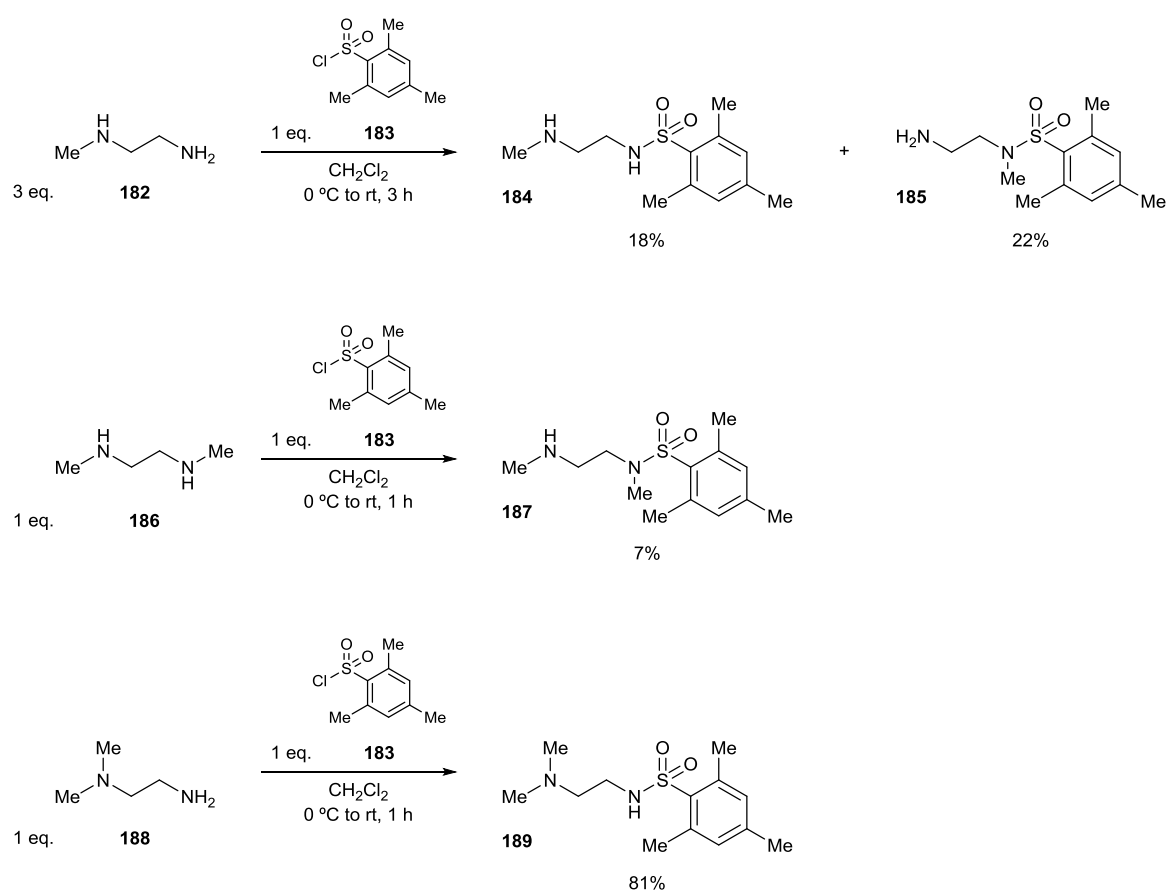
Scheme 3.8 Synthesis of *N*-methylated-*N*-mesitylsulfonamide ethylenediamine ligands **184**, **185**, **187** and **189**.
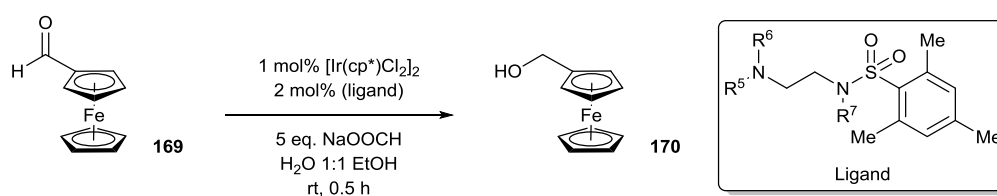
1 mol% [Ir(cp*)Cl$_2$]$_2$
2 mol% (ligand)

5 eq. NaOOCH
H$_2$O 1:1 EtOH
rt, 0.5 h

169 → 170

Ligand (R^1, R^2, R^3, R^4 substituted ethylenediamine)

Ligand	R^1	R^2	R^3	R^4	Conversion (%) [a]
172	H	H	H	H	2%
182	Me	H	H	H	2%
186	Me	Me	H	H	<1%
188	Me	H	Me	H	2%
190	Me	Me	Me	Me	0%

[a] determined by ratiometric electrochemical analysis.

Table 3.3 Screen of *N*-methyl ethylenediamine ligands within the iridium-catalysed transfer hydrogenation reaction.

1 mol% [Ir(cp*)Cl$_2$]$_2$
2 mol% (ligand)

5 eq. NaOOCH
H$_2$O 1:1 EtOH
rt, 0.5 h

169 → 170

Ligand (R^5, R^6, R^7 substituted mesitylsulfonamido-ethylenediamine)

Ligand	R^5	R^6	R^7	Conversion (%) [a]
175	H	H	H	>99%
184	Me	H	H	34%
185	H	H	Me	6%
187	Me	H	Me	0%
189	Me	Me	H	0%

[a] determined by ratiometric electrochemical analysis.

Table 3.4 Screen of *N*-methyl mesitylsulfonamido-ethylenediamine ligands within the iridium-catalysed transfer hydrogenation reaction.

Under the optimised conditions, ethylenediamine **172** and its mono- and di-methylated derivatives **182**, **186** and **188** were all found to be ineffective ligands within the transfer hydrogenation reaction. Additionally, and somewhat expectedly, tetramethylethylenediamine (TMEDA) **190** was shown to completely inhibit catalyst activity. This highlights the need for a sulfonamide-containing ligand in order to achieve high reaction rates. Further confirmation of this was shown by the best performing ligand found from the ligand screen as ligand **175** delivered

quantitative conversion after 30 minutes. Modifying **175** with a single methyl group at the primary amine position, ligand **184**, was shown to be enough to hamper the reaction but interestingly, was insufficient to shutdown reactivity completely. This was thought to be due to the fact the ligand is still equipped with a proton for activation of the substrate carbonyl towards hydride attack as well as a sulfonamide for metal insertion. Further methylation at this position, ligand **189**, and thus disabling proton-assisted activation of the substrate carbonyl, completely inhibits reactivity as no conversion was at all observed. Alternatively, additional methylation on the sulfonamide nitrogen, ligand **187**, and thus preventing metal insertion to form the active catalyst, also leads to a complete loss in catalytic activity. However, solely blocking the sulfonamide nitrogen with a methyl group, ligand **185**, was found to not be enough to completely inhibit the reaction as small conversion was still observed.
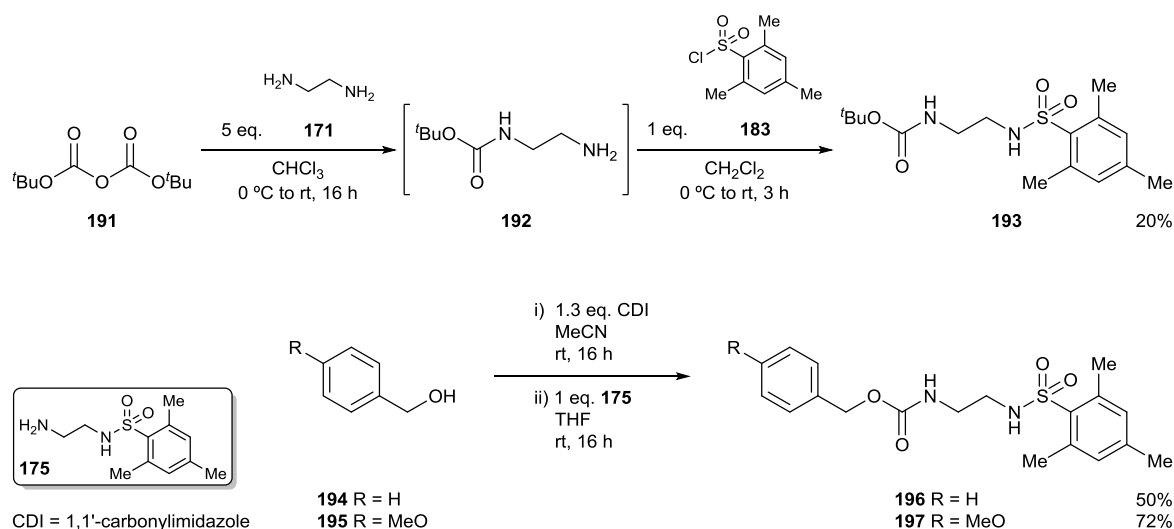
Scheme 3.9 Synthesis of *N*-carbamate-*N*-mesitylsulfonamide ethylenediamine ligands **193**, **196** and **197**.
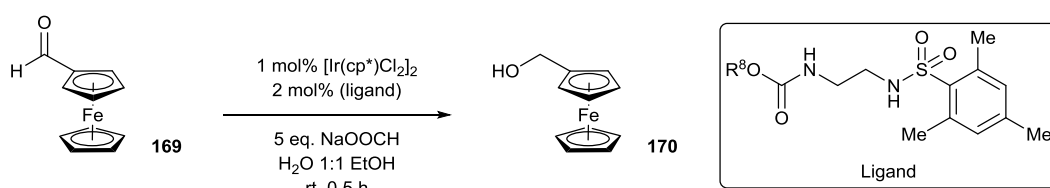
Ligand	R^8	Conversion (%) [a]
193	*t*Bu	7%
196	Bn	<1%
197	4-MeOBn	2%

[a] determined by ratiometric electrochemical analysis.

Table 3.5 Screen of *N*-carbamate *N*-mesitylesulfonamido-ethylenediamine ligands within the iridium-catalysed transfer hydrogenation reaction.

Clearly, functionalisation at the primary amine position of mesitylsulfonamide **175** was sufficient in hindering ligand acceleration within the transfer hydrogenation reaction. To investigate this further, a number of carbamate derivatives of ligand **175** were synthesised since these functional groups are more amenable to elimination than a methylene group (Scheme 3.9). When tested within the transfer hydrogenation reaction, the carbamate derivatives of ligand **175** were also found to be ineffective ligands (Table 3.5). Importantly, benzyl carbamates **196** and **197** delivered negligible conversions which could allow ligand release to potentially be achieved through the quinone–methide elimination mechanism.

3.1.4   Enzyme Substrate Design and Synthesis
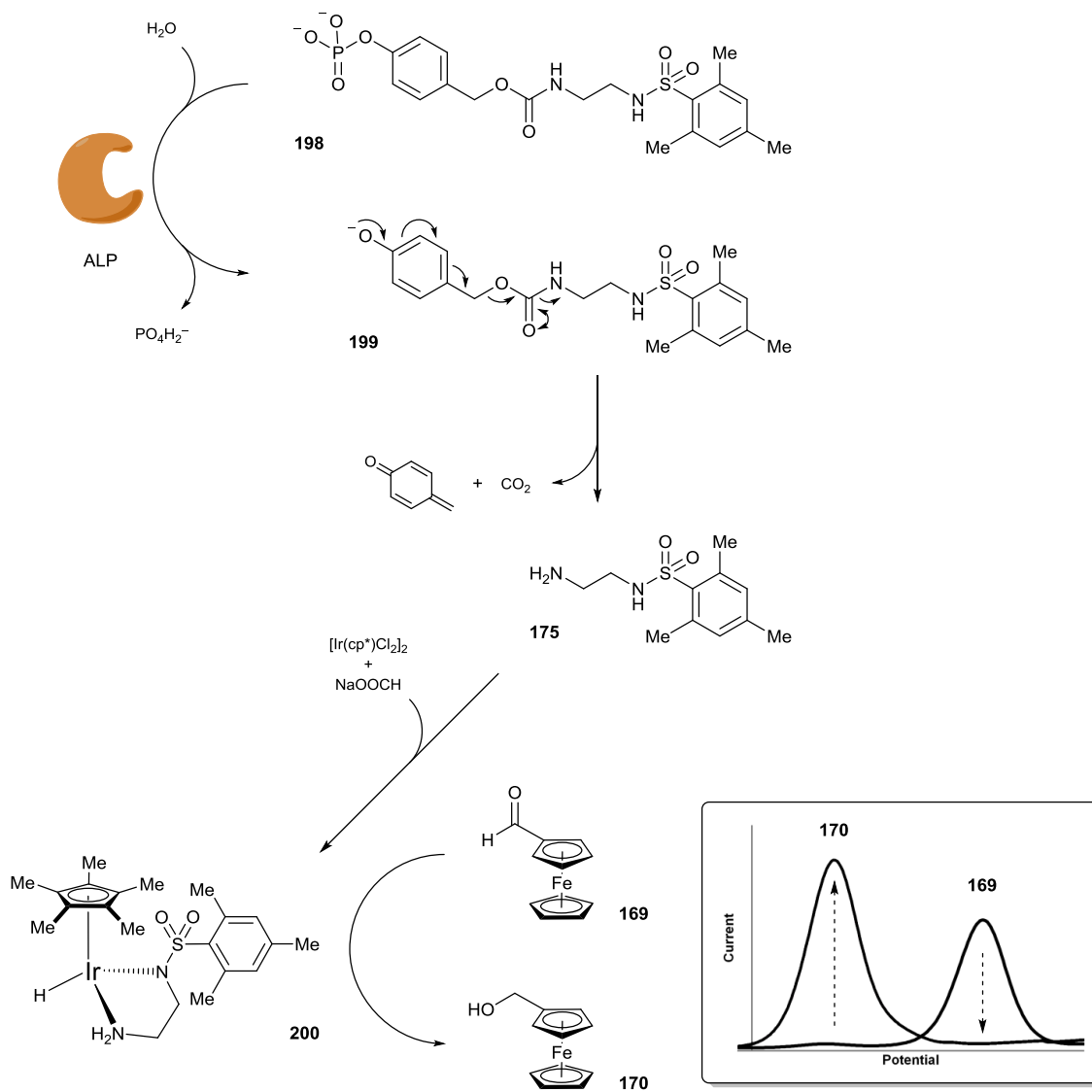
Scheme 3.10 Proposed mechanism for enzyme-triggered ligand release and ligand-accelerated transfer hydrogenation.

Consequently, compound **198** was designed armed with a phosphate trigger enabling ligand release to be achieved through ALP-catalysed hydrolysis (Scheme 3.10). Enzyme substrate **198** was subsequently termed a 'proligand' since it was designed not to act like a ligand in its current form, but could undergo a functional group transformation to create an active ligand. In principle, a low background reaction should be seen in the absence of an enzyme as the proligand should remain protected as carbamate **198**. Yet in the presence of the enzyme, enzyme-catalysed hydrolysis of the enzyme substrate would give phenolate **199**. 1,6-elimination and subsequent decarboxylation should then release ligand **175** into the system and once released, the ligand can bind to the iridium pre-catalyst to form active catalyst **200**, which would have an increased rate within the catalytic transfer hydrogenation reaction. This would lead to a faster turnover of ferrocenecarboxaldehyde **169** to ferrocenemethanol **170**, which could be monitored through ratiometric electrochemical analysis.
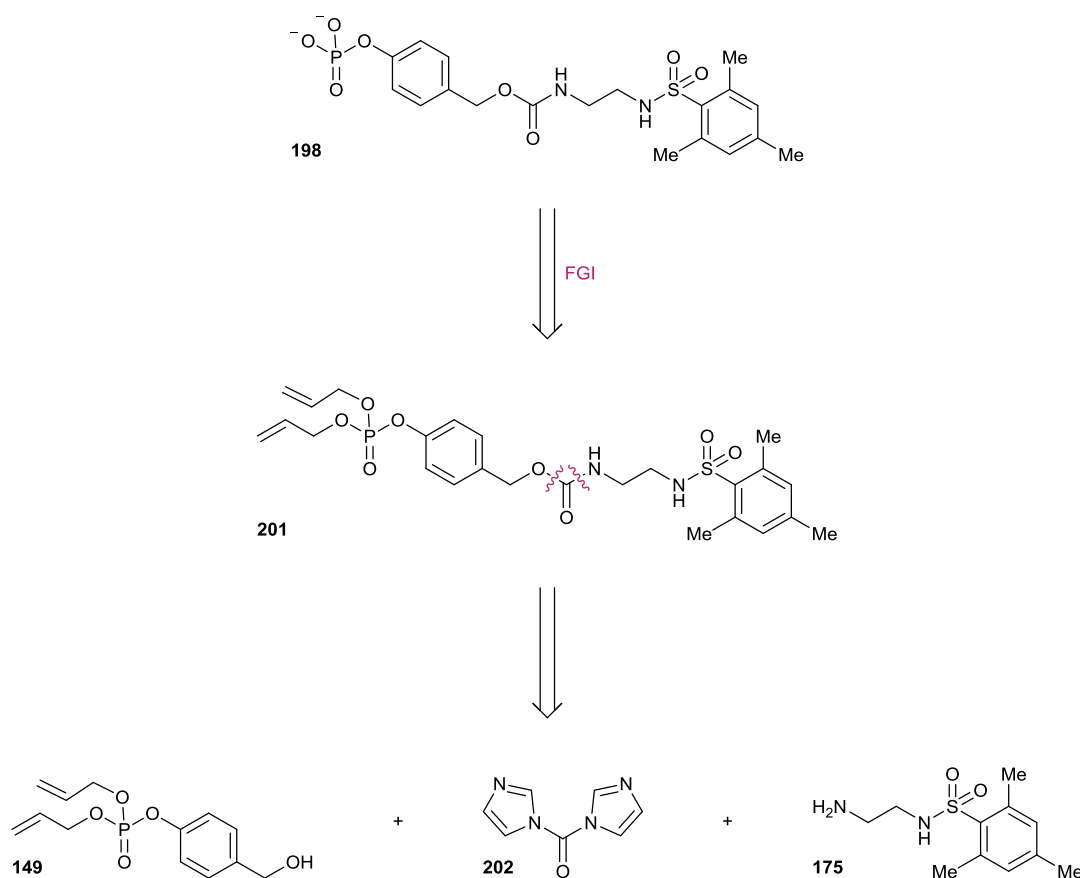
Scheme 3.11 Retrosynthetic analysis of proligand **198**.

To prove this concept, proligand **198** first had to be synthesised. Retrosynthetic analysis of **198** revealed that, after phosphate protection, bis-protected compound **201** could simply be achieved through coupling of ligand **175** with a bis-protected phosphoryl benzyl alcohol such as **149** through the use of a carbonyl coupling reagent such as 1,1'-carbonyldiimidazole (CDI) **202**

(Scheme 3.11). Towards this end, the synthesis of proligand **198** began with the coupling of previously synthesised benzyl alcohol **149** to optimal ligand **175** using CDI **202** under standard conditions, which afforded carbamate **201** in good yield (Scheme 3.12). The previously optimised allyl deprotection conditions were then applied to bis-allyl protected phosphate **201** and were also found to be effective for this substrate as full consumption of starting material was observed. However, owing to the poor solubility of product **198** in any solvent, purification by preparative reverse phase C_{18}-silica gel column chromatography or recrystallisation was unachievable. Fortunately, allyl deprotection typically occurs cleanly and owing to the polymer-supported catalyst and volatility of the reagents, crude compound **198** could still be obtained in high enough purity. Typically, ^{31}P NMR was a single peak corresponding to the product and ^{1}H NMR shows mainly product with sodium formate, arising from deprotonation of leftover formic acid from the deprotection step, as the sole minor impurity. Since sodium formate is used as the hydride source in the transfer hydrogenation reaction, this impurity was thought not to affect the outcome of any subsequent reactions and so proligand **198** was decided to be taken forward without further purification.
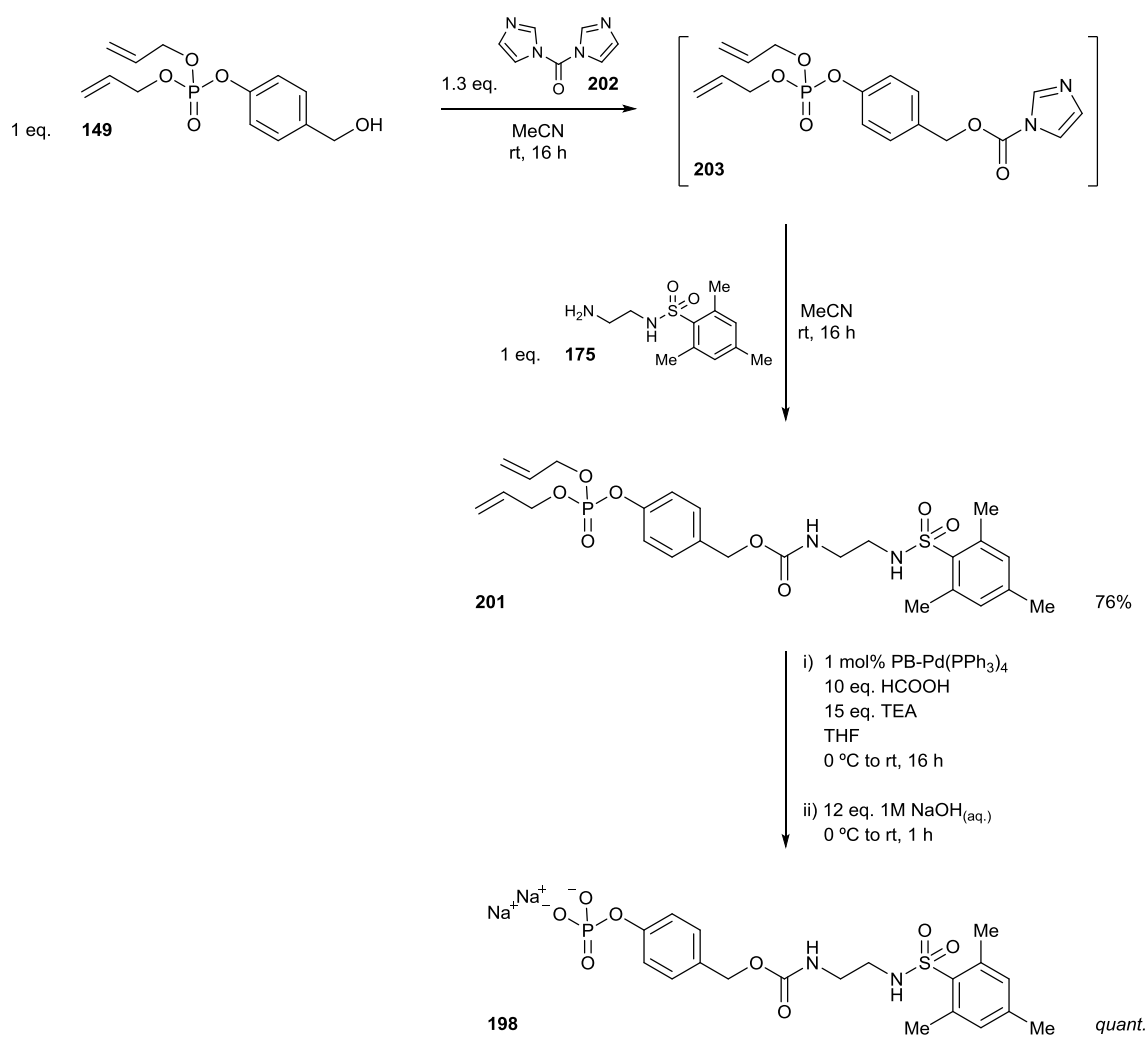
Scheme 3.12 Synthesis of proligand **198**.
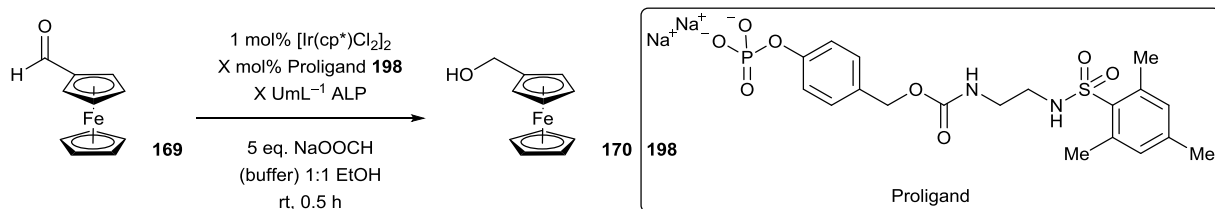
Proligand 198	ALP	Buffer	Yield (%) [a]
2 mol%	0 UmL^{-1}	H$_2$O	4%
2 mol%	100 UmL^{-1}	pH 9 Tris	95%
0 mol%	100 UmL^{-1}	pH 9 Tris	29%
0 mol%	100 UmL^{-1}	pH 9.8 CO$_3^{2-}$	0%
2 mol%	100 UmL^{-1}	pH 9.8 CO$_3^{2-}$	95%

[a] isolated yield.

Table 3.5 Background reactions.

With proligand **198** in hand, it was necessary to test it as a ligand within the transfer hydrogenation reaction (Table 3.5). In the absence of any enzyme, a low yield of ferrocenemethanol **170** was obtained showing that, in water, the proligand does not contribute to undesired reaction acceleration. Pleasingly, in the presence of ALP in its optimal pH 9 Tris buffer, a near quantitative yield of **170** was obtained with proligand **198**. To confirm whether conversion of ferrocenecarboxaldehyde **169** to ferrocenemethanol **170** was occurring through the proposed mechanism, the reaction was repeated in the absence of the proligand. Unfortunately, a significantly large background reaction was observed which could be due to either enzyme stabilisers or the enzyme itself, or components of the buffer solution. Since ethylenediamine- and ethanolamine-like compounds present in both the buffer and as enzyme stabilisers, or bidentate amino acid side-chains on the enzyme, could act as ligands themselves within the transfer hydrogenation reaction, the assay was repeated in an ALP-compatible buffer that did not contain these classes of structures. The change in buffer resulted in a dramatic reduction in the background rate as no conversion to ferrocenemethanol **170** whatsoever was observed. This points to components in the buffer, most probably tris(hydroxymethyl)aminomethane (Tris) itself, as the main culprit for the previously observed high background rate. To ensure the positive reaction maintained a high conversion despite the buffer change, the reaction was again repeated but this time with the inclusion of proligand **198**. Again, a high isolated yield of ferrocenemethanol **170** was obtained which, with greater certainty, can be attributed to enzyme triggered release of ligand **175** from the proligand and subsequent ligand-acceleration of the transfer hydrogenation reaction.

3.1.5   Mechanistic Studies

In order to determine that the observed conversion of ferrocenecarboxaldehyde **169** to ferrocenemethanol **170** was occurring through the proposed mechanism, a number of mechanistic studies were performed. First, to confirm that the proligand can be selectively hydrolysed by ALP, a buffered solution of **198** was exposed to ALP and the interaction monitored by ^{31}P NMR (Figure 3.5). Indeed, when a 50 mM buffered solution of **198** was treated with 5 UmL^{-1} of ALP, the peak at −0.15 ppm corresponding to proligand **198** slowly decreases over time. Concomitantly, a peak at 2.25 ppm corresponding to the free phosphate slowly increases over time. A repeat experiment in the absence of ALP did not lead to the deconstruction of proligand **198** over the same time period, which shows that dephosphorylation occurs only in the presence of ALP. Similarly to previous, the protic aqueous buffer required for enzyme activity prohibits the use of ^{1}H NMR to identify any reaction intermediates, such as quinone methide or 4-hydroxybenzyl alchohol, or product **175**. Additionally, attempts to isolate and characterise ligand **175** after the reaction was complete to confirm its release as a result of dephosphorylation were unsuccessful. For further mechanistic elucidation, an orthogonal reaction-monitoring technique was required.
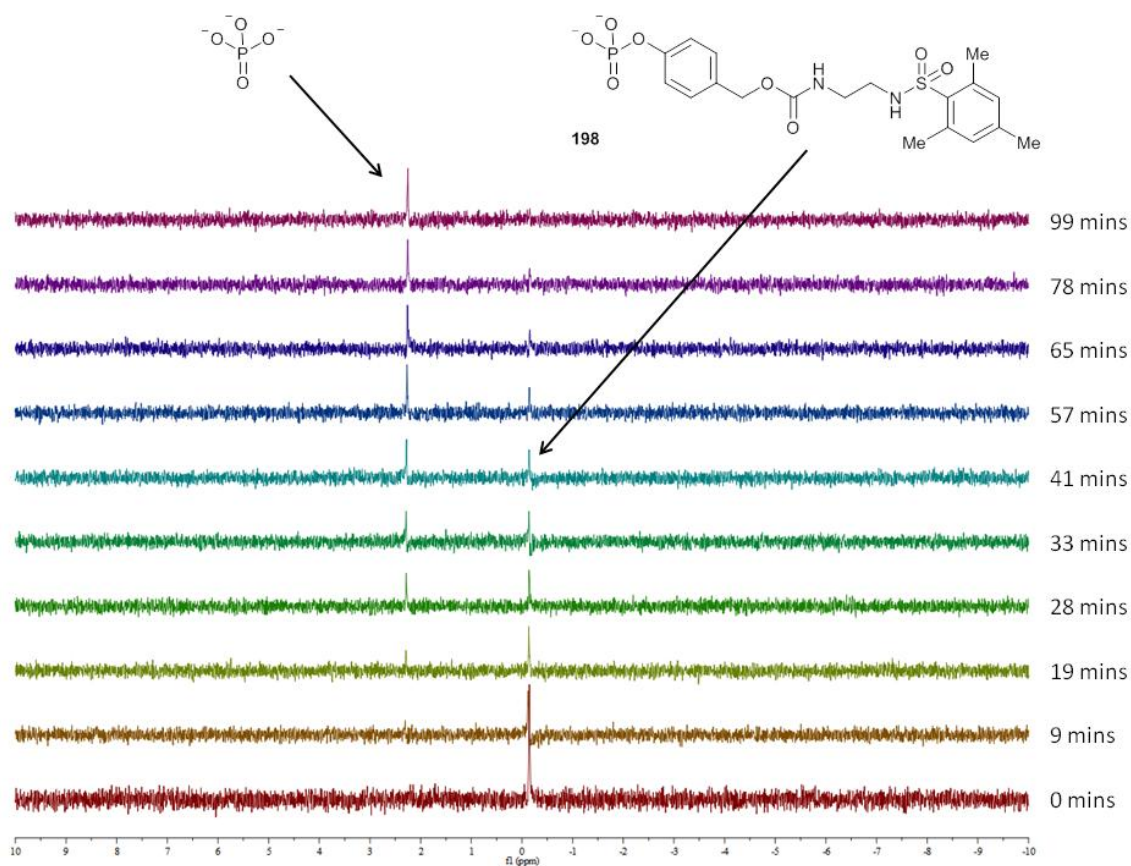
Figure 3.5 Stacked ^{31}P NMR spectra of proligand **198** over time after the addition of ALP.

In order to detect the intermediate phenol and elimination products such as quinone methide or 4-hydroxybenzyl alcohol as well as the production of ligand **175** from the reaction of proligand **198** with ALP, the reaction was then monitored using direct infusion electrospray ionisation ultrahigh resolution time-of-flight mass spectrometry (ESI-UHR-TOF MS). In negative ion mode, an initial 3 mM solution of **198** in water was directly injected at rate of 3 µLmin^{-1} for 10 minutes and over this time period, only the peak corresponding to the [M−H]⁻ mass ion for hydrogen phosphate **204** was observed (Figure 3.6). This confirms the stability of proligand **198** to both undesired hydrolysis as well as the ionisation technique used for MS analysis.
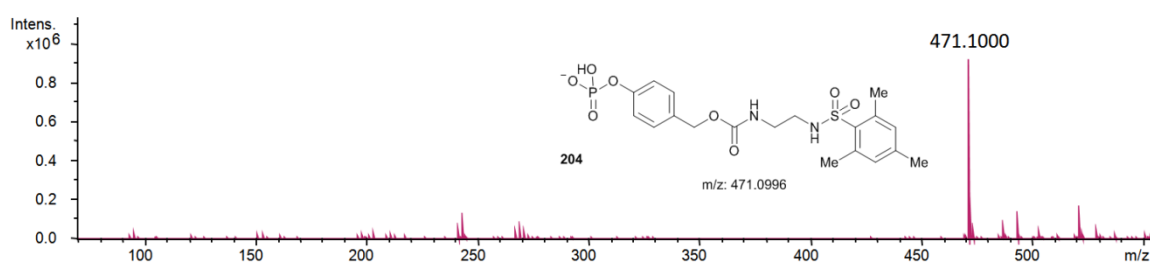
Figure 3.6 Accumulative averaged mass spectrum acquired over a 10 minute period of proligand **198** in water prior to the addition of ALP.
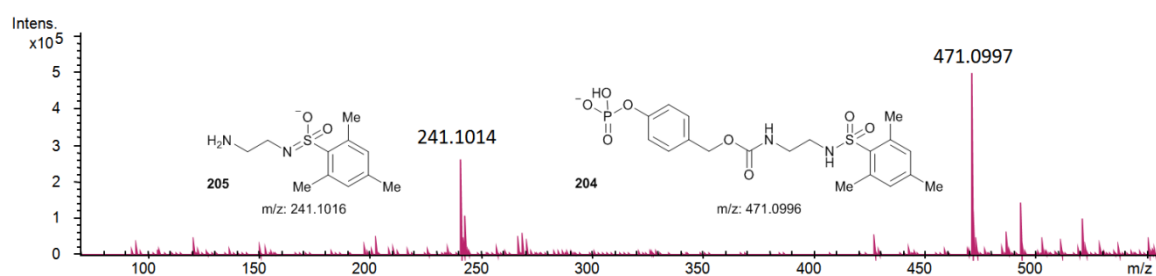
Figure 3.7 Accumulative averaged mass spectrum acquired over a 3 minute period of proligand **198** in water 6 minutes after the addition of ALP.
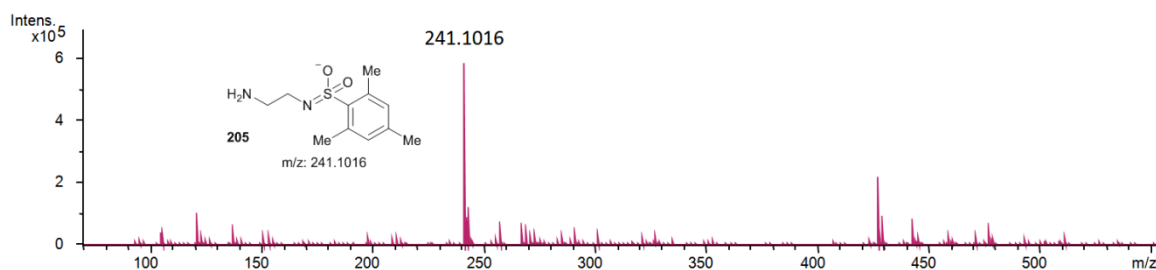
Figure 3.8 Accumulative averaged mass spectrum acquired over a 2 minute period of proligand **198** in water 29 minutes after the addition of ALP.

Upon the addition of a buffered solution of ALP, a peak corresponding to the [M−H]⁻ mass ion for deprotonated sulfonamide anion **205** becomes immediately apparent (Figure 3.7). This

shows that, once proligand **198** undergoes ALP-catalysed dephosphorylation, 1,6-elimination and decarboxylation of the intermediate phenolate **199** occurs and ligand **175** was released as desired. After a 30 minute reaction period, the peak corresponding to the [M−H]⁻ mass ion for **204** disappears indicating that full consumption of the enzyme substrate occurs over time as expected (Figure 3.8). Additionally, the peak corresponding to the [M−H]⁻ mass ion for **205** increases with intensity over time indicating that as proligand **198** was consumed, the concomitant production of ligand **175** also occurs. Clarification of this observation can be better provided through a plot of the intensities for both [M−H]⁻ mass ion peaks for **204** and **205** over time (Figure 3.9). The peak corresponding to the [M−H]⁻ ion for 4-hydroxybenzyl alcohol was not evident under these conditions, as loss of the phenolic proton would lead to a 1,6-elimination to release hydroxide and the resulting neutral quinone methide would be undetectable by MS in negative ion mode. Nevertheless, release of ligand **175** was indeed occurring as a direct result of enzyme-catalysed hydrolysis of proligand **198**.
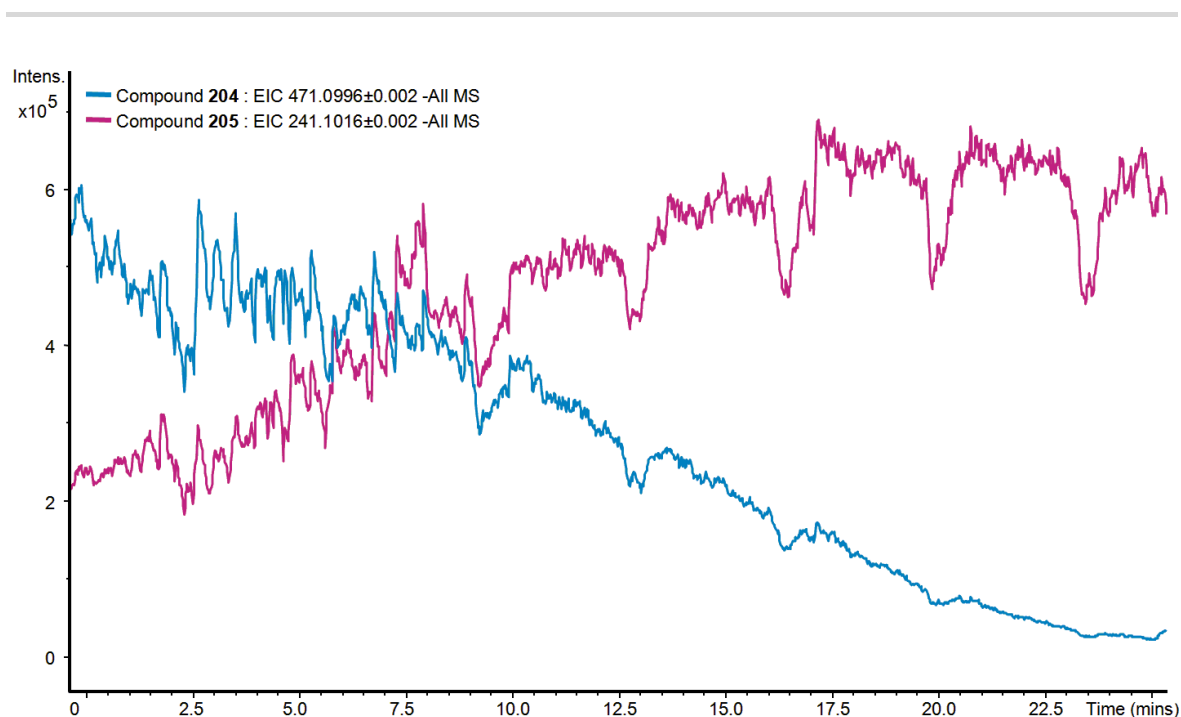
Figure 3.9 Peak intensities representing proligand **198** and ligand **175** over time after the addition of ALP.

Having proven that the iridium-catalysed transfer hydrogenation reaction could be selectively accelerated through enzyme activity and that this occurs through the programmed release of a ligand from a proligand, the next objective was to optimise the enzyme-triggered catalytic signal amplification methodology to increase the sensitivity of the ALP detection assay.

3.1.6. Optimisation of the Enzyme Detection Assay

Initially, a study into the optimal catalytic loading of the iridium–ligand catalyst **200** was first required in order to determine the concentration of proligand **198** needed to deliver efficient enzyme-triggered ligand-accelerated catalytic signal amplification. Specifically, identification of the lowest catalytic loading that delivered quantitative electrochemical conversion in the shortest amount of time was sought. Towards this end, ferrocenecarboxaldehyde **169** was exposed to different catalytic loadings of iridium catalyst **200** and the reaction was monitored every 3 minutes using ratiometric electrochemical analysis (Figure 3.10).
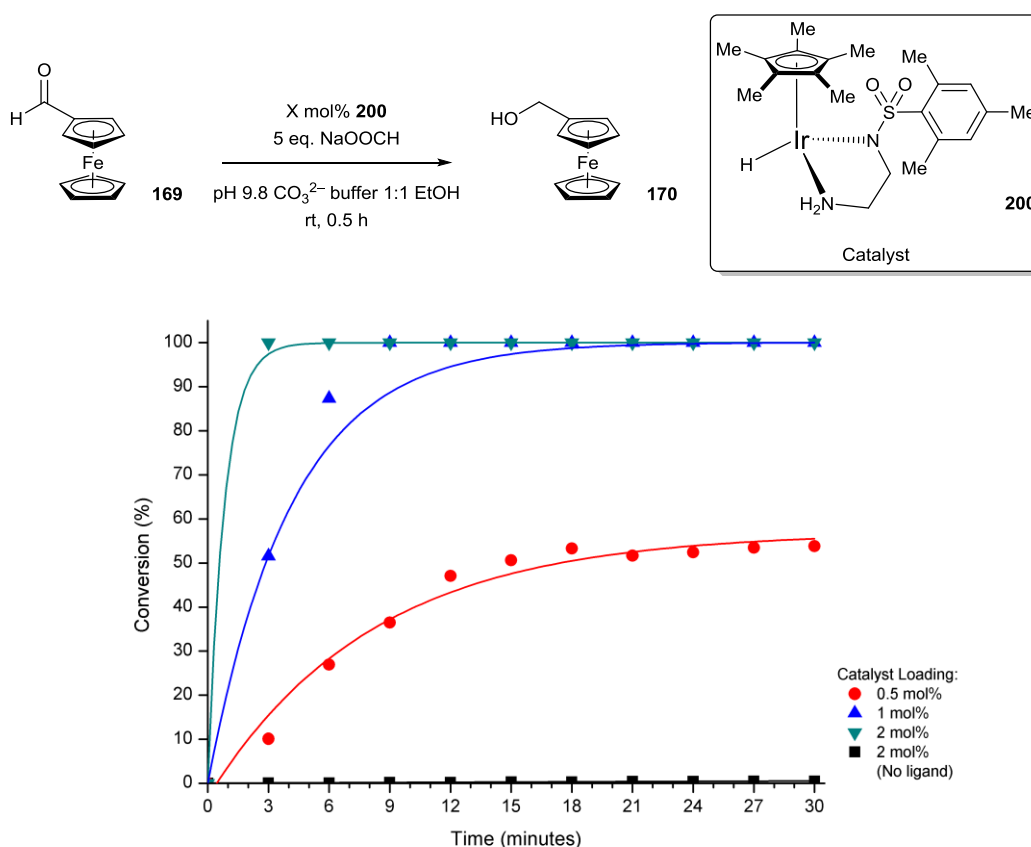
Figure 3.10 Electrochemical conversion of aldehyde **169** to alcohol **170** under different catalytic loadings at room temperature.

At a catalyst loading of 0.5 mol%, only ≈50% electrochemical conversion of ferrocenecarboxaldehyde **169** to ferrocenemethanol **170** was observed after 30 minutes at room temperature. Doubling the catalyst loading to 1 mol% afforded quantitative electrochemical conversion within the same time period. Doubling the catalytic loading again to 2 mol% delivered quantitative electrochemical conversion within just 3 minutes. Importantly, in the absence of the ligand, <1% conversion was observed after 30 minutes showing the dramatic signal change that can be achieved through ligand acceleration.

Encouraged by the efficiency of the iridium-catalysed transfer hydrogenation reaction at 2 mol%, the next step was to apply this catalytic loading towards the detection of ALP by replacing ligand **175** with proligand **198** (Figure 3.11). Pleasingly, in the presence of high concentrations of ALP (10 and 100 UmL^{-1}), positive conversions were indeed observed over a 30 minute reaction time. However, an ALP concentration of 1 UmL^{-1} could not be confidently discerned from the background rate, which had increased slightly through the use of proligand **198**. Nevertheless, the enzyme-triggered catalytic signal amplification methodology had been successfully demonstrated in one pot without the need for protection, separation or manipulation of the reagents, ideal for use within an automated POC device.
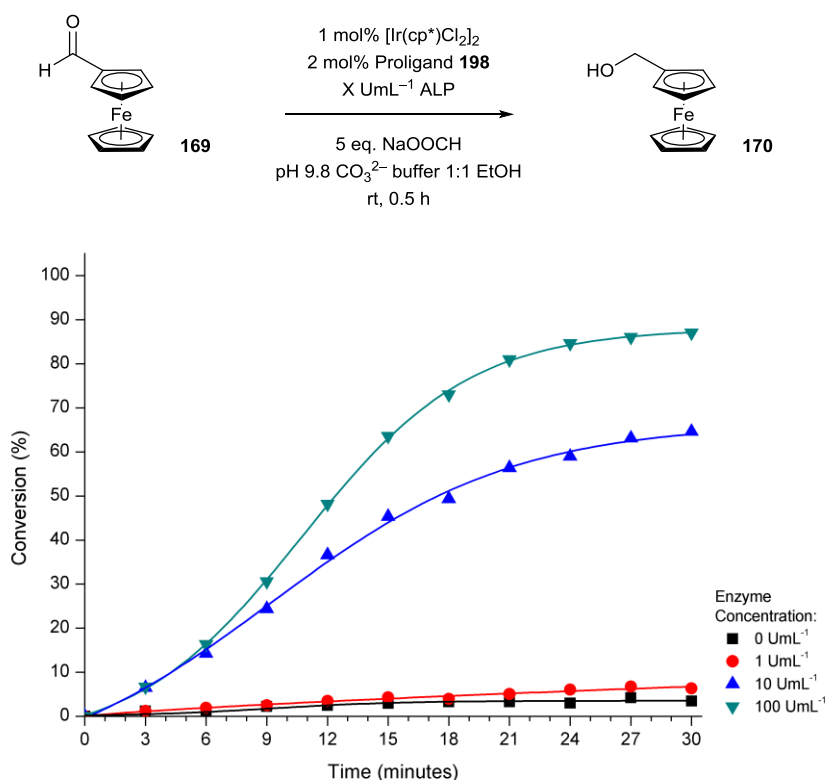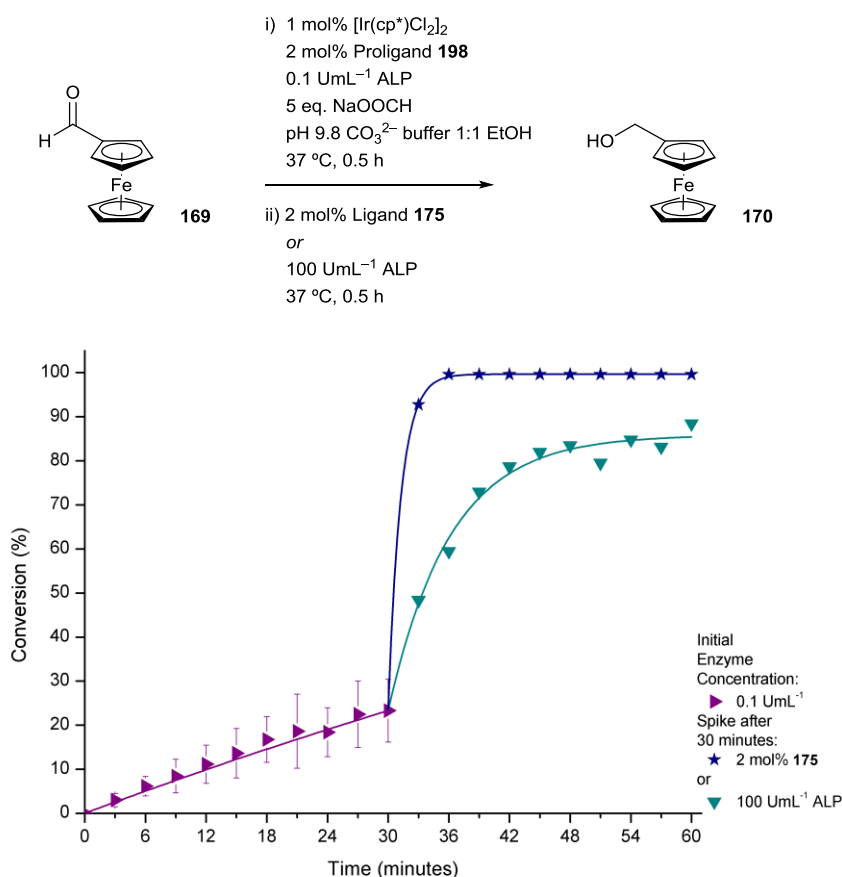

Figure 3.11 Electrochemical conversion of aldehyde **169** to alcohol **170** in the presence of different enzyme concentrations at room temperature.

Of particular interest is the sigmoidal shape of the reaction profiles as this indicates that there are two distinct phases to the enzyme-triggered catalytic signal amplification methodology. Initially, there is a catalyst activation period where enzyme-triggered ligand release and subsequent active catalyst complex formation is effectively rate limiting. Once a sufficient proportion of the enzyme substrate has been consumed and a significant number of ligands have been released, then the number of active catalysts in the system is increased which leads to the pseudo-exponential rate increase. After this, a standard reaction profile is observed where consumption of the starting material leads to a plateau in rate. These sigmoidal profiles are indicative of an exponential-type

signal amplification mechanism being in effect, as previously reported double catalyst, autoinductive and autocatalytic signal amplification methodologies have all shown similar reaction profiles.
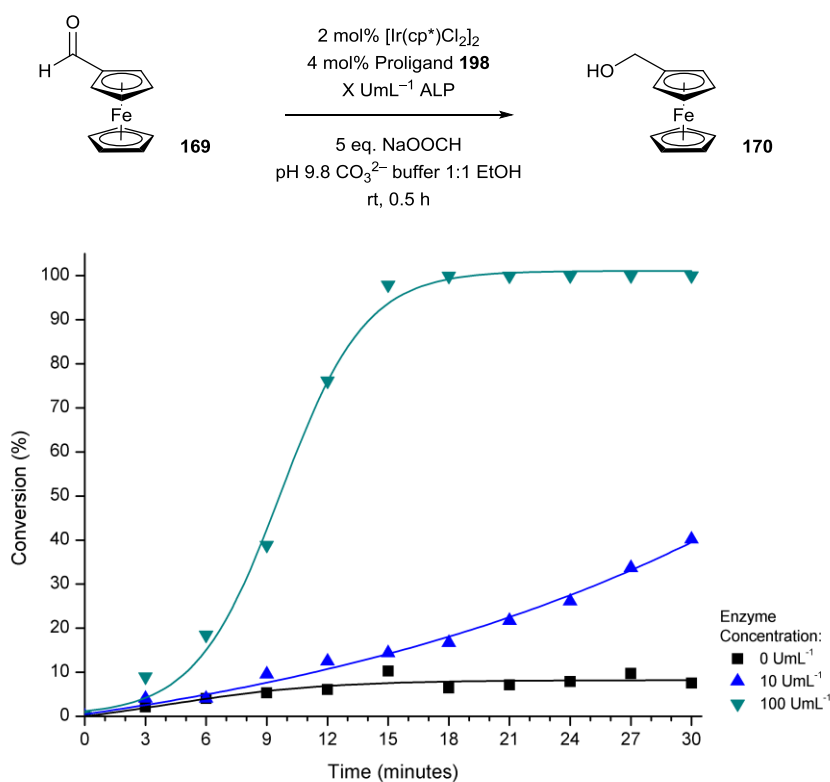
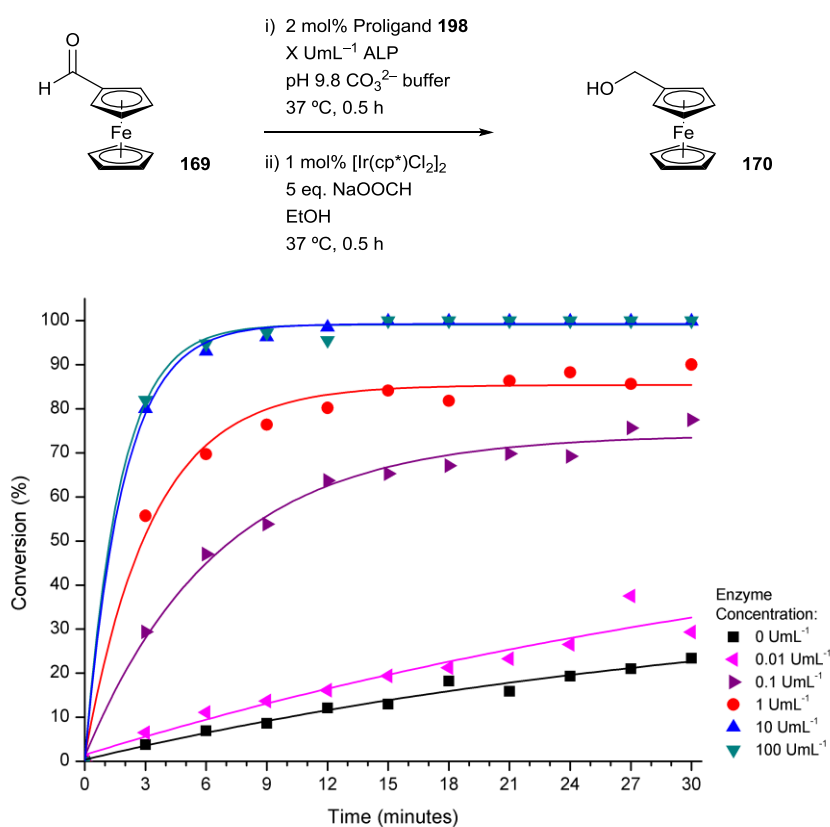**Figure 3.12** Electrochemical conversion of aldehyde **169** to alcohol **170** in the presence of different enzyme concentrations at room temperature.

In order to improve the sensitivity of the assay, iridium precatalyst and proligand **198** loading was doubled to 2 mol% and 4 mol% respectively, as it was thought that this would increase turnover of the aldehyde substrate (Figure 3.12). At an enzyme concentration of 100 UmL^{-1}, this led to an increase in conversion and a sharper exponential signal increase. However, since a larger amount of proligand **198** needs to be hydrolysed to achieve complete catalyst acceleration, a lower enzyme concentration of 10 UmL^{-1} was found to be unable to do this and as such, a longer catalyst activation period and an associated lower conversion was therefore observed. Additionally, the increase in catalytic loading also provided an increase in the undesired background reaction. Resultantly, the catalytic loading was returned to 2 mol% and a study into assay temperature was next to be performed to improve assay sensitivity.
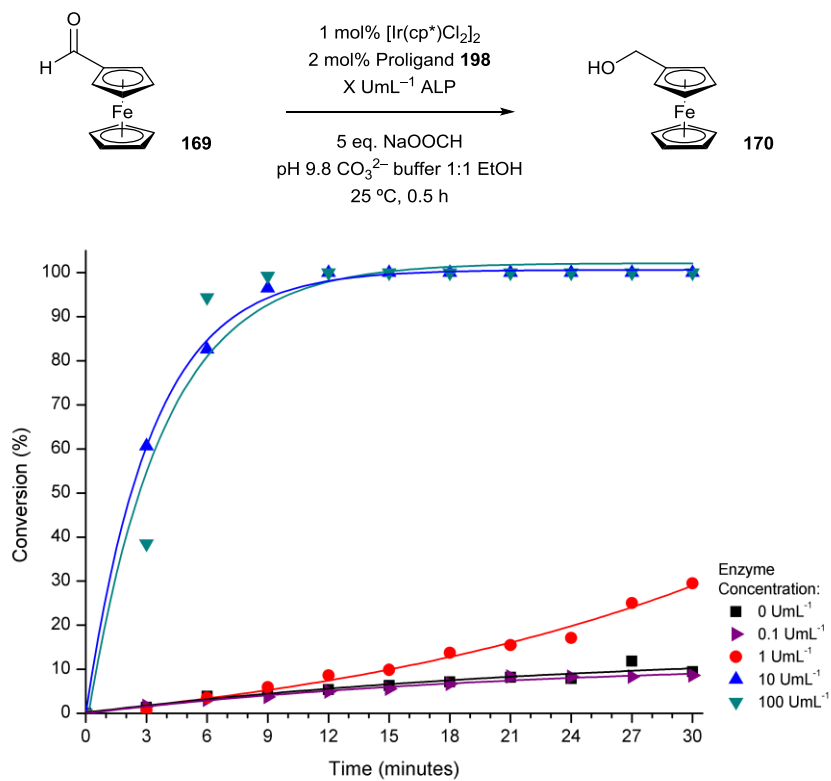
Figure 3.13 Electrochemical conversion of aldehyde **169** to alcohol **170** in the presence of different enzyme concentrations at 25 °C.
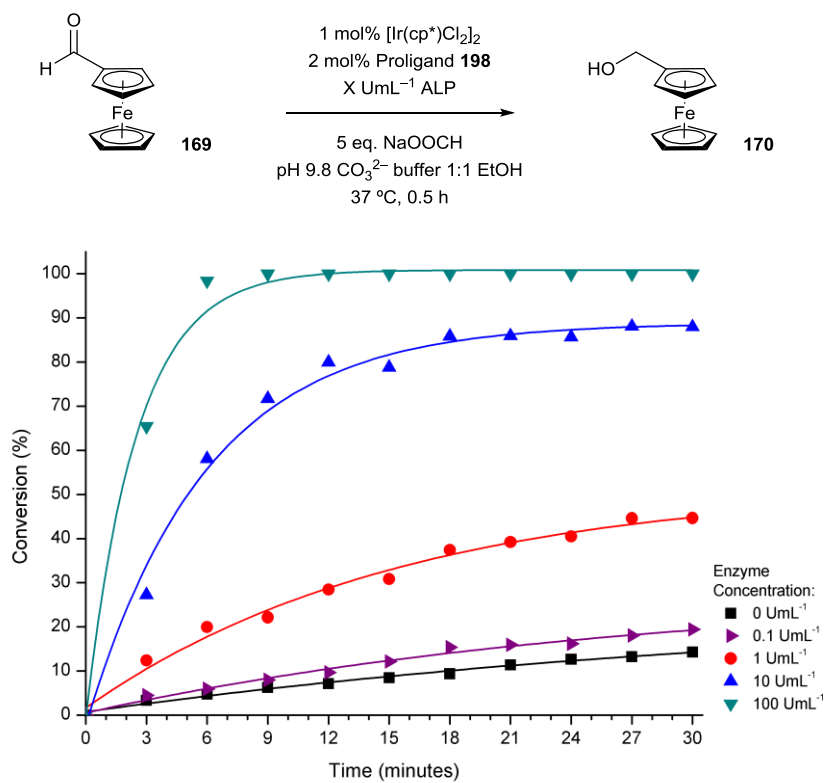
Figure 3.14 Electrochemical conversion of aldehyde **169** to alcohol **170** in the presence of different enzyme concentrations at 37 °C.

Increasing the temperature to 25 °C enabled quantitative conversions of ferrocenecarboxaldehyde **169** to ferrocenemethanol **170** within 30 minutes at enzyme concentrations of 10 UmL^{-1} and higher (Figure 3.13). The increase in temperature also allowed for an enzyme concentration of 1 UmL^{-1} to be distinguished from the background within the same timeframe. Incidentally, the background reaction is also increased due to the rise in temperature which prevents an enzyme concentration of less than 0.1 UmL^{-1} from being detected. Increasing the reaction temperature further, to 37 °C to coincide with the optimum working temperature of the enzyme also delivered an improvement to assay sensitivity as expected (Figure 3.14). Again, quantitative conversions were observed at high enzyme concentrations and at 1 UmL^{-1}, a much greater conversion was obtained. Despite another slight increase in the background reaction, an enzyme concentration of 0.1 UmL^{-1} was now distinguishable.

Figure 3.15 Electrochemical conversion of aldehyde **169** to alcohol **170** in the presence of an initial enzyme concentration of 0.1 UmL^{-1} at 37 °C. After 30 minutes, the assay was spiked with either 2 mol% of ligand **175** or 100 UmL^{-1} of ALP. Error bars indicate standard deviation ($n = 3$).

The proposed mechanism of this enzyme-triggered catalytic signal amplification methodology contains a number of potential bottlenecks which could limit the sensitivity of the assay. These were identified as enzyme-catalysed hydrolysis of proligand **198**, elimination and

release of ligand **175** from phenolate intermediate **199**, ligand–metal complexation to form active catalyst **200** and the iridium-catalysed transfer hydrogenation reaction itself. In order to determine which step was rate-limiting, specific spiking experiments were performed (Figure 3.15).

To begin with, the assay for the detection of 0.1 UmL^{-1} was performed analogous to previous and ran for 30 minutes, with sampling every 3 minutes. After this period, the assay was first spiked with ligand **175** to determine if either ligand release or enzyme-catalysed hydrolysis was rate limiting. Immediately after the introduction of ligand **175**, dramatic rate acceleration was observed with quantitative conversion being achieved within 6 minutes after ligand addition. This indicated that the iridium pre-catalyst was still available to undergo metal–ligand complexation to form active catalyst **200** as rapid transfer hydrogenation was seen after the addition of ligand **175**. To distinguish between whether enzyme-catalysed hydrolysis of proligand **198** or release of ligand **175** from intermediate phenolate **200** were rate limiting, the assay was repeated but after 30 minutes, the assay was spiked with 100 UmL^{-1} of ALP. Again, as a consequence of the spike, significant rate acceleration was observed. This indicates that at low concentrations of ALP, the enzyme substrate is not being hydrolysed quick enough to release sufficient amounts of ligand **175**. Therefore, enzyme-catalysed hydrolysis of proligand **198** was concluded as being the rate-limiting step of the enzyme-triggered catalytic signal amplification methodology.

Figure 3.16 Electrochemical conversion of aldehyde **169** to alcohol **170** in the presence of different enzyme concentrations at 37 °C with an additional 30 minute incubation period.

Armed with this knowledge, further attempts to improve the sensitivity of the signal amplification methodology were aimed at increasing the rate of enzyme-catalysed hydrolysis of proligand **198**. Towards this end, an incubation period, where the enzyme and the enzyme substrate were reacted together prior to the addition of the potentially interfering signal amplification reagents, was included within the procedure (Figure 3.16). The introduction of an incubation period allowed enzyme concentrations of 10 UmL^{-1} or higher to deliver quantitative conversions within 15 minutes. The sensitivity of the assay was also increased by an order of magnitude as an enzyme concentration of 0.01 UmL^{-1} could now be distinguished from the background rate.
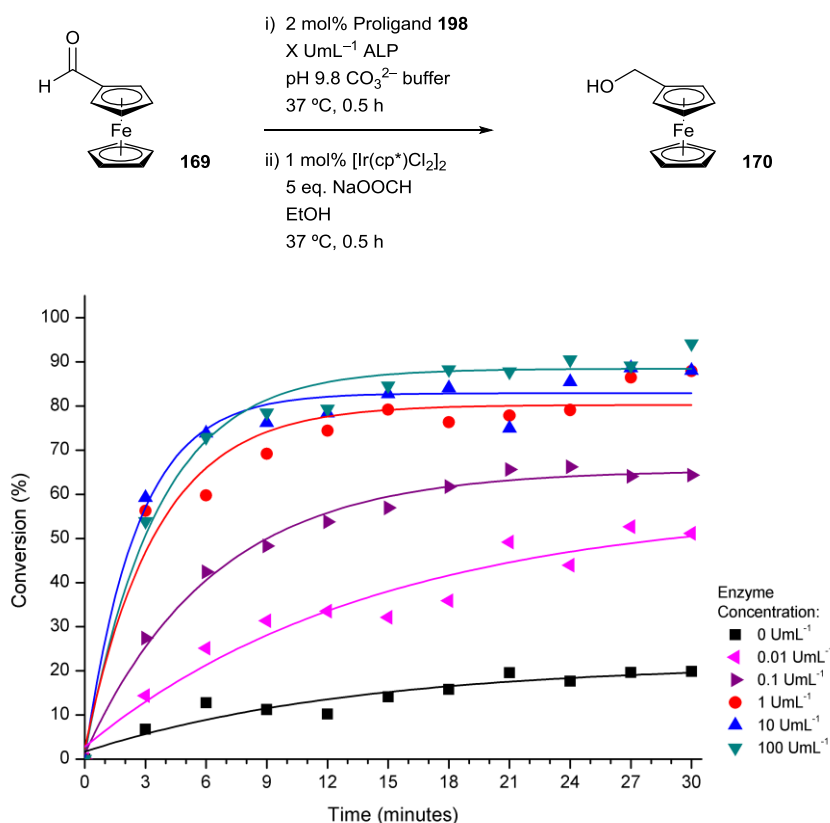
Figure 3.17 Electrochemical conversion of aldehyde **169** to alcohol **170** in the presence of different enzyme concentrations at 37 °C with a 30 minute incubation period at double concentration.

Looking to increase sensitivity further, the reaction concentration of the incubation period was investigated next (Figure 3.17). Doubling the concentration of the incubation delivered higher conversions for lower concentrations of ALP. However, the working range of the detection methodology becomes limited as quantitative electrochemical conversions were not observed under any concentration of ALP. Instead, high ALP concentrations across three orders of magnitude all delivered similar conversions of ≈80%. As a result, the concentration of the incubation period was returned to previous and the current optimised conditions were chosen to be applied towards a signal-amplified immunoassay.
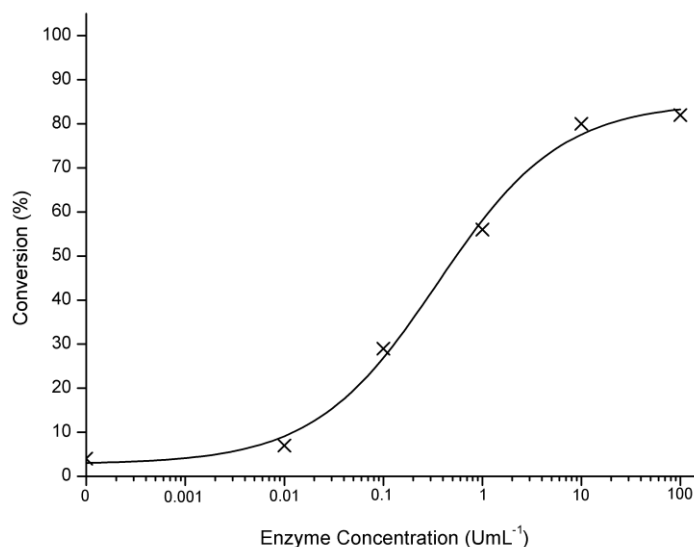
Figure 3.18 A plot of the electrochemical conversion of aldehyde **169** to alcohol **170** 3 minutes after the addition of the signal amplification reagents *vs.* the $\log_{10}$ of the ALP concentration. $R^2 = 0.99$.

Due to the rapid conversions seen under these conditions, a plot of the conversion obtained 3 minutes after the addition of the signal amplification reagents against the log of the enzyme concentration enabled a LOD for ALP to be calculated at 7.6 pM after a 33 minute total assay time at 37 °C (Figure 3.18). The significant background reaction observed with the signal amplification methodology means that this detection assay is not as sensitive as the reagent-based detection method previously described. However, it does have a bigger dynamic range as enzyme concentrations over 5 orders of magnitude can be accurately distinguished compared to 3 orders of magnitude seen with the reagent-based approach.

3.1.7 Application of Enzyme-Triggered Catalytic Signal Amplification towards Immunosorbent Assays

Prior to the application of enzyme-triggered catalytic signal amplification to an enzyme-linked immunosorbent assay (ELISA), the amplification methodology was tested with streptavidin-conjugated ALP. Again, this was to determine if the structural modification of the enzyme would prevent enzyme-catalysed hydrolysis of enzyme substrate **198** due to denaturisation or through steric hindrance. As such, a 1 mM solution of proligand **198** was incubated with varying concentrations of streptavidin–ALP for 30 minutes prior to the addition of the signal amplification reagents. After which, conversion of ferrocenecarboxaldehyde **169** to ferrocenemethanol **170** was monitored for a further 30 minutes *via* ratiometric electrochemical analysis (Figure 3.19).

Protein–enzyme conjugation did not appear to have a detrimental impact upon ALP-catalysed hydrolysis of proligand **198** or upon the iridium-catalysed transfer hydrogenation reaction

as positive electrochemical conversions were observed. Quantitative conversions were seen at streptavidin–ALP concentrations of 10 mgL^{-1} and higher, whilst a concentration of 0.01 mgL^{-1} could easily be distinguished from the background. Enzyme-triggered catalytic signal amplification again showed an excellent dynamic range as protein–enzyme concentrations over 4 orders of magnitude could be accurately determined. For completion, the assay was performed in the absence of proligand **198** to confirm that positive conversion was occurring through the proposed mechanism. Without the proligand, conversions lower than the background rate was seen showing that enzyme-catalysed hydrolysis of **198** was indeed responsible for quantitative conversions being observed.
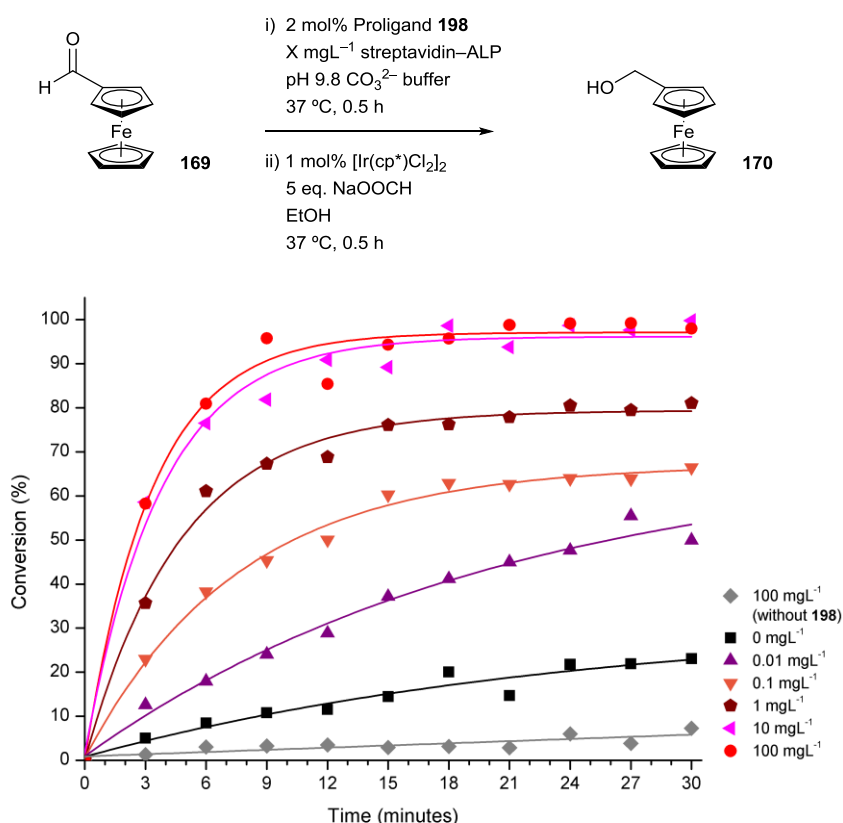
Figure 3.19 Electrochemical conversions of aldehyde **169** to alcohol **170** in the presence of different enzyme conjugate concentrations at 37 °C with a 30 minute incubation period.

As enzyme conjugation does not interfere with hydrolysis of the enzyme substrate or with organometallic catalyst activity, the next goal was to apply enzyme-triggered catalytic signal amplification to an immunosorbent assay for signal-amplified ratiometric electrochemical protein detection. C-reactive protein (CRP) was chosen once more as the model analyte which could be identified through a commercial ELISA kit that utilises ALP as the enzyme label. Again, the sandwich ELISA was constructed according to the manufacturer's procedure and incubated with a

1 mM solution of proligand **198** for 30 minutes prior to the addition of the signal amplification reagents (Figure 3.20).
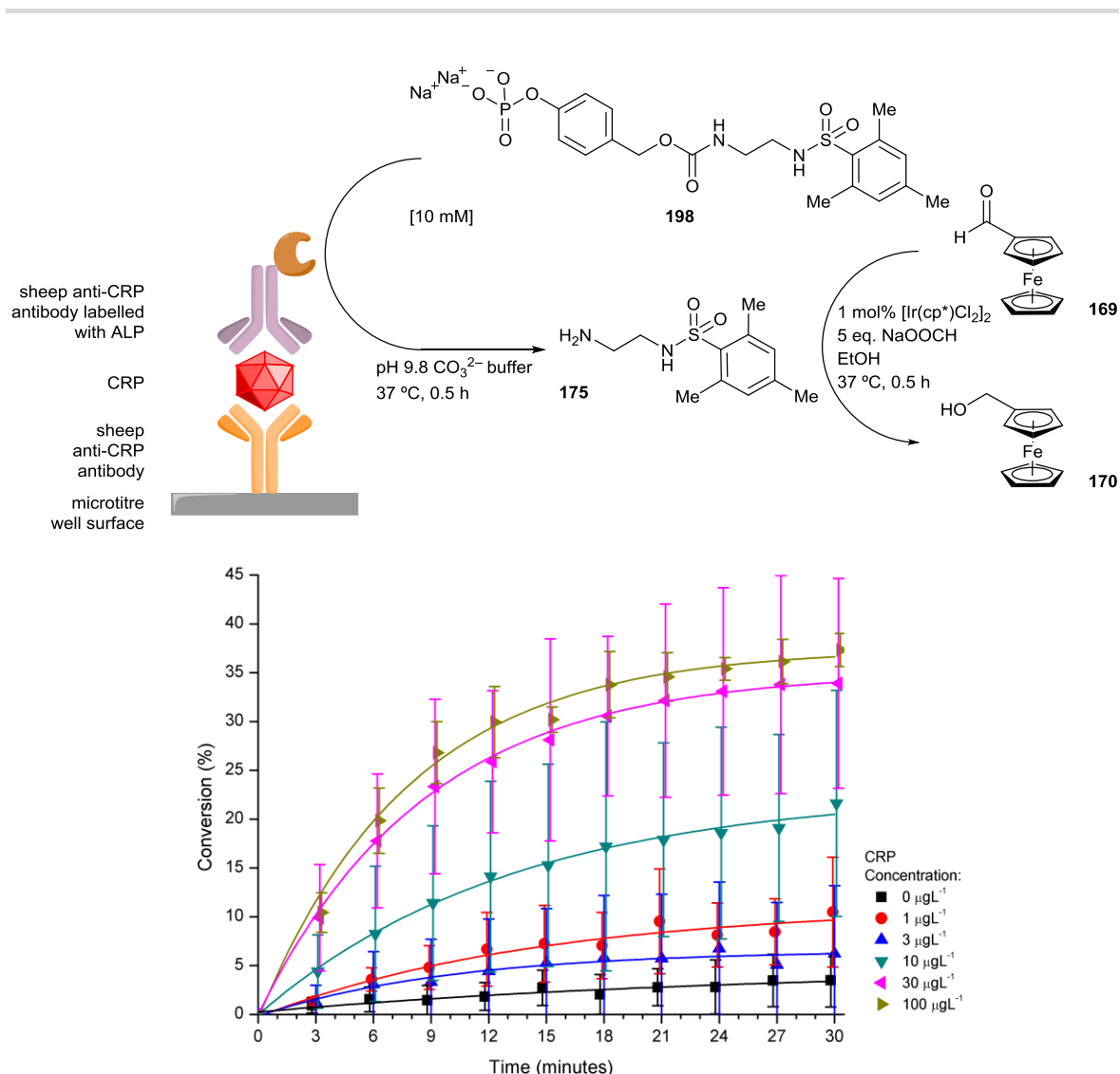
Figure 3.20 Electrochemical conversions of aldehyde **169** to alcohol **170** in the presence of different CRP concentrations at 37 °C after a 30 minute incubation period of proligand **198** with the sandwich complex. Error bars indicate standard deviation ($n = 3$).

Pleasingly, positive conversions were observed at all concentrations of CRP tested with high concentrations able to produce ≈35% conversion after 30 minutes. Interestingly, a CRP concentration of 1 μgL^{-1} delivered a higher average conversion than a CRP concentration of 3 μgL^{-1}, which does show the potential high sensitivity of the amplification methodology. However, the background rate is high enough to limit this sensitivity. Due to the use of a second amplifier, any error produced as a result of the first amplification step is amplified by the second, as indicated by the large error bars. Therefore, in attempting to achieve greater sensitivity, accuracy and reproducibility had been compromised.
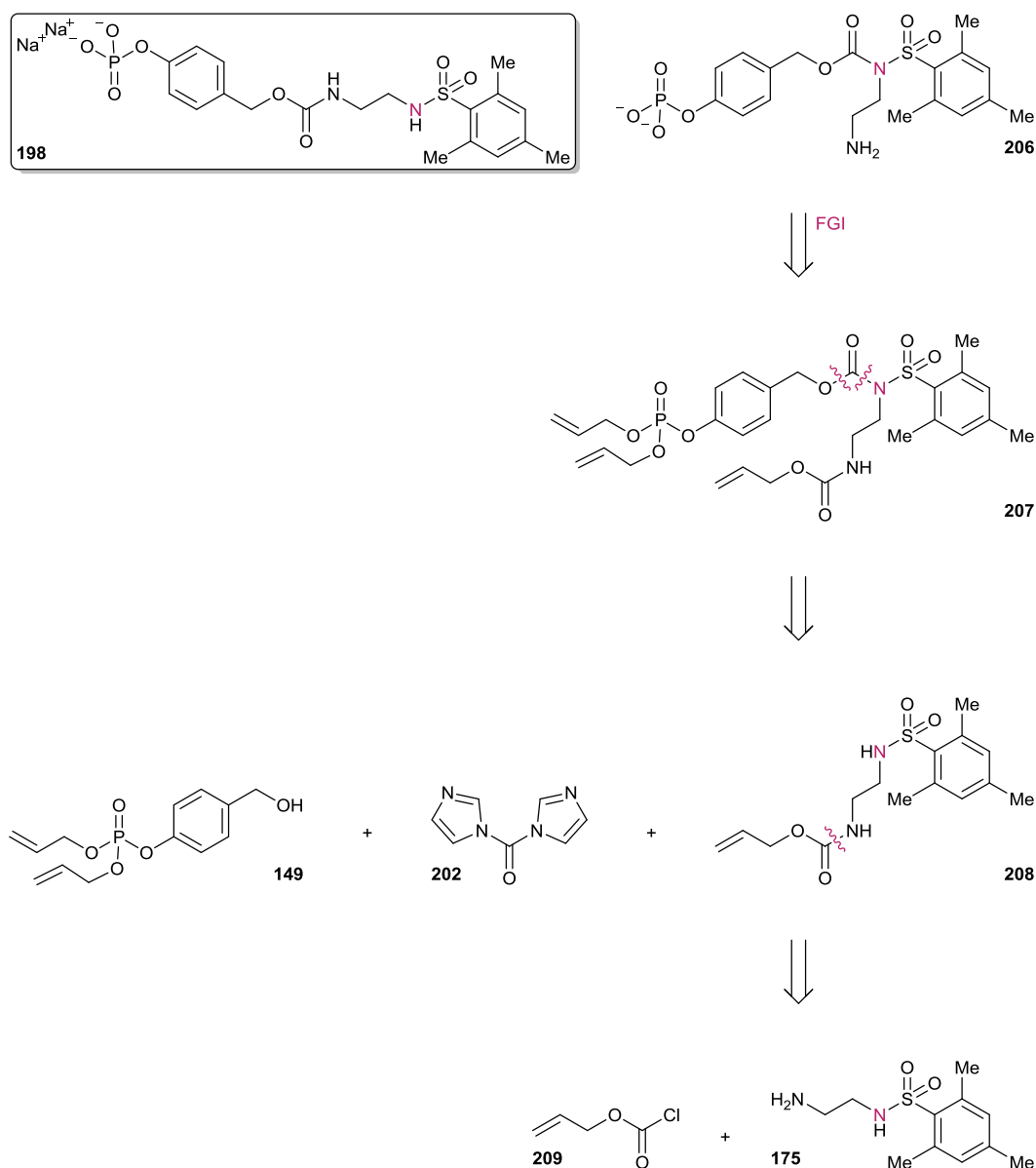
Scheme 3.13 Retrosynthetic analysis of proligand **206**.

In order to improve the signal amplification methodology, efforts were made to reduce the unsatisfactorily high background rate. From the results obtained where streptavidin-conjugated ALP was being detected (Figure 3.19), it was clear that a combination of both proligand **198** and the iridium precatalyst were contributing to the high background rate. Although contrary to the conclusions resulting from the ligand derivative screen (Table 3.4), this was considered to be due to that at the higher reaction temperatures iridium insertion into the sulfonamide N–H bond could occur to form a partially-active catalyst within the transfer hydrogenation reaction. It was thought that a structural adjustment of the proligand would prevent this metal insertion from occurring and could nullify the background reaction. Towards this end, a second generation proligand, compound

206, was designed. By simply moving the phosphate trigger and the benzyl linker attachment from the primary amine position to the sulfonamide nitrogen position would remove the acidic sulfonamide yet allow the same enzyme-triggered ligand release mechanism to remain in effect. Proligand **206** could be synthesised in much a similar way to the proligand **198** albeit with an added protection/deprotection step (Scheme 3.13). The amine protecting group was chosen to be an allyloxycarbonyl (alloc) group as deprotection of this group should occur in the same synthetic procedure as allyl deprotection of the phosphate group.
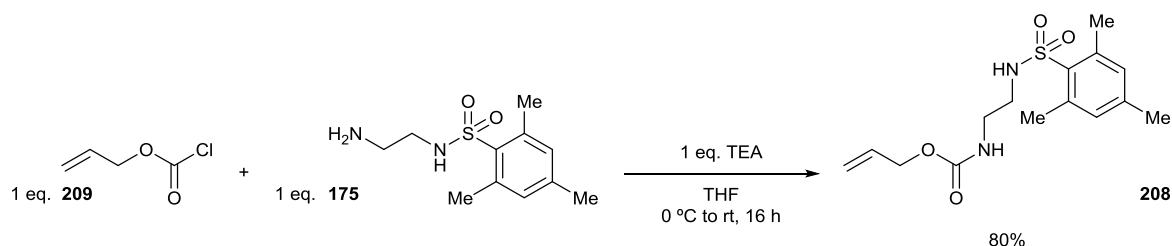
Scheme 3.14 Alloc protection of ligand **175**.
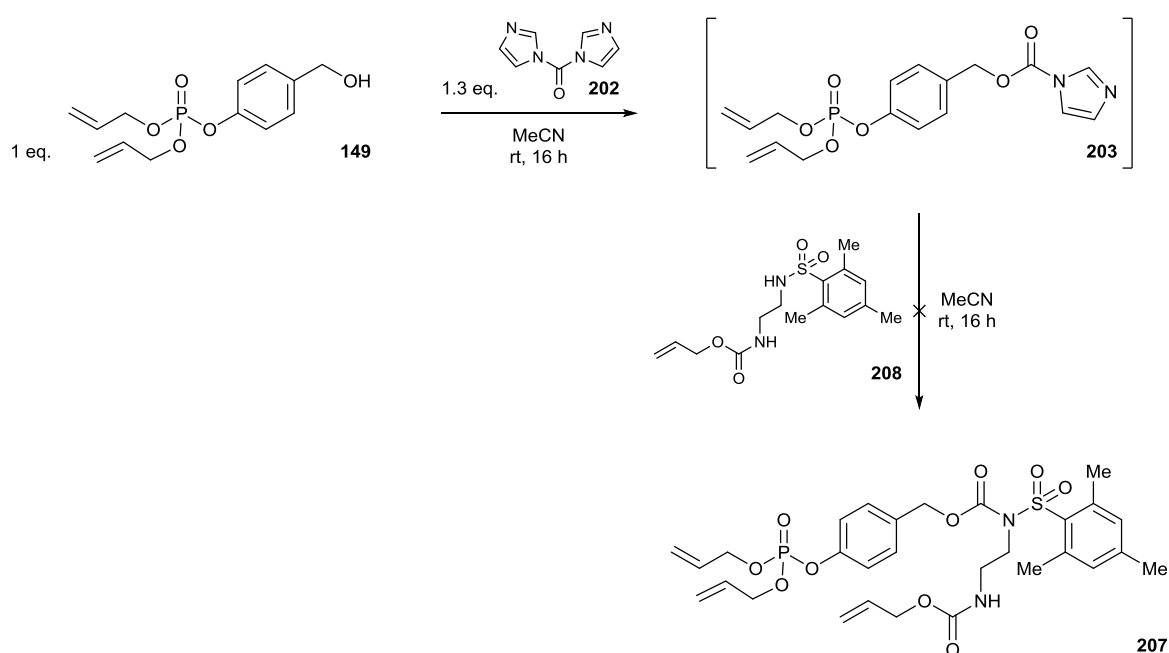
Scheme 3.15 Attempted synthesis of triallyl protected proligand **207**.

Thus, the synthesis of proligand **206** began with alloc protection of ligand **175** with allyl chloroformate **209** which proceeded in good yield (Scheme 3.14). Next, the synthesis of the triallyl protected proligand **207** was attempted analogous to previous where benzyl alcohol **149** could be coupled to the sulfonamide nitrogen of **208** through the use of carbonyl coupling reagent CDI **202** (Scheme 3.15). However, due to the poor nucleophilicity of the sulfonamide, the desired product

was not observed. To improve the reactivity between the coupling partners, it was decided to replace the carbonyl coupling reagent with the much more reactive phosgene, enabling coupling to go through the corresponding benzyl chloroformate. In addition, the use of a nucleophilic catalyst should greatly improve the electrophilicity of the intermediate chloroformate.

DMAP = 4-(dimethylamino)pyridine
DIPEA = *N,N*-diisopropylethylamine
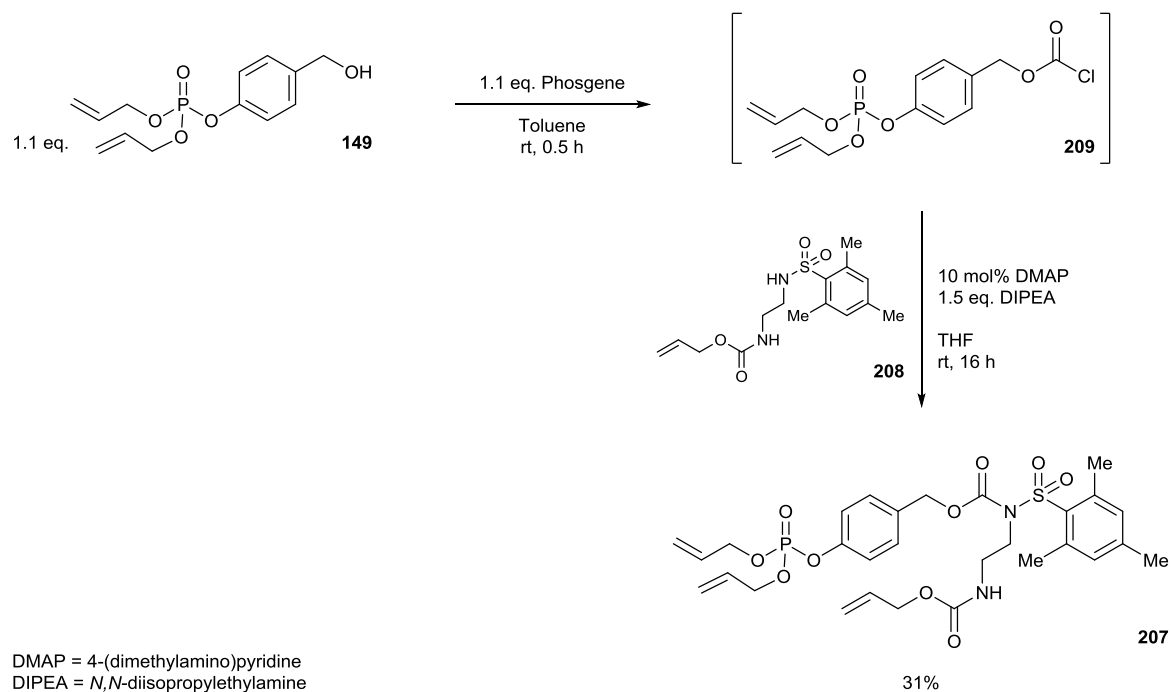
Scheme 3.16 Synthesis of triallyl protected proligand **207**.

Indeed, the use of phosgene as the carbonyl coupling reagent and 4-(dimethylamino)pyridine (DMAP) as the nucleophilic catalyst delivered the desired triallyl protected proligand **207** in moderate yield (Scheme 3.16). To obtain proligand **206**, deprotection of **207** was attempted using the standard optimised deallylation conditions (Scheme 3.17). However, despite the desired product being observed in the crude ^{1}H NMR, compound **198** was also observed in the inseparable mixture. This product is presumed to have formed from an intramolecular rearrangement through nucleophilic attack of the carbamate by the primary amine subsequent to alloc deprotection. Unable to successfully purify proligand **206** from **198**, another proligand was designed.
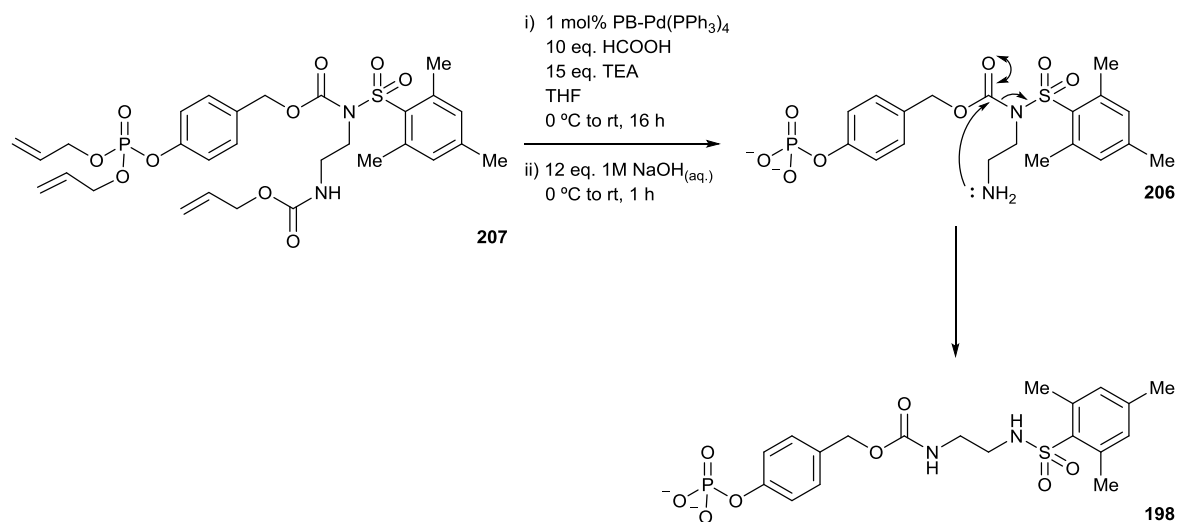
Scheme 3.17 Attempted synthesis of proligand **206**.
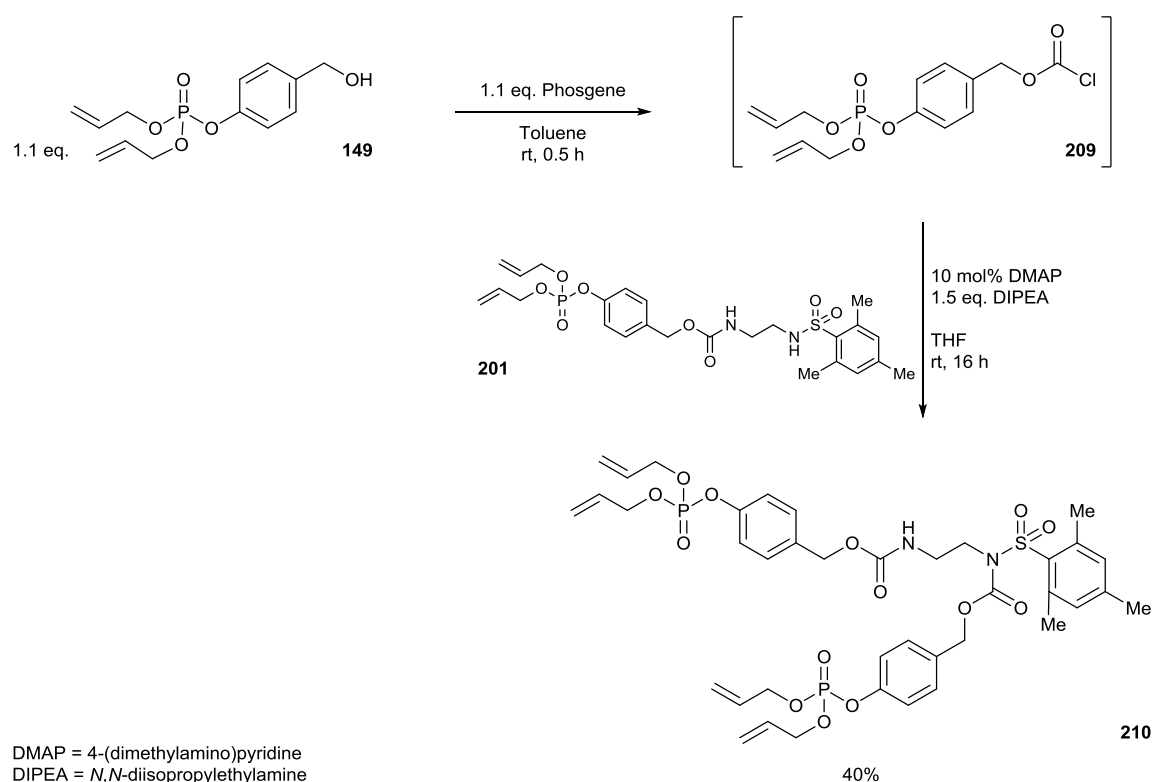
Scheme 3.18 Synthesis of tetraallyl protected proligand **210**.

To avoid the intramolecular rearrangement yet maintain functionalisation at the sulfonamide nitrogen, it was decided that attachment of another phosphate trigger and benzyl linker at this position would achieve the desired reduced background rate in the transfer hydrogenation reaction despite needing two enzyme-catalysed dephosphorylations to release the active ligand. In a similar procedure for the synthesis of **207**, tetraallyl protected bis-phosphate **210** was synthesised in moderate yield from previously prepared **201** (Scheme 3.18). With compound **210** in hand, it was

then exposed to the palladium-catalysed deallylation conditions to remove the four allyl protecting groups (Scheme 3.19). Initially, this was successfully achieved but the conditions used for disodium phosphate salt formation led to decomposition of the product. This was thought to be due to the hydroxide acting as a nucleophile and hydrolysing the *N*-sulfonyl carbamate linkage. Repeating the synthesis but using a milder base led to formation of the desired bis-phosphate salt in quantitative yield. The addition of an extra phosphate group greatly improved the water solubility of the proligand allowing purification of compound **211** to occur *via* preparative reverse phase column chromatography.
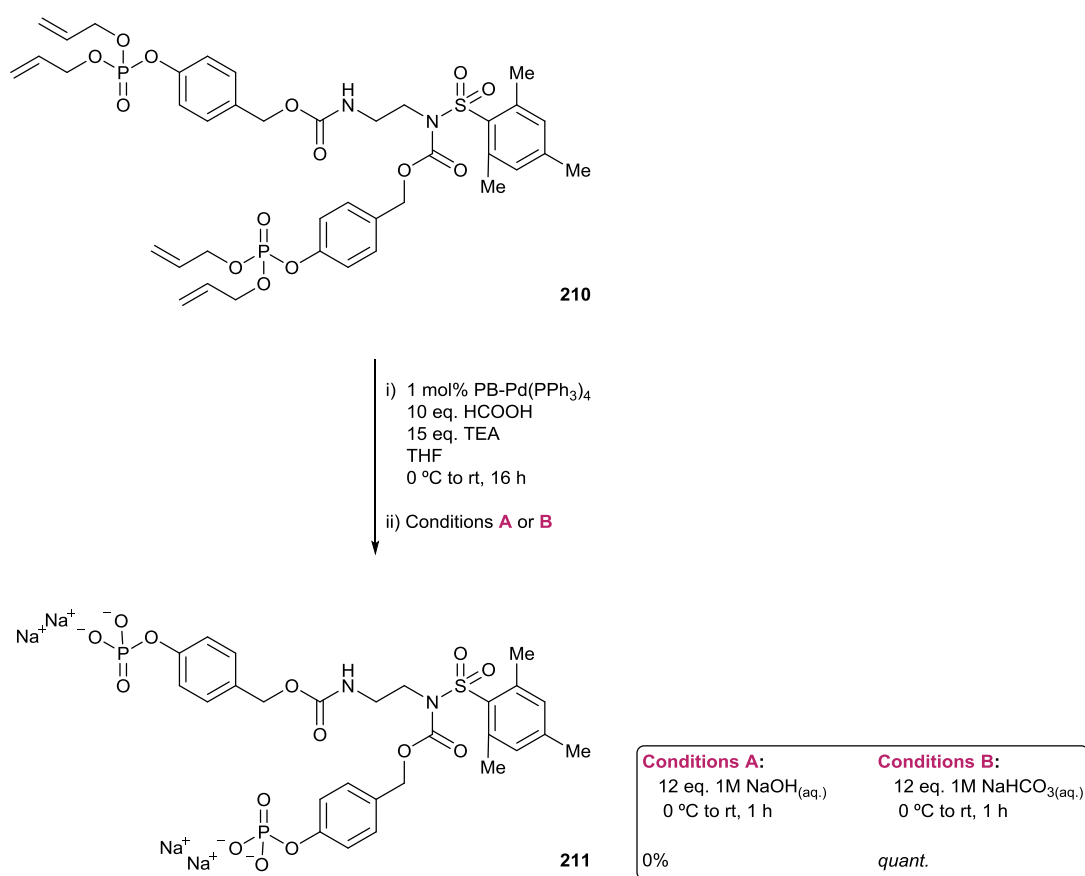
Scheme 3.19 Synthesis of bis-phosphate proligand **211**.

With bis-phosphate **211** in hand, it was then tested as the proligand within the enzyme-triggered catalytic signal amplification methodology (Figure 3.21). Initially, unconjugated ALP was used as the enzyme trigger to determine the background rate, if any, prior to testing **211** within the more procedurally complex ELISA. Pleasingly, in the presence of ALP, rapid conversion of ferrocenecarboxaldehyde **169** to ferrocenemethanol **170** was observed through ratiometric electrochemical analysis. Despite requiring two ALP-catalysed dephosphorylations of proligand **211** to release ligand **175**, this was shown not to significantly hinder reactivity as quantitative conversions were still obtained within 30 minutes. However, in the absence of ALP, a small

undesired background reaction was still present with ≈10% conversion being observed after 30 minutes. This indicates that the background reaction was not necessarily caused by iridium-insertion into the acidic sulfonamide N–H bond creating a partially-active catalyst. Nevertheless, with the improved water solubility of proligand **211** over proligand **198**, it was thought that **211** could still be used as the enzyme substrate within an ELISA and the undesired background reaction could be potentially minimised through a careful optimisation.
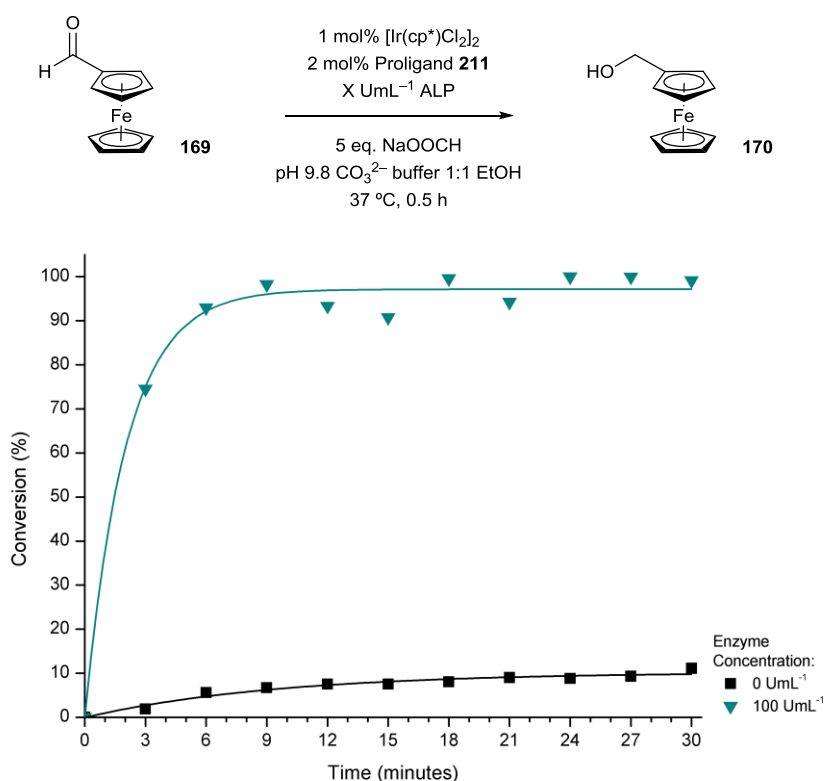
Figure 3.21 Electrochemical conversion of aldehyde **169** to alcohol **170** in the presence of different enzyme concentrations at 37 °C using proligand **211** as the enzyme substrate.

Once again, an ELISA was constructed for the detection of model analyte CRP which was tested at the highest concentration available as well as in its absence in order to obtain the detection range (Figure 3.22). In the absence of any CRP, a low background was indeed observed with a maximum 2% conversion reached over the course of the 30 minute assay. A conversion distinguishable from the background was seen in the presence of 100 μgL^{-1} of CRP but under these conditions, the signal amplification methodology barely delivered over 10% conversion. Pleased with the low background rate however, ways to improve conversion in the case of a positive scenario were next looked at.
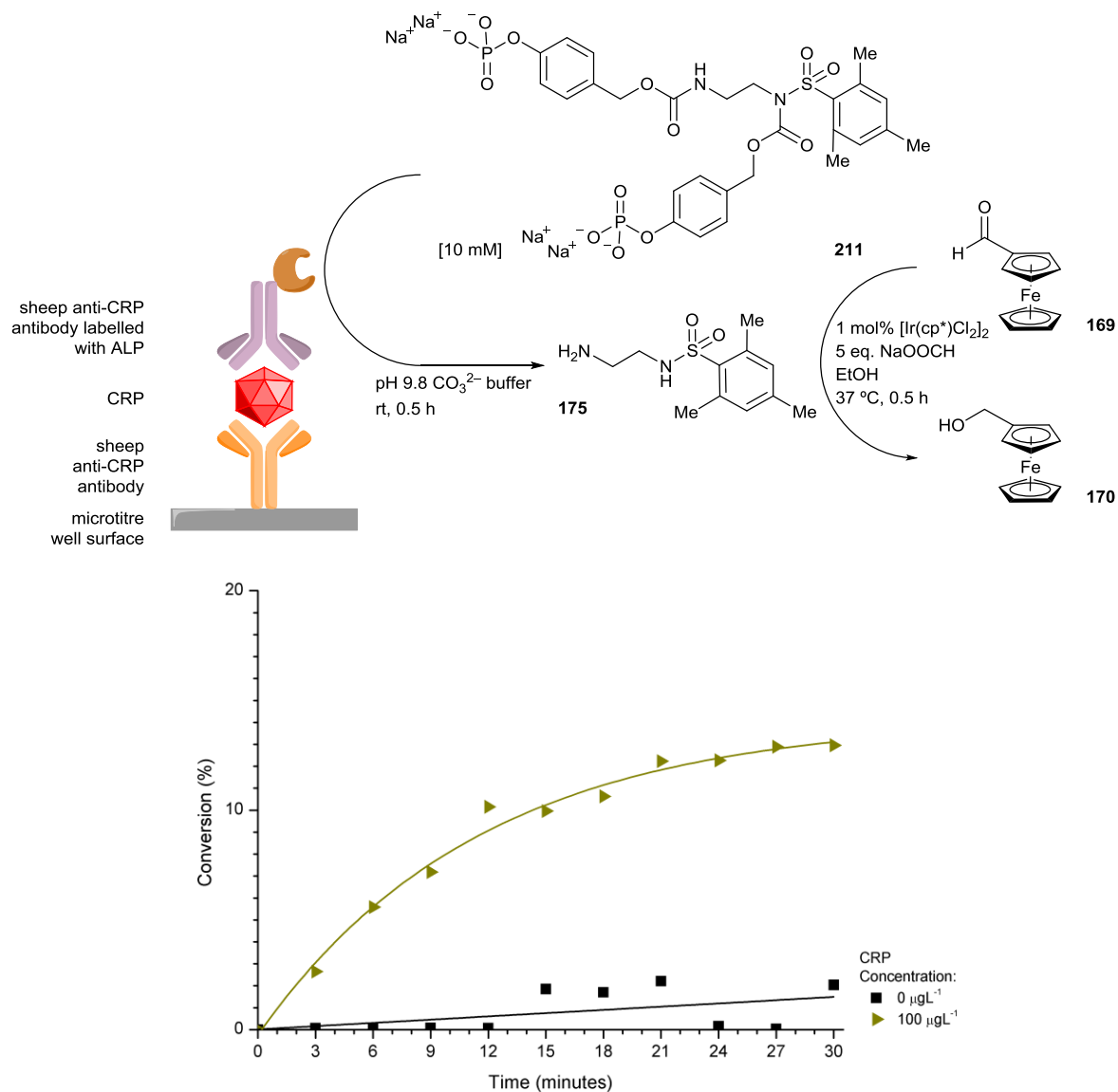
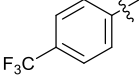**Figure 3.22** Electrochemical conversions of aldehyde **169** to alcohol **170** in the presence of different CRP concentrations at 37 °C after a 30 minute incubation period of proligand **211** with the sandwich complex at room temperature.

One method to improve the signal output was thought to simply increase the catalytic loading of the second catalytic amplifier of the signal amplification methodology. As such, the overall catalytic loading was increased to 12 mol% and again tested within an ELISA for CRP detection (Figure 3.23). The higher catalytic loading does indeed provide higher conversion within the methodology as greater than 50% conversion was observed after a 30 minute reaction time. However, much more strikingly is that this increase in signal was accompanied by a huge increase in background rate with nearly 50% conversion also being seen.

From this result it is clear that the background reaction is not caused by complexation of the proligand to the metal forming a partially-active catalyst. Instead, the background reaction was being caused by the iridium pre-catalyst itself acting as an active catalyst within the transfer hydrogenation reaction.
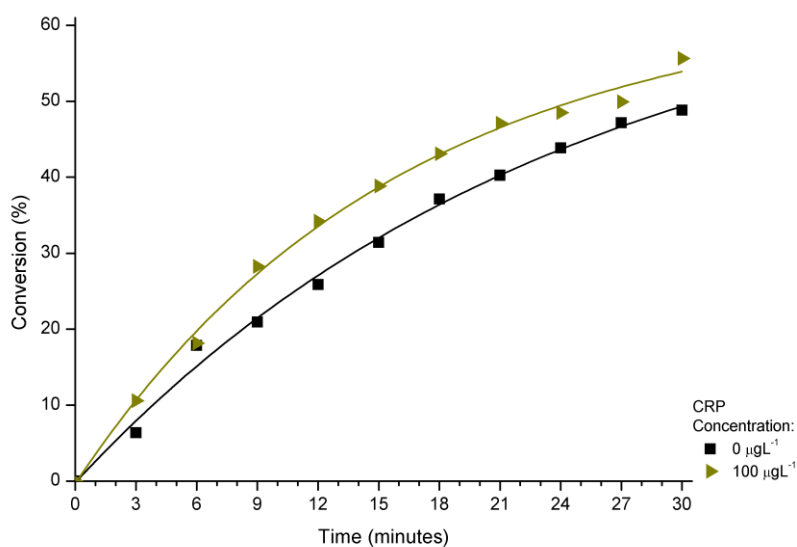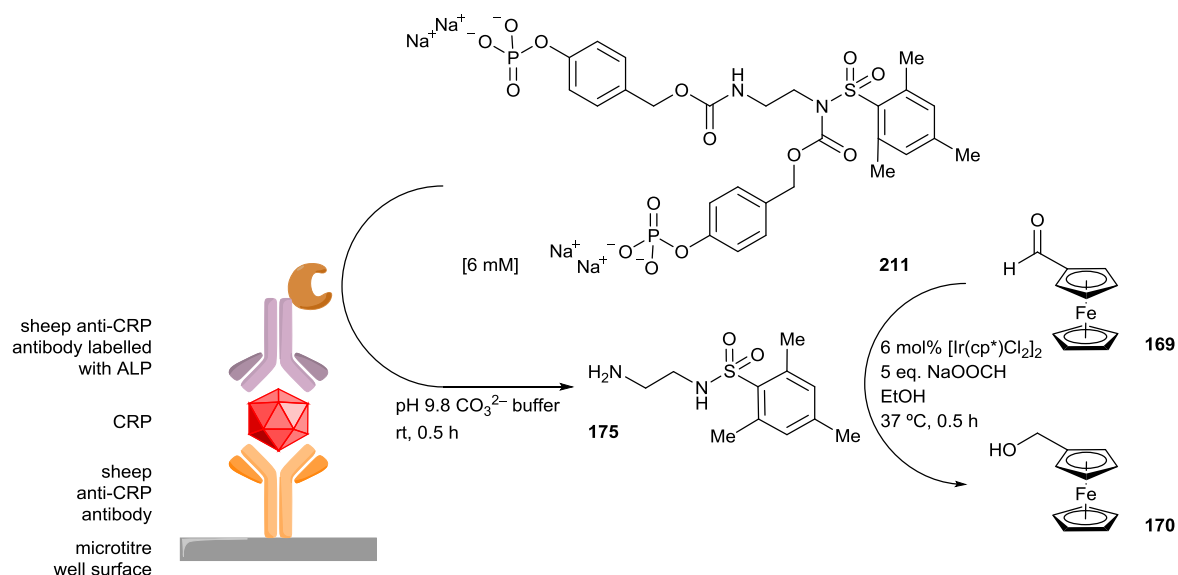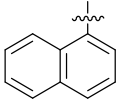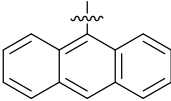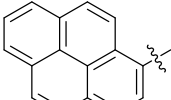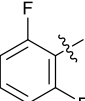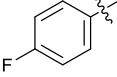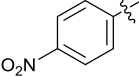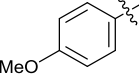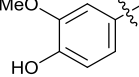
Figure 3.23 Electrochemical conversions of aldehyde **169** to alcohol **170** in the presence of different CRP concentrations at 37 °C with an overall catalytic loading of 12 mol% after a 30 minute incubation period of proligand **211** with the sandwich complex at room temperature.
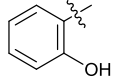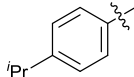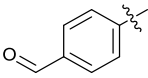
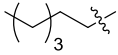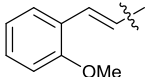## 3.2   Signal-Amplified Detection of Alkaline Phosphatase with Alternative Signal Readout

One of the major benefits of the enzyme-triggered catalytic signal amplification methodology developed herein, other than the signal amplification itself, is its modularity. For example, if an electrochemical enzyme substrate had been previously described, but the readout method required for a different application is fluorescence or colourimetric, then an entirely new enzyme substrate with those particular attributes would need to be developed. With this methodology however, the same enzyme substrate can always be used but the readout method can be easily changed by choosing an aldehyde that simply possesses the desired properties. This has an increased benefit

since many aldehydes are commercially available and do not require multiple procedures to synthesise unlike typical enzyme substrate development. To test this principle, the previously optimised conditions for ALP detection were applied to a range of different commercially-available aldehydes in both the presence and absence of ALP (Table 3.6).

$$R-CHO \xrightarrow[\substack{5 \text{ eq. NaOOCH} \\ \text{pH } 9.8 \text{ CO}_3^{2-} \text{ buffer } 1:1 \text{ EtOH} \\ 37 \text{ °C, } 0.5 \text{ h}}]{\substack{0.25 \text{ mol}\% [\text{Ir(cp*)Cl}_2]_2 \\ 0.5 \text{ mol}\% \text{ Proligand } \mathbf{198} \\ X \text{ UmL}^{-1} \text{ ALP}}} R-CH_2OH$$
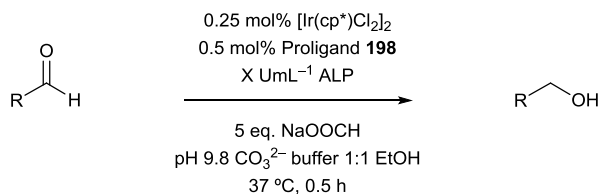
Product Number	R	Conversion (%) [a]	
		25 UmL^{-1} ALP	0 UmL^{-1} ALP
212		>99%	10%
213		77%	2%
214		95%	2%
215 [b]		52%	14%
216 [b]		>99%	4%
217 [b]		>99%	20%
218 [b]		>99%	21%
219		>99%	11%
220		48%	12%

221		>99%	13%
222		>99%	14%
223		>99% [c]	26%
224		>99%	n/a [d]
225		>99%	24%
226		75%	8%

[a] determined by ^{1}H NMR. [b] half catalytic loading. [c] combined conversion of **223** (≈75%) and 1,4-benzenedimethanol (≈25%). [d] neither product nor substrate observed by crude ^{1}H NMR.

Table 3.6 Application of enzyme-triggered catalytic signal amplification to different aldehydes for alternative signal readout.

Initially, a number of polyaromatic aldehydes were tried as this would allow enzyme detection through the amplification methodology to be achieved by fluorescence. 1-napthyl, 9-anthracenyl and 1-pyrenyl aldehydes all furnished excellent conversions in the presence of ALP yet delivered satisfactorily low conversions in its absence. This shows that the methodology could be utilised within an amplified enzyme detection assay with fluorescent signal readout. A number of fluorine-containing aromatic aldehydes were next used as the substrate which would enable ^{19}F NMR to be used as the readout method. Good conversions were also seen with these aldehydes but the more electron-withdrawing substrates were prone to high background conversions. This was confirmed with the very electron-withdrawing *p*-nitro substrate where half catalytic loadings were required to obtain acceptably low background conversions. Pleasingly, reduction of the nitro group itself was not observed.

Exploring the electronic demands of the substrate within the transfer hydrogenation reaction further, showed that electron-rich aromatic substrates were able to suppress these background reactions yet still provide quantitative conversions in the present of the enzyme. However, very electron-rich substrates such as vanillin deactivated the aldehyde enough to limit its reduction. Interestingly, when a dialdehyde was used as the substrate, the mono-alcohol was found to be the major product over the di-alcohol in a 3:1 ratio. The methodology was also found to not be limited to aromatic aldehydes as aliphatic substrates also furnished quantitative conversions in the presence of the enzyme. In the absence of the enzyme though, the cyclohexyl derivative

delivered a complex mixture of products as observed in the crude ^{1}H NMR spectrum, with no starting material or product being seen. Cinnamaldehydes were also shown to be excellent catalyst substrates within the methodology as the 2-methoxy derivative gave good conversion in the presence of the enzyme yet poor conversion in its absence. In addition, no reduction of the alkene was observed.

In the majority of cases, excellent conversions were obtained in the presence of the enzyme without needing to re-optimise the assay showing the potential applicability of the amplification methodology within detection methods that utilise alternative signal readouts. The excellent functional group tolerance could also lend this methodology towards applications other than sensing, such as stimuli-responsive materials and molecular computing. However, the iridium pre-catalyst also exhibits high background conversions with these aldehydes. Despite being able to minimise this through reducing the catalytic loading, any background could hinder the incorporation of this methodology within other sensing applications.

3.3   Conclusion

3.3.1   Project Summary

For the development of a signal-amplified enzyme-linked immunosorbent assay (ELISA) towards rapid and ultrasensitive electrochemical protein detection, a novel signal amplification methodology was designed and developed for the ratiometric detection of alkaline phosphatase (ALP). This methodology utilised a highly efficient iridium catalyst as the second catalytic amplifier within a double-catalyst signal amplification strategy, whose activity could be accelerated through ligand control. To accelerate catalytic activity selectively in the presence of ALP, an enzyme-triggered ligand release protocol was achieved through careful design of a proligand enzyme substrate, which bore an enzyme-selective phosphate trigger and benzyl linker attached to the ligand. The proligand itself was shown not to accelerate the iridium-catalysed transfer hydrogenation reaction but in the presence of ALP, hydrolysis of the proligand and consequent elimination of the linker was shown to release the active ligand, capable of accelerating the rate of the transfer hydrogenation reaction. The catalytic reaction could be monitored through ratiometric electrochemical analysis by using ferrocenecarboxaldehyde as the catalyst substrate since the corresponding product, ferrocenemethanol, had a significantly different oxidation potential from the starting aldehyde.

The enzyme-triggered catalytic signal amplification methodology was shown to go through the desired mechanism as ^{31}P NMR experiments revealed that hydrolysis of the proligand occurs selectively in the presence of ALP and mass spectrometry experiments identified that release of the ligand occurs as a direct result of enzyme-catalysed phosphate cleavage. A considerable optimisation was then performed to provide both further mechanistic insight as well as to find the

limit of detection for ALP activity, which was calculated to be 7.6 pM after a 33 minute assay reaction time. However, when applied to protein detection through an ELISA, a significant background rate was observed which limited the sensitivity of the assay. Also, the addition of a second amplifier to the detection methodology enhances any errors accrued from the first amplifier and as such, significant variation in positive results was observed.

The high background rate was considered to come from partial activation of the catalyst by the proligand in the absence of the enzyme. To prevent this, a second proligand was designed and synthesised where a second enzyme trigger and benzyl linker was affixed to another attachment point of the proligand. However, despite this modification, the undesired background reaction remained leading the conclusion that this was as a result of the iridium pre-catalyst itself being an active catalyst within the transfer hydrogenation reaction. Nevertheless, the versatility of the enzyme-triggered catalytic amplification methodology was shown through the enzyme-triggered catalytic reduction of a range of commercially-available aldehydes. Potentially, this enables amplified ALP detection through means other than electrochemistry, such as fluorescence or ^{19}F NMR, and the methodology could also be incorporated into systems other than sensing, where both signal transduction and signal amplification is needed.

3.3.2 Future Work

To increase the sensitivity and therefore the applicability of the enzyme-triggered catalytic signal amplification methodology, minimisation of the high background reaction would be paramount. Knowing that the cause of this background was the iridium pre-catalyst, then using a more inert pre-catalyst could reduce the background rate. From the ligand optimisation study, tetramethylethylenediamine (TMEDA) was shown to completely inhibit the transfer hydrogenation reaction and therefore, synthesis of an Ir·TMEDA complex such as **227** and testing it as the pre-catalyst within the transfer hydrogenation reaction would be the initial intention (Scheme 3.20).
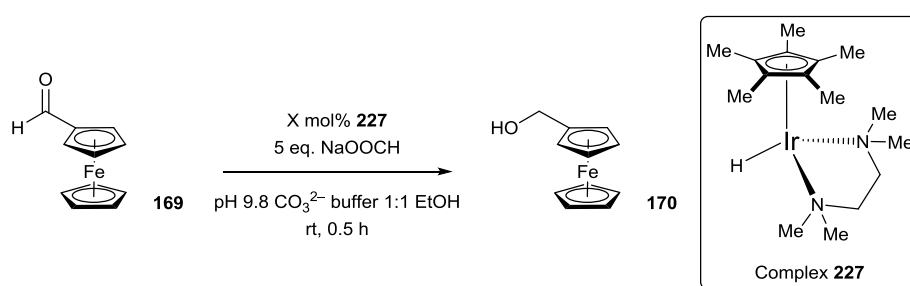
Scheme 3.20 Design of inert iridium complex **227** and its potential application as a precatalyst within the transfer hydrogenation reaction.

Once the background reaction has been minimised, the signal amplification methodology could then be applied to the signal-amplified detection of other analytes. Replacing the phosphate trigger of the proligand with other enzyme-cleavable functional groups would enable the amplified electrochemical ratiometric detection of other enzymes such as sulfatase, protease, esterase or glycosylase (Figure 3.24). Additionally, replacing the trigger with phenol protecting groups such as allyl or silyl groups would extend this methodology to the detection of palladium or fluoride respectively. Phenylboronic acids could also be used as the trigger moiety allowing for the amplified detection of hydrogen peroxide. This would also extend the signal amplification methodology towards an inverse horseradish peroxidase (HRP) detection assay as well as protein detection through HRP-labelled ELISAs.
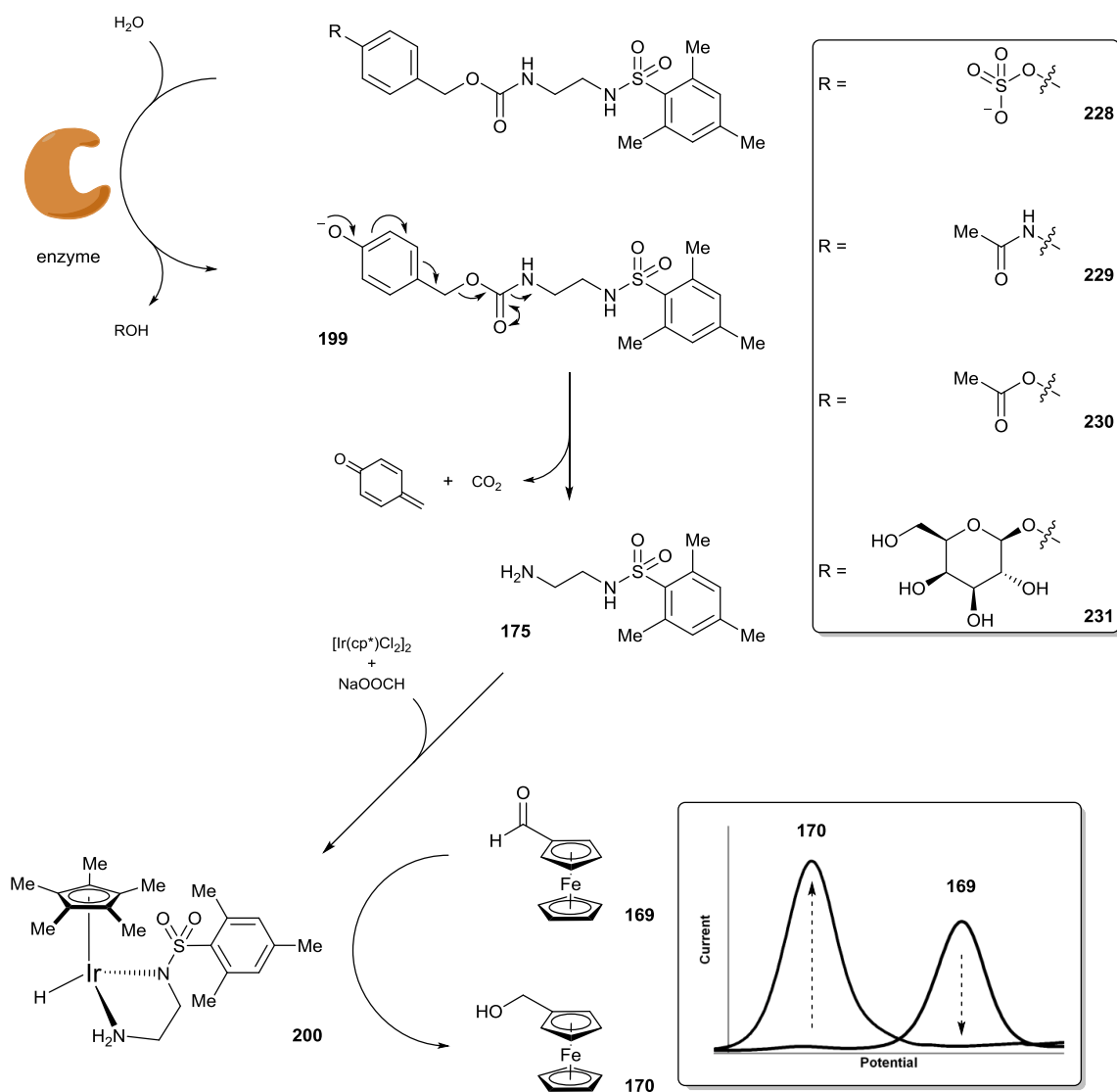
Figure 3.24 Potential application of enzyme-triggered catalytic signal amplification applied for sensitive ratiometric electrochemical detection of alternative enzymes.

As well as modifying the enzyme or analyte-selective substrate for alternative analyte detection, other aspects of the methodology could also be changed such as the catalyst substrate.

Although the aldehyde scope was briefly demonstrated, a more thorough optimisation using fluorescent or colourimetric substrates would greatly highlight the applicability of this methodology within detection assays that require signal readouts other than electrochemistry. Furthermore, since this is the first example of enzyme-triggered catalyst activation through ligand acceleration, further work should be aimed at other catalyst–ligand systems that could be used as the second catalytic amplifier within the methodology.

Chapter 4

Experimental

4.0   General Information

4.0.1   Instruments

Proton, carbon, fluorine and phosphorous nuclear magnetic resonance (NMR) spectra were recorded on Bruker 300, 400 or 500 MHz spectrometers or on an Agilent Technologies 500 MHz spectrometer (^{1}H NMR at 300 or 400 MHz, ^{13}C NMR at 75.5 or 101 MHz, ^{19}F at 376.5 or 470.5 MHz and ^{31}P NMR at 121.5 MHz) at 298 K unless otherwise stated. Chemical shifts for protons are reported in parts *per* million downfield from $Si(CH_3)_4$ and are referenced to residual protium in the deuterated solvent ($CHCl_3$ at 7.26 ppm, C_6H_6 at 7.16 ppm, H_2O at 4.79 ppm, DMSO at 2.50 ppm).[420] Chemical shifts for carbons are reported in parts *per* million downfield from $Si(CH_3)_4$ and are reference, where available, to the carbon resonances of the deuterated solvent ($CDCl_3$ at 77.0 ppm, C_6D_6 at 128.1 ppm, d_6–DMSO at 39.5 ppm).[420] Chemical shifts for fluorines are reported in parts *per* million downfield from $CFCl_3$. Chemical shifts for phosphorous' are reported in parts *per* million downfield from 85% H_3PO_4. NMR data are presented in the following format: chemical shift (number of equivalent nuclei by integration, multiplicity [app = apparent, br = broad, d = doublet, dd = doublet of doublets, dq = doublet of quartets, dt = doublet of triplets, ddd = doublet of doublet of doublets, ddt = doublet of doublet of triplets, m = multiplet, q = quartet, s = singlet, sept = septet, t = triplet], coupling constant [in Hz], assignment). Electrospray ionisation ultrahigh resolution time-of-flight mass spectrometry (ESI–UHR–TOF–MS) was performed on a Bruker maXis mass spectrometer. Electrospray ionisation high resolution time-of-flight mass spectrometry (ESI–HR–TOF–MS) was performed on a Bruker micrOTOF spectrometer. Infrared (IR) spectra were recorded on a Perkin–Elmer 1600 FT (Fourier transform) IR spectrophotometer, with absorbencies quoted as wavenumber (ν [in cm^{-1}]). Electrochemical analysis was performed on a Metrohm Autolab PGSTAT30 potentiostat controlled by a personal computer running General Purpose Electrochemical System (GPES) software. Melting points were obtained on a Bibby Sterilin SMP10 melting point machine and are uncorrected. Enzyme-linked immunosorbent assays (ELISAs) were incubated on a Benchmark Scientific H1000-M Incu-Shaker Mini. pH was measured using a Hanna Instruments HI 9321 pH meter and was calibrated prior to use.

4.0.2   Materials

Analytical thin-layer chromatography (TLC) was performed on aluminium-backed plates coated with Alugram® SIL G/UV$_{254}$ purchased from Macherey–Nagel and visualised with UV light (254 or 365 nm) and/or $KMnO_4$, 2,4-DNPH or ninhydrin staining where appropriate. Silica gel column chromatography was performed using 60 Å, 200–400 mesh particle size silica gel purchased from Sigma–Aldrich. Reverse phase C_{18}-silica gel column chromatography was carried out using VersaPak® 30g C18 cartridges (23 mm × 110 mm) preloaded with 20–45 μm spherical C_{18} bonded silica purchased from Sigma–Aldrich. High sensitivity

C-reactive protein (CRP) enzyme-linked immunosorbent assay (ELISA) kits were purchased from Kalon Biological Ltd. (Guildford, UK) and stored at 4 °C prior to use.

4.0.3 Chemicals

All reactions were performed in oven-dried glassware under an atmosphere of nitrogen at room temperature (≈18 °C) unless otherwise stated. All water used was purified through a Merck Millipore reverse osmosis purification system prior to use. Anhydrous acetonitrile (MeCN), anhydrous dichloromethane (CH_2Cl_2), anhydrous tetrahydrofuran (THF) and anhydrous toluene (PhMe) were dried and degassed by passing through anhydrous alumina columns using an Innovative Technology Inc. PS–400–7 solvent purification system (SPS) and stored under an atmosphere of argon prior to use. Anhydrous *N,N*-dimethylformamide (DMF) was purchased from Sigma–Aldrich and used as received. Hexane refers to high-pressure liquid chromatography (HPLC) grade hexane which was purchased from Sigma–Aldrich and used as received. Triethylamine (TEA), purchased from Sigma–Aldrich, was dried over KOH pellets and distilled before being stored under an atmosphere of nitrogen prior to use.[421] *N*-Chlorosuccinimide (NCS), purchased from Sigma–Aldrich, was rapidly recrystallised from glacial acetic acid and washed well with water before being dried *in vacuo* prior to use.[421] Dichloro(pentamethylcyclopentadienyl)iridium(III) dimer and ferrocenecarboxylic acid were purchased from Alfa Aesar and used as received. Oxalyl chloride was purchased from Fluorochem and used as received. NaOH and KOH pellets as well as anhydrous Na_2SO_4 were purchased from Acros Organics and used as received. Sand and $MgSO_4$ were purchased from Fisher Scientific and used as received. Polymer-bound tetrakis(triphenylphosphine)palladium was purchased from Sigma–Aldrich as a 200–400 mesh polymer, 2% cross-linked with divinylbenzene, labelled with 0.5–0.9 mmolg^{-1} palladium and used as received. Alkaline phosphatase (ALP) from bovine intestinal mucosa (≥2000 DEA units/mg) was purchased from Sigma–Aldrich as a lyophilised powder and stored at 4 °C prior to use. Streptavidin–alkaline phosphatase conjugate from *streptomyces avidinii* (700–2300 DEA units/mg) was purchased from Sigma–Aldrich as a lyophilised powder and stored at −20 °C prior to use. All other chemicals were purchased from Sigma–Aldrich and used as received. All buffers were freshly prepared according to previously published methods and carefully adjusted to the appropriate pH using either 1M NaOH $_{(aq.)}$ or 1M HCl $_{(aq.)}$.[422]

4.1 General Procedures

### 4.1.1 Synthetic Procedures

4.1.1.1 Procedure A
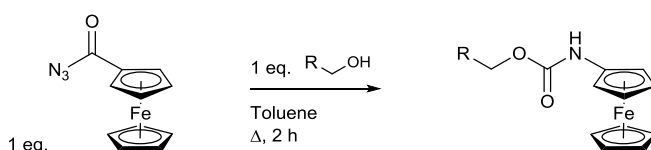
To a stirring solution of ferrocenoyl azide (1 eq.) in anhydrous toluene (3 mL / mmol) under argon was added the alcohol (1 eq.). The reaction mixture was then heated to reflux and stirred for 2 hours. The reaction mixture was then allowed to cool to room temperature before being concentrated *in vacuo* to afford the crude product.

4.1.1.2 Procedure B
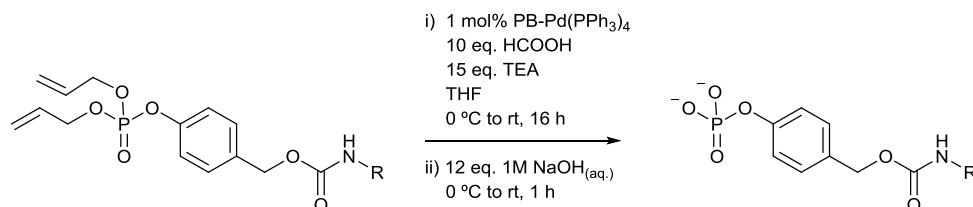
To a stirring solution of the 4-((bis(allyloxy)phosphoryl)oxy)benzyl carbamate (1 eq.) in anhydrous THF (10 mL / mmol) at 0 °C was added polymer-bound $Pd(PPh_3)_4$ (1 mol%) followed by formic acid (15 eq.) and anhydrous TEA (10 eq.). The reaction mixture was allowed to warm to room temperature and stirred for 16 hours. The reaction mixture was then filtered *via* gravity filtration and the filtrate concentrated *in vacuo*. The residue was then cooled to 0 °C and 1M $NaOH_{(aq.)}$ (12 eq.) was added slowly. The reaction mixture was allowed to warm to room temperature and stirred for 1 hour before being concentrated *in vacuo* to afford the crude product.
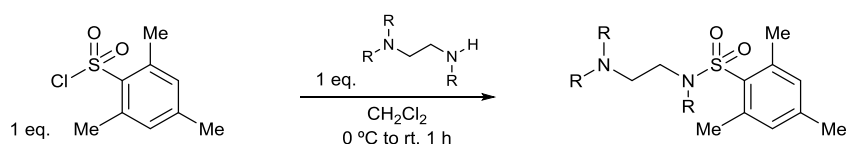
4.1.1.3 Procedure C
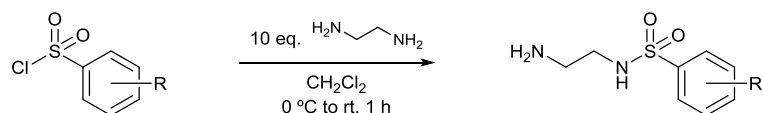
To a stirring solution of ethylenediamine (10 eq.) in anhydrous CH_2Cl_2 (2.5 mL / mmol) at 0 °C was added the sulfonyl chloride (1 eq.) in anhydrous CH_2Cl_2 (2.5 mL / mmol) dropwise. After complete addition, the reaction mixture was allowed to warm to room temperature and stirred for 1 hour. The reaction was then quenched with water and the organics separated. The aqueous layer was then extracted twice with CH_2Cl_2. The combined organics were then washed with water, then brine, dried over $MgSO_4$ and concentrated *in vacuo* to afford the crude product.

4.1.1.4 Procedure D
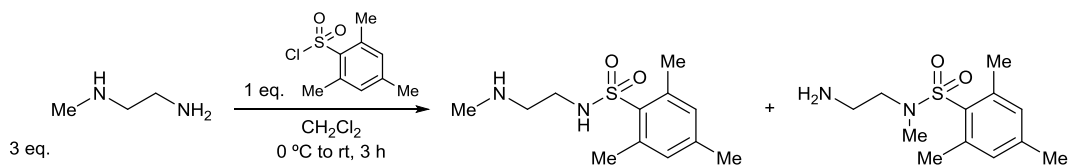
To a stirring solution of *N*-methylethylenediamine (3 eq.) in anhydrous CH$_2$Cl$_2$ (2.5 mL / mmol) at 0 °C was added mesitylsulfonyl chloride (1 eq.) in anhydrous CH$_2$Cl$_2$ (2.5 mL / mmol) dropwise. After complete addition, the reaction mixture was allowed to warm to room temperature and stirred for 3 hours. The reaction was then quenched with water and the organics separated. The aqueous layer was then extracted twice with CH$_2$Cl$_2$. The combined organics were then washed with water, then brine, dried over MgSO$_4$ and concentrated *in vacuo* to afford the crude product.

4.1.1.5 Procedure E

To a stirring solution of the ethylenediamine (1 eq.) in anhydrous CH$_2$Cl$_2$ (2.5 mL / mmol) at 0 °C was added mesitylsulfonyl chloride (1 eq.) in anhydrous CH$_2$Cl$_2$ (2.5 mL / mmol) dropwise. After complete addition, the reaction mixture was allowed to warm to room temperature and stirred for 1 hour. The reaction was then quenched with water and the organics separated. The aqueous layer was then extracted twice with CH$_2$Cl$_2$. The combined organics were then washed with water, then brine, dried over MgSO$_4$ and concentrated *in vacuo* to afford the crude product.

4.1.1.6 Procedure F
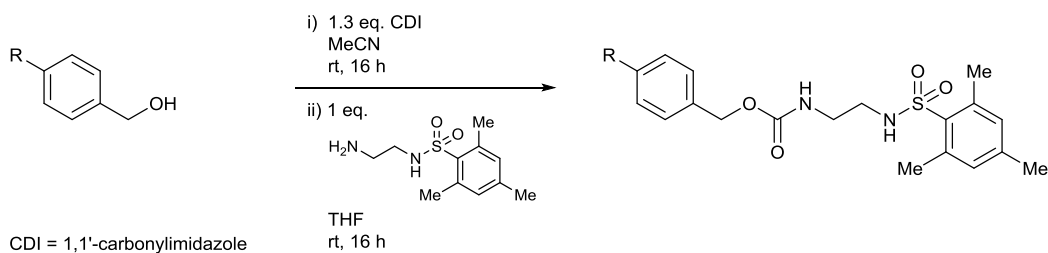
To a stirring solution of 1,1'-carbonyldiimidazole (1.3 eq.) in anhydrous MeCN (7.5 mL / mmol) at room temperature was added a solution of the benzyl alcohol (1 eq.) in anhydrous MeCN (7.5 mL / mmol) dropwise. After complete addition, the reaction mixture was left to stir for 16 hours before being concentrated *in vacuo* and the residue quenched with water. The aqueous layer was then extracted three times with CHCl$_3$. The combined organics were then washed with water, then brine, dried over Na$_2$SO$_4$ and concentrated *in vacuo*. The residue was then taken up in anhydrous THF (15 mL / mmol) and *N*-(2-aminoethyl)-2,4,6-trimethylbenzenesulfonamide **175** (1 eq.) was added in one portion. The reaction mixture

was then left to stir for 16 hours before being concentrated *in vacuo* and the residue quenched with water. The aqueous layer was then extracted three times with EtOAc. The combined organics were then washed twice with water and once with brine before being dried over Na$_2$SO$_4$ and concentrated *in vacuo* to afford the crude product.

4.1.1.7 Procedure G
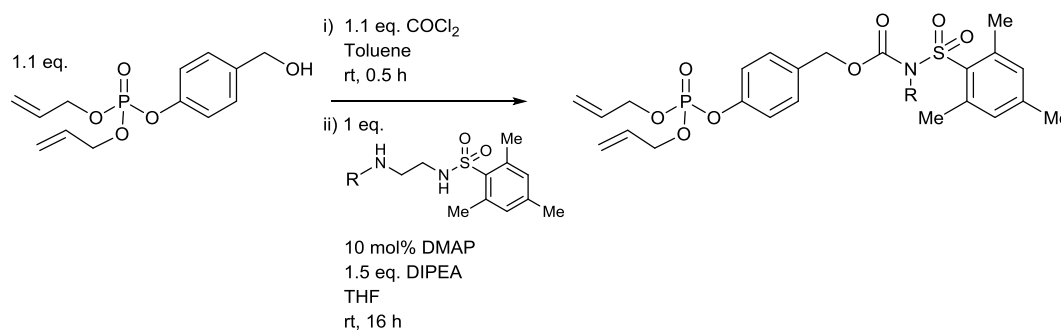
To a stirring solution of diallyl (4-(hydroxymethyl)phenyl) phosphate (1.1 eq.) in anhydrous toluene (1 mL / mmol) was added phosgene solution (≈20% in toluene) (1.1 eq.) dropwise and the reaction was allowed to stir at room temperature for 30 minutes before being concentrated *in vacuo*. The residue was then taken up into anhydrous THF (2 mL / mmol) and added dropwise to a stirring solution of the *N*-(2-aminoethyl)-sulfonamide (1 eq.), DIPEA (1.5 eq.) and DMAP (10 mol%) in anhydrous THF (3 mL / mmol). The reaction mixture was then allowed to stir for 16 hours at room temperature before being quenched with NaHCO$_3$ (sat.) and extracted three times with EtOAc. The combined organics were then washed with water, then brine before being dried over MgSO$_4$ and concentrated *in vacuo* to afford the crude product.

4.1.1.8 Procedure H
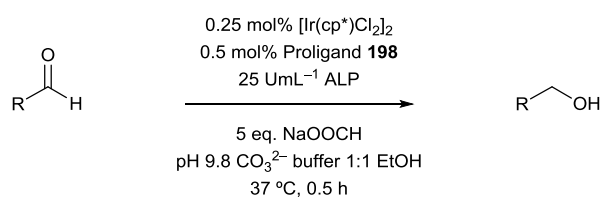
To a stirring solution of dichloro(pentamethylcyclopentadienyl)iridium(III) dimer (0.25 mol%), 4-((((2-((2,4,6-trimethylphenyl)sulfonamido)ethyl)carbamoyl)oxy) methyl)phenyl phosphate **198** (0.5 mol%) and sodium formate (5 eq.) in pH 9.8 0.05M sodium carbonate buffer (2 mL / mmol) was added alkaline phosphatase (25 UmL^{-1}) followed by a solution of the aldehyde (1 eq.) in ethanol (2 mL / mmol). The reaction mixture was then warmed to 37 °C and stirred for 30 minutes. The reaction was then quenched with water and extracted three times with EtOAc. The combined organics were dried over MgSO$_4$ and concentrated *in vacuo* to afford the crude product.

4.1.1.9 Procedure I
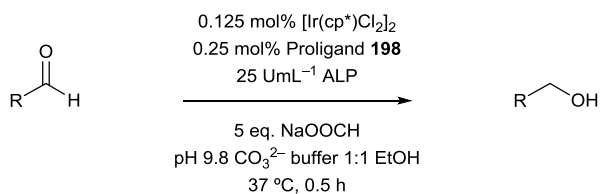
To a stirring solution of dichloro(pentamethylcyclopentadienyl)iridium(III) dimer (0.125 mol%), 4-((((2-((2,4,6-trimethylphenyl)sulfonamido)ethyl)carbamoyl)oxy) methyl)phenyl phosphate **198** (0.25 mol%) and sodium formate (5 eq.) in pH 9.8 0.05M sodium carbonate buffer (2 mL / mmol) was added alkaline phosphatase (25 UmL^{-1}) followed by a solution of the aldehyde (1 eq.) in ethanol (2 mL / mmol). The reaction mixture was then warmed to 37 °C and stirred for 30 minutes. The reaction was then quenched with water and extracted three times with EtOAc. The combined organics were dried over $MgSO_4$ and concentrated *in vacuo* to afford the crude product.

4.1.2 ^{31}P NMR Procedures

4.1.2.1 ALP-catalysed Dephosphorylation of Substrate 112
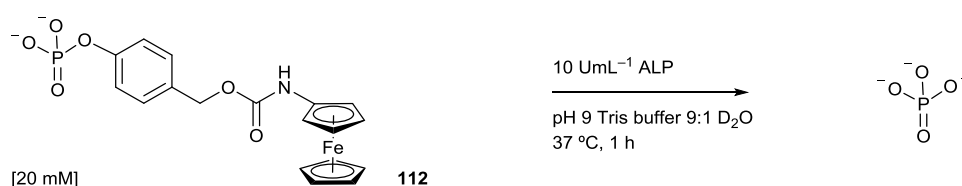
To 350 μL of a 28.6 mM solution of **112** in pH 9 Tris buffer in a clean, oven-dried Young's NMR tube was added 50 μL of D_2O, to achieve successful NMR locking, followed by 100 μL of a 50 UmL^{-1} solution of ALP in pH 9 Tris buffer. This achieved a 0.5 mL reaction volume that consisted of a 20 mM concentration of **112** and a 10 UmL^{-1} concentration of ALP. The tube was then sealed with a screw-top lid and the reaction mixture agitated through vertical inversion and reversion of the reaction vessel. The reaction was then injected into a 500 MHz NMR machine preheated to 310 K, locked to D_2O and shimmed prior to ^{31}P {^1H} data acquisition. Approximately every 5 minutes, the reaction vessel was ejected and agitated in the same manner as previous, before reinsertion into the NMR machine. To maintain accurate peak position, locking and shimming was performed prior to every acquisition. This process was repeated until full consumption of the starting material was observed.

4.1.2.1 ALP-catalysed Dephosphorylation of 198
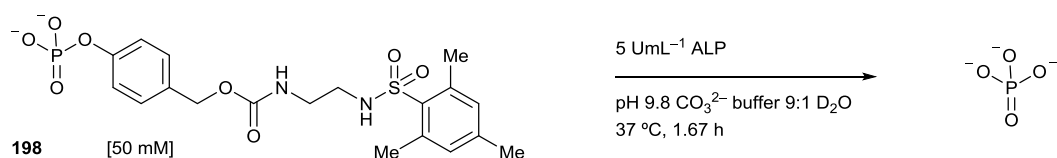
To 350 μL of a 72 mM solution of **198** in pH 9.8 CO_3^{2-} buffer in a clean, oven-dried Young's NMR tube was added 50 μL of D_2O, to achieve successful NMR locking, followed by 100 μL of a 25 UmL^{-1} solution of ALP in pH 9.8 CO_3^{2-} buffer. This achieved a 0.5 mL reaction volume that consisted of a 50 mM concentration of **198** and a 5 UmL^{-1} concentration of ALP. The tube was then sealed with a screw-top lid and the reaction mixture agitated through vertical inversion and reversion of the reaction vessel. The reaction was then injected into a 500 MHz NMR machine preheated to 310 K, locked to D_2O and shimmed prior to ^{31}P {^1H} data acquisition. Approximately every 10 minutes, the reaction vessel was ejected and agitated in the same manner as previous, before reinsertion into the NMR machine. To maintain accurate peak position, locking and shimming was performed prior to every acquisition. This process was repeated until full consumption of the starting material was observed.

4.1.3 Mass Spectrometry Procedure
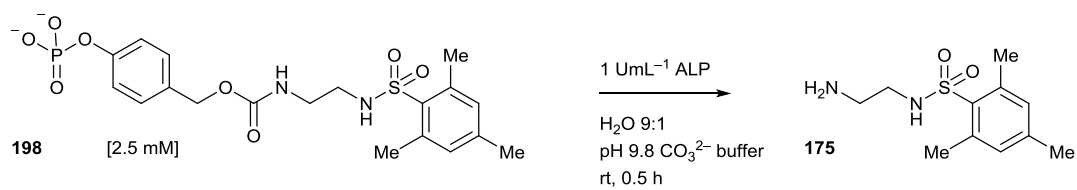
To 900 μL of a 2.8 mM solution of **198** in water was added 100 μL of a 10 UmL^{-1} solution of ALP to give a 1 mL reaction mixture that consisted of a 2.5 mM solution of **198** and a 1 UmL^{-1} solution of ALP. Immediately after ALP addition, the reaction mixture was taken up in a micro-syringe and directly infused at 3 μLmin^{-1} into an ESI–UHR–TOF mass spectrometer in negative ion mode. Spectra were recorded between 0–500 *m/z* over a reaction timeframe of 30 minutes and accumulative averaged mass spectra were generated between specific time points. Additionally, relative peak intensities for **198** at 471.0996 ± 0.002 *m/z* and for **175** at 241.1016 ± 0.002 were monitored over time.

4.1.4 Electrochemistry Procedures

All electrochemical analysis was conducted by direct application of the sample to a screen-printed electrochemical cell (GM Nameplate, Seattle) comprising of carbon working and counter electrodes and a silver (pseudo Ag/AgCl) reference electrode. All samples were analysed amperometrically using differential pulse voltammetry (modulation = 0.04 s, interval = 0.1 s, step potential = 3 mV, modulation amplitude = 49.95 mV). Peak integrals were obtained through the software's 'peak search' function (automatic search, linear baseline). Current was measured either through the software's 'peak search' function (automatic search, no baseline) or, when no peaks could be found, through the software's 'interpolate' function where the current at a specific voltage could be obtained.

4.1.4.1 Ratiometric Electrochemical Detection of ALP with Substrate 112
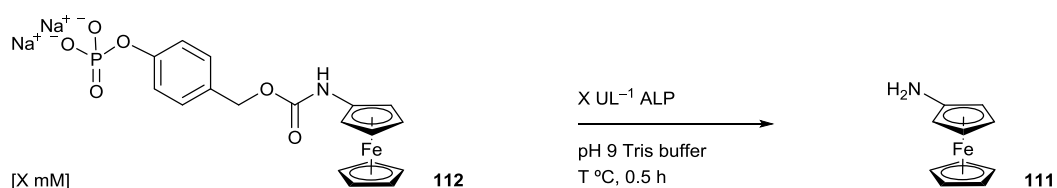

1 mL of ALP in pH 9 Tris buffer was charged to a 10 mL screw-top vial containing a magnetic flea and warmed to the desired temperature using a multi-vial, aluminium DrySyn® heating block upon a stirrer hotplate. 1 mL of 1 mM **112** was then added and the reaction sealed and stirred at 1000 rpm for 30 minutes. Every 3 minutes during the reaction, a 25 μL sample was taken and subjected to electrochemical analysis (initial voltage = −300 mV, end voltage = 200 mV).

4.1.4.2 Ratiometric Electrochemical Detection of Streptavidin–ALP with Substrate 112
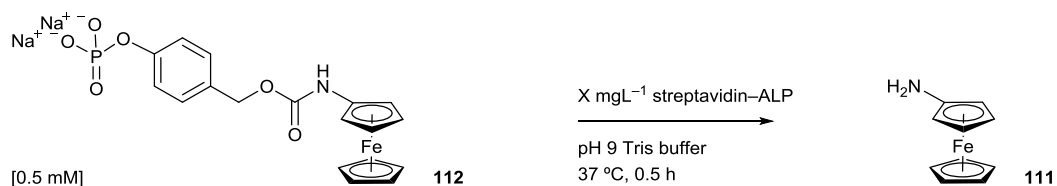

1 mL of streptavidin–ALP in pH 9 Tris buffer was charged to a 10 mL screw-top vial containing a magnetic flea and warmed 37 °C using a multi-vial, aluminium DrySyn® heating block upon a stirrer hotplate. 1 mL of 1 mM of **112** was then added and the reaction sealed and stirred at 1000 rpm for 30 minutes. Every 3 minutes during the reaction, a 25 μL sample was taken and subjected to electrochemical analysis (initial voltage = −300 mV, end voltage = 200 mV).

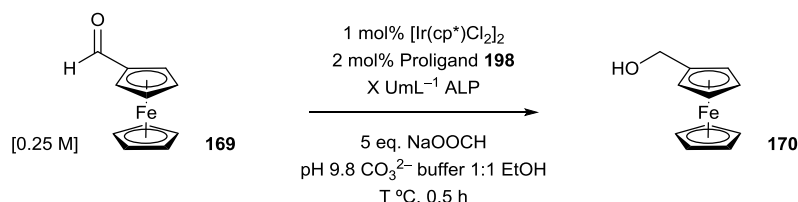### 4.1.4.3 Ratiometric Electrochemical Detection of CRP with Substrate 112
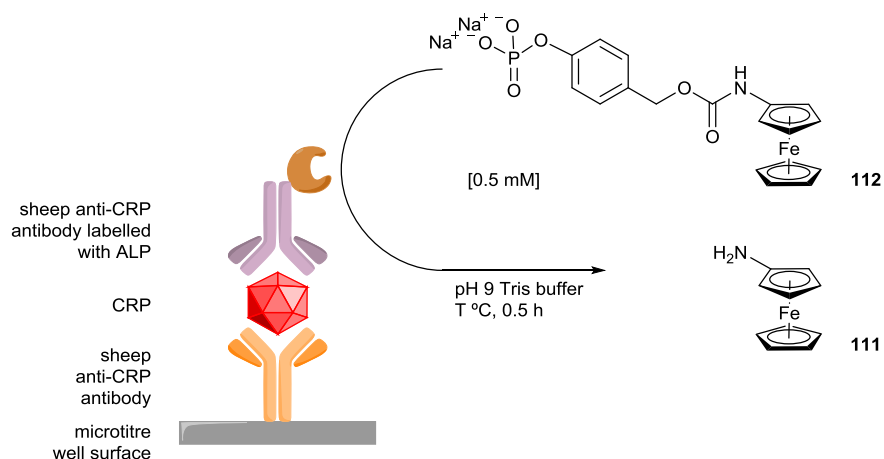
A sandwich ELISA was constructed according to the general procedure (4.1.5) before the addition of 100 μL of a 0.5 mM solution of **112** in pH 9 Tris buffer. The microwells were then mixed briefly on a plate shaker and incubated at either room temperature or 37 °C for 30 minutes. After this duration, a 25 μL sample was taken and subjected to electrochemical analysis (initial voltage = −300 mV, end voltage = 200 mV).

### 4.1.4.4 Amperometric Electrochemical Detection of CRP with AA2P 105
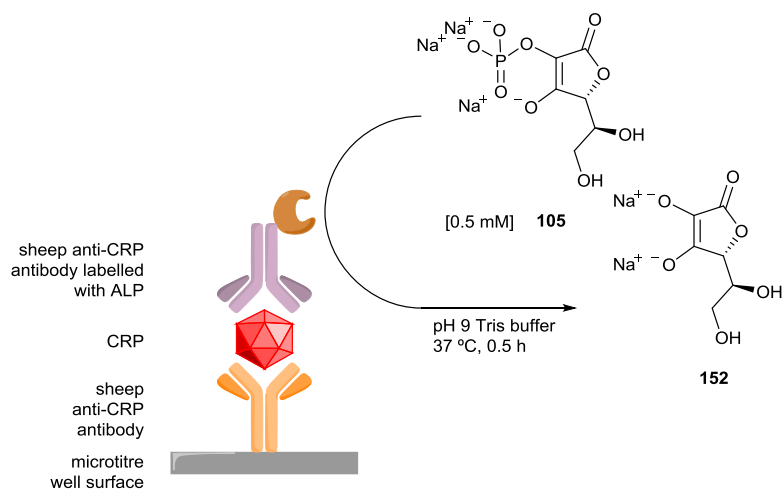
A sandwich ELISA was constructed according to the general procedure (4.1.5) before the addition of 100 μL of a 0.5 mM solution of AA2P **105** in pH 9 Tris buffer. The microwells were then mixed briefly on a plate shaker and incubated at 37 °C for 30 minutes. After this duration, a 25 μL sample was taken and subjected to electrochemical analysis (initial voltage = −200 mV, end voltage = 600 mV) and the current at 400 mV was measured.

### 4.1.4.5 Ratiometric Electrochemical Detection of ALP with Proligand **198**

To a 10 mL screw-top vial charged with a magnetic flea was added dichloro(pentamethylcyclopentadienyl)iridium(III) dimer (4 mg, 5 μmol, 1 mol%), 4-((((2-((2,4,6-trimethylphenyl)sulfonamido)ethyl)carbomyl)oxy)methyl)phenyl phosphate **198** (5 mg, 10 μmol, 2 mol%) and sodium formate (170 mg, 2.5 mmol, 5 eq.). 1 mL of 2 × the desired concentration of ALP in pH 9.8 CO_3^{2-} buffer was then added. Immediately thereafter, a 1 mL solution of ferrocenecarboxaldehyde **169** (107 mg, 0.5 mmol, 1 eq.) was then added in one portion. The reaction was then warmed to the desired temperature using a multi-vial, aluminium DrySyn® heating block upon a stirrer hotplate and stirred at 1000 rpm for 30 minutes. Every 3 minutes during the reaction, a 1 μL sample was taken from the reaction mixture and diluted into 999 μL of pH 9.8 CO_3^{2-} buffer. After shaking, a 100 μL sample of this solution was diluted into 900 μL of pH 9.8 CO_3^{2-} buffer to give a 25 μM ferrocene concentration. After shaking again, a 25 μL sample of this twice-diluted solution was subjected to electrochemical analysis (initial voltage = −200 mV, end voltage = 400 mV).

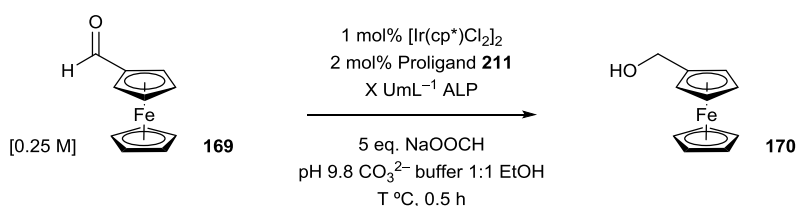### 4.1.4.6 Ratiometric Electrochemical Detection of Streptavidin–ALP with Proligand **198**
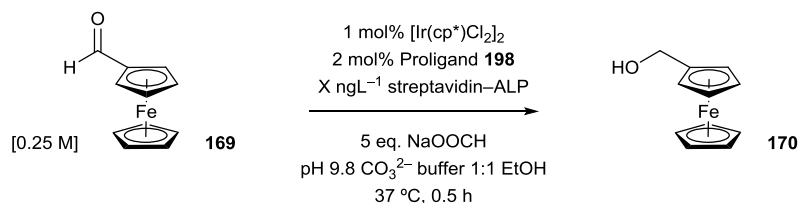
To a 10 mL screw-top vial charged with a magnetic flea was added dichloro(pentamethylcyclopentadienyl)iridium(III) dimer (4 mg, 5 μmol, 1 mol%), 4-((((2-((2,4,6-trimethylphenyl)sulfonamido)ethyl)carbomyl)oxy)methyl)phenyl phosphate **198** (5 mg, 10 μmol, 2 mol%) and sodium formate (170 mg, 2.5 mmol, 5 eq.). 1 mL of 2 × the desired concentration of streptavidin–ALP in pH 9.8 CO_3^{2-} buffer was then added. Immediately thereafter, a 1 mL solution of ferrocenecarboxaldehyde **169** (107 mg, 0.5 mmol, 1 eq.) was then added in one portion. The reaction was then warmed to the desired temperature using a multi-vial, aluminium DrySyn® heating block upon a stirrer hotplate and stirred at 1000 rpm for 30 minutes. Every 3 minutes during the reaction, a 1 μL sample was taken from the reaction mixture and diluted into 999 μL of pH 9.8 CO_3^{2-} buffer. After shaking, a 100 μL sample of this solution was diluted into 900 μL of pH 9.8 CO_3^{2-} buffer to give a 25 μM ferrocene concentration. After shaking again, a 25 μL sample of this twice-diluted solution was subjected to electrochemical analysis (initial voltage = −200 mV, end voltage = 400 mV).

4.1.4.7 Ratiometric Electrochemical Detection of CRP with Proligand 198
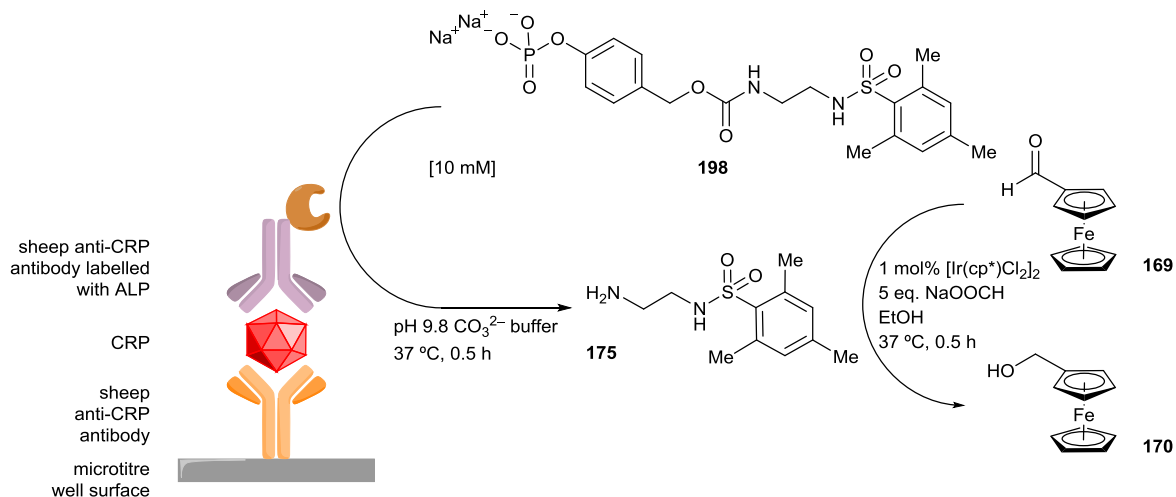
A sandwich ELISA was constructed according to the general procedure (4.1.5) before being washed (filled and aspirated with pH 9.8 CO_3^{2-} buffer) another four times to remove surfactants in the previous wash solution that were found to cause high background signals. 100 μL of a 10 mM solution of 198 in pH 9.8 CO_3^{2-} buffer (0.5 mg, 1 μmol, 2 mol%) was then added. The microwells were then mixed briefly on a plate shaker and incubated at 37 °C for 30 minutes. After this duration, the substrate solution was aspirated and added to a 1 mL screw-top sample vial charged with a magnetic flea as well as containing 10 μL of a 5 mM solution of dichloro(pentamethylcyclopentadienyl)iridium(III) dimer (0.4 mg, 0.5 μmol, 1 mol%), 90 μL of a 0.56 M solution of ferrocenecarboxaldehyde 169 (11 mg, 0.05 mmol, 1 eq.) and sodium formate (17 mg, 0.25 mmol, 5 eq.). The reaction was then warmed to 37 °C using a multi-vial, aluminium DrySyn® heating block upon a stirrer hotplate and stirred at 1000 rpm for 30 minutes. Every 3 minutes during the reaction, a 1 μL sample was taken from the reaction mixture and diluted into 999 μL of pH 9.8 CO_3^{2-} buffer to give a 25 μM ferrocene concentration. After shaking, a 25 μL sample of this diluted solution was subjected to electrochemical analysis (initial voltage = −200 mV, end voltage = 400 mV).

4.1.4.8 Ratiometric Electrochemical Detection of ALP with Proligand 211

To a 10 mL screw-top vial charged with a magnetic flea was added dichloro(pentamethylcyclopentadienyl)iridium(III) dimer (4 mg, 5 μmol, 1 mol%), 4-((((2-((2,4,6-trimethylphenyl)sulfonamido)ethyl)carbomyl)oxy)methyl)phenyl phosphate 211 (8 mg, 10 μmol, 2 mol%) and sodium formate (170 mg, 2.5 mmol, 5 eq.). 1 mL of 2 × the desired concentration of ALP in pH 9.8 CO_3^{2-} buffer was then added. Immediately thereafter, a 1 mL solution of ferrocenecarboxaldehyde 169 (107 mg, 0.5 mmol, 1 eq.) was then added in one portion. The reaction was then warmed to the desired temperature using a multi-vial, aluminium DrySyn® heating block upon a stirrer hotplate and stirred at 1000 rpm for 30 minutes. Every 3 minutes during the reaction, a 1 μL sample was taken from the reaction mixture

and diluted into 999 µL of pH 9.8 CO_3^{2-} buffer. After shaking, a 100 µL sample of this solution was diluted into 900 µL of pH 9.8 CO_3^{2-} buffer to give a 25 µM ferrocene concentration. After shaking again, a 25 µL sample of this twice-diluted solution was subjected to electrochemical analysis (initial voltage = −200 mV, end voltage = 400 mV).

4.1.4.9 Ratiometric Electrochemical Detection of CRP with Proligand 211
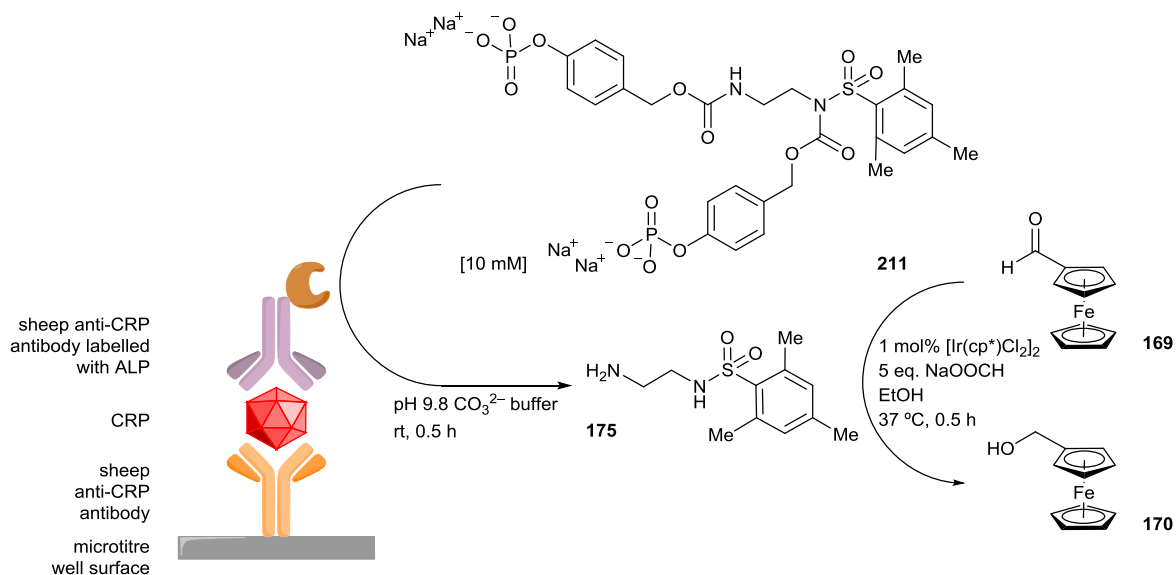
A sandwich ELISA was constructed according to the general procedure (4.1.5) before being washed (filled and aspirated with pH 9.8 CO_3^{2-} buffer) another four times to remove surfactants in the previous wash solution that were found to cause high background signals. 100 µL of a 10 mM solution of **211** in pH 9.8 CO_3^{2-} buffer (0.8 mg, 1 µmol, 2 mol%) was then added. The microwells were then mixed briefly on a plate shaker and incubated at 37 °C for 30 minutes. After this duration, the substrate solution was aspirated and added to a 1 mL screw-top sample vial charged with a magnetic flea as well as containing 10 µL of a 5 mM solution of dichloro(pentamethylcyclopentadienyl)iridium(III) dimer (0.4 mg, 0.5 µmol, 1 mol%), 90 µL of a 0.56 M solution of ferrocenecarboxaldehyde **169** (11 mg, 0.05 mmol, 1 eq.) and sodium formate (17 mg, 0.25 mmol, 5 eq.). The reaction was then warmed to 37 °C using a multi-vial, aluminium DrySyn® heating block upon a stirrer hotplate and stirred at 1000 rpm for 30 minutes. Every 3 minutes during the reaction, a 1 µL sample was taken from the reaction mixture and diluted into 999 µL of pH 9.8 CO_3^{2-} buffer to give a 25 µM ferrocene concentration. After shaking, a 25 µL sample of this diluted solution was subjected to electrochemical analysis (initial voltage = −200 mV, end voltage = 400 mV).

4.1.5   ELISA Construction for CRP Detection
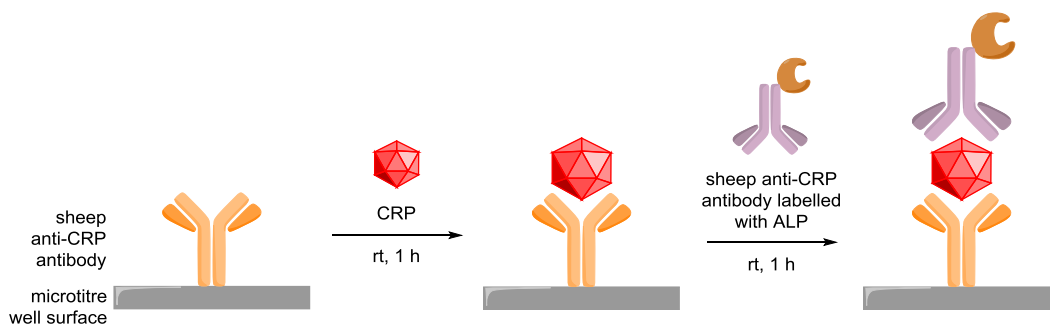
To a polystyrene microtitre well pre-coated with affinity-purified sheep anti-CRP antibodies, was added 50 µL of a standard, pre-diluted CRP concentration, mixed briefly on a plate shaker and incubated at room temperature for 1 hour. The microwells were then washed (filled and aspirated with a wash solution containing buffered saline and a commercial surfactant) four times before 100 µL of a solution containing affinity-purified sheep anti-CRP antibodies labelled with ALP, mixed briefly on a plate shaker and incubated at room temperature for 1 hour. The microwells were then washed (filled and aspirated with a wash solution containing buffered saline and a commercial surfactant) another four times to leave the constructed ALP-labelled sandwich immunoassay.
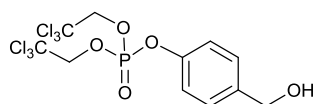
4.2 Compound Data

4.2.1 *4-Formylphenyl Bis(2,2,2-trichloroethyl) Phosphate* **128**
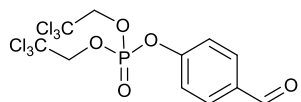
To a stirring solution of 4-hydroxybenzaldehyde (0.61g, 5 mmol, 1 eq.) in anhydrous THF (25 mL) at 0 °C was added anhydrous TEA (0.7 mL, 5 mmol, 1 eq.) followed by bis(2,2,2-trichloroethyl) phosphorochloridate (1.90 g, 5 mmol, 1 eq.). The reaction mixture was stirred at 0 °C for 30 minutes before being allowed to warm to room temperature. After stirring for 2 hours, the reaction was concentrated *in vacuo* and the residue quenched with NaHCO$_{3 \text{ (sat.)}}$ (20 mL). The aqueous layer was then extracted three times with CH$_2$Cl$_2$ (20 mL). The combined organics were dried over Na$_2$SO$_4$ and then concentrated *in vacuo* to afford the crude product. Purification by recrystallisation (hot Et$_2$O) gave the title compound as white needles (0.17 g, 7%). **MP**: 77–79 °C. **IR** (solid, cm^{-1}); ν 3068 (C–H), 2953 (C–H), 2862 (C–H), 1699 (C=O), 1272 (P=O), 1046 (P–O), 641 (C–Cl). **^{1}H NMR** (300 MHz, CDCl$_3$); δ$_\text{H}$ 9.98 (1H, s, C*H*O), 7.92 (2H, d, *J* = 8.4 Hz, Ar*H*), 7.45 (2H, dd, *J* = 8.4 Hz, $^4J_\text{H–P}$ = 0.9 Hz, Ar*H*), 4.74 (2H, dd, *J* = 12.7, $^3J_\text{H–P}$ = 7.1 Hz, C*H*$_2$), 4.70 (2H, dd, *J* = 12.7, $^3J_\text{H–P}$ = 7.1 Hz, C*H*$_2$). **^{13}C NMR** (75.5 MHz, CDCl$_3$); δ$_\text{C}$ 190.6 (*C*HO), 154.3 (d, $^2J_\text{C–P}$ = 7 Hz, Ar*C*), 134.2 (Ar*C*), 131.9 (Ar*C*), 121.0 (d, $^3J_\text{C–P}$ = 5 Hz, Ar*C*), 94.3 (d, $^3J_\text{C–P}$ = 11 Hz, *C*Cl$_3$), 77.8 (d, $^2J_\text{C–P}$ = 5 Hz, *C*CCl$_3$). **^{31}P {^{1}H} NMR** (121.5 MHz, CDCl$_3$); δ$_\text{P}$ −9.32. **HRMS** (ESI): calc'd for C$_{11}$H$_{10}$^{35}Cl$_6$O$_5$P [M+H]$^+$ *m/z* 462.8397, found 462.8429.

### 4.2.2   4-(Hydroxymethyl)phenyl Bis(2,2,2-trichloroethyl) Phosphate 129

To a stirring solution of 4-hydroxybenzaldehyde (0.49 g, 4 mmol, 1 eq.) in anhydrous THF (25 mL) at 0 °C was added anhydrous TEA (0.56 mL, 4 mmol, 1 eq.), followed by bis(2,2,2-trichloroethyl) phosphorochloridate (3.03 g, 8 mmol, 2 eq.). The reaction mixture was stirred at 0 °C for 30 minutes before being allowed to warm to room temperature. After stirring at room temperature for 2 hours, the reaction was concentrated *in vacuo* and the residue quenched with NaHCO$_3$ $_{(sat.)}$ (20 mL). The aqueous layer was then extracted three times with CH$_2$Cl$_2$ (20 mL). The combined organics were dried over Na$_2$SO$_4$ and concentrated *in vacuo*. The residue was then taken up into THF (30 mL) and cooled to 0 °C. Sodium borohydride (0.30 g, 8 mmol, 2 eq.) was then added portion-wise. The reaction was then concentrated *in vacuo* and the residue quenched with NH$_4$Cl $_{(sat.)}$ (30 mL). The aqueous layer was then extracted three times with EtOAc (30 mL). The combined organics were dried over Na$_2$SO$_4$ and then concentrated *in vacuo* to afford the crude compound. Purification by silica gel column chromatography (hexane 8:2 EtOAc, R$_f$ = 0.45) gave the title compound as a colourless oil (1.02 g, 55%). **IR** (film, cm^{-1}); ν 3412 (O–H), 2953 (C–H), 2876 (C–H), 1282 (P=O), 1025 (P–O), 637 (C–Cl). **^{1}H NMR** (300 MHz, CDCl$_3$); δ$_H$ 7.37 (2H, d, *J* = 8.1 Hz, Ar*H*), 7.26 (2H, d, *J* = 8.1 Hz, Ar*H*), 4.75–4.64 (6H, m, C*H*$_2$), 1.86 (1H, br s, O*H*). **^{13}C NMR** (75.5 MHz, CDCl$_3$); δ$_C$ 149.3 (d, $^2J_{C–P}$ = 7 Hz, Ar*C*), 138.9 (d, $^5J_{C–P}$ = 1 Hz, Ar*C*), 128.6 (Ar*C*), 120.4 (d, $^3J_{C–P}$ = 5 Hz, Ar*C*), 94.5 (d, $^3J_{C–P}$ = 11 Hz, *C*Cl$_3$), 77.7 (d, $^2J_{C–P}$ = 5 Hz, *C*CCl$_3$), 64.5 (*C*H$_2$OH). **^{31}P {^{1}H} NMR** (121.5 MHz, CDCl$_3$); δ$_P$ −8.66. **HRMS** (ESI): calc'd for C$_{11}$H$_{12}$^{35}Cl$_6$O$_5$P [M+H]$^+$ *m/z* 464.8554, found 464.8570.

### 4.2.3 Dibenzyl (4-(Hydroxymethyl)phenyl) Phosphate 136
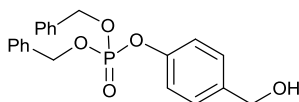
To a stirring solution of NCS (0.67 g, 5 mmol, 1 eq.) in anhydrous toluene (25 mL) under argon at 0 °C was added the dibenzyl phosphite (1.1 mL, 5 mmol, 1 eq.) drop-wise. The reaction mixture was allowed to warm to room temperature and stirred for 2 hours. The reaction mixture was then filtered *via* gravity filtration and concentrated *in vacuo*. The residue was then taken up into anhydrous THF (10 mL) and added drop-wise to a stirring solution of 4-hydroxybenzaldehyde (0.61 g, 5 mmol, 1 eq.) and anhydrous TEA (0.7 mL, 5 mmol, 1 eq.) in anhydrous THF (10 mL) at 0 °C. The reaction mixture was stirred at 0 °C for 30 minutes before being allowed to warm to room temperature. After stirring at room temperature for 2 hours, the reaction was concentrated *in vacuo* and the residue quenched with $NaHCO_3$ (sat.) (25 mL). The aqueous layer was then extracted three times with EtOAc (25 mL). The combined organics were dried over Na_2SO_4 and concentrated *in vacuo*. The residue was then taken up into THF (45 mL) and cooled to 0 °C. Sodium borohydride (0.38 g, 10 mmol, 2 eq.) was then added portion-wise. The reaction mixture was then allowed to warm to room temperature and stirred for 2 hours. The reaction was then concentrated *in vacuo* and the residue quenched with NH_4Cl (sat.) (50 mL). The aqueous layer was then extracted three times with EtOAc (25 mL). The combined organics were then dried over Na_2SO_4 and concentrated *in vacuo* to afford the crude product. Purification by silica gel column chromatography (hexane 1:1 EtOAc, R_f = 0.20) gave the title compound as a white solid (1.21 g, 63%). **MP**: 52–54 °C. **IR** (solid, cm^{-1}); ν 3367 (O–H), 3063 (C–H), 3029 (C–H), 2964 (C–H), 2893 (C–H), 2846 (C–H), 1245 (P=O), 1054 (P–O). **^{1}H NMR** (300 MHz, CDCl$_3$); δ_H 7.22–7.15 (10H, m, Ar*H*), 7.13 (2H, d, *J* = 8.5 Hz, Ar*H*), 6.96 (2H, dd, *J* = 8.5 Hz, $^4J_{H-P}$ = 1.0 Hz, Ar*H*), 4.96 (4H, d, $^2J_{H-P}$ = 8.4 Hz, ArC*H$_2$*OP), 4.46 (2H, s, ArC*H$_2$*OH), 3.25 (1H, br s, O*H*). **^{13}C NMR** (75.5 MHz, CDCl$_3$); δ_C 149.5 (d, $^2J_{C-P}$ = 7 Hz, Ar*C*), 138.4 (d, $^5J_{C-P}$ = 1 Hz, Ar*C*), 135.3 (d, $^3J_{C-P}$ = 7 Hz, Ar*C*), 128.7 (Ar*C*), 128.6 (Ar*C*), 128.2 (Ar*C*), 128.2 (Ar*C*), 128.0 (Ar*C*), 70.0 (d, $^2J_{C-P}$ = 6 Hz, *C*H$_2$OP), 64.0 (*C*H$_2$OH). **^{31}P {^{1}H} NMR** (121.5 MHz, CDCl$_3$); δ_P −5.53. **HRMS** (ESI): calc'd for C$_{21}$H$_{21}$NaO$_5$P [M+Na]$^+$ *m/z* 407.1019, found 407.1124.

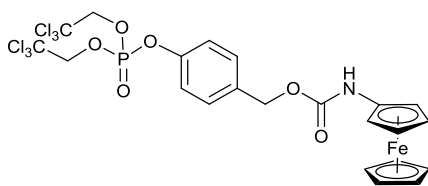### 4.2.4 Diallyl (4-(Hydroxymethyl)phenyl) Phosphate **149**
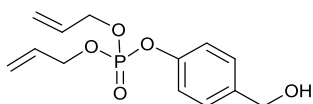
To a stirring solution of phosphorous trichloride (8.7 mL, 100 mmol, 2 eq.) in anhydrous THF (70 mL) at 0 °C was added a solution of allyl alcohol (13.6 mL, 200 mmol, 4 eq.) and anhydrous TEA (31 mL, 220 mmol, 4.4 eq.) in anhydrous THF (30 mL) drop-wise. After complete addition, the reaction mixture was allowed to warm to room temperature and stirred for 1 hour before being cooled back down to 0 °C. Water (50 mL) was then added slowly and the reaction mixture was allowed to warm to room temperature before being stirred for 0.5 hours. The organics were removed *in vacuo* and the aqueous residue extracted three times with EtOAc (50 mL). The combined organics were dried over Na_2SO_4 and concentrated *in vacuo*. The residue was then taken up in anhydrous toluene (75 mL) and added slowly to a stirring solution of NCS (11.7 g, 87.5 mmol, 1.75 eq.) in anhydrous toluene (75 mL) under argon at 0 °C. The reaction mixture was then allowed to warm to room temperature and left to stir for 16 hours. The reaction mixture was then filtered *via* gravity filtration and concentrated *in vacuo*. The residue was then taken up in anhydrous THF (50 mL) and added slowly to a stirring solution of 4-hydroxybenzaldehyde (6.1 g, 50 mmol, 1 eq.) and anhydrous TEA (10.5 mL, 75 mmol, 1.5 eq.) in anhydrous THF (50 mL) at 0 °C. The reaction mixture was allowed to warm to room temperature and stirred for 2 hours before being filtered *via* gravity filtration. The filtrate was then concentrated and the residue taken up in EtOAc (50 mL). The organics were then washed with $NaHCO_3$ (sat.) (50 mL) and the organics separated. The combined aqueous washings were then back-extracted twice with EtOAc (50 mL). The combined organics were then washed with water (50 mL), dried over Na_2SO_4 and concentrated *in vacuo*. The residue was then taken up in anhydrous THF (50 mL) and cooled to 0 °C. Sodium borohydride (3.8 g, 100 mmol, 2 eq.) was added portion-wise and the reaction mixture was then allowed to warm to room temperature and stirred for 2 hours. The reaction was then concentrated *in vacuo* and the residue quenched with NH_4Cl (sat.) (50 mL). The aqueous layer was then extracted three times with EtOAc (50 mL). The combined organics were then washed twice with 1M NaOH (aq.) (50 mL) and twice with water (50 mL) before being dried over Na_2SO_4 and concentrated *in vacuo* to afford the crude product. Purification by silica gel column chromatography (hexane 1:1 EtOAc, $R_f = 0.20$) gave the title compound as a colourless liquid (4.0 g, 28%). **IR** (film, cm^{-1}); ν 3419 (O–H), 2881 (C–H), 1651 (C=C), 1267 (P=O), 1013 (P–O), 988 (C=C–H). **^{1}H NMR** (300 MHz, CDCl$_3$); δ$_H$ 7.22 (2H, d, J = 8.6 Hz, Ar*H*), 7.08 (2H, d, J = 8.6 Hz, Ar*H*), 5.89–5.80 (2H, m, C=C*H*), 5.29 (2H, ddd, J = 17.1, 2.6, 1.5 Hz, C=C*H*$_2$), 5.18 (2H, ddd, J = 10.4, 2.6, 1.1 Hz, C=C*H*$_2$), 4.56–4.51 (6H, m, C*H*$_2$OP + C*H*$_2$OH), 2.90 (1H, br s, O*H*). **^{13}C NMR** (75.5 MHz, CDCl$_3$); δ$_C$ 149.7 (d, $^2J_{C-P}$ = 7 Hz, Ar*C*), 138.3 (d, $^5J_{C-P}$ = 1 Hz, Ar*C*), 132.0 (d, $^3J_{C-P}$ = 7 Hz, *C*HCH$_2$OP), 128.2 (Ar*C*), 119.9 (d, $^3J_{C-P}$ = 5 Hz, Ar*C*), 118.8 (*C*=CH), 68.9 (d, $^2J_{C-P}$ = 6 Hz, *C*H$_2$OP), 64.2 (*C*H$_2$OH). **^{31}P {^{1}H} NMR** (121.5 MHz, CDCl$_3$); δ$_P$ −5.52. **HRMS** (ESI): calc'd for C$_{13}$H$_{17}$NaO$_5$P [M+Na]$^+$ *m/z* 307.0706, found 307.0760.
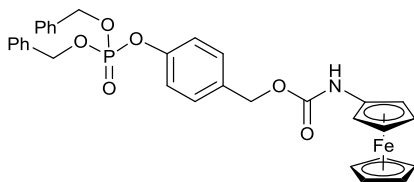
4.2.5   *Ferrocenoyl Azide* **117**
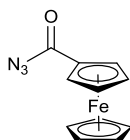
To a stirring suspension of ferrocenecarboxylic acid (2.00 g, 8.7 mmol, 1 eq.) in anhydrous CH_2Cl_2 (20 mL) and anhydrous DMF (1 drop) at 0 °C was added oxalyl chloride (1.5 mL, 17.4 mmol, 2 eq.) drop-wise. The reaction mixture was allowed to warm to room temperature and stirred for 3 hours. The reaction mixture was then concentrated *in vacuo* and the remaining residue was taken up in CH_2Cl_2 (20 mL) before being cooled to 0 °C. Tetrabutylammonium bromide (0.03 g, 0.1 mmol, 0.01 eq.) was then added followed by a solution of sodium azide (0.85 g, 13.1 mmol, 1.5 eq.) in water (4 mL). The reaction mixture was then allowed to warm to room temperature and left to stir for 16 hours. The reaction was then diluted with water (20 mL) and the organics separated. The aqueous layer was then extracted with CH_2Cl_2 (25 mL) and the combined organics were dried over $MgSO_4$ and concentrated *in vacuo* to afford the crude product. Purification by silica gel column chromatography (hexane 1:1 CH_2Cl_2, R_f = 0.45) gave the title compound as a crystalline orange solid (1.75 g, 79%). **MP**: 86–87 °C (lit.[367] 84–86 °C). **IR** (solid, cm^{-1}); 2149 (N_3), 1671 (C=O). **^{1}H NMR** (300 MHz, C_6D_6); δ_H 4.74 (2H, s, Fc*H*), 4.02 (2H, s, Fc*H*), 3.91 (5H, s, Fc*H*). **^{13}C NMR** (75.5 MHz, C_6D_6); δ_C 176.3 (*C*=O), 97.7 (Fc*C*), 72.7 (Fc*C*), 70.7 (Fc*C*), 70.4 (Fc*C*). NMR data in accordance with literature precedent.[367]

4.2.6   4-((Bis(2,2,2-trichloroethoxy)phosphoryl)oxy)benzyl Ferrocenylcarbamate 131
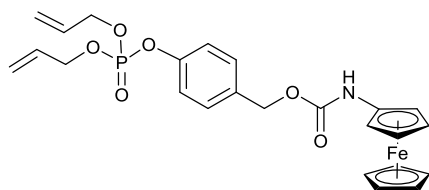

Ferrocenoyl azide (128 mg, 0.5 mmol) and 4-(hydroxymethyl)phenyl bis(2,2,2-trichloroethyl) phosphate **129** (233 mg, 0.5 mmol) were reacted together according to general procedure A to afford the crude product. Purification by silica gel column chromatography (hexane 8:2 EtOAc, R_f = 0.50) gave the title compound as an orange oil (108 mg, 31%). **IR** (film, cm^{-1}); ν 3096 (N–H), 3014 (C–H), 2953 (C–H), 1707 (C=O), 1287 (P=O), 1024 (P–O), 722 (C–Cl). **^{1}H NMR** (300 MHz, CDCl$_3$); δ_H 7.40 (2H, d, J = 8.5 Hz, ArH), 7.28 (2H, d, J = 8.5 Hz, ArH), 6.09 (1H, br s, NH), 5.13 (2H, s, ArCH_2), 4.85 (2H, dd, J = 11.1, $^3J_{H–P}$ = 6.9 Hz, POCH_2), 4.80 (2H, dd, J = 11.1, $^3J_{H–P}$ = 6.9 Hz, POCH_2), 4.48 (2H, s, FcH), 4.82 (5H, s, FcH), 3.98 (2H, s, FcH). **^{13}C NMR** (75.5 MHz, CDCl$_3$); δ_C 153.6 (C=O), 149.7 (d, $^2J_{C–P}$ = 7 Hz, ArC), 134.3 (ArC), 130.0 (ArC), 120.4 (d, $^3J_{C–P}$ = 5 Hz, ArC), 95.4 (FcC), 94.4 (d, $^3J_{C–P}$ = 11 Hz, CCl$_3$), 77.6 (d, $^2J_{C–P}$ = 5 Hz, CCCl$_3$), 69.3(FcC), 66.0 (ArCH_2), 64.6 (FcC), 61.0 (FcC). **^{31}P {^{1}H} NMR** (121.5 MHz, CDCl$_3$); δ_P −8.56. **HRMS** (ESI): calc'd for C$_{22}$H$_{20}$^{35}Cl$_6$FeNNaO$_6$P [M+Na]$^+$ m/z 713.8424, found 713.8407.

4.2.7   4-((Bis(benzyloxy)phosphoryl)oxy)benzyl Ferrocenylcarbamate 137

Ferrocenoyl azide (255 mg, 1 mmol) and dibenzyl (4-(hydroxymethyl)phenyl) phosphate **136** (384 mg, 1 mmol) were reacted together according to general procedure A to afford the crude product. Purification by silica gel column chromatography (hexane 1:1 EtOAc, R_f = 0.45) gave the title compound as an orange solid (271 mg, 44%). **MP**: 118–119 °C. **IR** (solid, cm^{-1}); ν 3093 (N–H), 3048 (C–H), 1721 (C=O), 1263 (P=O), 1075 (P–O). **^{1}H NMR** (300 MHz, CDCl$_3$); δ_H 7.33–7.30 (12H, m, ArH), 7.14 (2H, d, J = 8.2 Hz, ArH), 6.24 (1H, br s, NH), 5.13 (2H, s, ArCH_2), 5.10 (4H, s, POCH_2), 4.49 (2H, s, FcH), 4.15 (5H, s, FcH), 3.97 (2H, s, FcH). **^{13}C NMR** (75.5 MHz, CDCl$_3$); δ_C 153.7 (C=O), 150.5 (d, $J_{C–P}$ = 7 Hz, ArC), 135.4 (d, $J_{C–P}$ = 7 Hz, ArC), 133.4 (ArC), 129.8 (ArC), 128.8 (ArC), 128.7 (ArC), 128.1 (ArC), 120.2 (d, $J_{C–P}$ = 5 Hz, ArC), 95.4 (FcC), 70.0 (d, $J_{C–P}$ = 6 Hz, CH_2OP), 69.2 (FcC), 66.1 (CH_2OH), 64.5 (FcC), 61.0 (FcC). **^{31}P {^{1}H} NMR** (121.5 MHz, CDCl$_3$); δ_P −5.39. **HRMS** (ESI): calc'd for C$_{32}$H$_{31}$FeNO$_6$P [M+H]$^+$ m/z 612.1233, found 612.2169.

### 4.2.8   4-((Bis(allyloxy)phosphoryl)oxy)benzyl Ferrocenylcarbamate **150**


Ferrocenoyl azide (255 mg, 1 mmol) and diallyl (4-(hydroxymethyl)phenyl phosphate **149** (284 mg, 1 mmol) were reacted together according to general procedure A to afford the crude product. Purification by silica gel column chromatography (hexane 1:1 EtOAc (R_f = 0.45, KMnO$_4$)) gave the title compound as a dark orange oil (377 mg, 74%). **IR** (film, cm^{-1}); ν 3094 (N–H), 2953 (C–H), 1726 (C=O), 1259 (P=O), 1017 (P–O), 951 (C=C–H). **^{1}H NMR** (300 MHz, C$_6$D$_6$); δ_H 7.26 (2H, d, J = 8.3 Hz, ArH), 7.12 (2H, d, J = 8.3 Hz, ArH), 6.81 (1H, br s, NH), 5.71–5.58 (2H, m, C=CH), 5.14 (2H, dd, J = 17.1, 1.3 Hz, C=CH_2), 4.99 (2H, s, ArCH_2), 4.92 (2H, dd, J = 10.4, 1.3 Hz, C=CH_2), 4.47–4.33 (4H, m, CH_2OP + FcH), 4.10 (5H, s, FcH), 3.81 (2H, s, FcH). **^{13}C NMR** (75.5 MHz, C$_6$D$_6$); δ_C 154.1 (C=O), 150.9 (d, $^2J_{C-P}$ = 7 Hz, ArC), 134.3 (ArC), 132.5 (d, $^3J_{C-P}$ = 7 Hz, ArC), 130.1 (ArC), 120.5 (d, $^3J_{C-P}$ = 5 Hz), 118.4 (C=CH), 97.0 (FcC), 69.5 (ArCH_2), 68.9 (d, $^2J_{C-P}$ = 6 Hz, CH$_2$OP), 65.9 (ArCH_2), 64.5 (FcC), 60.9 (FcC). **^{31}P {^{1}H} NMR** (121.5 MHz, C$_6$D$_6$); δ_P −4.70. **HRMS** (ESI): calc'd for C$_{24}$H$_{26}$NaFeNO$_6$P [M+Na]$^+$ m/z 534.0745, found 534.0760.

4.2.9   2-(Trimethylsilyl)ethyl Ferrocenylcarbamate **151**
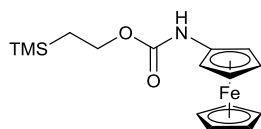
Ferrocenoyl azide (1.02 g, 4 mmol) and 2-(trimethylsilyl)ethanol (0.57 mL, 4 mmol) were reacted together according to general procedure A to afford the crude product. Purification by silica gel column chromatography (hexane 1:1 EtOAc (R_f = 0.82)) gave the title compound as a pale orange solid (1.09 g, 79%). **MP**: 87–89 °C. **IR** (solid, cm^{-1}); ν 3095 (N–H), 2954 (C–H), 2899 (C–H), 1698 (C=O), 1241 (Si–CH$_3$). **^{1}H NMR** (300 MHz, d_6–DMSO); δ_H 8.73 (1H, br s, NH), 4.46 (2H, s, FcH), 4.14–4.09 (7H, m, FcH + OCH_2), 3.91 (2H, s, FcH), 1.00 (2H, t, J = 8.1 Hz, SiCH_2), 0.05 (9H, s, SiCH_3). **^{13}C NMR** (75.5 MHz, d_6–DMSO); δ_C 153.8 (C=O), 97.0 (FcC), 68.7 (FcC), 63.5 (OCH$_2$), 61.9 (FcC), 59.8 (FcC), 17.3 (SiCH$_2$), −1.3 (SiCH$_3$). **HRMS** (ESI): calc'd for C$_{16}$H$_{23}$FeNNaO$_2$Si [M+Na]$^+$ m/z 368.0745, found 368.0748.

4.2.10 4-(((Ferrocenylcarbamoyl)oxy)methyl)phenyl Phosphate 112
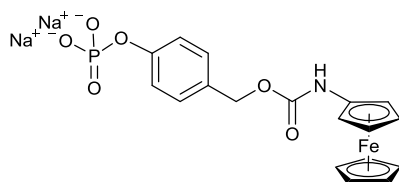
4-((Bis(allyloxy)phosphoryl)oxy)benzyl ferrocenylcarbamate **150** (377 mg, 0.74 mmol), polymer-bound Pd(PPh$_3$)$_4$ (11 mg, 7.4 μmol), formic acid (0.4 mL, 11.1 mmol), anhydrous TEA (1.0 mL, 7.4 mmol) and 1M NaOH$_{(aq.)}$ (8.8 mL, 8.8 mmol) were all reacted together according to general procedure B to afford the crude product. Purification by preparative reverse phase C18-silica gel column chromatography (water) gave the title compound as an amorphous orange solid (241 mg, 69%). **IR** (solid, cm^{-1}); ν 1687 (C=O), 1233 (P=O), 1071 (P–O). **^{1}H NMR** (300 MHz, D$_2$O); δ$_H$ 7.32 (2H, d, J = 8.3 Hz, ArH), 7.17 (2H, d, J = 8.3 Hz, ArH), 5.05 (2H, s, CH_2), 4.47 (2H, s, FcH), 4.17 (5H, s, FcH), 4.03 (2H, s, FcH). **^{13}C NMR** (75.5 MHz, D$_2$O); δ$_C$ 156.5 (C=O), 154.2 (d, $^2J_{C–P}$ = 6 Hz, ArC), 130.3 (ArC), 129.5 (ArC), 120.8 (d, $^3J_{C–P}$ = 5 Hz, ArC), 95.1 (FcC), 69.7 (ArCH_2), 67.2 (FcC), 65.2 (FcC), 61.8 (FcC). **^{31}P {^{1}H} NMR** (121.5 MHz, D$_2$O); δ$_P$ 0.95. **HRMS** (ESI); calc'd for C$_{18}$H$_{18}$FeNO$_6$P [M−H]$^-$: m/z 430.0143, found 430.0180. **E$_{ox}$** (1 mM, pH 9 Tris buffer): 85 mV $vs.$ Ag/AgCl.

4.2.11 4-(((((2-((2,4,6-Trimethylphenyl)sulfonamido)ethyl)carbomyl)oxy)methyl)phenyl Phosphate 198
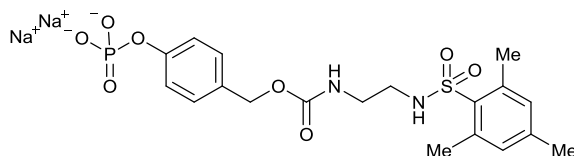
4-((Bis(allyloxy)phosphoryl)oxy)benzyl (2-((2,4,6-trimethylphenyl)sulfonamido)ethyl) carbamate **201** (276 mg, 0.5 mmol), polymer-bound Pd(PPh$_3$)$_4$ (7 mg, 5 μmol), formic acid (0.3 mL, 7.5 mmol) and anhydrous TEA (0.7 mL, 5 mmol) and 1M NaOH$_{(aq.)}$ (6 mL, 6 mmol) were all reacted together according to general procedure B to afford the crude product as a white solid (257 mg, $quant.$). **MP**: 255–260 °C (decomp.). **IR** (solid, cm^{-1}); ν 3299 (N–H), 1707 (C=O), 1382 (SO$_2$–N), 1255 (P=O), 1153 (SO$_2$–N), 1095 (S=O), 1015 (P–O). **^{1}H NMR** (300 MHz, D$_2$O/NaOD); δ$_H$ 7.23 (2H, d, J = 8.2 Hz, ArH), 7.12 (2H, d, J = 8.2 Hz, ArH), 6.92 (2H, s, ArH), 4.79 (2H, s, ArCH_2), 2.93 (2H, m, SO$_2$NHCH_2), 2.78 (2H, br s, CO$_2$NHCH_2), 2.49 (6H, s, ArCH_3), 2.16 (3H, s, ArCH_3). **^{31}P {^{1}H} NMR** (121.5 MHz, D$_2$O/NaOD); δ$_P$ 1.05. **HRMS** (ESI); calc'd for C$_{19}$H$_{24}$N$_2$O$_8$PS [M−H]$^-$: m/z 471.0991, found 471.1025.

*4.2.12 Aminoferrocene **111***
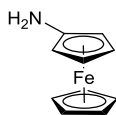
2-(Trimethylsilyl)ethyl ferrocenylcarbamate **151** (1.04 g, 3 mmol, 1 eq.) was dissolved in a 1M TBAF in THF solution (12 mL, 12 mmol, 4 eq.) and heated to 50 °C for 2 hours. After allowing to cool to room temperature, the reaction mixture was concentrated and the residue was quenched with water (20 mL). The aqueous layer was then extracted three times with CH_2Cl_2 (20 mL). The combined organics were then dried over $MgSO_4$ and concentrated *in vacuo* to afford the crude product. Purification by silica gel column chromatography (hexane 8:2 EtOAc, R_f = 0.20) gave the title compound as an orange crystalline solid (0.51 g, 85%). **MP**: 151–153 °C decomp. (lit.[423] 155 °C decomp.). **^{1}H NMR** (300 MHz, C_6D_6); δ_H 3.98 (5H, s, Fc*H*), 3.73 (2H, s, Fc*H*), 3.69 (2H, s, Fc*H*), 1.86 (2H, br s, NH$_2$). **^{13}C NMR** (75.5 MHz, C_6D_6); δ_C 106.7 (Fc*C*), 69.1 (Fc*C*), 63.5 (Fc*C*), 58.3 (Fc*C*). **E_{ox}** (1 mM, pH 9 Tris buffer): −130 mV *vs.* Ag/AgCl. NMR data in accordance with literature precedent.[383]

4.2.13 Ferrocenemethanol **170**
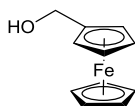
Dichloro(pentamethylcyclopentadienyl)iridium(III) dimer (0.4 mg, 0.5 μmol, 0.005 mol%) and *N*-(2-aminoethyl)-4-methylbenzenesulfonamide **171** (0.2 mg, 1 μmol, 0.01 mol%) were suspended in degassed and distilled water (0.6 mL) and heated to 80 °C. The reaction mixture was allowed to stir for 1 hour before being cooled to room temperature. Sodium formate (340 mg, 5 mmol, 5 eq.) and ferrocenecarboxaldehyde (214 mg, 1 mmol, 1 eq.) were then added and heated to 80 °C. The reaction mixture was allowed to stir for 1 hour before being cooled to room temperature. The reaction mixture was then diluted with water (6 mL) and extracted three times with Et$_2$O (6 mL). The combined organics were then dried over MgSO$_4$ and concentrated *in vacuo* to afford the crude product. Purification by silica gel column chromatography (CHCl$_3$, R$_f$ = 0.22) gave the title compound as a crystalline yellow solid (153 mg, 71%). **MP**: 76–78 °C (lit.[424] 77 °C). **¹H NMR** (300 MHz, C$_6$D$_6$); δ$_H$ 4.17 (2H, d, *J* = 5.5 Hz, C*H*$_2$), 4.05 (2H, t, *J* = 1.7 Hz, Fc*H*), 3.94–3.92 (7H, m, Fc*H*), 1.36 (1H, br t, *J* = 5.5 Hz, O*H*). **¹³C NMR** (75.5 MHz, C$_6$D$_6$); δ$_C$ 89.5 (Fc*C*), 69.0 (Fc*C*), 68.7 (Fc*C*), 68.5 (Fc*C*), 61.1 (*C*H$_2$). **E$_{ox}$** (1 mM, pH 9 Tris buffer): −170 mV *vs.* Ag/AgCl. **E$_{ox}$** (1 mM, pH 9.8 CO$_3$$^{2-}$ buffer): −5 mV *vs.* Ag/AgCl. NMR data in accordance with literature precedent.[425]

4.2.14 N-(2-Aminoethyl)-4-methylbenzenesulfonamide 171
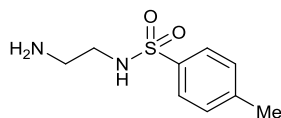
4-Methylbenzenesulfonyl chloride (1.77 g, 10 mmol) was reacted according to general procedure C to afford the crude product. Purification by silica gel column chromatography (CH$_2$Cl$_2$ 9:1 MeOH + 1% TEA, R$_f$ = 0.10) gave the title compound as a white solid (1.06 g, 49%). **MP**: 121–122 °C (lit.[426] 122–123 °C). **^{1}H NMR** (300 MHz, d_6-DMSO); δ$_H$ 7.66 (2H, d, J = 8.2 Hz, ArH), 7.37 (2H, d, J = 8.2 Hz, ArH), 3.37 (2H, br s, NH_2), 2.68 (2H, br t, J = 6.5 Hz, CH_2NH), 2.49 (2H, br t, J = 6.5 Hz, CH_2NH$_2$), 2.36 (3H, s, CH_3). **^{13}C NMR** (75.5 MHz, d_6-DMSO); δ$_C$ 142.8 (ArC), 138.1 (ArC), 130.0 (ArC), 126.9 (ArC), 46.6 (CH$_2$NH), 41.7 (CH$_2$NH$_2$), 21.3 (ArCH$_3$). NMR data in accordance with literature precedent.[419]

4.2.15 N-(2-Aminoethyl)benzenesulfonamide 173
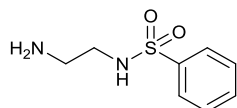
Benzenesulfonyl chloride (1.28 mL, 10 mmol) was reacted according to general procedure C to afford the crude product. Purification by silica gel column chromatography (CH$_2$Cl$_2$ 9:1 MeOH + 1% TEA, R$_f$ = 0.10) gave the title compound as a beige solid (0.49 g, 25%). **MP**: 50–56 °C (lit.[419] 67–69 °C). **^{1}H NMR** (300 MHz, d_6-DMSO); δ$_H$ 7.79 (2H, m, ArH), 7.59 (3H, m, ArH), 3.90 (2H, br s, NH_2), 2.73 (2H, br t, J = 6.4 Hz, CH_2NH), 2.52 (2H, m, CH_2NH$_2$). **^{13}C NMR** (75.5 MHz, d_6-DMSO); δ$_C$ 140.6 (ArC), 132.3 (ArC), 129.2 (ArC), 126.4 (ArC), 46.0 (CH$_2$NH), 41.3 (CH$_2$NH$_2$). NMR data in accordance with literature precedent.[419]

4.2.16 N-(2-Aminoethyl)-4-(tert-butyl)benzenesulfonamide 174

4-(*tert*-Butyl)benzenesulfonyl chloride (2.33 g, 10 mmol) was reacted according to general procedure C to afford the crude product. Purification by silica gel column chromatography (CH$_2$Cl$_2$ 9:1 MeOH + 1% TEA, R$_f$ = 0.10) gave the title compound as a white solid (1.87 g, 77%). **MP**: 117–119 °C (lit.[419] 79–81 °C). **^{1}H NMR** (300 MHz, d_6-DMSO); δ$_H$ 7.70 (2H, d, J = 8.7 Hz, ArH), 7.59 (2H, d, J = 8.7 Hz, ArH), 3.36 (2H, br s, NH_2), 2.69 (2H, br t, J = 6.4 Hz, CH_2NH), 2.50 (2H, m, CH_2NH$_2$), 1.29 (9H, s, CH_3). **^{13}C NMR** (75.5 MHz, d_6-DMSO); δ$_C$ 155.2 (ArC), 137.7 (ArC), 126.3 (ArC), 126.0 (ArC), 46.2 (CH$_2$NH), 41.4 (CH$_2$NH$_2$), 34.8 (C(CH$_3$)$_3$), 30.8 (C(CH$_3$)$_3$). NMR data in accordance with literature precedent.[419]

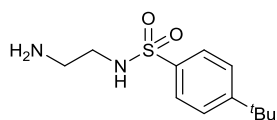### 4.2.17 N-(2-Aminoethyl)-2,4,6-trimethylbenzenesulfonamide 175

2,4,6-Trimethylbenzenesulfonyl chloride (2.19 g, 10 mmol) was reacted according to general procedure C to afford the crude product. Purification by silica gel column chromatography (CH_2Cl_2 9:1 MeOH + 1% TEA, R_f = 0.10) gave the title compound as a white solid (1.87 g, 77%). **MP**: 96–99 °C (lit.[427] 90 °C). **^{1}H NMR** (300 MHz, d_6-DMSO); δ_H 7.01 (2H, s, Ar*H*), 3.31 (2H, br s, N*H$_2$*), 2.68 (2H, br t, *J* = 6.5 Hz, C*H$_2$*NH), 2.54 (6H, s, ArC*H$_3$*), 2.47 (2H, br t, *J* = 6.5 Hz, C*H$_2$*NH$_2$), 2.24 (3H, s, ArC*H$_3$*). **^{13}C NMR** (75.5 MHz, d_6-DMSO); δ_C 141.6 (Ar*C*), 138.6 (Ar*C*), 134.9 (Ar*C*), 132.0 (Ar*C*), 45.7 (*C*H$_2$NH), 41.6 (*C*H$_2$NH$_2$), 22.9 (Ar*C*H$_3$), 20.7 (Ar*C*H$_3$). NMR data in accordance with literature precedent.[419]

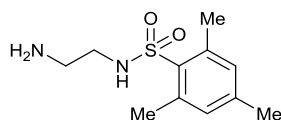### 4.2.18 N-(2-Aminoethyl)-2,4,6-triisopropylbenzenesulfonamide 176

2,4,6-Triisopropylbenzenesulfonyl chloride (3.03 g, 10 mmol) was reacted according to general procedure C to afford the crude product. Purification by silica gel column chromatography (CH_2Cl_2 9:1 MeOH + 1% TEA, R_f = 0.10) gave the title compound as a white solid (2.52 g, 77%). **MP**: 124–126 °C (lit.[419] 120–122 °C). **^{1}H NMR** (300 MHz, d_6-DMSO); δ_H 7.21 (2H, s, Ar*H*), 4.13 (2H, sept, *J* = 6.7 Hz, C*H*(CH$_3$)$_2$), 3.39 (2H, br s, N*H$_2$*), 2.89 (1H, sept, *J* = 6.9 Hz, C*H*(CH$_3$)$_2$), 2.78 (2H, br t, *J* = 6.4 Hz, C*H$_2$*NH), 2.53 (2H, br t, *J* = 6.4 Hz, C*H$_2$*NH$_2$), 2.49 (1H, br t, *J* = 1.8 Hz, N*H*), 1.20–1.17 (18H, m, CH(C*H$_3$*)$_2$). **^{13}C NMR** (75.5 MHz, d_6-DMSO); δ_C 152.2 (Ar*C*), 149.9 (Ar*C*), 133.6 (Ar*C*), 123.8 (Ar*C*), 45.7 (*C*H$_2$NH), 41.7 (*C*H$_2$NH$_2$), 33.7 (*C*H(CH$_3$)$_2$), 29.1 (*C*H(CH$_3$)$_2$), 25.1 (CH(*C*H$_3$)$_2$), 23.8 (CH(*C*H$_3$)$_2$). NMR data in accordance with literature precedent.[419]
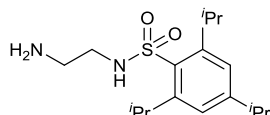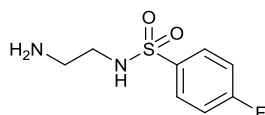
4.2.19 N-(2-Aminoethyl)-4-fluorobenzenesulfonamide 177

4-Fluorobenzenesulfonyl chloride (2.45 g, 10 mmol) was reacted according to general procedure C to afford the crude product. Purification by silica gel column chromatography (CH_2Cl_2 9:1 MeOH + 1% TEA, R_f = 0.10) gave the title compound as a white solid (0.46 g, 21%). **MP**: 81–85 °C. **IR** (solid, cm^{-1}); ν 3349 (N–H), 3298 (N–H), 3068 (C–H), 2951 (C–H), 2897 (C–H), 2854 (C–H), 2591 (N–H), 1658 (N–H), 1590 (N–H), 1512 (N–H), 1490 (N–H), 1315 (SO$_2$–N), 1286 (C–F), 1155 (SO$_2$–N), 1063 (S=O). **^{1}H NMR** (400 MHz, d_6-DMSO); δ_H 7.86 (2H, m, Ar*H*), 7.43 (2H, m, Ar*H*), 3.50 (2H, br s, N*H$_2$*), 2.73 (2H, br t, *J* = 6.4 Hz, C*H$_2$*NH),

2.52 (2H, m, CH_2NH$_2$). ^{13}**C NMR** (101 MHz, d_6-DMSO); δ$_C$ 164.1 (d, $^1J_{C-F}$ = 251 Hz, ArC), 137.0 (d, $^4J_{C-F}$ = 3 Hz, ArC), 129.5 (d, $^3J_{C-F}$ = 9 Hz, ArC), 116.3 (d, $^2J_{C-F}$ = 23 Hz, ArC), 46.2 (CH$_2$NH), 41.3 (CH$_2$NH$_2$). ^{19}**F NMR** (376.5 MHz, d_6-DMSO); δ$_F$ −107.2. **HRMS** (ESI); calc'd for C$_8$H$_{12}$ FN$_2$O$_2$S [M+H]$^+$: m/z 219.0598, found 219.0547.

4.2.20 N-(2-Aminoethyl)-4-bromobenzenesulfonamide **178**

4-Bromobenzenesulfonyl chloride (2.56 g, 10 mmol) was reacted according to general procedure C to afford the crude product. Purification by silica gel column chromatography (CH$_2$Cl$_2$ 9:1 MeOH + 1% TEA, R$_f$ = 0.10) gave the title compound as a white solid (1.84 g, 66%). **MP**: 127–128 °C (lit.[428] 124–126 °C). **IR** (solid, cm^{-1}); ν 3350 (N–H), 3299 (N–H), 3056 (C–H), 2951 (C–H), 2861 (C–H), 2582 (N–H), 1591 (N–H), 1574 (N–H), 1491 (N–H), 1316 (SO$_2$–N), 1145 (SO$_2$–N), 1065 (S=O), 662 (C–Br). ^{1}**H NMR** (300 MHz, d_6-DMSO); δ$_H$ 7.81 (2H, d, J = 8.7 Hz, ArH), 7.72 (2H, d, J = 8.7 Hz, ArH), 3.48 (2H, br s, NH_2), 2.73 (2H, br t, J = 6.5 Hz, CH_2NH), 2.50 (2H, m, CH_2NH$_2$). ^{13}**C NMR** (75.5 MHz, d_6-DMSO); δ$_C$ 139.9 (ArC), 132.3 (ArC), 128.5 (ArC), 126.1 (ArC), 46.2 (CH$_2$NH), 41.3 (CH$_2$NH$_2$). **HRMS** (ESI); calc'd for C$_8$H$_{12}$BrN$_2$O$_2$S [M+H]$^+$: m/z 278.9797, found 278.9715.

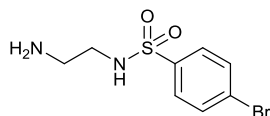## 4.2.21 N-(2-Aminoethyl)-4-methoxybenzenesulfonamide **179**
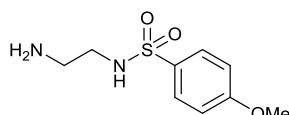
4-Methoxybenzenesulfonyl chloride (2.07 g, 10 mmol) was reacted according to general procedure C to afford the crude product. Purification by silica gel column chromatography (CH$_2$Cl$_2$ 9:1 MeOH + 1% TEA, R$_f$ = 0.10) gave the title compound as a white crystalline solid (0.84 g, 37%). **MP**: 95–97 °C (lit.[429] 90–91 °C). **IR** (solid, cm^{-1}); ν 3367 (N–H), 3307 (N–H), 3056 (C–H), 2944 (C–H), 2839 (C–H), 2603 (N–H), 1595 (N–H), 1577 (N–H), 1495 (N–H), 1319 (SO$_2$–N), 1143 (SO$_2$–N), 1092 (C–O). ^{1}**H NMR** (300 MHz, d_6-DMSO); δ$_H$ 7.71 (2H, d, J = 8.9 Hz, ArH), 7.09 (2H, d, J = 8.9 Hz, ArH), 3.82 (3H, s, OCH_3), 3.36 (2H, br s, NH_2), 2.67 (2H, br t, J = 6.5 Hz, CH_2NH), 2.49 (2H, t, J = 6.5 Hz, CH_2NH$_2$). ^{13}**C NMR** (75.5 MHz, d_6-DMSO); δ$_C$ 162.4 (ArC), 132.6 (ArC), 129.0 (ArC), 114.6 (ArC), 56.0 (OCH$_3$), 46.5 (CH$_2$NH), 41.7 (CH$_2$NH$_2$). **HRMS** (ESI); calc'd for C$_9$H$_{14}$N$_2$O$_3$S [M+H]$^+$: m/z 231.0803, found 231.0785.

4.2.22 N-(2-Aminoethyl)-4-nitrobenzenesulfonamide 180
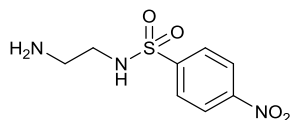
4-Nitrobenzenesulfonyl chloride (2.22 g, 10 mmol) was reacted according to general procedure C to afford the crude product. Purification by silica gel column chromatography (CH$_2$Cl$_2$ 9:1 MeOH + 1% TEA, R$_f$ = 0.10) gave the title compound as a pale-yellow crystalline solid (0.71 g, 29%). **MP**: 147–150 °C (lit.[430] 149–150 °C). **IR** (solid, cm^{-1}); ν 3362 (N–H), 3274 (N–H), 3111 (C–H), 2931 (C–H), 2868 (C–H), 1602 (N–H), 1528 (NO$_2$), 1469 (N–H), 1349 (NO$_2$), 1297 (SO$_2$–N), 1154 (SO$_2$–N), 1055 (S=O). **^{1}H NMR** (300 MHz, d_6-DMSO); δ$_H$ 8.40 (2H, d, J = 8.9 Hz, ArH), 8.03 (2H, d, J = 8.9 Hz, ArH), 3.67 (2H, br s, NH_2), 2.78 (2H, br t, J = 6.5 Hz, CH_2NH), 2.51 (2H, t, J = 6.5 Hz, CH_2NH$_2$). **^{13}C NMR** (75.5 MHz, d_6-DMSO); δ$_C$ 149.9 (ArC), 146.7 (ArC), 128.4 (ArC), 124.9 (ArC), 46.4 (CH$_2$NH), 41.7 (CH$_2$NH$_2$). **HRMS** (ESI); calc'd for C$_8$H$_{12}$N$_3$O$_4$S [M+H]$^+$: m/z 246.0543, found 246.0482.

4.2.23 N-(2-Aminoethyl)-4-(trifluoromethyl)-benzenesulfonamide 181
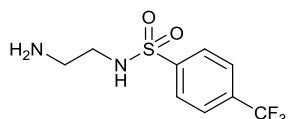
4-(Trifluoromethyl)benzenesulfonyl chloride (2.45 g, 10 mmol) was reacted according to general procedure C to afford the crude product. Purification by silica gel column chromatography (CH$_2$Cl$_2$ 9:1 MeOH + 1% TEA, R$_f$ = 0.10) gave the title compound as a white crystalline solid (1.58 g, 59%). **MP**: 112–114 °C (lit.[419] 103–105 °C). **^{1}H NMR** (400 MHz, d_6-DMSO); δ$_H$ 8.03–8.00 (4H, m, ArH), 3.59 (2H, br s, NH_2), 2.77 (2H, br t, J = 6.0 Hz, CH_2NH), 2.53 (2H, br t, J = 6.0 Hz, CH_2NH$_2$). **^{13}C NMR** (101 MHz, d_6-DMSO); δ$_C$ 145.1 (ArC), 132.6 (q, $^2J_{C–F}$ = 32 Hz, ArC), 127.9 (ArC), 126.9 (q, $^3J_{C–F}$ = 4 Hz, ArC), 124.0 (q, $^1J_{C–F}$ = 273 Hz, ArC), 46.6 (CH$_2$NH), 41.8 (CH$_2$NH$_2$). **^{19}F NMR** (376.5 MHz, d_6-DMSO); δ$_F$ −61.6. NMR data in accordance with literature precedent.[419]

4.2.24 2,4,6-Trimethyl-N-(2-(methylamino)ethyl)benzenesulfonamide 184


N-Methylethylenediamine (1.0 mL, 11.5 mmol) and mesitylsulfonyl chloride (838 mg, 3.8 mmol) were reacted together according to general procedure D to afford the crude product. Purification by silica gel column chromatography (CHCl$_3$ 9:1 MeOH + 1% TEA, R$_f$ = 0.10) gave the title compound as a pale-yellow amorphous solid (180 mg, 18%). **IR** (film, cm^{-1}); ν 3318 (N–H), 2975 (N–H), 2935 (C–H), 2846 (C–H), 1603 (N–H), 1563 (N–H), 1310 (SO$_2$–N), 1146 (SO$_2$–N). **^{1}H NMR** (300 MHz, CDCl$_3$); δ$_H$ 6.92 (2H, s, Ar*H*), 3.95 (2H, br s, N*H$_2$*), 2.94–2.91 (2H, m, C*H$_2$*NHSO$_2$), 2.69–2.65 (2H, m, C*H$_2$*NHCH$_3$), 2.61 (6H, s, ArC*H$_3$*), 2.31 (3H, s, NHC*H$_3$*), 2.26 (3H, s, ArC*H$_3$*). **^{13}C NMR** (75.5 MHz, CDCl$_3$); δ$_C$ 142.1 (Ar*C*), 139.1 (Ar*C*), 133.5 (Ar*C*), 131.9 (Ar*C*), 49.8 (*C*H$_2$NHSO$_2$), 41.1 (*C*H$_2$NHCH$_3$), 35.4 (N*C*H$_3$), 22.9 (Ar*C*H$_3$), 20.9 (Ar*C*H$_3$). **HRMS** (ESI); calc'd for C$_{12}$H$_{21}$N$_2$O$_2$S [M+H]$^+$: *m/z* 257.1324, found 257.1357.

4.2.25 N-(2-Aminomethyl)-N,2,4,6-tetramethylbenzenesulfonamide 185
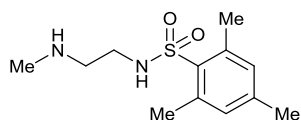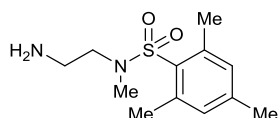

N-Methylethylenediamine (1.0 mL, 11.5 mmol) and mesitylsulfonyl chloride (838 mg, 3.8 mmol) were reacted together according to general procedure D to afford the crude product. Purification by silica gel column chromatography (CHCl$_3$ 9:1 MeOH + 1% TEA, R$_f$ = 0.05) gave the title compound as a dark-yellow amorphous solid (550 mg, 56%). **IR** (film, cm^{-1}); ν 3357 (N–H), 2975 (N–H), 2935 (C–H), 1603 (N–H), 1563 (N–H), 1309 (SO$_2$–N), 1143 (SO$_2$–N). **^{1}H NMR** (300 MHz, CDCl$_3$); δ$_H$ 6.84 (2H, s, Ar*H*), 3.11 (2H, t, *J* = 6.2 Hz, C*H$_2$*NSO$_2$), 2.74 (2H, t, *J* = 6.2 Hz, C*H$_2$*NH$_2$), 2.62 (3H, s, NC*H$_3$*), 2.50 (6H, s, ArC*H$_3$*), 2.19 (3H, s, ArC*H$_3$*), 1.27 (2H, br s, N*H$_2$*). **^{13}C NMR** (75.5 MHz, CDCl$_3$); δ$_C$ 142.3 (Ar*C*), 140.0 (Ar*C*), 132.1 (Ar*C*), 131.8 (Ar*C*), 51.9 (*C*H$_2$NSO$_2$), 39.3 (*C*H$_2$NH$_2$), 32.9 (N*C*H$_3$), 22.6 (Ar*C*H$_3$), 20.7 (Ar*C*H$_3$). **HRMS** (ESI); calc'd for C$_{12}$H$_{21}$N$_2$O$_2$S [M+H]$^+$: *m/z* 257.1324, found 257.1363.

4.2.26 N,2,4,6-Tetramethyl-N-(2-(methylamino)ethyl)benzenesulfonamide **187**
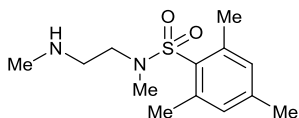
N,N'-Dimethylethylenediamine (1.1 mL, 10 mmol) was reacted according to general procedure E to afford the crude product. Purification by silica gel column chromatography (CH$_2$Cl$_2$ 9:1 MeOH + 1% TEA, R$_f$ = 0.10) gave the title compound as a yellow oil (201 mg, 7%). **IR** (film, cm^{-1}); ν 2937 (C–H), 1603 (N–H), 1564 (N–H), 1312 (SO$_2$–N), 1148 (SO$_2$–N). **^{1}H NMR** (300 MHz, CDCl$_3$); δ_H 6.90 (2H, s, Ar*H*), 3.22 (2H, t, *J* = 6.4 Hz, C*H*$_2$NSO$_2$), 2.74–2.69 (5H, m, C*H*$_2$NH + C*H*$_3$NSO$_2$), 2.56 (6H, s, ArC*H*$_3$), 2.32 (3H, s, C*H*$_3$NH), 2.25 (3H, s, ArC*H*$_3$), 1.56 (1H, br s, N*H*). **^{13}C NMR** (75.5 MHz, CDCl$_3$); δ_C 142.5 (Ar*C*), 140.3 (Ar*C*), 132.1 (Ar*C*), 132.0 (Ar*C*), 48.9 (*C*H$_2$NSO$_2$), 48.2 (*C*H$_2$NH), 36.0 (*C*H$_3$NSO$_2$), 33.3 (*C*H$_3$NH), 22.8 (Ar*C*H$_3$), 20.9 (Ar*C*H$_3$). **HRMS** (ESI); calc'd for C$_{13}$H$_{23}$N$_2$O$_2$S [M+H]$^+$: *m/z* 271.1480, found 271.1517.

4.2.27 N-(Dimethylamino)ethyl)-2,4,6-trimethylbenzenesulfonamide **189**
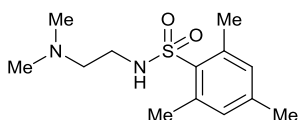
N,N-Dimethylethylenediamine (1.1 mL, 10 mmol) was reacted according to general procedure E to afford the crude product. Purification by silica gel column chromatography (CH$_2$Cl$_2$ 9:1 MeOH + 1% TEA, R$_f$ = 0.10) gave the title compound as pale-yellow oil (2.20 g, 81%). **IR** (film, cm^{-1}); ν 3303 (N–H), 2943 (C–H), 2862 (C–H), 2824 (C–H), 2775 (C–H), 1604 (N–H), 1564 (N–H), 1319 (SO$_2$–N), 1152 (SO$_2$–N). **^{1}H NMR** (300 MHz, CDCl$_3$); δ_H 6.95 (2H, s, Ar*H*), 5.45 (1H, br s, N*H*), 2.95–2.91 (2H, m, C*H*$_2$NH), 2.64 (6H, s, ArC*H*$_3$), 2.39–2.35 (2H, m, C*H*$_2$N(CH$_3$)$_2$), 2.29 (3H, s, ArC*H*$_3$), 2.15 (6H, s, N(C*H*$_3$)$_2$). **^{13}C NMR** (75.5 MHz, CDCl$_3$); δ_C 142.1 (Ar*C*), 139.2 (Ar*C*), 133.5 (Ar*C*), 131.9 (Ar*C*), 57.0 (*C*H$_2$N(CH$_3$)$_2$), 44.7 (CH$_2$N(*C*H$_3$)$_2$), 39.4 (*C*H$_2$NH), 22.8 (Ar*C*H$_3$), 20.9 (Ar*C*H$_3$). **HRMS** (ESI); calc'd for C$_{13}$H$_{23}$N$_2$O$_2$S [M+H]$^+$: *m/z* 271.1480, found 271.1504.

4.2.28 tert-Butyl (2-((2,4,6-Trimethylphenyl)sulfonamido)ethyl)carbamate 193
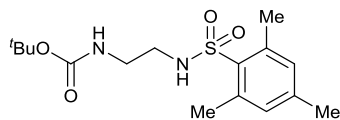
To a stirring solution of ethylenediamine (0.67 mL, 10 mmol, 5 eq.) in chloroform (50 mL) at 0 °C was added di-*tert*-butyl dicarbonate (436 mg, 2 mmol, 1 eq.) in chloroform (50 mL) dropwise. After complete addition, the reaction mixture was allowed to warm to room temperature and left to stir for 16 hours. The reaction was then quenched with $NaHCO_{3\ (sat.)}$ (50 mL) and the organics separated. The organics were then washed with brine before being dried over Na_2SO_4 and concentrated *in vacuo*. The residue was then taken up in anhydrous CH_2Cl_2 (10 mL) and cooled to 0 °C. A solution of 2,4,6-trimethylbenzenesulfonyl chloride (437 mg, 2 mmol, 1 eq.) in anhydrous CH_2Cl_2 (50 mL) was then added dropwise. After complete addition, the reaction mixture was then quenched with water (50 mL) and the organics separated. The aqueous layer was then extracted twice with CH_2Cl_2 (50 mL). The combined organics were then washed with water (50 mL), dried over Na_2SO_4 and concentrated *in vacuo* to afford the crude product. Purification by silica gel column chromatography (hexane 8:2 EtOAc, R_f = 0.20) gave the title compound as a white solid (137 mg, 20%). **MP**: 86–88 °C (lit.[431] 91–94 °C). **¹H NMR** (300 MHz, CDCl₃); δ_H 6.92 (2H, s, Ar*H*), 5.57 (1H, br s, N*H*SO₂), 5.04 (1H, br s, N*H*CO₂), 3.20–3.19 (2H, m, C*H₂*NHSO₂), 3.00–2.94 (2H, m, C*H₂*NHCO₂), 2.60 (6H, s, ArC*H₃*), 2.27 (3H, s, ArC*H₃*), 1.39 (9H, s, C(C*H₃*)₃). **¹³C NMR** (75.5 MHz, CDCl₃); δ_C 156.5 (*C*=O), 142.2 (Ar*C*), 139.1 (Ar*C*), 133.5 (Ar*C*), 132.0 (Ar*C*), 79.7 (*C*(CH₃)₃), 43.0 (*C*H₂NHSO₂), 40.3 (*C*H₂NHCO₂), 28.3 (C(*C*H₃)₃), 22.9 (Ar*C*H₃), 20.9 (Ar*C*H₃). NMR data in accordance with literature precedent.[431]

4.2.29 Benzyl (2-((2,4,6-Trimethylphenyl)sulfonamido)ethyl)carbamate 196
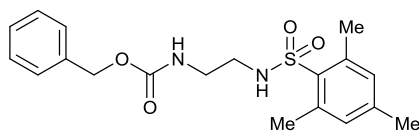
Benzyl alcohol (0.52 mL, 5 mmol), 1,1'-carbonyldiimidazole (1.05 g, 6.5 mmol) and *N*-(2-aminoethyl)-2,4,6-trimethylbenzenesulfonamide **175** (1.21 g, 5 mmol) were reacted together according to general procedure F to afford the crude product. Purification by silica gel column chromatography (hexane 7:3 EtOAc, R_f = 0.35) gave the title compound as a white solid (0.95 g, 50%). **MP**: 125–126 °C. **IR** (solid, cm^{-1}); ν 3435 (N–H), 3200 (N–H), 2956 (C–H), 1680 (C=O), 1604 (N–H), 1311 (SO$_2$–N), 1149 (SO$_2$–N), 1094 (C–O), 1046 (S=O). ^{1}**H NMR** (300 MHz, CDCl$_3$); δ_H 7.34–7.29 (5H, m, Ar*H*), 6.92 (2H, s, Ar*H*), 5.47 (1H, br s, N*H*SO$_2$), 5.34 (1H, br s, N*H*CO$_2$), 5.05 (2H, s, ArC*H$_2$*), 3.30–3.24 (2H, m, C*H$_2$*NHSO$_2$), 3.01–2.99 (2H, m, C*H$_2$*NHCO$_2$), 2.60 (6H, s, ArC*H$_3$*), 2.28 (3H, s, ArC*H$_3$*). ^{13}**C NMR** (75.5 MHz, CDCl$_3$); δ_C 157.0 (*C*=O), 142.4 (Ar*C*), 139.1 (Ar*C*), 136.4 (Ar*C*), 133.4 (Ar*C*), 132.1 (Ar*C*), 128.6 (Ar*C*), 128.2 (Ar*C*), 128.1 (Ar*C*), 66.9 (Ar*C*H$_2$), 42.7 (*C*H$_2$NHSO$_2$), 40.8 (*C*H$_2$NHCO$_2$), 23.0 (Ar*C*H$_3$), 21.0 (Ar*C*H$_3$). **HRMS** (ESI); calc'd for C$_{19}$H$_{24}$N$_2$O$_4$SNa [M+Na]$^+$: *m/z* 399.1354, found 399.1322.

4.2.30 4-Methoxybenzyl (2-((2,4,6-Trimethylphenyl)sulfonamido)ethyl)carbamate 197
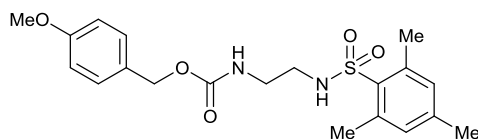
4-Methoxybenzyl alcohol (0.12 mL, 1 mmol), 1,1'-carbonyldiimidazole (221 mg, 1.3 mmol) and *N*-(2-aminoethyl)-2,4,6-trimethylbenzenesulfonamide **175** (242 mg, 1 mmol) were reacted together according to general procedure F to afford the crude product. Purification by silica gel column chromatography (hexane 1:1 EtOAc, R_f = 0.55) gave the title compound as a white crystalline solid (283 mg, 72%). **MP**: 78–79 °C. **IR** (solid, cm^{-1}); ν 3328 (N–H), 2939 (C–H), 1682 (C=O), 1616 (N–H), 1329 (SO$_2$–N), 1157 (SO$_2$–N), 1077 (C–O), 1027 (S=O). ^{1}**H NMR** (300 MHz, CDCl$_3$); δ_H 7.27 (2H, d, *J* = 8.6 Hz, Ar*H*), 6.93 (2H, d, *J* = 8.6 Hz, Ar*H*), 5.21 (1H, br t, *J* = 5.4 Hz, N*H*SO$_2$), 5.10 (1H, br t, *J* = 5.7 Hz, N*H*CO$_2$), 5.00 (2H, s, ArC*H$_2$*), 3.80 (3H, s, OC*H$_3$*), 3.29–3.24 (2H, m, C*H$_2$*NHSO$_2$), 3.04–2.98 (2H, m, C*H$_2$*NHCO$_2$), 2.60 (6H, s, ArC*H$_3$*), 2.29 (3H, s, ArC*H$_3$*). ^{13}**C NMR** (75.5 MHz, CDCl$_3$); δ_C 159.7 (*C*=O), 157.1 (Ar*C*), 142.4 (Ar*C*), 139.2 (Ar*C*), 133.5 (Ar*C*), 132.2 (Ar*C*), 130.1 (Ar*C*), 128.4 (Ar*C*), 114.0 (Ar*C*), 66.9 (Ar*C*H$_2$), 55.4 (O*C*H$_3$), 42.9 (*C*H$_2$NHSO$_2$), 40.9 (*C*H$_2$NHCO$_2$), 23.0 (Ar*C*H$_3$), 21.1 (Ar*C*H$_3$). **HRMS** (ESI); calc'd for C$_{20}$H$_{26}$N$_2$O$_5$SNa [M+Na]$^+$: *m/z* 429.1460, found 429.1455.

4.2.31 4-((Bis(allyloxy)phosphoryl)oxy)benzyl (2-((2,4,6-Trimethylphenyl)sulfonamido)ethyl)carbamate 201
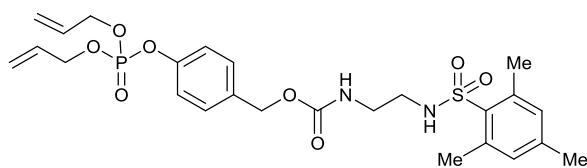
Diallyl (4-(hydroxymethyl)phenyl) phosphate **149** (1.86 g, 6.5 mmol), 1,1'-carbonyldiimidazole (1.36 g, 8.4 mmol) and *N*-(2-aminoethyl)-2,4,6-trimethylbenzenesulfonamide **175** (2.71 g, 8.4 mmol) were reacted together according to general procedure F to afford the crude product. Purification by silica gel column chromatography (hexane 1:1 EtOAc, R_f = 0.10) gave the title compound as a colourless oil (2.71 g, 76%). **IR** (film, cm^{-1}); ν 3299 (N–H), 2942 (C–H), 1707 (C=O), 1605 (N–H), 1324 (SO$_2$–N), 1255 (P=O), 1153 (SO$_2$–N), 1095 (C–O), 1015 (P–O), 989 (C=C–H). **^{1}H NMR** (300 MHz, CDCl$_3$); δ_H 7.23 (2H, d, *J* = 8.3 Hz, Ar*H*), 7.12 (2H, d, *J* = 8.3 Hz, Ar*H*), 6.87 (2H, s, Ar*H*), 5.88 (2H, app ddd, *J* = 22.6, 11.0, 5.6 Hz, C=C*H*), 5.78 (2H, br t, *J* = 5.8 Hz, CO$_2$N*H*), 5.32 (2H, ddd, *J* = 17.1, 2.9, 1.4 Hz, C=C*H*$_2$), 5.21 (2H, dd, *J* = 10.4, 1.4 Hz, C=C*H*$_2$), 4.95 (2H, s, ArC*H*$_2$), 4.59 (4H, ddd, *J* = 8.4, 5.7, 1.3 Hz, C*H*$_2$OP), 3.17 (2H, app q, *J* = 5.5 Hz, C*H*$_2$NHSO$_2$), 2.91 (2H, app q, *J* = 5.5 Hz, C*H*$_2$NHCO$_2$), 2.54 (6H, s, ArC*H*$_3$), 2.22 (3H, s, ArC*H*$_3$). **^{13}C NMR** (75.5 MHz, CDCl$_3$); δ_C 156.8 (*C*=O), 150.2 (d, $J_{C–P}$ = 7 Hz, Ar*C*), 142.1 (Ar*C*), 139.0 (Ar*C*), 133.6 (Ar*C*), 132.0 (Ar*C*), 132.0 (*C*HCH$_2$OP), 131.9 (Ar*C*), 129.6 (Ar*C*), 121.1 (d, $J_{C–P}$ = 5 Hz, Ar*C*), 118.8 (*C*=CH), 69.0 (d, $J_{C–P}$ = 5 Hz, *C*H$_2$OP), 65.9 (*C*H$_2$O$_2$C), 42.5 (*C*H$_2$NHSO$_2$), 40.7 (*C*H$_2$NHCO$_2$), 22.9 (Ar*C*H$_3$), 20.9 (Ar*C*H$_3$). **^{31}P NMR** (121.5 MHz, CDCl$_3$); δ_P −5.65. **HRMS** (ESI); calc'd for C$_{25}$H$_{33}$N$_2$O$_8$PS [M+H]$^+$: *m/z* 553.1773, found 553.1765.

4.2.32 Allyl (2-((2,4,6-Trimethylphenyl)sulfonamido)ethyl)carbamate 208
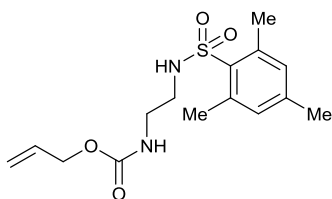
To a stirring solution of *N*-(2-aminoethyl)-2,4,6-trimethylbenzenesulfonamide **175** (2.42 g, 10 mmol, 1 eq.) in anhydrous THF (100 mL) at 0 °C was added allyl chloroformate (1.3 mL, 10 mmol, 1 eq.) dropwise, followed by anhydrous TEA (1.4 mL, 10 mmol, 1 eq.). The reaction mixture was allowed to warm to room temperature and left to stir for 16 hours before being concentrated *in vacuo*. The residue was then quenched with NaHCO$_3$ (sat.) (50 mL) and extracted three times with EtOAc (50 mL). The combined organics were then washed with water (50 mL), then brine (50 mL) before being dried over MgSO$_4$ and concentrated *in vacuo* to afford the crude product. Purification by silica gel column chromatography (hexane 1:1 EtOAc, R$_f$ = 0.50) gave the title compound as a white solid (2.61 g, 80%). **MP**: 82–83 °C. **IR** (solid, cm^{-1}); ν 3365 (N–H), 3287 (N–H), 2942 (C–H), 1699 (C=O), 1603 (N–H), 1323 (SO$_2$–N), 1152 (SO$_2$–N), 1072 (C–O), 1013 (S=O), 990 (C=C–H). **^{1}H NMR** (300 MHz, CDCl$_3$); δ$_H$ 6.92 (2H, s, Ar*H*), 5.85 (1H, ddt, *J* = 17.2, 10.5, 5.5 Hz, C=C*H*), 5.61 (1H, br t, *J* = 5.5 Hz, SO$_2$N*H*), 5.42 (1H, br s, CO$_2$N*H*), 5.25 (1H, dd, *J* = 17.2, 1.4 Hz, C=C*H$_2$*), 5.16 (1H, dd, *J* = 10.5, 1.4 Hz, C=C*H$_2$*), 4.49 (2H, d, *J* = 5.5 Hz, OC*H$_2$*), 3.26 (2H, app q, *J* = 5.7 Hz, SO$_2$NHC*H$_2$*), 3.00 (2H, app q, *J* = 5.7 Hz, CO$_2$NHC*H$_2$*), 2.59 (6H, s, ArC*H$_3$*), 2.27 (3H, s, ArC*H$_3$*). **^{13}C NMR** (75.5 MHz, CDCl$_3$); δ$_C$ 156.9 (*C*=O), 142.3 (Ar*C*), 139.1 (Ar*C*), 133.5 (Ar*C*), 132.7 (H$_2$*C*=C), 132.0 (Ar*C*), 117.7 (H$_2$*C*=C), 65.7 (O*C*H$_2$), 42.7 (SO$_2$NH*C*H$_2$), 40.7 (CO$_2$NH*C*H$_2$), 22.9 (*C*H$_3$), 20.9 (*C*H$_3$). **HRMS** (ESI); calc'd for C$_{15}$H$_{22}$N$_2$NaO$_4$S [M+Na]$^+$: *m/z* 349.1198, found 349.1211.

4.2.33 4-((Bis(allyloxy)phosphoryl)oxy)benzyl

(2(((Allyoxy)carbonyl)amino)ethyl)(mesitylsulfonyl)carbamate **207**
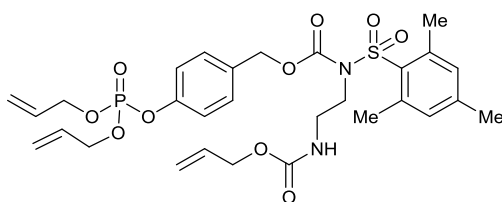
Diallyl (4-(hydroxymethyl)phenyl) phosphate **149** (182 mg, 0.64 mmol), phosgene solution (0.3 mL, 0.64 mmol), allyl (2-((2,4,6-trimethylphenyl)sulfonamido)ethyl)carbamate **208** (191 mg, 0.59 mmol), DIPEA (0.2 mL, 0.88 mmol) and DMAP (7 mg, 0.059 mmol) were all reacted together according to general procedure G to afford the crude product. Purification by silica gel column chromatography (hexane 1:1 EtOAc, R_f = 0.40) gave the title compound as an amorphous pale-yellow solid (114 mg, 31%). **IR** (film, cm^{-1}); ν 1719 (C=O), 1604 (N–H), 1346 (SO$_2$–N), 1221 (P=O), 1167 (SO$_2$–N), 1017 (P–O), 930 (C=C–H). **^{1}H NMR** (300 MHz, CDCl$_3$); δ$_H$ 7.08 (2H, d, J = 7.8 Hz, ArH), 6.96 (2H, d, J = 7.8 Hz, ArH), 6.83 (2H, s, ArH), 5.99–5.84 (3H, m, C=CH), 5.39–5.15 (7H, m, C=CH_2 + NH), 4.97 (2H, s, ArCH_2), 4.65–4.55 (6H, m, C=CHCH_2), 4.04 (2H, br s, CH_2), 3.49 (2H, br s, CH_2), 2.41 (6H, s, ArCH_3), 2.27 (3H, s, ArCH_3). **^{13}C NMR** (75.5 MHz, CDCl$_3$); δ$_C$ 156.4 (SO$_2$NC=O), 152.4 (NHC=O), 150.8 (d, $^2J_{C-P}$ = 7 Hz, PO$_4$ArC), 143.3 (SO$_2$ArC), 139.9 (ArC), 139.9 (ArC), 133.9 (ArC), 132.0 (H$_2$C=C), 131.9 (H$_2$C=C), 131.2 (ArC), 130.1 (ArC), 120.1 (d, $^3J_{C-P}$ = 5 Hz, ArC), 118.8 (H$_2$$C$=C), 117.4 (H$_2$$C$=C), 68.9 (d, $^2J_{C-P}$ = 5 Hz, PO$_4$$CH_2$), 68.3 (NHCO$_2$$CH_2$), 65.6 (Ar$CH_2$), 46.2 ($CH_2$), 40.5 ($CH_2$), 22.3 ($CH_3$), 21.0 ($CH_3$). **^{31}P {^{1}H} NMR** (121.5 MHz, CDCl$_3$); δ$_P$ −5.38. **HRMS** (ESI); calc'd for C$_{29}$H$_{38}$N$_2$O$_{10}$PS [M+H]$^+$: m/z 637.1985, found 637.1979.

4.2.34 4-((Bis(allyloxy)phosphoryl)oxy)benzyl   (2-((((4-((Bis(allyloxy)phosphoryl)oxy)carbonyl)

amino)ethyl)(mesitylsulfonyl)carbamate **210**
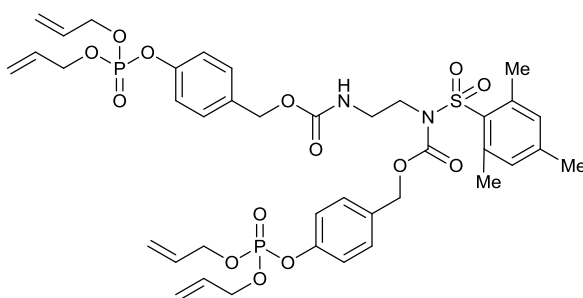
Diallyl (4-(hydroxymethyl)phenyl) phosphate **149** (313 mg, 1.1 mmol), phosgene solution (0.6 mL, 1.1 mmol), 4-((bis(allyloxy)phosphoryl)oxy)benzyl   (2-((2,4,6-trimethylphenyl)sulfonamido)ethyl) carbamate **201** (553 mg, 1 mmol), DIPEA (0.3 mL, 1.5 mmol) and DMAP (12 mg, 0.1 mmol) were all reacted together according to general procedure G to afford the crude product. Purification by silica gel column chromatography (hexane 1:1 EtOAc, R_f = 0.10) gave the title compound as a colourless oil (346 mg, 40%). **IR** (film, cm^{-1}); ν 1719 (C=O), 1346 (SO$_2$–N), 1218 (P=O). **^{1}H NMR** (300 MHz, CDCl$_3$); δ$_H$ 7.34 (2H, d, J = 8.3 Hz, ArH), 7.18 (2H, d, J = 8.3 Hz), 7.09 (2H, d, J = 8.3 Hz, ArH), 6.96 (2H, d, J = 8.3 Hz, ArH), 6.85 (2H, s, ArH), 5.93 (4H, dtd, J = 16.7, 10.7, 5.4 Hz, C=CH), 5.40–5.33 (4H, m, C=CH_2), 5.29–5.23 (5H, m,

C=CH_2 + NH), 5.08 (2H, s, ArCH_2), 4.97 (2H, s, ArCH_2), 4.66–4.60 (8H, m, C=CHCH_2), 4.06 (2H, t, J = 5.4 Hz, SO$_2$NCH_2), 3.52 (2H, app q, J = 5.4 Hz, NHCH_2), 2.42 (6H, s, ArCH_3), 2.29 (3H, s, ArCH_3). **^{13}C NMR** (75.5 MHz, CDCl$_3$); δ_C 156.6 (SO$_2$NC=O), 152.5 (NHC=O), 150.9 (d, J = 7 Hz, PO$_4$ArC), 150.4 (d, J = 7 Hz, PO$_4$ArC), 143.5 (SO$_2$ArC), 140.0 (ArC), 133.9 (ArC), 133.7 (ArC), 132.2 (H$_2$C=C), 132.1 (H$_2$C=C), 132.0 (ArC), 131.3 (ArC), 130.3 (ArC), 129.7 (ArC), 120.2 (d, $^3J_{C–P}$ = 5 Hz, ArC), 120.1 (d, $^3J_{C–P}$ = 5 Hz, ArC), 119.0 (H$_2$$C$=C), 118.8 (H$_2$$C$=C), 69.0 (d, $^2J_{C–P}$ = 6 Hz, PO$_4$$CH_2$), 69.0 (d, $^2J_{C–P}$ = 6 Hz, PO$_4$$CH_2$), 68.5 (Ar$CH_2$), 66.1 (Ar$CH_2$), 46.3 ($CH_2$), 40.6 ($CH_2$), 22.4 ($CH_3$), 21.1 ($CH_3$). **^{31}P {^{1}H} NMR** (121.5 MHz, CDCl$_3$); δ_P −5.35, −5.37. **HRMS** (ESI); calc'd for C$_{39}$H$_{49}$N$_2$O$_{14}$P$_2$S [M+H]$^+$: m/z 863.2380, found 863.2391.

4.2.35 4-(7-(Mesitylsulfonyl)-3,8-dioxo-10-(4-(phosphonatooxy)phenyl)-2,9-dioxa-4,7-diazadecyl) phenyl Phosphate 211
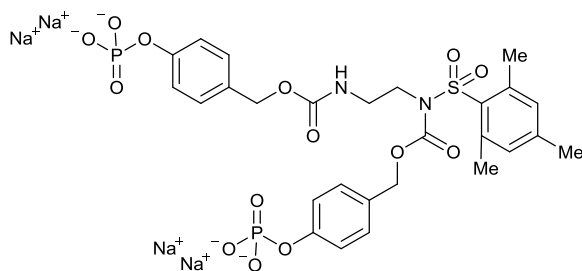
To a stirring solution of 4-((bis(allyloxy)phosphoryl)oxy)benzyl(2-((((4-((bis(allyloxy)phosphoryl)oxy) carbonyl)amino)ethyl)(mesitylsulfonyl)carbamate **210** (346 mg, 0.4 mmol, 1 eq.) in anhydrous THF (4 mL) at 0 °C was added polymer-bound Pd(PPh$_3$)$_4$ (57 mg, 0.04 mmol, 0.1 eq.) followed by formic acid (0.2 mL, 6 mmol, 15 eq.) then anhydrous TEA (0.6 mL, 4 mmol, 10 eq.). The reaction mixture was allowed to warm to room temperature and left to stir for 16 hours. The reaction was then filtered *via* gravity filtration and the filtrate concentrated *in vacuo*. The residue was then cooled to 0 °C and 1M NaHCO$_{3(aq.)}$ (5.6 mL, 5.6 mmol, 14 eq.) was added slowly. The reaction mixture was allowed to warm to room temperature and stirred for 1 hour before being concentrated *in vacuo* to afford the crude product. Purification by preparative reverse phase C18-silica gel column chromatography (water) gave the title compound as a white solid (316 mg, *quant.*). **MP**: 275–280 °C (decomp.). **IR** (solid, cm^{-1}); ν 1619 (C=O), 1425 (P=O). **^{1}H NMR** (300 MHz, CDCl$_3$); δ$_H$ 7.16 (2H, d, *J* = 8.3 Hz, Ar*H*), 7.03–7.00 (6H, m, Ar*H*), 6.57 (2H, s, Ar*H*, Ar*H*), 4.58 (2H, s, ArC*H*$_2$), 4.38 (2H, s, ArC*H*$_2$), 2.78 (2H, br s, SO$_2$NC*H*$_2$), 2.55 (2H, br s, O$_2$CNHC*H*$_2$), 2.32 (6H, s, ArC*H*$_3$), 1.84 (3H, s, ArC*H*$_3$). **^{13}C NMR** (75.5 MHz, CDCl$_3$); δ$_C$ 158.0 (C=O), 153.9 (d, $^2J_{C–P}$ = 6 Hz, PO$_4$Ar*C*), 153.3 (d, $^2J_{C–P}$ = 6 Hz, PO$_4$Ar*C*), 140.4 (Ar*C*), 138.4 (Ar*C*), 137.1 (Ar*C*), 135.4 (Ar*C*), 131.5 (Ar*C*), 130.5 (Ar*C*), 130.1 (Ar*C*), 129.3 (Ar*C*), 129.2 (Ar*C*), 120.7 (d, $^3J_{C–P}$ = 4 Hz, Ar*C*), 68.7 (ArC*H*$_2$), 63.8 (ArC*H*$_2$), 44.1 (NC*H*$_2$), 42.4 (N C*H*$_2$), 23.0 (C*H*$_3$), 20.3 (C*H*$_3$). **^{31}P {^{1}H} NMR** (121.5 MHz, CDCl$_3$); δ$_P$ 1.26, 1.15.

4.2.36 Naphthalen-1-ylmethanol 212
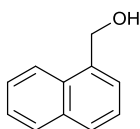
Dichloro(pentamethylcyclopentadienyl)iridium(III) dimer (1 mg, 0.00125 mmol), 4-((((2-((2,4,6-trimethylphenyl)sulfonamido)ethyl)carbamoyl)oxy) methyl)phenyl phosphate **198** (1.3 mg, 0.0025 mmol), sodium formate (170 mg, 2.5 mmol), alkaline phosphatase (2.5 mg, 10 Umg^{-1}) and 1-naphthaldehyde (68 μL, 0.5 mmol) were all reacted together according to general procedure H to afford the crude product. Purification by silica gel column chromatography (hexane 9:1 EtOAc) gave the title compound as a colourless oil. **^{1}H NMR** (300 MHz, CDCl$_3$); δ$_H$ 8.13–8.10 (1H, m, ArH), 7.91–7.88 (1H, m, ArH), 7.84–7.81 (1H, m, ArH), 7.59–7.42 (4H, m, ArH), 5.13 (2H, s, CH_2), 1.95 (1H, br s, OH). **^{13}C NMR** (75.5 MHz, CDCl$_3$); δ$_C$ 136.3 (ArC), 133.9 (ArC), 131.3 (ArC), 128.8 (ArC), 128.7 (ArC), 126.5 (ArC), 126.0 (ArC), 125.5 (ArC), 125.4 (ArC), 123.8 (ArC), 63.8 (CH_2). NMR data in accordance with literature precedent.[432]

4.2.37 Anthracen-9-ylmethanol 213
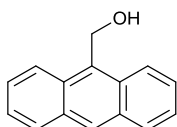
Dichloro(pentamethylcyclopentadienyl)iridium(III) dimer (1 mg, 0.00125 mmol), 4-((((2-((2,4,6-trimethylphenyl)sulfonamido)ethyl)carbamoyl)oxy) methyl)phenyl phosphate **198** (1.3 mg, 0.0025 mmol), sodium formate (170 mg, 2.5 mmol), alkaline phosphatase (2.5 mg, 10 Umg^{-1}) and anthracene-9-carboxaldehyde (103 mg, 0.5 mmol) were all reacted together according to general procedure H to afford the crude product. Purification by silica gel column chromatography (hexane 9:1 EtOAc) gave the title compound as a pale yellow crystalline solid. **MP**: 161–164 °C. (lit.[433] 159–162 °C). **^{1}H NMR** (300 MHz, CDCl$_3$); δ$_H$ 8.44 (1H, s, ArH), 8.37 (2H, d, J = 8.7 Hz, ArH), 8.02 (2H, d, J = 8.2 Hz, ArH), 7.58–7.46 (4H, m, ArH), 5.61 (2H, s, CH_2), 1.87 (1H, br s, OH). **^{13}C NMR** (75.5 MHz, CDCl$_3$); δ$_C$ 131.6 (ArC), 131.1 (ArC), 130.2 (ArC), 129.3 (ArC), 128.5 (ArC), 126.6 (ArC), 125.2 (ArC), 124.0 (ArC), 57.5 (CH_2). NMR data in accordance with literature precedent.[434]

4.2.38 Pyren-1-ylmethanol 214

Dichloro(pentamethylcyclopentadienyl)iridium(III) dimer (1 mg, 0.00125 mmol), 4-((((2-((2,4,6-trimethylphenyl)sulfonamido)ethyl)carbamoyl)oxy) methyl)phenyl phosphate **198** (1.3 mg, 0.0025 mmol),

sodium formate (170 mg, 2.5 mmol), alkaline phosphatase (2.5 mg, 10 Umg^{-1}) and pyrene-1-carboxaldehyde (115 mg, 0.5 mmol) were all reacted together according to general procedure H to afford the crude product. Purification by silica gel column chromatography (hexane 9:1 EtOAc) gave the title compound as a pale yellow crystalline solid. **MP**: 94–98 °C. (lit.[435] 124–126 °C). **^{1}H NMR** (300 MHz, CDCl$_3$); δ_H 8.26 (1H, d, J = 9.2 Hz, ArH), 8.17 (2H, d, J = 7.6 Hz, ArH), 8.09–7.94 (6H, m, ArH), 5.31 (2H, s, CH_2), 2.02 (1H, br s, OH). **^{13}C NMR** (75.5 MHz, CDCl$_3$); δ_C 133.8 (ArC), 131.3 (ArC), 131.3 (ArC), 130.8 (ArC), 128.8 (ArC), 127.9 (ArC), 127.5 (ArC), 127.5 (ArC), 126.0 (ArC), 126.0 (ArC), 125.4 (ArC), 125.3 (ArC), 124.9 (ArC), 124.8 (ArC), 123.0 (ArC), 63.8 (CH_2). NMR data in accordance with literature precedent.[435]

4.2.39 2,6-Difluorobenzyl Alcohol 215

Dichloro(pentamethylcyclopentadienyl)iridium(III) dimer (1 mg, 0.00125 mmol), 4-((((2-((2,4,6-trimethylphenyl)sulfonamido)ethyl)carbamoyl)oxy) methyl)phenyl phosphate **198** (1.3 mg, 0.0025 mmol), sodium formate (340 mg, 5 mmol), alkaline phosphatase (2.5 mg, 10 Umg^{-1}) and 2,6-difluorobenzaldehyde (108 μL, 1 mmol) were all reacted together according to general procedure I to afford the crude product. Purification by silica gel column chromatography (hexane 9:1 EtOAc) gave the title compound as a colourless oil. **^{1}H NMR** (300 MHz, CDCl$_3$); δ_H 7.31–7.21 (1H, m, ArH), 6.95–6.85 (2H, m, ArH), 4.78 (2H, s, CH_2), 2.05 (1H, br s, OH). **^{13}C NMR** (75.5 MHz, CDCl$_3$); δ_C 161.7 (dd, $^1J_{C–F}$ = 249 Hz & $^3J_{C–F}$ = 8 Hz, ArC), 130.0 (t, $^3J_{C–F}$ = 10 Hz, ArC), 116.4 (t, $^2J_{C–F}$ = 19 Hz, ArC), 111.5 (dd, $^2J_{C–F}$ = 25 Hz & $^4J_{C–F}$ = 8 Hz, ArC), 53.1 (t, $^3J_{C–F}$ = 4 Hz, CH_2). **^{19}F NMR** (470.5 MHz, CDCl$_3$); δ_F −116.6. NMR data in accordance with literature precedent.[436]

4.2.40 4-Fluorobenzyl Alcohol 216

Dichloro(pentamethylcyclopentadienyl)iridium(III) dimer (1 mg, 0.00125 mmol), 4-((((2-((2,4,6-trimethylphenyl)sulfonamido)ethyl)carbamoyl)oxy) methyl)phenyl phosphate **198** (1.3 mg, 0.0025 mmol), sodium formate (340 mg, 5 mmol), alkaline phosphatase (2.5 mg, 10 Umg^{-1}) and 4-fluorobenzaldehyde (94 μL, 1 mmol) were all reacted together according to general procedure I to afford the crude product. Purification by silica gel column chromatography (hexane 9:1 EtOAc) gave the title compound as a colourless oil. **^{1}H NMR** (300 MHz, CDCl$_3$); δ_H 7.35–7.29 (2H, m, ArH), 7.08–7.00 (2H, m, ArH), 4.64 (2H, s, CH_2), 1.97 (1H, br s, OH). **^{13}C NMR** (75.5 MHz, CDCl$_3$); δ_C 162.4 (d, $^1J_{C–F}$ = 246 Hz, ArC), 136.7 (d, $^4J_{C–F}$ = 3 Hz, ArC), 128.9 (d, $^3J_{C–F}$ = 8 Hz, ArC), 115.5 (d, $^2J_{C–F}$ = 21 Hz, ArC), 64.7 (CH_2). **^{19}F NMR** (470.5 MHz, CDCl$_3$); δ_F −114.9. NMR data in accordance with literature precedent.[437]

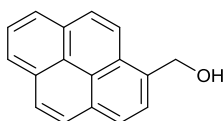### 4.2.41 4-(Trifluoromethyl)benzyl Alcohol 217

Dichloro(pentamethylcyclopentadienyl)iridium(III) dimer (1 mg, 0.00125 mmol), 4-((((2-((2,4,6-trimethylphenyl)sulfonamido)ethyl)carbamoyl)oxy) methyl)phenyl phosphate 198 (1.3 mg, 0.0025 mmol), sodium formate (340 mg, 5 mmol), alkaline phosphatase (2.5 mg, 10 Umg^{-1}) and 4-(trifluoromethyl)benzaldehyde (136 µL, 1 mmol) were all reacted together according to general procedure I to afford the crude product. Purification by silica gel column chromatography (hexane 9:1 EtOAc) gave the title compound as a colourless oil. **^{1}H NMR** (300 MHz, CDCl$_3$); δ_H 7.57 (2H, d, J = 8.1 Hz, ArH), 7.39 (2H, d, J = 8.1 Hz, ArH), 4.65 (2H, s, CH_2), 3.24 (1H, br s, OH). **^{13}C NMR** (75.5 MHz, CDCl$_3$); δ_C 144.8 (q, $^{4}J_{C–F}$ = 1 Hz, ArC), 129.8 (q, $^{2}J_{C–F}$ = 32 Hz, ArC), 126.9 (ArC), 125.5 (q, $^{3}J_{C–F}$ = 32 Hz, ArC), 124.3 (q, $^{1}J_{C–F}$ = 272 Hz, ArC), 64.3 (CH_2). **^{19}F NMR** (470.5 MHz, CDCl$_3$); δ_F −62.5. NMR data in accordance with literature precedent.[438]

4.2.42 4-Nitrobenzyl Alcohol 218

Dichloro(pentamethylcyclopentadienyl)iridium(III) dimer (1 mg, 0.00125 mmol), 4-((((2-((2,4,6-trimethylphenyl)sulfonamido)ethyl)carbamoyl)oxy) methyl)phenyl phosphate 198 (1.3 mg, 0.0025 mmol), sodium formate (340 mg, 5 mmol), alkaline phosphatase (2.5 mg, 10 Umg^{-1}) and 4-nitrobenzaldehyde (153 mg, 1 mmol) were all reacted together according to general procedure I to afford the crude product. Purification by silica gel column chromatography (hexane 9:1 EtOAc) gave the title compound as a white solid. **MP**: 89–91 °C (lit.[439] 91–93 °C). **^{1}H NMR** (300 MHz, CDCl$_3$); δ_H 8.18 (2H, d, J = 8.2 Hz, ArH), 7.51 (2H, d, J = 8.2 Hz, ArH), 4.82 (2H, s, CH_2), 2.29 (1H, br s, OH). **^{13}C NMR** (75.5 MHz, CDCl$_3$); δ_C 148.4 (ArC), 147.3 (ArC), 127.1 (ArC), 123.8 (ArC), 64.0 (CH_2). NMR data in accordance with literature precedent.[440]
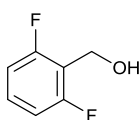
4.2.43 4-Methoxybenzyl Alcohol 219

Dichloro(pentamethylcyclopentadienyl)iridium(III) dimer (1 mg, 0.00125 mmol), 4-((((2-((2,4,6-trimethylphenyl)sulfonamido)ethyl)carbamoyl)oxy) methyl)phenyl phosphate 198 (1.3 mg, 0.0025 mmol), sodium formate (170 mg, 2.5 mmol), alkaline phosphatase (2.5 mg, 10 Umg^{-1}) and p-anisaldehyde (61 µL, 0.5 mmol) were all reacted together according to general procedure H to afford the crude product. Purification by silica gel column chromatography (hexane 9:1 EtOAc) gave the title compound as a

colourless oil. **^{1}H NMR** (300 MHz, CDCl$_3$); δ_H 7.20 (2H, d, J = 8.7 Hz, Ar*H*), 6.81 (2H, d, J = 8.7 Hz, Ar*H*), 4.51 (2H, s, C*H*$_2$), 3.72 (3H, s, OC*H*$_3$), 1.89 (1H, br s, O*H*). **^{13}C NMR** (75.5 MHz, CDCl$_3$); δ 159.3 (Ar*C*), 133.2 (Ar*C*), 128.8 (Ar*C*), 114.0 (Ar*C*), 65.1 (*C*H$_2$), 55.4 (O*C*H$_3$). NMR data in accordance with literature precedent.[441]

4.2.44   4-Hydroxy-3-methoxybenzyl Alcohol **220**

Dichloro(pentamethylcyclopentadienyl)iridium(III) dimer (1 mg, 0.00125 mmol), 4-((((2-((2,4,6-trimethylphenyl)sulfonamido)ethyl)carbamoyl)oxy) methyl)phenyl ph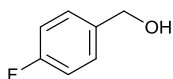osphate **198** (1.3 mg, 0.0025 mmol), sodium formate (170 mg, 2.5 mmol), alkaline phosphatase (2.5 mg, 10 Umg^{-1}) and vanillin (76 mg, 0.5 mmol) were all reacted together according to general procedure H to afford the crude product. Purification by silica gel column chromatography (hexane 9:1 EtOAc) gave the title compound as a white solid. **MP**: 114–115 °C (lit.[442] 112–114 °C). **^{1}H NMR** (300 MHz, d_6-DMSO); δ_H 8.80 (1H, s, ArO*H*), 6.88 (1H, s, Ar*H*), 6.74–6.68 (2H, m, Ar*H*), 5.02 (1H, t, J = 5.7 Hz, CH$_2$O*H*), 4.38 (2H, d, J = 5.7 Hz, C*H*$_2$OH), 3.75 (3H, s OC*H*$_3$). **^{13}C NMR** (75.5 MHz, d_6-DMSO); δ_C 147.4 (Ar*C*), 145.3 (Ar*C*), 133.6 (Ar*C*), 119.2 (Ar*C*), 115.1 (Ar*C*), 111.1 (Ar*C*), 63.1 (*C*H$_2$), 55.5 (O*C*H$_3$). NMR data in accordance with literature precedent.[443]

4.2.45   2-Hydroxybenzyl Alcohol **221**
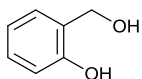
Dichloro(pentamethylcyclopentadienyl)iridium(III) dimer (1 mg, 0.00125 mmol), 4-((((2-((2,4,6-trimethylphenyl)sulfonamido)ethyl)carbamoyl)oxy) methyl)phenyl phosphate **198** (1.3 mg, 0.0025 mmol), sodium formate (170 mg, 2.5 mmol), alkaline phosphatase (2.5 mg, 10 Umg^{-1}) and salicylaldehyde (53 µL, 0.5 mmol) were all reacted together according to general procedure H to afford the crude product. Purification by silica gel column chromatography (hexane 9:1 EtOAc) gave the title compound as a white crystalline solid. **MP**: 82–84 °C. (lit.[444] 82–84 °C). **^{1}H NMR** (300 MHz, CDCl$_3$); δ_H 7.34 (1H, br s, ArO*H*), 7.24–7.18 (1H, m, Ar*H*), 7.04 (1H, dd, J = 7.4, 1.3 Hz, Ar*H*), 6.89–6.83 (2H, m, Ar*H*), 4.85 (2H, s, C*H*$_2$), 2.46 (1H, br s, CH$_2$O*H*). **^{13}C NMR** (75.5 MHz, CDCl$_3$); δ_C 156.1 (Ar*C*), 129.7 (Ar*C*), 128.0 (Ar*C*), 124.8 (Ar*C*), 120.3 (Ar*C*), 116.6 (Ar*C*), 64.7 (*C*H$_2$). NMR data in accordance with literature precedent. [443]
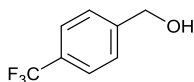
4.2.46 4-Isopropylbenzyl Alcohol **222**

Dichloro(pentamethylcyclopentadienyl)iridium(III) dimer (1 mg, 0.00125 mmol), 4-((((2-((2,4,6-trimethylphenyl)sulfonamido)ethyl)carbamoyl)oxy) methyl)phenyl phosphate **198** (1.3 mg, 0.0025 mmol), sodium formate (170 mg, 2.5 mmol), alkaline phosphatase (2.5 mg, 10 Umg^{-1}) and cuminaldehyde (76 µL, 0.5 mmol) were all reacted together according to general procedure H to afford the crude product. Purification by silica gel column chromatography (hexane 9:1 EtOAc) gave the title compound as a colourless oil. **¹H NMR** (300 MHz, CDCl$_3$); δ$_H$ 7.31 (2H, d, J = 8.2 Hz, ArH), 7.24 (2H, d, J = 8.2 Hz, ArH), 4.66 (2H, s, CH_2), 2.92 (1H, sept, J = 6.9 Hz, CH), 1.71 (1H, br s, OH), 1.26 (6H, d, J = 6.9 Hz, CH_3). **¹³C NMR** (75.5 MHz, CDCl$_3$); δ$_C$ 148.5 (ArC), 138.3 (ArC), 127.2 (ArC), 126.7 (ArC), 65.3 (CH_2), 33.9 (CH), 24.1 (CH_3). NMR data in accordance with literature precedent.[445]
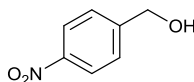
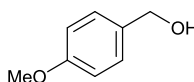### 4.2.47 4-(Hydroxymethyl)benzaldehyde **223**
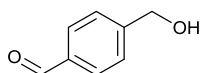
Dichloro(pentamethylcyclopentadienyl)iridium(III) dimer (1 mg, 0.00125 mmol), 4-((((2-((2,4,6-trimethylphenyl)sulfonamido)ethyl)carbamoyl)oxy) methyl)phenyl phosphate **198** (1.3 mg, 0.0025 mmol), sodium formate (170 mg, 2.5 mmol), alkaline phosphatase (2.5 mg, 10 Umg^{-1}) and terephthalaldehyde (67 mg, 0.5 mmol) were all reacted together according to general procedure H to afford the crude product. Purification by silica gel column chromatography (hexane 9:1 EtOAc) gave the title compound as a white solid. **MP**: 41–43 °C (lit.[446] 43–44 °C). **¹H NMR** (300 MHz, CDCl$_3$); δ$_H$ 9.98 (1H, s, CHO), 7.85 (2H, d, J = 8.1 Hz, ArH), 7.51 (2H, d, J = 8.1 Hz, ArH), 4.79 (2H, s, CH_2), 2.28 (1H, br s, OH). **¹³C NMR** (75.5 MHz, CDCl$_3$); δ$_C$ 192.2 (C=O, 148.0 (ArC), 135.8 (ArC), 130.1 (ArC), 127.1 (ArC), 64.6 (CH_2). NMR data in accordance with literature precedent.[447]

4.2.48 Cyclohexanemethanol **224**
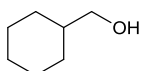
Dichloro(pentamethylcyclopentadienyl)iridium(III) dimer (1 mg, 0.00125 mmol), 4-((((2-((2,4,6-trimethylphenyl)sulfonamido)ethyl)carbamoyl)oxy) methyl)phenyl phosphate **198** (1.3 mg, 0.0025 mmol), sodium formate (170 mg, 2.5 mmol), alkaline phosphatase (2.5 mg, 10 Umg^{-1}) and cyclohexanecarboxaldehyde (61 µL, 0.5 mmol) were all reacted together according to general procedure H to afford the crude product. Purification by silica gel column chromatography (hexane 9:1 EtOAc) gave the title compound as a colourless oil. **¹H NMR** (300 MHz, CDCl$_3$); δ$_H$ 3.44 (2H, d, J = 6.3 Hz, CH_2), 1.77–1.66 (5H,

m, C*H*), 1.56 (1H, br s, O*H*), 1.53–1.41 (1H, m, C*H*), 1.32–1.21 (3H, m, C*H*), 1.00–0.83 (2H, m, C*H*). ^{13}C NMR (75.5 MHz, CDCl$_3$); δ_C 69.0 (*C*H$_2$OH), 40.7 (*C*H), 29.7 (*C*H$_2$), 26.7 (*C*H$_2$), 26.0 (*C*H$_2$). NMR data in accordance with literature precedent.[432]
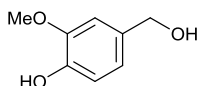
4.2.49 *1-Octanol* **225**
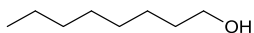
Dichloro(pentamethylcyclopentadienyl)iridium(III) dimer (1 mg, 0.00125 mmol), 4-((((2-((2,4,6-trimethylphenyl)sulfonamido)ethyl)carbamoyl)oxy) methyl)phenyl phosphate **198** (1.3 mg, 0.0025 mmol), sodium formate (170 mg, 2.5 mmol), alkaline phosphatase (2.5 mg, 10 Umg^{-1}) and octanal (79 µL, 0.5 mmol) were all reacted together according to general procedure H to afford the crude product. Purification by silica gel column chromatography (hexane 9:1 EtOAc) gave the title compound as a colourless oil. ^{1}**H NMR** (300 MHz, CDCl$_3$); δ_H 3.64 (2H, t, *J* = 6.6 Hz, C*H*$_2$OH), 1.61–1.52 (2H, m, C*H*$_2$), 1.39–1.28 (11H, m, C*H*$_2$ + O*H*), 0.88 (3H, t, *J* = 6.8 Hz, C*H*$_3$). ^{13}**C NMR** (75.5 MHz, CDCl$_3$); δ 63.2 (*C*H$_2$OH), 33.0 (*C*H$_2$), 29.5 (*C*H$_2$), 29.4 (*C*H$_2$), 25.9 (*C*H$_2$), 22.8 (*C*H$_2$), 14.2 (*C*H$_3$). NMR data in accordance with literature precedent.[437]

4.2.50 *2-Methoxycinnamyl Alcohol* **226**
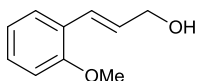
Dichloro(pentamethylcyclopentadienyl)iridium(III) dimer (1 mg, 0.00125 mmol), 4-((((2-((2,4,6-trimethylphenyl)sulfonamido)ethyl)carbamoyl)oxy) methyl)phenyl phosphate **198** (1.3 mg, 0.0025 mmol), sodium formate (170 mg, 2.5 mmol), alkaline phosphatase (2.5 mg, 10 Umg^{-1}) and 2-Methoxycinnamaldehyde (81 mg, 0.5 mmol) were all reacted together according to general procedure H to afford the crude product. Purification by silica gel column chromatograph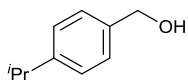y (hexane 9:1 EtOAc) gave the title compound as a colourless oil. ^{1}**H NMR** (300 MHz, CDCl$_3$); δ_H 7.44 (1H, dd, *J* = 7.6, 1.7 Hz, Ar*H*), 7.27–7.21 (1H, m, Ar*H*), 6.96–6.86 (3H, m, Ar*H* + Ar*CH*), 6.38 (1H, dt, *J* = 16.0, 5.9 Hz, CH$_2$C*H*), 4.32 (2H, d, *J* = 5.0 Hz, C*H*$_2$OH), 3.84 (3H, s, OC*H*$_3$), 1.81 (1H, br s, O*H*). ^{13}**C NMR** (75.5 MHz, CDCl$_3$); δ_C 156.8 (Ar*C*), 129.4 (Ar*C*), 128.9 (Ar*C*), 127.1 (Ar*C*), 126.2 (Ar*C*), 125.8 (Ar*C*), 120.8 (*C*=CHCH$_2$), 110.9 (CH*C*HCH$_2$), 64.3 (*C*H$_2$), 55.5 (O*C*H$_3$). NMR data in accordance with literature precedent.[448]

Chapter 5

References

1. R. G. Macfarlane, *Nature*, 1964, **202**, 498.

2. G. Wald, *Science*, 1965, **150**, 1028.

3. A. L. Lehninger, D. L. Nelson and M. M. Cox, *Lehninger Principles of Biochemistry*, W. H. Freeman, New York, 4th edn., 2004, ch. 12, pp. 421–439.

4. G. Krauss, *Biochemistry of Signal Transduction and Regulation*, Wiley–VCH, Weinheim, 3rd edn., 2008, ch. 3, pp. 115–149.

5. J. M. Bowness, *Science*, 1966, **152**, 1370.

6. P. Scrimin and L. J. Prins, *Chem. Soc. Rev.*, 2011, **40**, 4488.

7. Y.-W. Tang, G. W. Procop and D. H. Persing, *Clin. Chem.*, 1997, **43**, 2021.

8. S. Bell, *Annu. Rev. Anal. Chem.*, 2009, **2**, 297.

9. M. Vanderlaan, B. E. Watkins and L. Stanker, *Environ. Sci. Technol.*, 1988, **22**, 247.

10. S. C. Andras, J. B. Power, E. C. Cocking and M. R. Davey, *Mol. Biotechnol.*, 2001, **19**, 29.

11. R. K. Saiki, D. H. Gelfand, S. Stoffel, S. J. Scharf, R. Higuchi, G. T. Horn, K. B. Mullis and H. A. Erlich, *Science*, 1988, **239**, 487.

12. N. Arnheim and H. Erlich, *Annu. Rev. Biochem.*, 1992, **61**, 131.

13. *The Polymerase Chain Reaction*, eds. K. B. Mullis, F. Ferré and R. A. Gibbs, Birkhäuser, Boston, 1994, pp. 233–415.

14. P. Gill and A. Ghaemi, *Nucleosides Nucleotides Nucleic Acids*, 2008, **27**, 224.

15. L. Yan, J. Zhou, Y. Zheng, A. S. Gamson, B. T. Roembke, S. Nakayama and H. O. Sintim, *Mol. BioSyst.*, 2014, **10**, 970.

16. P. Craw and W. Balachandran, *Lab Chip*, 2012, **12**, 2469.

17. Y. V. Gerasimova and D. M. Kolpashchikov, *Chem. Soc. Rev.*, 2014, **43**, 6405.

18. M. Zhang, Y.-M. Guan and B.-C. Ye, *Chem. Commun.*, 2011, **47**, 3478.

19. F. Wang, J. Elbaz and I. Willner, *J. Am. Chem. Soc.*, 2012, **134**, 5504.

20. S. Sando, T. Sasaki, K. Kanatani and Y. Aoyama, *J. Am. Chem. Soc.*, 2003, **125**, 15720.

21. Z. J. Gartner, B. N. Tse, R. Grubina, J. B. Doyon, T. M. Snyder and D. R. Liu, *Science*, 2004, **305**, 1601.

22. A. Shibata, T. Uzawa, Y. Nakashima, M. Ito, Y. Nakano, S. Shuto, Y. Ito and H. Abe, *J. Am. Chem. Soc.*, 2013, **135**, 14172.

23. H. Wang, Y. Wang, S. Liu, J. Yu, W. Xu, Y. Guo and J. Huang, *Chem. Commun.*, 2015, **51**, 8377.

24. J. Nie, M.-Z. Zhao, W. J. Xie, L.-Y. Cai, Y.-L. Zhou and X.-X. Zhang, *Chem. Sci.*, 2015, **6**, 1225.

25. F. Wang, C.-H. Lu and I. Willner, *Chem. Rev.*, 2014, **114**, 2881.

26. *Metal-catalyzed Cross-coupling Reactions*, eds. A. de Meijere and F. Diederich, Wiley–VCH, Weinheim, 2nd edn., 2004.

27. C. E. Garrett and K. Prasad, *Adv. Synth. Catal.*, 2004, **346**, 889.

28. F. Song, A. L. Garner and K. Koide, *J. Am. Chem. Soc.*, 2007, **129**, 12354.

29. J. Tsuji, *Organic Synthesis with Palladium Compounds*, Springer–Verlag, Berlin, 1980, pp. 125–132.

30. B. M. Trost, *Acc. Chem. Res.*, 1980, **13**, 385.

31. C. G. Frost, J. Howarth and J. M. J. Williams, *Tetrahedron: Asymmetry*, 1992, **3**, 1089.

32. J. M. Williams and K. Koide, *Ind. Eng. Chem. Res.*, 2013, **52**, 8612.

33. K. C. Majumdar, S. Alam and B. Chattopadhyay, *Tetrahedron*, 2008, **64**, 597.

34. A. L. Garner and K. Koide, *J. Am. Chem. Soc.*, 2008, **130**, 16472.

35. A. L. Garner and K. Koide, *Chem. Commun.*, 2009, 86.

36. A. L. Garner, F. Song and K. Koide, *J. Am. Chem. Soc.*, 2009, **131**, 5163.

37. F. Song, E. J. Carder, C. C. Kohler and K. Koide, *Chem. – Eur. J.*, 2010, **16**, 13500.

38. W. R. Kitley, P. J. Santa Maria, R. A. Cloyd and L. M. Wysocki, *Chem. Commun.*, 2015, **51**, 8520.

39. M. Santra, S.-K. Ko, I. Shin and K. H. Ahn, *Chem. Commun.*, 2010, **46**, 3964.

40. B. Zhu, C. Gao, Y. Zhao, C. Liu, Y. Li, Q. Wei, Z. Ma, B. Du and X. Zhang, *Chem. Commun.*, 2011, **47**, 8656.

41. J. Jiang, H. Jiang, W. Liu, X. Tang, X. Zhou, W. Liu and R. Liu, *Org. Lett*. 2011, **13**, 4922.

42. M. E. Jun and K. H. Ahn, *Org. Lett.*, 2010, **12**, 2790.

43. H. N. Kim, M. H. Lee, H. J. Kim, J. S. Kim and J. Yoon, *Chem. Soc. Rev.*, 2008, **37**, 1465.

44. H. Li, J. Fan and X. Peng, *Chem. Soc. Rev.*, 2013, **42**, 7943.

45. M. P. Tracey, D. Pham and K. Koide, *Chem. Soc. Rev.*, 2015, DOI: 10.1039/C4CS00323C.

46. J.-P. Goddard and J.-L. Reymond, *Trends in Biotechnology*, 2004, **22**, 363.

47. J.-L. Reymond, V. S. Fluxá and N. Maillard, *Chem. Commun.*, 2009, 34.

48. X. Li, X. Gao, W. Shi and H. Ma, *Chem. Rev.*, 2014, 114, 590.

49. D. J. Yee, V. Balsanek and D. Sames, *J. Am. Chem. Soc.*, 2004, 126, 2282.

50. T. M. Penning, M. E. Burczynski, J. M. Jez, C.-F. Hung, H. K. Lin, H. Ma, M. Moore, N. Palackal and K. Ratnam, *Biochem. J.*, 2000, **351**, 67.

51. M. Halim, D. J. Yee and D. Sames, *J. Am. Chem. Soc.*, 2008, **130**, 14123.

52. H. Yun and S. J. Danishefsky, *J. Org. Chem.*, 2003, **68**, 4519.

53. G. Chen, D. J. Yee, N. G. Gubernator and D. Sames, *J. Am. Chem. Soc.*, 2005, **127**, 4544.

54. A. S. Kalgutkar, D.K. Dalvie, N. Castagnoli and T. J. Taylor, *Chem. Res. Toxicol.*, 2001, **14**, 1139.

55. R. B. Silverman, *Acc. Chem. Res.*, 1995, **28**, 335.

56. P. M. Lizardi, X. Huang, Z. Zhu, P. Bray-Ward, D. C. Thomas and D. C. Ward, *Nature Genetics*, 1998, **19**, 225.

57. M. M. Ali, F. Li, Z. Zhang, K. Zhang, D.-K. Kang, J. A. Ankrum, X. C. Le and W. Zhao, *Chem. Soc. Rev.*, 2014, **43**, 3324.

58. W. Zhao, M. M. Ali, M. A. Brook and Y. Li, *Angew. Chem., Int. Ed.*, 2008, **47**, 6330.

59. B. Schweitzer, S. Wiltshire, J. Lambert, S. O'Malley, K. Kukanskis, Z. Zhu, S. F. Kingsmore, P. M. Lizardi and D. C. Ward, *Proc. Natl. Acad. Sci. U. S. A.*, 2000, **97**, 10113.

60. Q. Xue, Z. Wang, L. Wang and W. Jiang, *Bioconjugate Chem.*, 2012, **23**, 734.

61. C. Ding, H. Liu, N. Wang and Z. Wang, *Chem. Commun.*, 2012, **48**, 5019.

62. T. Sano, C. L. Smith and C. R. Cantor, *Science*, 1992, **258**, 120.

63. C. M. Niemeyer, M. Adler and R. Wacker, *Trends Biotechnol.*, 2005, **23**, 208.

64. M. Adler, R. Wacker and C. M. Niemeyer, *Analyst*, 2008, **133**, 702.

65. R. M. Dirks and N. A. Pierce, *Proc. Natl. Acad. Sci. U. S. A.*, 2004, **101**, 15275.

66. J. M. Jean and K. B. Hall, *Proc. Natl. Acad. Sci. U. S. A.*, 2000, **98**, 37.

67. J. Huang, Y. Wu, Y. Chen, Z. Zhu, X. Yang, C. J. Yang, K. Wang and W. Tan, *Angew. Chem., Int. Ed.*, 2011, **50**, 401.

68. H. M. T. Choi, V. A. Beck and N. A. Pierce, *ACS Nano*, 2014, **8**, 4284.

69. J. Zhuang, L. Fu, M. Xu, H. Yang, G. Chen and D. Tang, *Anal. Chim. Acta*, 2013, **783**, 17.

70. H. D. Sikes, R. R. Hansen, L. M. Johnson, R. Jenison, J. W. Birks, K. L. Rowlen and C. N. Bowman, *Nat. Mater.*, 2008, **7**, 52.

71. R. R. Hansen, H. D. Sikes and C. N. Bowman, *Biomacromolecules*, 2007, **9**, 355.

72. H. D. Sikes, R. Jenison and C. N. Bowman, *Lab Chip*, 2009, **9**, 653.

73. R. R. Hansen, H. J. Avens, R. Shenoy and C. N. Bowman, *Anal. Bioanal. Chem.*, 2008, **392**, 167.

74. H. J. Avens and C. N. Bowman, *Acta Biomater.*, 2010, **6**, 83.

75. A. Sagi, R. Weinstain, N. Karton and D. Shabat, *J. Am. Chem. Soc.*, 2008, **130**, 5434.

76. N. Jourdain, R. P. Carlón and J.-L. Reymond, *Tetrahedron Lett.*, 1998, **39**, 9415.

77. S. T. Phillips and A. M. DiLauro, *ACS Macro Lett.*, 2014, **3**, 298.

78. R. Weinstain, A. Sagi, N. Karton and D. Shabat, *Chem. – Eur. J.*, 2008, **14**, 6857.

79. C. de las Heras Alarcón, S. Pennadam and C. Alexander, *Chem. Soc. Rev.*, 2005, **34**, 276.

80. W. Wang and C. Alexander, *Angew. Chem., Int. Ed.*, 2008, **47**, 7804.

81. *Rapid Detection of Infectious Agents*, eds. S. Spector, M. Bendinelli and H. Friedman, Plenum Press, New York, 1998, ch. 10, pp. 159–173.

82. M. N. Bobrow, T. D. Harris, K. J. Shaughnessy and G. J. Litt, *J. Immunol. Methods*, 1989, **125**, 279.

83. H. M. Kerstens, P. J. Poddighe and A. G. Hanselaar, *J. Histochem. Cytochem.*, 1995, **43**, 347.

84. A. J. Gross and I. W. Sizer, *J. Biomol. Chem.*, 1959, **234**, 1611.

85. E. P. Diamandis and T. K. Christopoulos, *Clin. Chem.*, 1991, **37**, 625.

86. I. M. Grumbach and R. W. Veh, *J. Histochem. Cytochem.*, 1995, **43**, 31.

87. S.-M. Hsu, L. Raine and H. Fanger, *J. Histochem. Cytochem.*, 1981, **29**, 577.

88. M. Wilchek and E. A. Bayer, *Anal. Biochem.*, 1988, **171**, 1.

89. E. A. Bayer and M. Wilchek, *Methods Biochem. Anal.*, 1980, **26**, 1.

90. N. L. Rossi and C. A. Mirkin, *Chem. Rev.*, 2005, **105**, 1547.

91. J. Wang, *Small*, 2005, **1**, 1036.

92. J. Lei and H. Ju, *Chem. Soc. Rev.*, 2012, **41**, 2122.

93. X. Yu, B. S. Munge, V. Patel, G. Jensen, A. Bhirde, J. D. Gong, S. N. Kim, J. Gillespie, J. S. Gutkind, F. Papadimitrakopoulos and J. F. Rusling, *J. Am. Chem. Soc.*, 2006, **128**, 11199.

94. B. Munge, G. Liu, G. Collins and J. Wang, *Anal. Chem.*, 2005, **77**, 4662.

95. B. S. Munge, A. L. Coffey, J. M. Doucette, B. K. Somba, R. Malhotra, V. Patel, J. S. Gutkind and J. F. Rusling, *Angew. Chem., Int. Ed.*, 2011, **50**, 7915.

96. K. Saha, S. S. Agasti, C. Kim, X. Li and V. M. Rotello, *Chem. Rev.*, 2012, **112**, 2739.

97. J.-M. Nam, S.-J. Park and C. A. Mirkin, *J. Am. Chem. Soc.*, 2002, **124**, 3820.

98. J.-M. Nam, C. S. Thaxton and C. A. Mirkin, *Science*, 2003, **301**, 1884.

99. C. S. Thaxton, H. D. Hill, D. G. Georganopoulou, S. I. Stoeva and C. A. Mirkin, *Anal. Chem.*, 2005, **77**, 8174.

100. T. A. Taton, C. A. Mirkin and R. L. Letsinger, *Science*, 2000, **289**, 1757.

101. B.-K. Oh, J.-M. Nam, S. W. Lee and C. A. Mirkin, *Small*, 2006, **2**, 103.

102. J.-M. Nam, S. I. Stoeva and C. A. Mirkin, *J. Am. Chem. Soc.*, 2004, **126**, 5932.

103. S. I. Stoeva, J.-S. Lee, C. S. Thaxton and C. A. Mirkin, *Angew. Chem., Int. Ed.*, 2006, **45**, 3303.

104. S. I. Stoeva, J.-S. Lee, J. E. Smith, S. T. Rosen and C. A. Mirkin, *J. Am. Chem. Soc.*, 2006, **128**, 8378.

105. U. Kreibig and L. Genzel, *Surf. Sci.*, 1985, **156**, 678.

106. R. Elghanian, J. J. Storhoff, R. C. Mucic, R. L. Letsinger and C. A. Mirkin, *Science*, 1997, **277**, 1078.

107. J. Liu and Y. Lu, *J. Am. Chem. Soc.*, 2003, **125**, 6642.

108. Y. Lu and J. Liu, *Curr. Opin. Biotechnol.*, 2006, **17**, 580.

109. D. G. Blackmond, *Angew. Chem., Int. Ed.*, 2009, **48**, 386.

110. O. V. Makhlynets and I. V. Korendovych, *Biomolecules*, 2014, **4**, 402.

111. B. Kobe and B. E. Kemp, *Nature*, 1999, **402**, 373.

112.   C.-W. Wang, W.-T. Yu, H.-P. Lai, B.-Y. Lee, R.-C. Gao and K.-T. Tan, *Anal. Chem.*, 2015, **87**, 4231.

113.   O. R. Miranda, H.-T. Chen, C.-C. You, D. E. Mortenson, X.-C. Yang, U. H. F. Bunz and V. M. Rotello, *J. Am. Chem. Soc.*, 2010, **132**, 5285.

114.   M. De, S. Rana, H. Akpinar, O. R. Miranda, R. R. Arvizo, U. H. F. Bunz and V. M. Rotello, *Nat. Chem.*, 2009, **1**, 461.

115.   M. De, C.-C. You, S. Srivastava and V. M. Rotello, *J. Am. Chem. Soc.*, 2007, **129**, 10747.

116.   O. R. Miranda, X. Li, L. Garcia-Gonzalez, Z.-J. Zhu, B. Yan, U. H. F. Bunz and V. M. Rotello, *J. Am. Chem. Soc.*, 2011, **133**, 9650.

117.   C.-C. You, O. R. Miranda, B. Gider, P. S. Ghosh, I.-B. Kim, B. Erdogan, S. A. Krovi, U. H. F. Bunz and V. M. Rotello, *Nat. Nanotechnol.*, 2007, **2**, 318.

118.   P. Miao, Y. Tang, B. Wang, J. Yin and L. Ning, *TrAC, Trends Anal. Chem.*, 2015, **67**, 1.

119.   A. Saghatelian, K. M. Guckian, D. A. Thayer and M. R. Ghadiri, *J. Am. Chem. Soc.*, 2003, **125**, 344.

120.   N. C. Gianneschi and M. R. Ghadiri, *Angew. Chem., Int. Ed.*, 2007, **46**, 3955.

121.   V. Pavlov, B. Shlyahovsky and I. Willner, *J. Am. Chem. Soc.*, 2005, **127**, 6522.

122.   B. M. G. Janssen, W. Engelen and M. Merkx, *ACS Synth. Biol.*, 2015, **4**, 547.

123.   A. Villaverde, *FEBS Lett.*, 2003, **554**, 169.

124.   J. D. Fischer, G. L. Holliday and J. M. Thornton, *Bioinformatics*, 2010, **26**, 2496.

125.   C. Andreini, I. Bertini, G. Cavallaro, G. L. Holliday and J. M. Thornton, *Bioinformatics*, 2009, **25**, 2088.

126.   P. Simon, C. Dueymes, M. Fontecave, J.-L. Décout, *Angew. Chem., Int. Ed.*, 2005, **44**, 2764.

127.   M. Liu, J. Fu, C. Hejesen, Y. Yang, N. W. Woodbury, K. Gothelf, Y. Liu and H. Yan, *Nat. Commun.*, 2013, **4**, 2127.

128.   J. Leblond and A. Petitjean, *ChemPhysChem*, 2011, **12**, 1043.

129.   N. Graf and R. Krämer, *Chem. Commun.*, 2006, 4375.

130.   M. Göritz and R. Krämer, *J. Am. Chem. Soc.*, 2005, **127**, 18016.

131.   N. Graf, S. Kassube and R. Krämer, *Bioorg. Med. Chem. Lett.*, 2008, **18**, 4786.

132.   N. Graf, M. Göritz and R. Krämer, *Angew. Chem., Int. Ed.*, 2006, **45**, 4013.

133.   J. Brunner, A. Mokhir and R. Kraemer, *J. Am. Chem. Soc.*, 2003, **125**, 12410.

134.   R. Bonomi, A. Cazzolaro, A. Sansone, P. Scrimin and L. J. Prins, *Angew. Chem., Int. Ed.*, 2011, **50**, 2307.

135.   F. Manea, F. B. Houillon, L. Pasquato and P. Scrimin, *Angew. Chem., Int. Ed.*, 2004, **43**, 6165.

136.   L. Zhu and E. V. Anslyn, *Angew. Chem., Int. Ed.*, 2006, **45**, 1190.

137.   L. Kovbasyuk and R. Krämer, *Chem. Rev.*, 2004, **104**, 3161.

138. J. G. Millán and L. J. Prins, in *Supramolecular Systems in Biomedical Fields*, ed. H.-J. Schneider, The Royal Society of Chemistry, Cambridge, 2013, ch. 2, pp. 7–34.

139. L. Zhu, V. M. Lynch and E. V. Anslyn, *Tetrahedron*, 2004, **60**, 7267.

140. M. Meldal and C. W. Tornøe, *Chem. Rev.*, 2008, **108**, 2952.

141. Q. Wu and E. V. Anslyn, *J. Am. Chem. Soc.*, 2004, **126**, 14682.

142. R. F. Heck, *J. Am. Chem. Soc.*, 1968, **90**, 5518.

143. Q. Wu and E. V. Anslyn, *J. Mater. Chem.*, 2005, **15**, 2815.

144. R. J. T. Houk and E. V. Anslyn, *New J. Chem.*, 2007, **31**, 729.

145. K. Sonogashira, Y. Tohda and N. Hagihara, *Tetrahedron Lett.*, 1975, **16**, 4467.

146. S. C.Ritter and B. König, *Chem. Commun.*, 2006, 4694.

147. W. G. Lewis, F. G. Magallon, V. V. Fokin and M. G. Finn, *J. Am. Chem. Soc.*, 2004, **126**, 9152.

148. M. J. Wiester, P. A. Ulmann and C. A. Mirkin, *Angew. Chem., Int. Ed.*, 2011, **50**, 114.

149. J. R. Farrell, C. A. Mirkin, I. A. Guzei, L. M. Liable-Sands and A. L. Rheingold, *Angew. Chem., Int. Ed.*, 1998, **37**, 465.

150. N. C. Gianneschi, P. A. Bertin, S. T. Nguyen, C. A. Mirkin, L. N. Zakharov and A. L. Rheingold, *J. Am. Chem. Soc.*, 2003, **125**, 10508.

151. E. N. Jacobsen, *Acc. Chem. Res.*, 2000, **33**, 421.

152. C. G. Oliveri, P. A. Ulmann, M. J. Wiester and C. A. Mirkin, *Acc. Chem. Res.*, 2008, **41**, 1618.

153. K. B. Hansen, J. L. Leighton and E. N. Jacobsen, *J. Am. Chem. Soc.*, 1996, **44**, 10924.

154. N. C. Gianneschi, S. T. Nguyen and C. A. Mirkin, *J. Am. Chem. Soc.*, 2005, **127**, 1644.

155. G. Greiner and I. Maier, *J. Chem. Soc., Perkin Trans. 2*, 2002, 1005.

156. M. S. Masar III, N. C. Gianneschi, C. G. Olivieri, C. L. Stern, S. T. Nguyen and C. A. Mirkin, *J. Am. Chem. Soc.*, 2007, **129**, 10149.

157. H. J. Yoon, J. Kuwabara, J.-H. Kim and C. A. Mirkin, *Science*, 2010, **330**, 66.

158. M. R. ten Breteler, Z. Zhong, P. J. Dijkstra, A. R. A. Palmans, J. Peeters and J. Feijen, *J. Polym. Sci., Part A: Polym. Chem.*, 2007, **45**, 429.

159. T. Zauner, R. Berger-Hoffman, K. Müller, R. Hoffman and T. Zuchner, *Anal. Chem.*, 2011, **83**, 7356.

160. D. R. Edwards and G. Murphy, *Nature*, 1998, **394**, 527.

161. H. K. Yoon, S. T. Jung, J.-H. Kim and T. H. Yoo, *Biotechnol. Bioprocess Eng.*, 2012, **17**, 1113.

162. J. V. Olsen, S.-E. Ong and M. Mann, *Mol. Cell. Proteomics*, 2004, **3**, 608.

163. A. Light and H. Janska, *Trends Biochem. Sci.*, 1989, **14**, 110.

164. A. Holzinger, E. M. Maier, C. Bück, P. U. Mayerhofer, M. Kappler, J. C. Haworth, S. P. Moroz, H.-B. Hadorn, J. E. Sadler and A. A. Roscher, *Am. J. Hum. Genet.*, 2002, **70**, 20.

165. I. Yamashina, *Biochim. Biophys. Acta*, 1956, **20**, 433.

166. H. Kim, H. K. Yoon and T. H. Yoo, *Chem. Commun.*, 2014, **50**, 10155.

167. R. N. Jones, H. W. Wilson, W. J. Novick, A. L. Barry and C. Thornsberry, *J. Clin. Microbiol.*, 1982, **15**, 954.

168. C. Gialeli, A. D. Theocharis and N. K. Karamanos, *FEBS J.*, 2010, **278**, 16.

169. S. S. Shekhawat and I. Ghosh, *Curr. Opin. Chem. Biol.*, 2011, **15**, 789.

170. S. S. Shekhawat, J. R. Porter, A. Sriprasad and I. Ghosh, *J. Am. Chem. Soc.*, 2009, **131**, 15284.

171. L. Pauling, R. B. Corey and H. R. Branson, *Proc. Natl. Acad. Sci. U. S. A.*, 1951, **37**, 205.

172. F. H. C. Crick, *Nature*, 1952, **170**, 882.

173. S. S. Shekhawat, S. T. Campbell and I. Ghosh, *ChemBioChem*, 2011, **12**, 2353.

174. D. S. Tawfik, B. S. Green, R. Chap, M. Sela and Z. Eshhar, *Proc. Natl. Acad. Sci. U. S. A.*, 1993, **90**, 373.

175. C. Créminon and F. Taran, *Chem. Commun.*, 2015, **51**, 7996.

176. A. L. Garner and K. D. Janda, *Angew. Chem., Int. Ed.*, 2010, **49**, 9630.

177. A. L. Garner and K. D. Janda, *ChemBioChem*, 2011, **12**, 523.

178. A. L. Garner and K. D. Janda, *Chem. Commun.*, 2011, **47**, 7512.

179. Y. Tian, Y. Hu and C. Mao, *ChemBioChem*, 2006, **7**, 1862.

180. R. R. Breaker, *Nat. Biotechnol.*, 1997, **15**, 427.

181. J. Li, Y. Jia, J. Zheng, W. Zhong, G. Shen, R. Yang, W. Tan, *Chem. Commun.*, 2013, **49**, 6137.

182. S. Sando, A. Narita, K. Abe and Y. Aoyama, *J. Am. Chem. Soc.*, 2005, **127**, 5300.

183. S. Tyagi and F. R. Kramer, *Nat. Biotechnol.*, 1996, **14**, 303.

184. A. Narita, K. Ogawa, S. Sando and Y. Aoyama, *Angew. Chem., Int. Ed.*, 2006, **45**, 2879.

185. M. Sinz, G. Wallace and J. Sahi, *AAPS J.*, 2008, **10**, 391.

186. E. Sella and D. Shabat, *J. Am. Chem. Soc.*, 2009, **131**, 9934.

187. D. A. Tomalia, H. Baker, J. Dewald, M. Hall, G. Kallos, S. Martin, J. Roeck, J. Ryder and P. Smith, *Polym. J.*, 1985, **17**, 117.

188. D. Astruc, E. Boisselier and C. Ornelas, *Chem. Rev.*, 2010, **110**, 1857.

189. F. M. H. de Groot, C. Albrecht, R. Koekkoek, P. H. Beusker and H. W. Scheeren, *Angew. Chem., Int. Ed.*, 2003, **42**, 4490.

190. M. L. Szalai, R. M. Kevwitch and D. V. McGrath, *J. Am. Chem. Soc.*, 2003, **125**, 15688.

191. R. J. Amir, N. Pessah, M. Shamis and D. Shabat, *Angew. Chem., Int. Ed.*, 2003, **42**, 4494.

192. M. Avital-Schmilovici and D. Shabat, *Soft Matter*, 2010, **6**, 1073.

193. E. Sella and D. Shabat, *Chem. Commun.*, 2008, 5701.

194. J. Simon, S. Salzbrunn, G. K. S. Prakash, N. A. Petasis and G. A. Olah, *J. Org. Chem.*, 2001, **66**, 633.

195. A. Baeyer and V. Villiger, *Ber. Dtsch. Chem. Ges.*, 1899, **32**, 3625.

196. H. D. Dakin, *Am. Chem. J.*, 1909, **42**, 477.

197. L.-C. Lo and C.-Y. Chu, *Chem. Commun.*, 2003, 2728.

198. S. Gnaim and D. Shabat, *Acc. Chem. Res.*, 2014, **47**, 2970.

199. R. Perry-Feigenbaum, E. Sella and D. Shabat, *Chem. – Eur. J.*, 2011, **17**, 12123.

200. M. Avital-Shmilovici and D. Shabat, *Bioorg. Med. Chem.*, 2010, **18**, 3643.

201. M. A. Swiderska and J.-L. Reymond, *Nat. Chem.*, 2009, **1**, 527.

202. E. Sella, A. Lubelski, J. Klafter and D. Shabat, *J. Am. Chem. Soc.*, 2010, **132**, 3945.

203. N. Karton-Lifshin and D. Shabat, *New J. Chem.*, 2012, **36**, 386.

204. E. Sella, R. Weinstain, R. Erez, N. Z. Burns, P. S. Baran and D. Shabat, *Chem.Commun.*, 2010, **46**, 6575.

205. K. Yeung, K. M. Schmid and S. T. Phillips, *Chem. Commun.*, 2013, **49**, 394.

206. E. Sella and D. Shabat, *Org. Biomol. Chem.*, 2013, **11**, 5074.

207. M. S. Baker and S. T. Phillips, *J. Am. Chem. Soc.*, 2011, **133**, 5170.

208. M. S. Baker and S. T. Phillips, *Org. Biomol. Chem.*, 2012, **10**, 3595.

209. V. F. Hodge and M. O. Stallard, *Environ. Sci. Technol.*, 1986, **20**, 1058.

210. A. D. Brooks, K. Yeung, G. G Lewis and S. T. Phillips, *Anal. Methods*, 2015, **7**, 7186.

211. J.-A. Gu, V. Mani and S.-T. Huang, *Analyst*, 2015, **140**, 346.

212. G. A. M. King, *Chem. Soc. Rev.*, 1978, **7**, 297.

213. G. A. M. King, *Origins Life*, 1977, **8**, 39.

214. L. E. Orgel, *Nature*, 1992, **358**, 203.

215. W. S. Zielinski and L. E. Orgel, *Nature*, 1987, **327**, 346.

216. D. Sievers and G. Von Kiedrowski, *Nature*, 1994, **369**, 221.

217. G. von Kiedrowski, B. Wlotzka, J. Helbing, M. Matzen and S. Jordan, *Angew. Chem., Int. Ed.*, 1991, **30**, 423.

218. N. Paul and G. F. Joyce, *Curr. Opin. Chem. Biol.*, 2004, **8**, 634.

219. V. Patzke and G. von Kiedrowski, *ARKIVOC*, 2007, 293.

220. D. H. Lee, J. R. Granja, J. A. Martinez, K. Severin and M. R. Ghadiri, *Nature*, 1996, **382**, 525.

221. V. Rotello, J.-I. Hong and J. Rebek, *J. Am. Chem. Soc.*, 1991, **113**, 9422.

222. K. Soai, S. Niwa and H. Hori, *J. Chem. Soc., Chem. Commun.*, 1990, 982.

223. K. Soai, T. Shibata, H. Morioka and K. Choji, *Nature*, 1995, **378**, 767.

224. K. Soai, T. Shibata and I. Sato, *Acc. Chem. Res.*, 2000, *33*, 382.

225. M. H. Todd, *Chem. Soc. Rev.*, 2002, **31**, 211.

226. K. Mikami and M. Yamanaka, *Chem. Rev.*, 2003, **103**, 3369.

227. T. Kawasaki, Y. Matsumura, T. Tsutsumi, K. Suzuki, M. Ito and K. Soai, *Science*, 2009, **24**, 492.

228.   J. L. Bada, *Nature*, 1995, **374**, 594.

229.   D. G. Blackmond, *Proc. Natl. Acad. Sci. U. S. A.*, 2004, **101**, 5732.

230.   K. Soai, *Top. Curr. Chem.*, 2008, **284**, 1.

231.   H. J. Yoon and C. A. Mirkin, *J. Am. Chem. Soc.*, 2008, **130**, 11590.

232.   M. Frenklach and D. Clary, *Ind. Eng. Chem. Fundamen.*, 1983, **22**, 433.

233.   H. Mohapatra, K. M. Schmid and S. T. Phillips, *Chem. Commun.*, 2012, **48**, 3018.

234.   K. Arimitsu, M. Miyamoto and K. Ichimura, *Angew. Chem., Int. Ed.*, 2000, **39**, 3425.

235.   J. S. Robbins, K. M. Schmid and S. T. Phillips, *J. Org. Chem.*, 2013, **78**, 3159.

236.   P. Theato, B. S. Sumerlin, R. K. O'Reilly and T. H. Epps III, *Chem. Soc. Rev.*, 2013, **42**, 7055.

237.   R. J. Amir and D. Shabat, *Chem. Commun.*, 2004, 1614.

238.   R. J. Amir, E. Danieli and D. Shabat, *Chem. – Eur. J.*, 2007, **13**, 812.

239.   S. A. Jenekhe and J. A. Osaheni, *Science*, 1994, **265**, 765.

240.   T. M. Swager, *Acc. Chem. Res.*, 1998, **31**, 201.

241.   Q. Zhou and T. M. Swager, *J. Am. Chem. Soc.*, 1995, **117**, 7017.

242.   B. L. Allwood, N. Spencer, H. Shahriari-Zavareh, J. F. Stoddart and D. J. Williams, *J. Chem. Soc., Chem. Commun.*, 1987, 1064.

243.   Q. Zhou and T. M. Swager, *J. Am. Chem. Soc.*, 1995, **117**, 12593.

244.   I. A. Levitsky, J. Kim and T. M. Swager, *J. Am. Chem. Soc.*, 1999, **121**, 1466.

245.   D. T. McQuade, A. E. Pullen and T. M. Swager, *Chem. Rev.*, 2000, **100**, 2537.

246.   S. W. Thomas III, G. D. Joly and T. M. Swager, *Chem. Rev.*, 2007, **107**, 1339.

247.   H. N. Kim, Z. Guo, W. Zhu, J. Yoon and H. Tian, *Chem. Soc. Rev.*, 2011, **40**, 79.

248.   K. Doré, S. Dubus, H.-A. Ho, I. Lévesque, M. Brunette, G. Corbeil, M. Boissinot, G. Boivin, M. G. Bergeron, D. Boudreau and M. Leclerc, *J. Am. Chem. Soc.*, 2004, **126**, 4240.

249.   X. Feng, L. Liu, S. Wang and D. Zhu, *Chem. Soc. Rev.*, 2010, **39**, 2411.

250.   H.-A. Ho, M. Boissinot, M. G. Bergeron, G. Corbeil, K. Doré, D. Boudreau and M. Leclerc, *Angew. Chem., Int. Ed.*, 2002, **41**, 1548.

251.   H. A. Ho, K. Doré, M. Boissinot, M. G. Bergeron, R. M. Tanguay, D. Boudreau and M. Leclerc, *J. Am. Chem. Soc.*, 2005, **127**, 12673.

252.   K. Doré, M. Leclerc and D. Boudreau, *Reviews in Fluorescence 2007*, eds. C. D. Geddes and J. R. Lakowicz, Springer, New York, 2009, ch. 9, pp. 179–197.

253.   K. Doré, M. Leclerc and D. Boudreau, *J. Fluoresc.*, 2006, **16**, 259.

254.   J. Chen, S. Körner, S. L. Craig, D. M. Rudkevich and J. Rebek, *Nature*, 2002, **415**, 385.

255.   J. Chen, S. Körner, S. L. Craig, S. L. Craig, D. M. Rudkevich and J. Rebek, *Proc. Natl. Acad. Sci. U. S. A.*, 2002, **99**, 2593.

256.   J. N. Weinstein, S. Yoshikami, P. Henkart, R. Blumenthal and W. A. Hagins, *Science*, 1977, **195**, 489.

257.   I. López Arbeloa, *J. Photochem.*, 1982, **18**, 161.

258.   C. Li and S. Liu, *Chem. Commun.*, 2012, **48**, 3262.

259.   G. Das, P. Talukdar and S. Matile, *Science*, 2002, **298**, 1600.

260.   S. Matile, *Chem. Soc. Rev.*, 2001, **30**, 158.

261.   M. Komoszynski and A. Wojtczak, *Biochim. Biophys. Acta*, 1996, **1310**, 233.

262.   T. Takeuchi and S. Matile, *J. Am. Chem. Soc.*, 2009, **131**, 18048.

263.   N. Sakai, J. Mareda and S. Matile, *Acc. Chem. Res.*, 2005, **38**, 79.

264.   S. Matile, H. Tanaka and S. Litvinchuk, *Top. Curr. Chem.*, 2007, **277**, 219.

265.   Y. Takaoka, K. Kiminami, K. Mizusawa, K. Matsuo, M. Narazaki, T. Matsuda and I. Hamachi, *J. Am. Chem. Soc.*, 2011, **133**, 11725.

266.   K. Matsuo, R. Kamada, K. Mizusawa, H. Imai, Y. Takayama, M. Narazaki, T. Matsuda, Y. Takaoka and I. Hamachi, *Chem. – Eur. J.*, 2013, **19**, 12875.

267.   K. Mizusawa, Y. Takoka and I. Hamachi, *J. Am. Chem. Soc.*, 2012, **134**, 13386.

268.   T. Yoshii, K. Mizusawa, Y. Takaoka and I. Hamachi, *J. Am. Chem. Soc.*, 2014, **136**, 16635.

269.   A. P. Esser-Kahn, S. A. Odom, N. R. Sottos, S. R. White and J. S. Moore, *Macromolecules*, 2011, **44**, 5539.

270.   A. P. Blum, J. K. Kammeyer, A. M. Rush, C. E. Callmann, M. E. Hahn and N. C. Gianneschi, *J. Am. Chem. Soc.*, 2015, **137**, 2140.

271.   M. A. Azagarsamy, P. Sokkalingam and S. Thayumanavan, *J. Am. Chem. Soc.*, 2009, **131**, 14184.

272.   A. J. Harnoy, I. Rosenbaum, E. Tirosh, Y. Ebenstein, R. Shaharabani, R. Beck and R. J. Amir, *J. Am. Chem. Soc.*, 2014, **136**, 7531.

273.   G. Liu, X. Wang, J. Hu, G. Zhang and S. Liu, *J. Am. Chem. Soc.*, 2014, **136**, 7492.

274.   M. Xue and J. I. Zink, *J. Am. Chem. Soc.*, 2013, **135**, 17659.

275.   M. Xue, D. Cao, J. F. Stoddart and J. I. Zink, *Nanoscale*, 2012, **4**, 7569.

276.   C. Wang, Z. Li, Y.-L. Zhao, J. W. Gaines, O. A. Bozdemir, M. W. Ambrogio, M. Frasconi, Y. Y. Botros, J. I. Zink and J. F. Stoddart, *Angew. Chem., Int. Ed.*, 2012, **51**, 5460.

277.   D. Tarn, C. E. Ashley, M. Xue, E. C. Carnes, J. I. Zink and C. J. Brinker, *Acc. Chem. Res.*, 2013, **46**, 792.

278.   N. A. Peppas and A. S. Hoffman, *Biomaterials Science: An Introduction to Materials in Medicine*, eds. B. D. Ratner, A. S. Hoffman, F. J. Schoen and J. E. Lemons, Elsevier, Oxford, 3rd ed., 2004, ch. 1.2.5, pp. 166–179.

279.   M. D. Segarra-Maset, V. J. Nebot, J. F. Miravet and B. Escuder, *Chem. Soc. Rev.*, 2013, **42**, 7086.

280.   J. Hu, G. Zhang and S. Liu, *Chem. Soc. Rev.*, 2012, **41**, 5933.

281.   A. Richtar, G. Paschew, S. Klatt, J. Lienig, K.-F. Arndt and H.-J. Adler, *Sensors*, 2008, **8**, 561.

282. D. Buenger, F. Topuz and J. Groll, *Prog. Polym. Sci.*, 2012, **37**, 1678.

283. Z. M. Shakhsher, I. Odeh, S. Jabr and W. R. Seitz, *Microchim. Acta*, 2004, **144**, 147.

284. L. A. DeLouise, P. M. Fauchet, B. L. Miller and A. A. Pentland, *Adv. Mater.*, 2005, **17**, 2199.

285. Z. Zhu, C. Wu, H. Liu, Y. Zou, X. Zhang, H. Kang, C. J. Yang and W. Tan, *Angew. Chem., Int. Ed.*, 2010, **49**, 1052.

286. J. Liu and Y. Lu, *Angew. Chem., Int. Ed.*, 2005, **45**, 90.

287. F. L. Bates, D. French and R. E. Rundle, *J. Am. Chem. Soc.*, 1943, **65**, 142.

288. L. Yan, Z. Zhu, Y. Zou, Y. Huang, D. Liu, S. Jia, D. Xu, M. Wu, Y. Zhou, S. Zhou and C. J. Yang, *J. Am. Chem. Soc.*, 2013, **135**, 3748.

289. M. Ikeda, T. Tanida, T. Yoshii and I. Hamachi, *Adv. Mater.*, 2011, **23**, 2819.

290. M. Ikeda, R. Ochi and I. Hamachi, *Lab Chip*, 2010, **10**, 3325.

291. A. Wada, S. Tamaru, M. Ikeda and I. Hamachi, *J. Am. Chem. Soc.*, 2009, **131**, 5321.

292. M. Ikeda, T. Yoshii, T. Matsui, T. Tanida, H. Komatsu and I. Hamachi, *J. Am. Chem. Soc.*, 2011, **133**, 1670.

293. M. Ikeda, R. Ochi, A. Wada and I Hamachi, *Chem. Sci.*, 2010, **1**, 491.

294. T. Yoshii, S. Onogi, H. Shigemitsu and I. Hamachi, *J. Am. Chem. Soc.*, 2015, **137**, 3360.

295. M. S. Hershfield, L. J. Roberts II, N. J. Ganson, S. J. Kelly, I. Santisteban, E. Scarlett, D. Jaggers and J. S. Sundy, *Proc. Natl. Acad. Sci. U. S. A.*, 2010, **107**, 14351.

296. M. Ikeda, T. Tanida, T. Yoshii, K. Kurotani, S. Onogi, K. Urayama and I. Hamachi, *Nat. Chem.*, 2014, **6**, 511.

297. D.-G. Cho and J. L. Sessler, *Chem. Soc. Rev.*, 2009, **38**, 1647.

298. S. Goggins, C. Naz, B. J. Marsh, *Chem. Commun.*, 2015, **51**, 561.

299. http://www.atlasgenetics.com/the-company (accessed June 2015).

300. R. W. Peeling, K. K. Holmes, D. Mabey and A. Ronald, *Sex Transm. Infect.*, 2006, **82**, v1.

301. A. Y. Peleg and D. C. Hooper, *N. Engl. J. Med.*, 2010, **362**, 1804.

302. B. J. Marsh, J. O. Sharp, S. E. Flower, C. G. Frost and Atlas Genetics Ltd., *Int. Pat.*, WO2012/085591, 2012.

303. N. J. Ronkainen, H. B. Halsall and W. R. Heineman, *Chem. Soc. Rev.*, 2010, **39**, 1747.

304. J. Wang, *Biosens. Bioelectron.*, 2006, **21**, 1887.

305. S. C. Hillier, C. G. Frost, A. T. A. Jenkins, H. T. Braven, R. W. Keay, S. E. Flower and J. M. Clarkson, *Bioelectrochemistry*, 2004, **63**, 307.

306. S. C. Hillier, S. E. Flower, C. G. Frost, A. T. A. Jenkins, R. W. Keay, H. T. Braven and J. M. Clarkson, *Electrochem. Commun.*, 2004, **6**, 1227.

307. J. O. Sharp, PhD Thesis, University of Bath, 2012.

308. B. J. Marsh, L. Hampton, S. Goggins and C. G. Frost, *New J. Chem.*, 2014, **38**, 5260.

309.   D. M. Pearce, D. P. Shenton, J. Holden and C. A. Gaydos, *IEEE Trans. Biomed. Eng.*, 2011, **58**, 755.

310.   K. A. Fenton and C. M. Lowndes, *Sex Transm. Infect.*, 2004, **80**, 255.

311.   L. Babuin and A. S. Jaffe, *Can. Med. Assoc. J.*, 2005, **173**, 1191.

312.   J. A. Ramos-Vara, *Vet. Pathol.*, 2005, **42**, 405.

313.   J. S. Bonifacino, E. S. Dell'Angelica and T. A. Springer, *Curr. Protoc. Mol. Biol.*, 2001, **48**, 1.

314.   B. Weeke, *Scand. J. Immunol. Suppl.*, 1973, **1**, 47.

315.   J. P. Gosling, *Clin. Chem.*, 1990, **36**, 1408.

316.   *Immunoassay*, eds. E. P. Diamandis and T. K. Christopoulos, Academic Press, London, 1996, ch. 1, pp. 1–3.

317.   L. E. Miles and C. N. Hales, *Nature*, 1968, **219**, 186.

318.   S. Avrameas, *Immunochemistry*, 1969, **6**, 43.

319.   B. K. van Weemen and A. H. W. M. Schuurs, *FEBS Lett.*, 1971, **15**, 232.

320.   E. Engvall and P. Perlmann, *Immunochemistry*, 1971, **8**, 871.

321.   R. Lequin, *Clin. Chem.*, 2005, **51**, 2415.

322.   D. M. Kemeny and S. Chantler, *ELISA and Other Solid Phase Immunoassays*, eds. D. M. Kemeny and S. J. Challacombe, John Wiley & Sons Ltd, Colchester, 1988, ch. 1, pp. 1–29.

323.   S. Chantler and J. A Diment, *Immunoassays for the 80s*, eds. A. Voller, A. Bartlett and D. Bidwell, MTP Press, Lancaster, ch. 28, pp. 417–430.

324.   R. H. Yolken and F. J. Leister, *J. Clin. Microbiol.*, 1980, **13**, 738.

325.   D. M. Kemeny and D. Richards, *Immunological Techniques in Microbiology*, vol. 24, eds. J. M. Grange, A. Fox and N. L. Morgan, Blackwell, Oxford, 1987, pp. 49–57.

326.   C. Blake and B. J. Gould, *Analyst*, 1984, **109**, 533.

327.   N. C. Veitch, *Phytochemistry*, 2004, **65**, 249.

328.   A.-C. Lee, G. Liu, C.-K. Heng, S.-N. Tan, T.-M. Lim and Y. Lin, *Electroanalysis*, 2008, **20**, 2040.

329.   Q. Husain, *Crit. Rev. Biotechnol.*, 2010, **30**, 41.

330.   F. H. Ko and H. G. Monbouquette, *Biotechnol. Prog.*, 2006, **22**, 860.

331.   U. Sharma, D. Pal and R. Prasad, *Ind. J. Clin. Biochem.*, 2014, **29**, 269.

332.   K. R. Wehnmeyer, H. B. Halsall and W. R. Heineman, *Clin. Chem.*, 1985, **31**, 1546.

333.   H. T. Tang, C. E. Lunte, H. B. Halsall and W. R. Heineman, *Anal. Chim. Acta*, 1988, **214**, 187.

334.   L. Della Ciana, G. Bernacca, C. De Nitti and A. Massaglia, *J. Immunol. Methods*, 1996, **193**, 51.

335.   C. Fernández-Sánchez and A. Costa-García, *Biosens. Bioelectron.*, 1997, **12**, 403.

336.   F. Tie, A. Pan, B. Ru, W. Wang and Y. Hu, *J. Immunol. Methods*, 1992, **149**, 115.

337.   M. P. Kreuzer, C. K. O'Sullivan and G. G. Guilbault, *Anal. Chim. Acta*, 1999, **393**, 95.

338.   S Kobayashi and H. Higashimura, *Prog. Polym. Sci.*, 2003, **28**, 1015.

339.   C. Fernández-Sánchez and A. Costa-García, *Electroanalysis*, 1998, **10**, 249.

340.   M. S. Wilson and R. D. Rauh, *Biosens. Bioelectron.*, 2004, **20**, 276.

341.   A. Kokado, H. Arakawa and M. Maeda, *Anal. Chim. Acta*, 2000, **407**, 119.

342.   A. Preeschaworapun, Z. Dai, Y. Xiang, O. Chailapakul and J. Wang, *Talanta*, 2008, **76**, 424.

343.   B. Habibi and M. H. Pournaghi-Azar, *Electrochim. Acta*, 2010, **55**, 5492.

344.   M. Díaz-González, M. B. González-García and A. Costa-García, *Electroanalysis*, 2005, **17**, 1901.

345.   D. R. van Staveren and N. Metzler-Nolte, *Chem. Rev.*, 2004, **104**, 5931.

346.   C. Degrand, B. Limoges and S. Rapicault, *J. Pharm. Biomed. Anal.*, 1996, **14**, 1343.

347.   C. J. McNeil, I. J. Higgins and J. V. Bannister, *Biosensors*, 1987/88, **3**, 199.

348.   A. La Gal La Salle, B. Limoges, C. Degrand and P. Brossier, *Anal. Chem.*, 1995, **67**, 1245.

349.   A. La Gal La Salle, B. Limoges and C. Degrand, *J. Electroanal. Chem.*, 1994, **379**, 281.

350.   B. Limoges and C. Degrand, *Anal. Chem.*, 1996, **68**, 4141.

351.   J. M. Fowler, D. K. Y. Wong, H. B. Halsall and W. R. Heineman, *Electrochemical Sensors, Biosensors and their Biomedical Applications*, eds. X. Zhang, H. Ju and J. Wang, Academic Press, London, 1st edn., 2008, ch. 5, pp. 115–140.

352.   R. Y. Tsien and A. T. Harootunian, *Cell Calcium*, 1990, **11**, 93.

353.   J. Fan, M. Hu, P. Zhan and X. Peng, *Chem. Soc. Rev.*, 2013, **42**, 29.

354.   Y. Du, B. J. Lim, Y. S. Jiang, J. L. Sessler and A. D. Ellington, *Anal. Chem.*, 2014, **86**, 8010.

355.   C. H. Fan, K. W. Plaxco and A. J. Heeger, *Proc. Natl. Acad. Sci. U. S. A.*, 2003, **100**, 9134.

356.   F. Gao, L. Du, Y. Zhang, D. Tang and Y. Du, *Anal. Chim. Acta*, 2015, **883**, 67.

357.   K. Ren, J. Wu, F. Yan and H. Ju, *Sci. Rep.*, 2014, **4**, 4360.

358.   K. Ren, J. Wu, F. Yan, Y. Zhang and H. Ju, *Biosens. Bioelectron.*, 2015, **66**, 345.

359.   E. Xiong, L. Wu, J. Zhou, P. Yu, X. Zhang and J. Chen, *Anal. Chim. Acta*, 2015, **853**, 242.

360.   X. Chai, L. Zhang and Y. Tian, *Anal. Chem.*, 2014, **86**, 10668.

361.   X. Zhang, L. Wu, J. Zhou, X. Zhang and J. Chen, *J. Electroanal. Chem.*, 2015, **742**, 97.

362.   A. Sagi, J. Rishpon and D. Shabat, *Anal. Chem.*, 2006, **78**, 1459.

363.   J. Li, X. Luo, Q. Wang, L.-M. Zheng, T. W. Doyle and S.-H. Chen, *Bioorg. Med. Chem. Lett.*, 1998, **8**, 3159.

364.   L. J. Silverberg, J. L. Dillon and P. Vemishetti, *Tetrahedron Lett.*, 1996, **37**, 771.

365.   M. Golkowski and T. Ziegler, *Molecules*, 2011, **16**, 4695.

366. S. W. Chaikin and W. G. Brown, *J. Am. Chem. Soc.*, 1949, **71**, 122.

367. J. Lapić, G. Pavlović, D. Siebler, K. Heinze and V. Rapić, *Organometallics*, 2008, **27**, 726.

368. C. Schotten, *Ber. Dtsch. Chem. Ges.*, 1884, **17**, 2544.

369. E. Baumann, *Ber. Dtsch. Chem. Ges.*, 1886, **19**, 3218.

370. T. Curtius, *Ber. Dtsch. Chem. Ges.*, 1890, **23**, 3023.

371. H. Franzyk, M. K. Christensen, R. M. Jørgensen, M. Meldal, H. Cordes, S. Mouritsen and K. Bock, *Bioorg. Med. Chem.*, 1997, **5**, 21.

372. G. W. Kenner, A. R. Todd and F. J. Weymouth, *J. Chem. Soc.*, 1952, 3875.

373. K.-H. Chen, J.-S. Yang, C.-Y. Hwang and J.-M. Fang, *Org. Lett.*, 2008, **10**, 4401.

374. J. Perruchon, R. Ortmann and M. Schlitzer, *Synthesis*, 2007, **22**, 3553.

375. J. Kotlarska, K. Binnemans and W. Dehaen, *Tetrahedron*, 2013, **69**, 9947.

376. M. Tercel, G. J. Atwell, S. Yang, A. Ashoorzadeh, R. J. Stevenson, K. J. Botting, Y. Gu, S. Y. Mehta, W. A. Denny, W. R. Wilson and F. B. Pruijn, *Angew. Chem., Int. Ed.*, 2011, **50**, 2606.

377. J. D. Patrone, J. Yao, N. E. Scott and G. D. Dotson, *J. Am. Chem. Soc.*, 2009, **131**, 16340.

378. T. Tsuji, K. Suzuki, T. Nakamura, T. Goto, Y. Sekiguchi, T. Ikeda, T. Fukuda, T. Takemoto, Y. Mizuno, T. Kimura, Y. Kawase, F. Nara, T. Kagari, T. Shimozato, C. Yahara, S. Inaba, T. Honda, T. Izumi, M. Tamura and T. Nishi, *Bioorg. Med. Chem.*, 2014, **22**, 4246.

379. S. Hanashima, S. Manabe, K. Inamori, N. Taniguchi and Y. Ito, *Angew. Chem., Int. Ed.*, 2004, **43**, 5674.

380. K. Shimada, Y. Kaburgi and T. Fukuyama, *J. Am. Chem. Soc.*, 2003, **125**, 4048.

381. Y. G. Wang, R. Takeyama and Y. Kobayashi, *Angew. Chem., Int. Ed.*, 2006, **45**, 3320.

382. M. Oikawa, H. Furuta, Y. Suda and S. Kusumoto, *Tetrahedron Lett.*, 1999, **40**, 5199.

383. D. C. D. Butler and C. J. Richards, *Organometallics*, 2002, **21**, 5433.

384. R. Q. Thompson, M. Porter, C. Stuver, H. B. Halsall, W. R. Heineman, E. Buckley and M. R. Smyth, *Anal. Chim. Acta*, 1993, **271**, 223.

385. Y.-H. Hsieh, C. A. Gaydos, M. T. Hogan, O. M. Uy, J. Jackman, M. Jett-Goheen, A. Albertie, D. T. Dangerfield II, C. R. Neustadt, Z. S. Wiener and A. M. Rompalo, *PLoS ONE*, 2011, **6**, e19263.

386. L. Michaelis and M. L. Menten, *Biochem. Z.*, 1913, **49**, 333.

387. K. A. Johnson and R. S. Goody, *Biochemistry*, 2011, **50**, 8264.

388. R. B. McComb, G. N. Bowers and S. Posen, *Alkaline Phosphatase*, Plenum Press, New York, 1979, ch. 7.8, pp. 334–337.

389. S. Black, I. Kushner and D. Samols, *J. Biol. Chem.*, 2004, **279**, 48487.

390. S. Goggins, B. J. Marsh, C. G. Frost and Atlas Genetics Ltd., *U.K. Pat.*, 1405003.3, 2014.

391.   S. Goggins, B. J. Marsh, A. T. Lubben and C. G. Frost, *Chem. Sci.*, 2015, **6**, 4978.

392.   N. Malou and D. Raoult, *Trends Microbiol.*, 2011, **19**, 295.

393.   X. Pei, B. Zhang, J. Tang, B. Liu, W. Lai and D. Tang, *Anal. Chim. Acta,* 2013, **758**, 1.

394.   Y. Zhang, Y. Guo, Y. Xianyu, W. Chen, Y. Zhao and X. Jiang, *Adv. Mater.*, 2013, **25**, 3802.

395.   J. Das, M. A. Aziz and H. Yang, *J. Am. Chem. Soc.*, 2006, **128**, 16022.

396.   E. J. Nam, E. J. Kim, A. W. Wark, S. Rho, H. Kim and H. J. Lee, *Analyst*, 2012, **137**, 2011.

397.   R. Polsky, R. Gill, L. Kaganovsky and I. Willner, *Anal. Chem.*, 2006, **78**, 2268.

398.   W. Qu, Y. Liu, D. Liu, Z. Wang and X. Jiang, *Angew. Chem., Int. Ed.*, 2011, **50**, 3442.

399.   R. de la Rica and M. M. Stevens, *Nat. Nanotechnol.*, 2012, **7**, 821.

400.   P. D. Howes, S. Rana and M. M. Stevens, *Chem. Soc. Rev.*, 2014, **43**, 3835.

401.   R. de la Rica and M. M. Stevens, *Nat. Protoc.*, 2013, **8**, 1759.

402.   A. Johannsson and D. L. Bates, *ELISA and Other Solid Phase Immunoassays*, eds. D. M. Kemeny and S. J. Challacombe, John Wiley & Sons Ltd, Colchester, 1988, ch. 4, pp. 86.

403.   O. H. Lowry, *Mol. Cell. Biochem.*, 1980, **32**, 135.

404.   H. Yang, *Curr. Opin. Chem. Biol.*, 2012, **16**, 422.

405.   Z. Gao, L. Hou, M. Xu and D. Tang, *Sci. Rep.*, 2014, **4**, 3966.

406.   J.-H. Kim, H.-W. Chung and T. R. Lee, *Chem. Mater.*, 2006, **18**, 4115.

407.   S. Ge, F. Liu, W. Liu, M. Yan, X. Song and J. Yu, *Chem. Commun.*, 2014, **50**, 475.

408.   C.-J. Li and T.-H. Chan, *Comprehensive Organic Reactions in Aqueous Media*, John Wiley & Sons Ltd, Hoboken, 2nd edn., 2007.

409.   J. F. Hull, Y. Himeda, W.-H. Wang, B. Hashiguchi, R. Periana, D. J. Szalda, J. T. Muckerman and E. Fujita, *Nat. Chem.*, 2012, **4**, 383.

410.   N. D. McDaniel, F. J. Coughlin, L. L. Tinker and S. Bernhard, *J. Am. Chem. Soc.*, 2008, **130**, 210.

411.   J. M. McFarland and M. B. Francis, *J. Am. Chem. Soc.*, 2005, **127**, 13490.

412.   R. Kawahara, K. Fujita and R. Yamaguchi, *J. Am. Chem. Soc.*, 2010, **132**, 15108.

413.   R. Kawahara, K. Fujita and R. Yamaguchi, *J. Am. Chem. Soc.*, 2012, **134**, 3643.

414.   T. Abura, S. Ogo, Y. Watanabe and S. Fukuzumi, *J. Am. Chem. Soc.*, 2003, **125**, 4149.

415.   X. Wu, X. Li, A. Zanotti-Gerosa, A. Pettman, J. Liu, A. J. Mills and J. Xiao, *Chem. – Eur. J.*, 2008, **14**, 2209.

416.   V. Köhler, Y. M. Wilson, M. Dürrenberger, D. Ghislieri, E. Churakova, T. Quinto, L. Knörr, D. Häussinger, F. Hollmann, N. J. Turner and T. R. Ward, *Nat. Chem.*, 2013, **5**, 93.

417.   Y. Wei, D. Xue, Q. Lei, C. Wang and J. Xiao, *Green Chem.*, 2013, **15**, 629.

418. X. Wu, J. Liu, X. Li, A. Zanotti-Gerosa, F. Hancock, D. Vinci, J. Ruan and J. Xiao, *Angew. Chem. Int. Ed.*, 2006, **45**, 6718.

419. J. Tan, W. Tang, Y. Sun, Z. Jiang, F. Chen, L. Xu, Q. Fan and J. Xiao, *Tetrahedron*, 2011, **67**, 6206.

420. H.E. Gottlieb, V. Kotlyar and A. Nudelman, *J. Org. Chem.*, 1997, **62**, 7512.

421. *Purification of Laboratory Chemicals* 3rd ed., C. L. L. Chai and W. L. F. Amarego, Pergamon Press, Oxford, 1988.

422. R. B. McComb and G. N. Bowers, *Clin. Chem.*, 1972, **18**, 97.

423. D. van Leusen and B. Hessen, *Organometallics*, 2001, **20**, 224.

424. M. Merabet-Khellasi, L. Aribi-Zouioueche and O. Riant, *Tetrahedron: Asymmetry*, 2009, **20**, 1371.

425. D. Kalita, M. Morisue and Y. Kobuke, *New J. Chem.*, 2006, **30**, 77.

426. Z. Zhang, S. Mikkola and H. Lönnberg, *Org. Biomol. Chem.*, 2003, **1**, 854.

427. T. Aubineau and J. Cossy, *Chem. Commun.*, 2013, **49**, 3303.

428. A. V. Kirsanov and N. A. Kirsanova, *Zh. Obshch. Khim.*, 1962, **32**, 887.

429. M. S. Abdel-Maksoud, M.-R. Kim, M. I. El-Gamal, M. M. G. El-Din, J. Tae, H. S. Choi, K.-T. Lee, K. H. Yoo and C.-H. Oh, *Eur. J. Med. Chem.*, 2015, **95**, 453.

430. F. B. Zienty, *J. Am. Chem. Soc.*, 1945, **67**, 1138.

431. D. G. Batt, J. J. Petraitis, G. C. Houghton, D. P. Modi, G. A. Cain, M. H. Corjay, S. A. Mousa, P. J. Bouchard, M. S. Forsythe, P. B. Harlow, F. A. Barbera, S. M. Spitz, R. R. Wexler and P. K. Jadhav, *J. Med. Chem.*, 2000, **43**, 41.

432. U. Ragnarsson, L. Grehn, L. S. Monteiro and H. L. S. Maia, *Synlett*, 2013, **15**, 2386.

433. R.Khan, T. P. Singh and M. D. Singh, *Synlett*, 2014, **25**, 696.

434. N. Mase, T. Ando, F. Shibagaki, A. Sugita, T. Narumi, M. Toda, N. Watanabe and F. Tanaka, *Tetrahedron Lett.*, 2014, **55**, 1946.

435. S. Chen, L. Wang, N. E. Fahmi, S. J. Benkovic and S. M. Hecht, *J. Am. Chem. Soc.*, 2012, **134**, 18883.

436. T. Schaefer, R. Sebastian, J. Peeling, G. H. Penner and K. Koh, *Can. J. Chem.*, 1989, **67**, 1015.

437. N. S. Shaikh, K. Junge and M. Beller, *Org. Lett.*, 2007, **9**, 5429.

438. A. P. Dieskau, J.-M. Begouin and B. Plietker, *Eur. J. Org. Chem.*, 2011, **2011**, 5291.

439. G. Nagendra, T. M. Vishwanatha and V. V. Sureshbabu, *Tetrahedron Lett.*, 2012, **53**, 5059.

440. N. Murai, M. Yonaga and K. Tanaka, *Org. Lett.*, 2012, **14**, 1278.

441. R. Cano, M. Yus and D. J. Ramón, *Tetrahedron*, 2011, **67**, 8079.

442. M. R. Naimi-Jamal, J. Mokhtari, M. G. Dekamin and G. Kaupp, *Eur. J. Org. Chem.*, **2009**, *2009*, 3567.

443. Y. Zhou, G. Gao, H. Li and J. Qu, *Tetrahedron Lett.*, 2008, **49**, 3260.

444. H.-J. Li, Y.-Y. Wu, Q.-X. Wu, R. Wang, C.-Y. Dai, Z.-L. Shen, C.-L. Xie and Y.-C. Wu, *Org. Biomol. Chem.*, 2014, **12**, 3100.

445. B. Basu, B. Mandal, S. Das, P. Das and A. K. Nanda, *Beilstein J. Org. Chem.*, 2008, **4**, 53.

446. C. B. Kelly, M. A. Mercadante, T. A. Hamlin, M. H. Fletcher and N. E. Leadbeater, *J. Org. Chem.*, 2012, **77**, 8131.

447. E. Kawabata, K. Kikuchi, Y. Urano, H. Kojima, A. Odani and T. Nagano, *J. Am. Chem. Soc.*, 2005, **127**, 818.

448. C. Morrill and R. H. Grubbs, *J. Am. Chem. Soc.*, 2005, **127**, 2842.